# Tectonic and microfabric studies along the Penninic Front between Pelvoux and Argentera massifs (Western Alps, France).

**Inauguraldissertation**

Zur Erlangung der Würde eines Doktors der Philosophie vorgelegt der Philosophisch-Naturwissenschaftlichen Fakultät der Universität Basel

von

Ghislain Trullenque

aus Frankreich

Basel, 2005

Je n'ai jamais fait comme tout le monde et je ne compte pas commencer aujourd'hui. Certaines personnes voient en cela une marque d'arrogance. Je leur réponds que ce n'est pas le cas, bien loin de là.

Je ne vais donc pas commencer ce mémoire, comme cela se fait habituellement, par une belle citation que j'aurais entendue quelque part, ou prise au hasard dans un livre que je n'aurais pas lu dans son intégralité. Je ne vais pas non plus dédier ce manuscrit à une ou plusieurs personnes proches. J'ai certes mis tous mes efforts, toute ma patience ainsi que toute mon application à la rédaction des pages qui vont suivre, mais comme tout travail de recherche, celui-ci se veut incomplet, perfectible et soumis à la critique. Les personnes à qui je pense en ce moment méritent bien mieux.

Je ne vais pas non plus longuement remercier toutes celles et ceux qui ont travaillé à mes cotés. Stefan, Bernhard, Renée, Holger, Karsten, il suffit d'avoir vu une seule fois l'enthousiasme qui vous a animé pendant ces années pour comprendre que tout discours de remerciement est superflu.
Stefan, je préfère te remercier de m'avoir donné, contre toute attente de ma part, la possibilité de finir mes trois premiers mois de prise de contact avec la géologie de terrain. Tu m'as accordé ta confiance malgré un début que je qualifierais de catastrophique et je t'en suis reconnaissant. Ce n'est pas la peine d'en dire plus, tu te souviens, cela ne fait aucun doute.
Merci Bernhard de m'avoir apporté ton soutient et tes encouragements pendant cette première semaine difficile. Merci aussi d'avoir toujours pris le temps de corriger, souvent dans l'urgence, telle ou telle figure, tel ou tel abstract.
Merci Renée, Holger, Karsten de m'avoir ouvert les portes de vos laboratoires. Merci de m'avoir spontanément accueilli dans vos équipes alors que mon sujet ne le prévoyait pas du tout au départ.

Je n'arrive pas non plus à remercier Alexandre, Sébastien, Markus, Boubou, RLB, Stefano, Tjerk, Nynke, Kamil, Almar, Zoltan, Pierre, Reizi, Déa, Matthias, Mihai, James, Heike, Johann, Kathy, Isa, Willy, Silvio, Koni, Nathalie, Verena, Stephane, Hans, Frau Glanzmann, Horst, Fred, Richy, Jeanette, Monsieur Fäh ou Cédric d'avoir partagé autant de bons moments avec moi, au sein de l'institut et bien plus encore. Nous avons pris tant de plaisir à être ensemble, pourquoi vous remercier ? Je ferais bien mieux de remercier le hasard de m'avoir permis de vous rencontrer et je souhaite sincèrement que nous gardions contact après mon départ.

# Table of contents

**Chapter 2:** Microfabrics of calcite ultramylonites recording coaxial and non-coaxial deformation kinematics: Examples from the Rocher de l'Yret shear zone (Western Alps).

**Chapter 3:** Microfabric analysis of calcitic marbles from the area investigated in the western Alps and the Gavarnie basal contact (central Pyrenees).

# INTRODUCTION

## Aim of the study

This study covers two key topics.

A first aim of the present study is to contribute to a better understanding of the formation of the arc of the Western Alps. This semi-circular arc has a radius of about 150 kilometers and is limited by the SW-NE trending northern subalpine chains to the north and by the NW-SE striking southern subalpine chains to the south. The southern segment of the arc, extending from the Pelvoux to the Argentera external crystalline massifs, is subject of this study (figures a and b).

In spite of a century of geological investigations, there is no general agreement concerning the formation of this arc. One of the key problems is related to the apparent 90° divergence in the direction of thrusting between the areas north and south of the Pelvoux massif, respectively. Several models aiming to explain the formation of this arc have been proposed (Vialon et al. 1989 and Platt et al. 1989, Ricou 1984, Ricou and Siddans 1986 and Butler et al. 1986).

Ceriani et al. (2001) recently proposed the hypothesis according to which the Adriatic indenter triggered WNW-thrusting along a major out of sequence thrust: the Roselend thrust (RT, figure a). According to these authors, displacements along this structure were kinematically linked to dextral movements along the Insubric line to the north and along sinistral strike slip at the rear of Argentera massif. Besides testing this hypothesis, this study also aims to integrate the work of Ceriani et al. (2001) into a coherent model that also includes the presence of SW-directed thrusting south of Pelvoux. This last feature remained unexplained by Ceriani et al. (2001) who based their hypothesis on work north of the Pelvoux massif.

The second key topic of this work is a complete microfabric analysis of calcite ultramylonites found at the eastern rim of the Pelvoux massif. WNW-directed emplacement of internal Subriançonnais and Briançonnais units led to impressive mylonitisation of Eocene nummulitic limestones at the eastern rim of the Pelvoux massif.

One major problem with calcite fabrics published so far is that, for a given sense of shear, *c*-axis maxima oriented either normal to foliation, or alternatively oriented oblique, rotated with or against the sense of shear, have been described. Hence, in the absence of a coherent model of texture evolution, calcite *c*-axis orientation could not be used as a reliable shear sense criterion. Based on two types of microfabrics developed under coaxial and non-coaxial kinematics a model of calcite *c*-axis distribution is proposed by this study. This model will be compared to results of microfabric analysis from calcite

ultramylonites found within the investigated area, and along a shear zone from the central Pyrenees.

This thesis forms part of a larger project dealing with the arc of the French-Italian Alps and was substantially supported by the Swiss National Science Foundation (project 20-555559.98 titled: The Penninic units of the Western Alps along the ECORS-CROP transect and the formation of the arc of the Western Alps.).

The main part of this project was carried out at the Geological-Paleontological Institute of Basel University. While Bernhard Fügenschuh and Stefan Schmid were involved in the field studies, Renée Heilbronner and Holger Stünitz contributed to the microstructural and the X-ray texture goniometry analysis of the calcite ultramylonites. Karsten Kunze from the ETH Zürich substantially participated in treatment of the textural data and the numerical modeling of textures. However, the author of this thesis acquired all the data and is primarily responsible for their interpretation with the help of the persons mentioned above.

**Geographical and geological setting of the field study area situated between the Pelvoux and Argentera massifs**

The 1/250000 French geological map, sheet Gap (Kerckhove et al. 1979) was used as an overview map for the whole area (figure a). The working area extends from the "Col du Lautaret" in the north to the Allos / Mont Pelat massif in the south, from Gap in the west to Vinacio in the east (figure b).

The key area of the field study was located at the eastern and southeastern rim of the Pelvoux massif (figure c) covered by the 1/50000 BRGM geological maps Guillestre (Debelmas et al. 1966), Orcières (Debelmas et al. 1980), Saint Christophe en Oisans (Barféty et al. 1984) and Briançon (Barféty et al. 1995). This triangular zone extends about 60 kilometers N/S and 45 kilometers E/W in its largest part (figure c). It represents the direct southern continuation of the area investigated by Ceriani (2001) in a precursor project. Elevations vary from 800 meters in the main valleys to 4102 meters (Barre des Ecrins summit).

This area lies along the Roselend thrust (Ceriani et al. 2001), a major tectonic feature separating the Subriançonnais and Briançonnais nappe stack from the externally located Dauphinois domain. The latter is overlain by the Helmenthoid Flysch nappes of Piemont Ligurian origin (i.e. the Embrunais Ubaye nappe stack), emplaced onto the Dauphinois domain early on and before the thrusting of the internal Penninic units along the Roselend thrust.

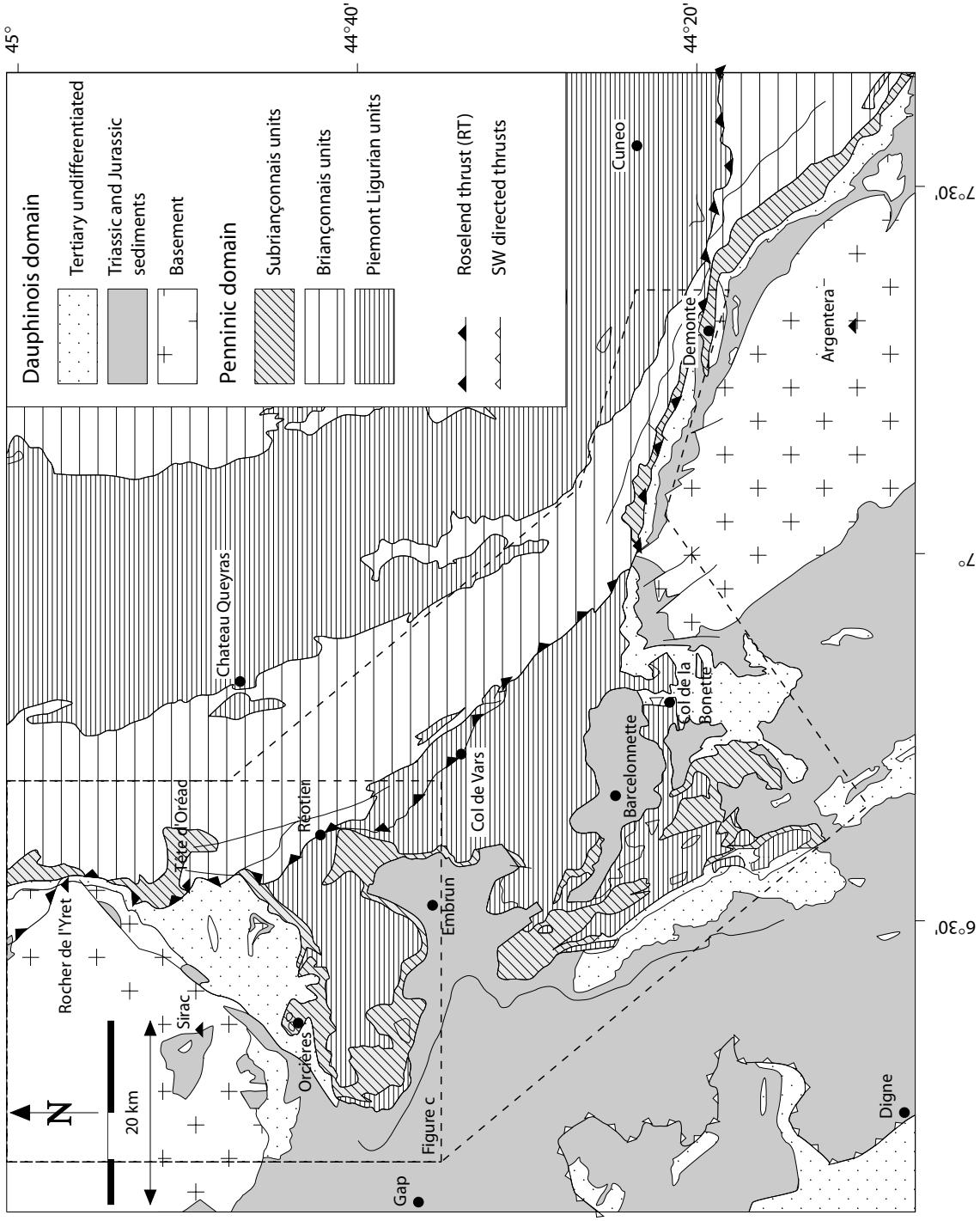


**Figure a:** Simplified geological overview of the area between Pelvoux and Argentera massifs after Kerckhove et al. (1979). Dashed lines indicate the outlines of figure c and of the entire working area of this study, respectively.

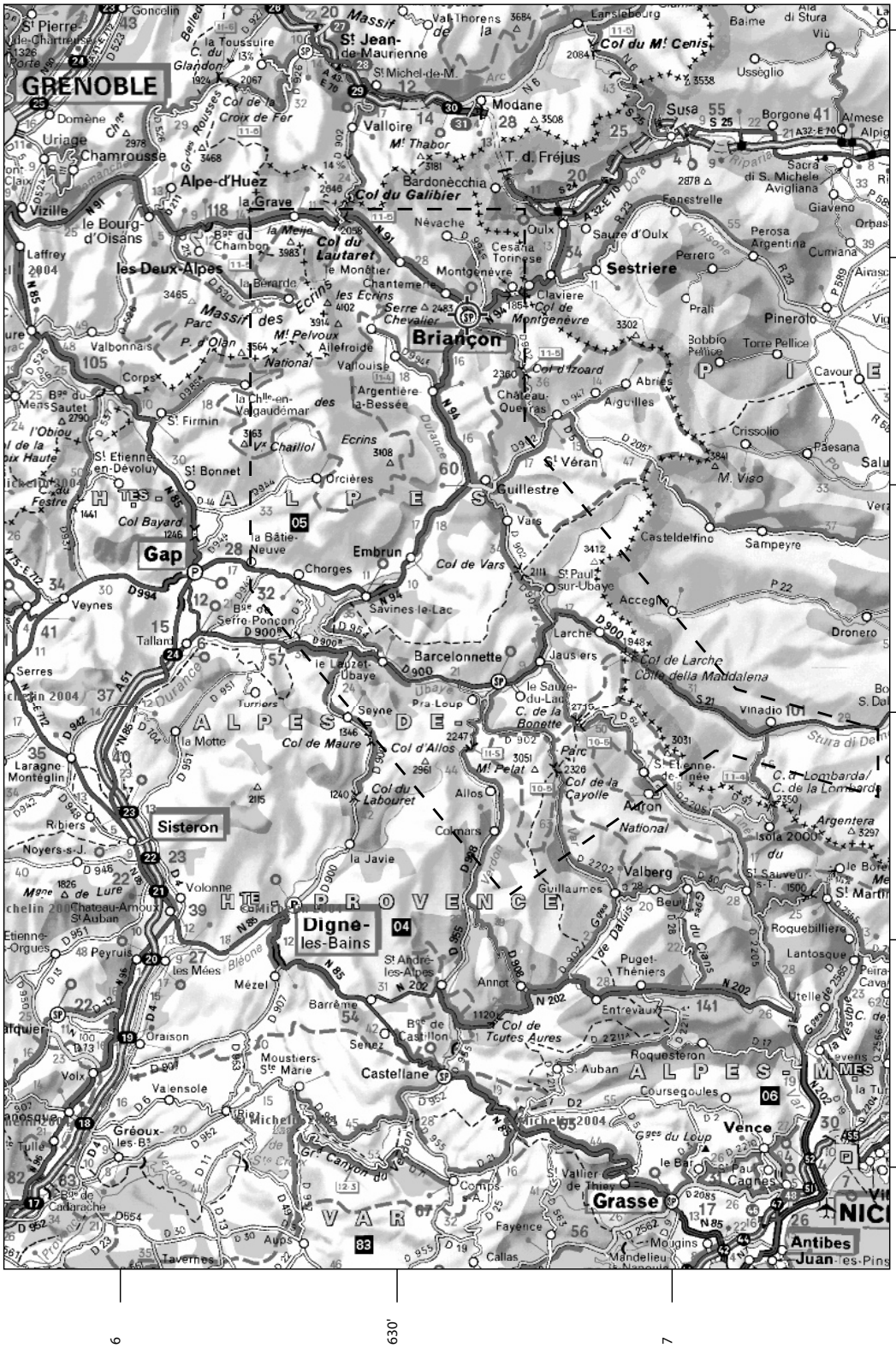


**Figure b:** Geographical map of the Dauphinois domain between Grenoble and Nice. The study area is outlined by the black dashed line.

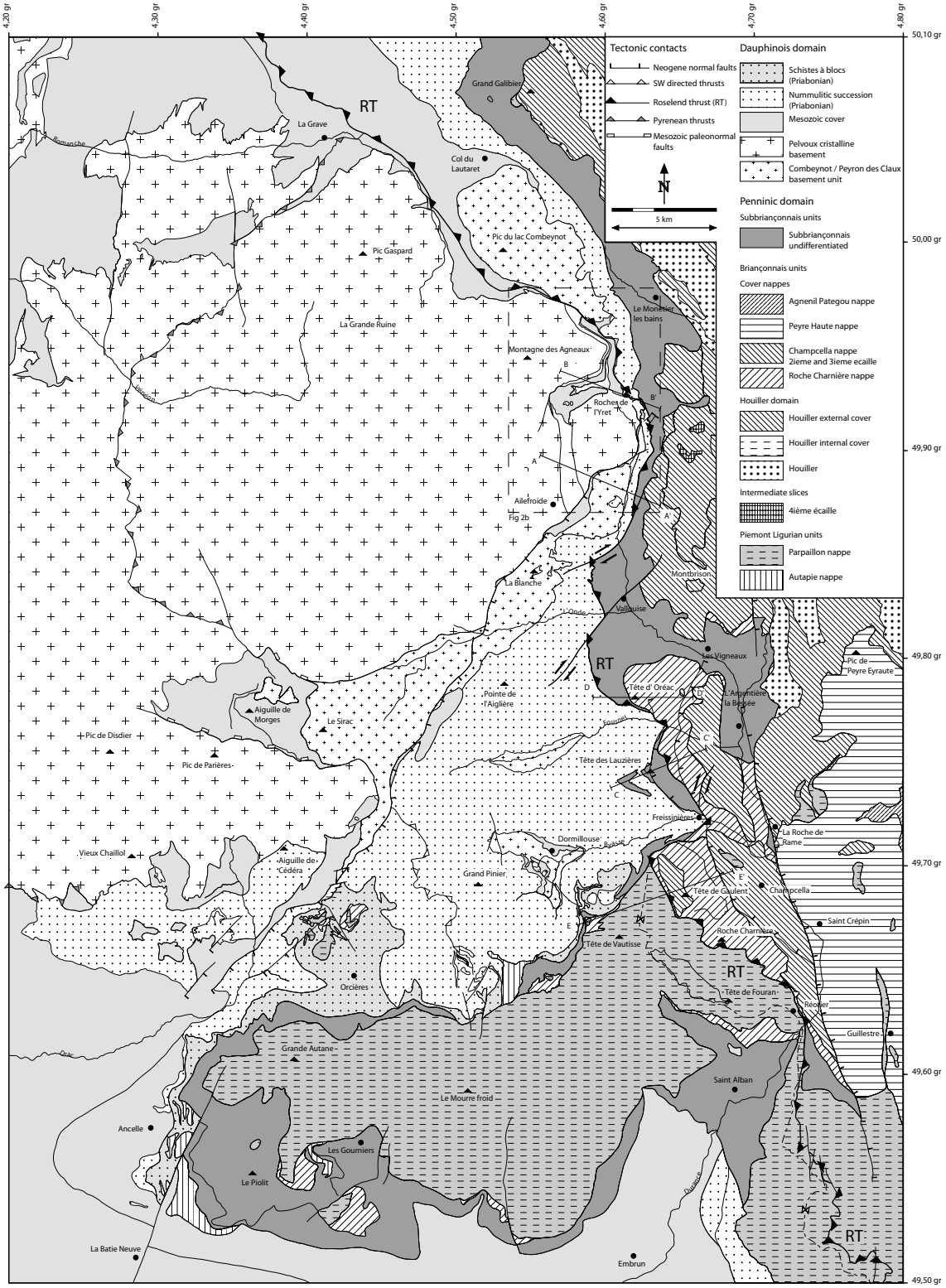


**Figure c:** Structural map of the eastern rim of the Pelvoux massif after Barféty et al. 1984, 1995 and Debelmas et al. 1966, 1980. See figure a for location.

**Organisation of the thesis**

This dissertation consists, besides this introduction, of three main chapters briefly characterised below, and of a final synthesis summarising the main results of the present work. This final synthesis is based on the discussions and conclusions presented in the individual chapters.

**Chapter 1:** Apparent divergence of thrusting directions north and south of the Pelvoux massif: implications for the evolution of the western Alpine arc.
Ghislain Trullenque, Bernhard Fügenschuh and Stefan M. Schmid; manuscript prepared for submission to "Tectonics".

After presenting the main geological units, the tectonic setting of the investigated area is discussed according to the new structural data acquired by the first author. Our model, based on three deformation phases, includes and confirms the hypothesis of Ceriani et al. (2001). We consider that the 90° divergence of thrusting directions recorded from north to south of Pelvoux is only an apparent one in the sense that it is the product of polyphase deformation. Clear overprinting relationships indicate that SW and NW-directed thrust systems developed totally independently, SW-thrusting is clearly post-dating NW-thrusting. All models involving a gradual change of contemporaneous thrusting directions are therefore not appropriate to explain the formation of the arc of the Western Alps. Based on these findings, a new model for the evolution of the arc of the Western Alps is proposed.

**Chapter 2:** Microfabrics of calcite ultramylonites recording coaxial and non-coaxial deformation kinematics: Examples from the Rocher de l'Yret shear zone (Western Alps)
Ghislain Trullenque, Karsten Kunze, Renee Heilbronner, Holger Stünitz and Stefan M. Schmid; manuscript submitted for publication to "Tectonophysics".

This study is based on a collection of 85 samples of mylonitised nummulitic limestone found at the eastern rim of the Pelvoux massif. The very specific structural setting of the outcrop investigated allows for the recognition of two types of microfabrics developed under coaxial and non-coaxial kinematics, respectively.

A new type of oblique *c*-axis orientation is described by means of a complete microfabric analysis, and the applicability of calcite textures as shear sense indicators is discussed.

**Chapter 3:** Microfabric analysis of calcitic marbles from the investigated area and the Gavarnie basal contact (central Pyrenees).

This chapter aims to provide examples for the application of the microfabric model presented in chapter 2, these being relevant for the conclusions reached in chapter 1.

Strain type evolutions (coaxial dominated to non-coaxial dominated) and strain partionning processes are evidenced within the main tectonic contacts of the investigated area and along the Gavarnie basal shear zone (central Pyrenees, France). The Pyrenean samples were provided by J.H.P. De Bresser from the experimental rock deformation laboratory at Utrecht University, who also made valuable contributions regarding this part of the microfabric analysis.

**Appendices**

This last part of the thesis provides appendices regarding the presentation of datasets and structural insights from the eastern rim of the Pelvoux massif (Appendix A), the complete textural and microstructural dataset from the Rocher de l'Yret shear zone presented in chapter 2 (Appendix B) and a metamorphic study of the Dauphinois domain at the south-eastern rim of the Pelvoux massif (Appendix C).

The data presented in these three appendices contributed to the overall interpretation of both the field and microfabric related parts of this study, respectively. Appendices A and B will be referred to in chapters 1, 2 and 3. The data presented in Appendix C are planned for publication at a later stage.

# 1. APPARENT DIVERGENCE OF THRUSTING DIRECTIONS NORTH AND SOUTH OF THE PELVOUX MASSIF: IMPLICATIONS FOR THE EVOLUTION OF THE WESTERN ALPINE ARC.

Ghislain Trullenque[a], Bernhard Fügenschuh[a] and Stefan M. Schmid[a].

[a] Department of Geosciences, Basel University, CH-4056 Basel, Switzerland

**Corresponding author:**

Ghislain Trullenque
Dept. of Geosciences
Basel University
Bernoullistr. 30-32
CH-4056 Basel
Switzerland

Tel. +41 - 61 - 267 3607
Fax. +41 - 61 - 267 3613
Email: ghislain.trullenque@unibas.ch

**Keywords:**
Western Alps, Dauphinois domain, shear sense analysis, polyphase tectonics, nappe stacking.

## Abstract.

In the Western Alps, the Penninic Basal Contact (PBC, Ceriani et al. 2001) defines the tectonic boundary between the external Dauphinois domain and the internal Penninic units.

During the Eocene, the PBC corresponds to the suture between Dauphinois and Subriançonnais/Briançonnais domains related to the subduction of the Valais ocean (Ceriani et al. 2001). In the Oligo-Miocene, i.e. during a second and post-collisional stage, Eocene structures were passively transported towards the WNW along a major out-of-sequence thrust, the Roselend thrust (RT), partially coinciding with and reactivating the PBC. Structural analysis of key outcrops combined with microfabric investigations of calcite ultramylonites allowed to trace the southern continuation of the RT in a broad shear zone at the rim of the Pelvoux massif and further South along the Briançonnais front (Tricart 1980) at the rear of the Embrunais Ubaye nappe stack. The RT finally branches into a sinistral strike slip zone NE of the Argentera massif.

The area south of the Pelvoux massif is additionally characterized by SW-directed thrusting, a feature totally absent north of it. Detailed investigations of outcrops found along strike of the RT, the basal decollement of both Dauphinois para-autochtonous Tertiary cover and Helmenthoid Flysch of the Embrunais Ubaye nappe stack reveal that top-SW thrusting is a younger (i.e. D2) event, overprinting earlier features linked to D1 WNW-directed displacements.

The youngest deformation event found in the area (D3) is consistent with normal faulting along the Durance system.

On a larger scale, it is concluded that the whole Adriatic indenter was thrusted onto the European plate along the RT during Oligo-Miocene times. Activity along this structure is linked to dextral movements along the Rhone-Simplon line and sinistral movements at the rear of the Argentera massif. Additionally, it is proposed that the onset of D2 SW-directed movements finds its origin in the opening of the western Mediterranean basin and the formation of the Appenine chain in middle Miocene times.

## 1.1 Introduction.

The formation of the Alpine nappe stack results from the closure of the Valaisan and Piemont-Ligurian oceanic domains, separated from each other by the Briançonnais micro-continent. During and after Tertiary collision between the Apulian and European plates, intensively deformed Penninic units were thrusted onto the European foreland along a major tectonic contact, referred to as Pennine/Penninic Front or Pennine/Penninic Frontal Thrust (Merle and Brun 1984, Mosar et al. 1996, Bagnoud et al. 1998, Spencer 1992, Seward and Mancktelow 1994, Bürgisser and Ford 1998).

Based on detailed mapping and a structural analysis in the area between the Arc and Isère valleys east of the Belledonne massif, Ceriani et al. (2001), Ceriani (2001), Ceriani and Schmid (2004) documented a polyphase history of this major tectonic contact. In Eocene times, the Penninic Basal Contact (PBC) (Ceriani et al. 2001) was active as a sinistrally transpressive zone during and after subduction of the Valaisan ocean. This episode was followed by Oligocene to Early Miocene WNW-directed out of sequence thrusting along the so-called Roselend Thrust (RT), partially reactivating the former PBC but propagating further into the Dauphinois domain at the rear of the Grandes Rousses massif. In their model, Ceriani et al. (2001), who only worked north of the Pelvoux massif, suggested that the RT may join the Briançonnais Front (BF) (Tricart 1980, 1986) at the rear of the Embrunais-Ubaye nappe stack south of the Pelvoux massif, in order to finally branch into a broad sinistral strike slip zone at the rear of the Argentera massif. A detailed study confirming or rejecting this hypothesis is still missing, however.

The structural setting of the Dauphinois domain south of the Pelvoux massif is, in comparison to the area N of the Pelvoux massif, additionally complicated by relicts of early Alpine structures. Moreover, top-SW directed kinematics have been described by many authors (e.g. Fry 1989, Bürgisser 1998, Bürgisser and Ford 1998, Lickorish and Ford 1998, Lickorish et al. 2002, Ford et al. 1999, Ford and Lickorish 2004) whereby it remained unclear as to whether this top-SW thrusting predates, is contemporaneous with, or postdates the top-WNW thrusting along the Roselend thrust.

The significance and amount of SW-directed thrusting, only observed in the Dauphinois domain south of the Pelvoux massif, is a matter of debate in the literature. Several models aim to combine top-SW displacements with the top-NW directed movements, observed north of the Pelvoux massif. Bürgisser (1998) formulated two groups of hypotheses: the “radial” and the “corner” hypotheses.

The radial hypothesis includes models such as that of Vialon et al. (1989) or a model proposed by Platt et al. (1989). According to Vialon et al. (1989), the radial thrusting pattern is generated by counterclockwise rotation of the translation direction

of the Mont Blanc-Belledonne-Pelvoux block along the western sidewall of the Apulian indenter, that moved northwestward. This rotation was accompanied by helical dextral strike slip faults (so-called Ring shear model). According to Platt et al. (1989), a three-dimensional radial orogenic wedge might develop ahead of a rounded indenter because of the combination of the plate motion vector and the topographically driven body forces (gravity) generated perpendicular to the trend of the orogenic wedge.

The corner hypothesis includes models such as those proposed by Ricou (1984), Ricou and Siddans (1986) and the model of Butler et al. (1986). The model of Ricou (1984), Ricou and Siddans (1986) involves indentation of the Adria indenter in two steps. According to this hypothesis, the Adria indenter moved towards the north during a first deformation phase, active from late Cretaceous to the Eocene. Deformation was accommodated along major N-S strike slip zones within the orogen. In a second episode, from the Oligocene to the Pliocene, the counterclokwise change in the translation path of Adria caused the SW-directed thrusting recorded in the Dauphinois domain south of Pelvoux. Deformation within the orogen was then accommodated by dextral strike slip along NE/SW striking faults (Dietrich and Durney 1986). Laubscher (1971, 1991) also came to a similar model that proposes a polyphase translation path of the Adria indenter. The model of Butler et al. (1986) involves a linear plate motion by at least 140 km towards WNW, inducing considerable thickening within the internal parts of the orogen. SW-directed thrusting within the southern sub-alpine chains is interpreted as a consequence of a lateral gravitational collapse of the orogen. In this model, such SW-directed displacements constitute a later, totally independent thrust system compared to the structures related to the NW-directed movements.

Bürgisser (1998) described clear evidence for SW-directed thrusting along the basal decollement of the Eocene cover of the southernmost parts of the Pelvoux massif and at the base of the Embrunais Ubaye nappe stack. According to this author, SW-directed deformation appears to be contemporaneous with NW-directed thrusting recorded north of the Pelvoux massif. The coeval activity of top-NW and top-SW thrusting, respectively, has also been proposed by Lickhorisch et al. (2002).

It is the aim of this contribution to test the hypothesis of Ceriani et al. (2001) and, provided it is found to be adequate, its integration into a coherent model. Thereby the evidence for top-SW movements will also be taken into account. These are in fact recorded in the area between Pelvoux and Argentera massifs, but not explained by the model of Ceriani et al. (2001). The present structural analysis also includes investigations of the basal contact of the Penninic Embrunais Ubaye nappe stack. No general agreement was found in the existing literature concerning the original direction of emplacement of these internal units of Briançonnais and Piemont-Ligurian origin onto the Dauphinois

domain.

We will present the results of an examination of the main tectonic contacts, particularly focussing on the kinematics of movement. Detailed maps in key areas are used to constrain the present day geometry of the region. Particular emphasis will be given to clear overprinting relationships in order to analyse the kinematic evolution of the area. All this will finally lead to a new interpretation of the tectonic evolution of the southern part of the western Alpine arc on the large scale.

## 1.2 Geological setting.

This detailed structural analysis first concentrates on the eastern and southeastern parts of the rim of the Pelvoux massif (figs 1.1 and 1.2). As already outlined by Bürgisser (1998), this area is of crucial importance for understanding the role of SW-directed kinematics, since such SW-directed thrusting is not recorded further north. In order to verify our findings in the area near the Pelvoux massif on a larger scale, we extended our study further towards the SE by investigating the Roselend thrust northeast and at the rear of the Argentera massif, where it affects both Dauphinois and Subriançonnais/ Briançonnais domains (fig 1.3).

Three main structural domains are distinguished in the working area, namely 1) the external Dauphinois domain, 2) the Embrunais-Ubaye nappe stack, consisting of basal slices of Subriançonnais origin, overlain by flysch of Piemont-Ligurian origin and 3) the Penninic units behind the "Briançonnais Front" in the sense of Tricart (1980, 1986), largely coinciding with the Roselend thrust as postulated by Ceriani et al. (2001) (fig 1.3). East of the Roselend thrust Briançonnais units predominate and are locally overlain by Piemont-Liguria derived flysch, while slices of Subriançonnais origin are found along a westernmost strip in the Pelvoux area only. The main geological characteristics of these units are briefly described below.

### 1.2.1 The Dauphinois domain.

The Dauphinois domain is part of the European margin and composed of Variscan basement carrying a thick Mesozoic to Tertiary sedimentary cover. During Mesozoic rifting, the eastern margin of the European plate was substantially thinned. Formation of major tilted crustal blocks allowed for the deposition of thick Mesozoic sedimentary series in asymmetric half grabens. These half grabens, intensively described in literature (Tricart et al. 1988, Davies 1982, Gillcrist et al. 1987, Butler 1989, Coward et al. 1991, Huyghe and Mugnier 1995, Lazarre et al. 1996, Sue et al. 1997) were inverted

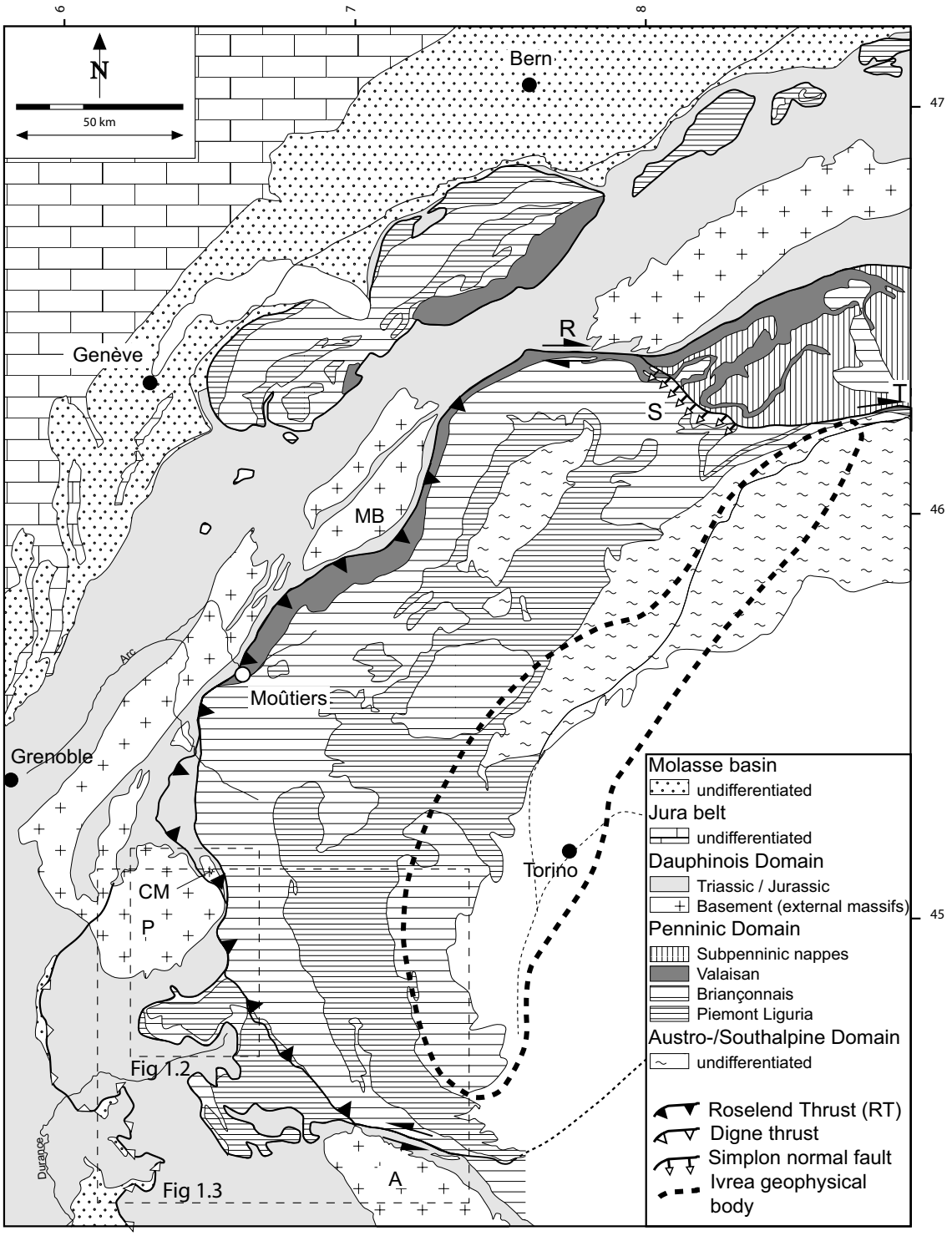


**Figure 1.1:** Simplified geological overview of the arc of the Western Alps. (A: Argentera massif, CM: Combeynot massif, MB: Mont Blanc massif, P: Pelvoux massif, R: Rhone-Simplon line, S: Simplon normal fault, T: Tonale line) ; after Froitzheim et al. (1996), Ceriani et al. (2001) and Schmid et al. (2004).

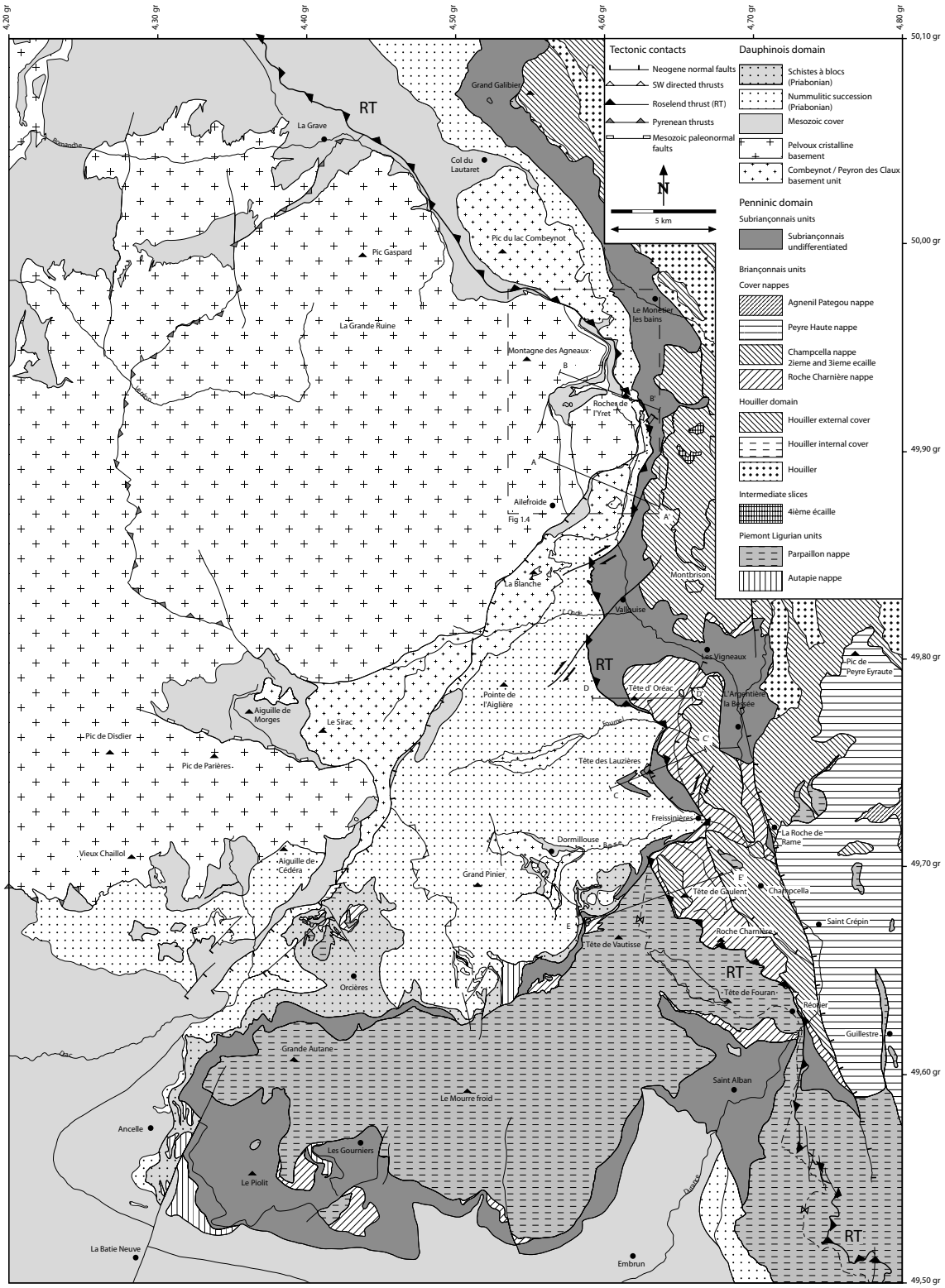


**Figure 1.2:** Structural map of the study area after Barbier et al. (1976); Barféty et al. (1984, 1996); Debelmas et al. (1966, 1980); Kerckhove et al. (1969, 1988).

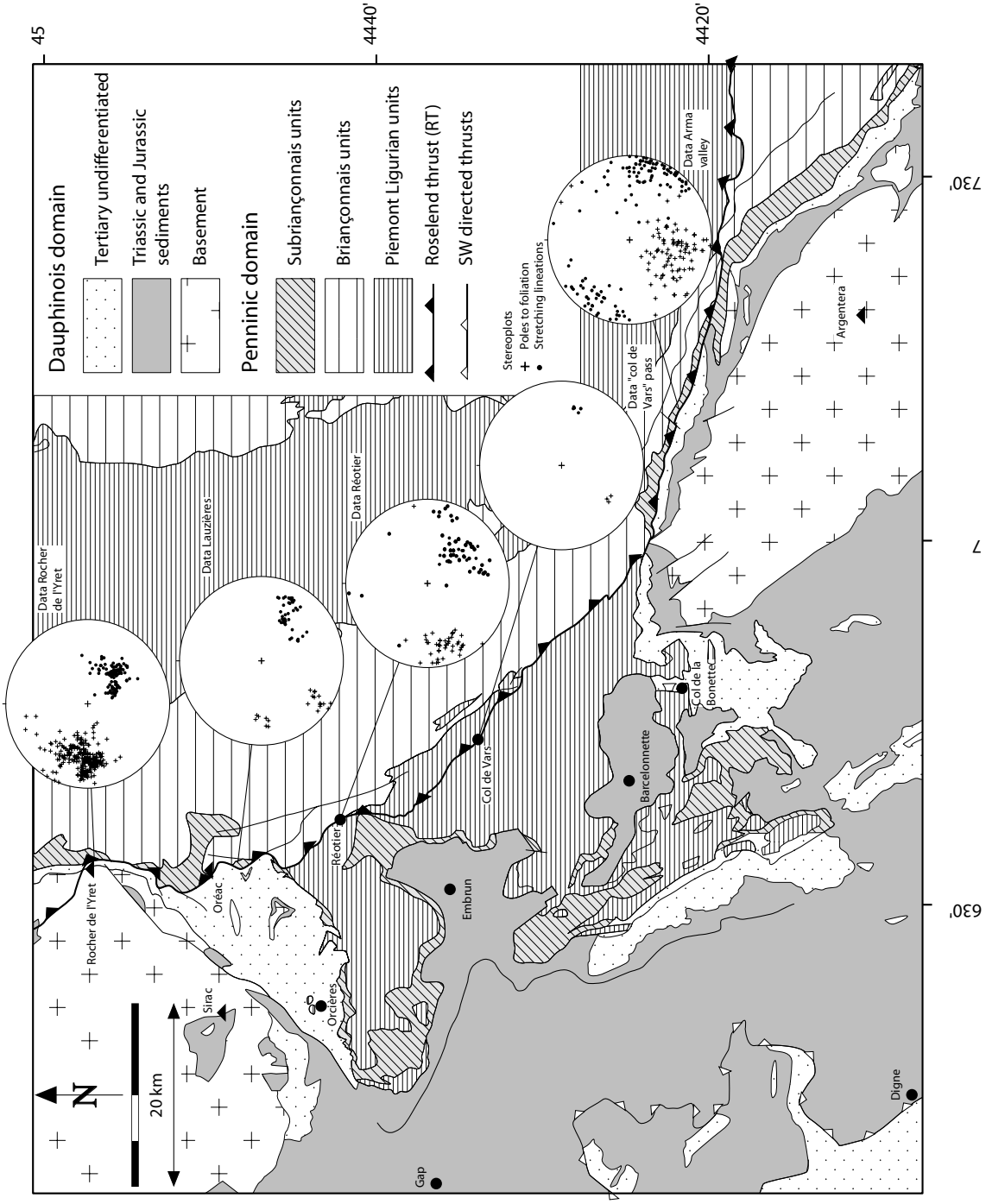


**Figure 1.3:** Simplified geological overview of the area between Pelvoux and Argentera massifs, after Kerckhove et al. (1980) and Bigi et al. (1983). Note the constant ESE-WNW oriented stretching lineations found along the Roselend thrust.

during Alpine orogeny and relics are directly observable within the Pelvoux massif and immediately north of it. Paleo-normal faults, such as the famous "Col d'Ornon" fault (Barféty et al. 1979, Lemoine et al. 1981) are mostly NE-SW striking.

Mesozoic strata are discordantly overlain by a conglomerate formation (Gupta 1997), followed by the classical "Priabonian trilogy" (Ravenne 1987, Apps et al. 2004), which comprises, from base to top:

1) shallow water nummulitic limestone of variable thickness (0 – 50 m).
2) hemipelagic globigerina marls (0 – 50 m).
3) the Champsaur sandstone formation, a regular alternance of turbiditic sandstones and shales (Perriaux and Uselle 1968, Waibel 1990), whose thickness varies from 700 to 1200 meters. In some areas immediately south of the Pelvoux massif, the silici-clastic deposits contain up to 50% of volcanic detritus (Debrand-Passard et al. 1984, Bürgisser 1998).

### 1.2.2 The Embrunais-Ubaye nappe stack.

The Embrunais Ubaye nappe stack comprises the Autapie nappe, overlain by the Parpaillon nappe. Both of them build up the Cretaceous age Helmenthoid flysch of Piemont-Liguria origin. These flysch units are locally underlain by slivers referred to as "Subriançonnais", although the facies of some of these slivers rather reminds of that found in the classical Briançonnais, rather than that found in the Subbriançonnais north of Pelvoux.

A marine tectono-sedimentary melange, the so-called "schistes à blocs" formation (Kerckhove 1969), formed in front of the advancing Autapie nappe. It marks the end of sedimentation within the Priabonian basin of the Dauphinois. This "schistes à blocs" unit is found without tectonic discontinuity on top of the Champsaur series and hence is considered as part of the Dauphinois (figs 1.2 and 1.3). It comprises an association of decimetric to metric sandstone and limestone blocks, mostly derived from the Autapie nappe and embedded in a black marly matrix.

Within the investigated area, the Autapie nappe is preserved as slices only, intensively folded together with the underlying Dauphinois series. The Parpaillon nappe, on the other hand, is much better preserved and it consists, from base to top, of the following succession (Kerckhove 1969):

1) silicic black schists with centimetric sandstone layers, the so-called "complexe de base".
2) Helminthoid flysch with massive sandstone layers, the so-called "Embrunais sandstones" (varying thickness of 0 to 100 m).

3) Calcareous Helminthoid flysch showing a regular internal stratification (500 to 800 m).

According to Fry (1989), Lickorish and Ford (1998), Merle and Brun (1984), the early emplacement of the Embrunais Ubaye nappe stack onto the Dauphinois domain is dated from the Early Oligocene (Rupelian). Numerous relics of helmenthoid flysch on top of the Briançonnais units clearly demonstrate that the Embrunais Ubaye nappe stack was originally derived from a more internal paleogeograhic position with respect to the Briançonnais units.

### 1.2.3 The Subriançonnais domain.

The Subriançonnais domain in the paleogeographic sense formed the passive margin of the Briançonnais during the opening of the Valais ocean. Its tectonic position is between the underlying Dauphinois units and the overlying Briançonnais units. It is presently exposed in the "Argentière window" near Oreac (figs 1.2 and 1.3) (a half window according to Barféty 1968) and was first recognized by Gignoux et al. (1933), Gignoux and Moret (1938). The age of the different stratigraphic units within this half window ranges from upper Oxfordian ("Terres noires" unit) to Cretaceous calcschists. The stratigraphically youngest formation of the Subbriançonnais units is the "black flysch" formation of Lutetian age, consisting of an alternance of centimetric to decimetric layers of black schists and fine-grained sandstones. This black flysch formation includes large olistoliths such as, for example, the Dogger limestone slice found below the "Tête des Lauzières" summit (see cross section in figure 1.11c and Debelmas 1955).

In map view (except for the above mentioned Argentière half window) the Subriançonnais unit usually forms a narrow band bordering the Briançonnais domain east and south of the Pelvoux massif. This thinning might be explained by late normal faulting, dissecting the Subriançonnais and Briançonnais front (Tricart et al. 1996), or alternatively, by intense shearing of the units at the eastern rim of the Pelvoux massif (Rocher de l'Yret shear zone, see chapter 2).

Finally, as mentioned above, slices related to the Subriançonnais are also found in a presently more external position, namely at the base of the Embrunais Ubaye nappe stack. These slices, together with Triassic dolomitic limestone units of Briançonnais paleogeographic origin, are interpreted as having been scraped off from the external border of the Eocene accretionary prism developed within the Briançonnais domain during the emplacement of the Helmenthoid flysch nappes onto Dauphinois. Their attribution to the "Subriançonnais" more reflects their present structural position (below or in front of the Briançonnais behind the Roselend thrust) rather than their pealeogeographic origin.

### 1.2.4 The Briançonnais domain.

The present geometry of the various Briançonnais tectonic units in the investigated area results from several deformation phases, described in detail by Tricart (1980, 1986), referred to as "Tectonique I to IV" by this author. The geometry of the Briançonnais domain indicates stacking of several nappes, some of them formely representing sedimentary infills of grabens developed within the Briançonnais platform during Mesozoic rifting ("in sequence" tectonics, Tricart et al. 1988). The actual order of stacking (from base to top) corresponds to their initial W-E paleogeographic distribution (Tricart et al. 1988, Claudel 1999).

The stratigraphy of the Briançonnais domain is described in great detail in the literature (see Claudel 1999 and references therein) and might be summarized as follows. A Devonian to Carboniferous age substratum is overlain by a Mesozoic and Tertiary cover. The Mesozoic series are dominantly calcareous and are often separated from their initial substratum due to decollement within the Upper Scythian evaporite formation. Within the western Briançonnais domain, the following nappes are classically described in literature (from base to top of the nappe stack): the "Roche Charnière" nappe, the "Champcella" nappe, the "3ieme écaille" nappe (Termier 1903) and the "Peyre-Haute" nappe.

*The "Roche Charnière" nappe:* This nappe is also known as the frontal Briançonnais nappe. It is mainly exposed in the area of the BRGM geological map "Guillestre" (Debelmas et al. 1966) between the Tête d'Oréac and Roche Charnière summits. Further north, this nappe is tectonically reduced to lenses marking the contact between Subriançonnais and Briançonnais domains, i.e. below the Montbrison massif.

*The "Champcella" nappe:* This nappe is also known as "Nappe de la Tête d'Aval du massif de Montbrison" and corresponds to the "2ième écaille" defined by Termier (1903) and later investigated by Goguel (1940, 1942) and Debelmas (1955). In the southern part of the investigated area, this nappe forms the "Gaulent" klippe and is found further east between Gaulent massif and Champcella village. In the north, this nappe builds up the major part of the Montbrison massif (fig 1.2).

*The "3ième écaille" nappe:* This nappe is also known as "Tête d'Amont du massif de Montbrison" nappe. It lies horizontally on top of the black flysch unit of the underlying "Champcella nappe" and remains relatively unaffected by folding or internal slicing.

*The "Peyre Haute" nappe:* This nappe is mainly exposed within the area covered by the "Guillestre" BRGM geological map (Debelmas et al. 1966). It is either thrust on top of the black flysch or onto the so-called "neo-Cretaceous" calcschists of the underlying "3ième écaille nappe". Numerous syn-rift paleo-normal faults are well preserved within

this nappe.

Finally, isolated klippen of crystalline basement, referred to as "4ième écaille" (Termier 1903) can be found. These basement units, well visible in the northern part of the investigated area east of the Rocher de l'Yret shear zone, are either interpreted as remnants of slices from the Acceglio zone (Debelmas 1983, Lemoine 1951, Termier 1903) or large-scale olistoliths (Barféty et al. 1992).

## 1.3 Deformation history.

Relics of pre-alpine (or early Alpine) structures can be observed at the southeastern rim of the Pelvoux massif, although largely overprinted by later Alpine deformation. Locally, three Alpine deformation phases (D1, D2 and D3) that post-date early Alpine structures formed before the deposition of the Priabonian-age nummulitic limestone can be defined and are briefly described below.

Shear sense have been deduced on mesoscopic and microscopic scale using criteria proposed by Simpson and Schmid (1983), Passchier and Trow (1996), in combination with the application of the model of calcite texture evolution presented in chapter 2 of this thesis.

### 1.3.1 Early Alpine structures.

Pre-Priabonian compressive deformation has been recognized in several places within the Pelvoux massif, either as inverted Mesozoic grabens (Lazarre et al. 1996, Sue et al. 1997, Lemoine et al. 2000), or as thrusting that affects the crystalline basement and its Mesozoic cover (Ford 1996). The Ailefroide syncline (figs 1.2 and 1.4) at the eastern rim of the Pelvoux massif is interpreted as an initial paleograben, inverted during this early Alpine phase (Lemoine et al. 2000 and next session). According to Lazarre et al. (1996), Sue et al. (1997), Lemoine et al. (2000), inversion occurred during the "Pyreneo-Provencal" phase of deformation, also known as the "early Alpine" stage.

This early Alpine stage, classically divided in a Pre-Senonian (Turonian) phase (Siddans 1979, Debrand-Passard et al. 1984, Flandrin 1967, Debelmas 1983) followed by a Late Cretaceous to Late Eocene Pyrenean-Provençal phase (Flandrin 1967, Graham 1978, Goguel 1963, Lemoine 1972), produced east-west trending structures, well visible in the thick Mesozoic sequences of the Diois and Baronnies regions (Gratier et al. 1989, Siddans 1979).

The structures resulting from the Pyrenean-Provencal phase are also well visible in the reconstruction map of the substrate to the Tertiary foreland basin deposition from

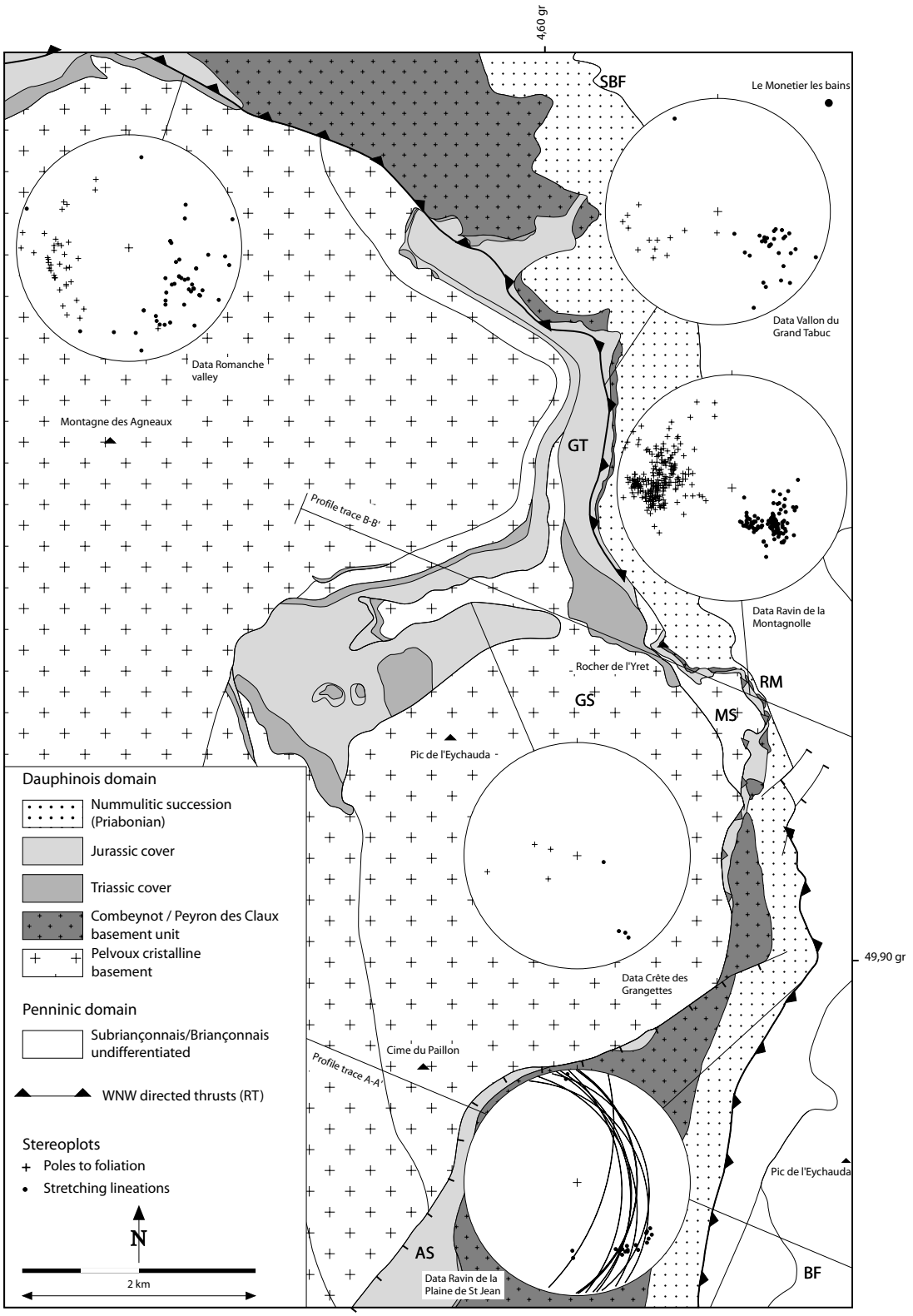


**Figure 1.4:** Structural map of the eastern rim of the Pelvoux massif (AS: Ailefroide syncline, BF: Briançonnais front, GS: Grangettes slice, GT: Grand Tabuc valley, MS: Montagnolle slice, RM: Ravin de la Montagnolle valley, SBF: Subriançonnais front). The Combeynot-Peyron des Claux unit is considered as a separate basement slice found in a higher structural position compared to the Pelvoux massif sensus stricto. See text for discussion.

Ravenne et al. (1987). The overall sense of transport during this compressional phase is top to the north.

According to Ford (1996), the "Pyrenean" phase is responsible for the early exhumation of the Pelvoux massif. The condensed Mesozoic cover series of Pelvoux at the "Crête des Grangettes" (fig 1.4) reflect this early exhumation of the massif (Gidon 1954, Debelmas and Kerckhove 1980, Lemoine et al. 1986). Moreover, increasing exhumation and erosion of Mesozoic series from the Argentera massif in the South to the Pelvoux massif in the North, provided a continuous older substratum for the Tertiary nummulitic transgression (Haug 1894, Ravenne et al. 1987).

### 1.3.2 D1 structures.

What is referred here as "D1", corresponds to the first phase of deformation that affected the Dauphinois units after the "Pyreneo-Provencal phase" during Oligocene to Early Miocene times. Note however that it corresponds to the third phase affecting the Penninic Sub-Briançonnais and Briançonnais units (see correlation table in Ceriani et al, 2001; Ceriani & Schmid 2004). It is the major deformation phase encountered in the investigated area since it is related to the thrusting along the Roselend thrust, Oligocene to Lower Miocene out-of-sequence thrust (Ceriani et al. 2001). Based on the constantly WNW-directed kinematic indicators measured directly along tectonic contacts associated with the Roselend thrust, and/or deduced from the analysis of calcite ultra-mylonites found in their direct footwall (see chapter 3), it becomes clear that the RT becomes amalgamated with the frontal thrust of the Subriançonnais units south of the Rocher de l'Yret peak (figs 1.2, 1.4 and 1.5). The geology of the Yret massif will be presented in more details when describing the cross sections (session 1.5). The Dauphinois domain, reduced to some hundred meters in thickness, suffered extreme lamination as attested by impressive mylonitisation of the nummulitic limestone formation (see chapter 2). All shear sense indicators found in this area immediately south of the one investigated by Ceriani et al. (2001) show a top to WNW sense of shearing.

Further south, the RT then joins the basal contact of the Roche Charnière unit below the "Tête d'Oréac" summit at the entrance of the Fournel valley (figs 1.2 and 1.5). The underlying Champsaur sandstones, dipping parallel to the RT (see cross section description), develops a penetrative foliation, well visible at the contact with the underlying Globigerina marls unit. The upper part of the Priabonian Globigerina marls often shows a first schistosity S1 that is sub-parallel to the S0 bedding planes of these sandstone levels (fig 1.6). In thin section, it appears that S1 is composed by alternating coarse layers formed by calcite crystals and more detritical levels. We interpret this S1

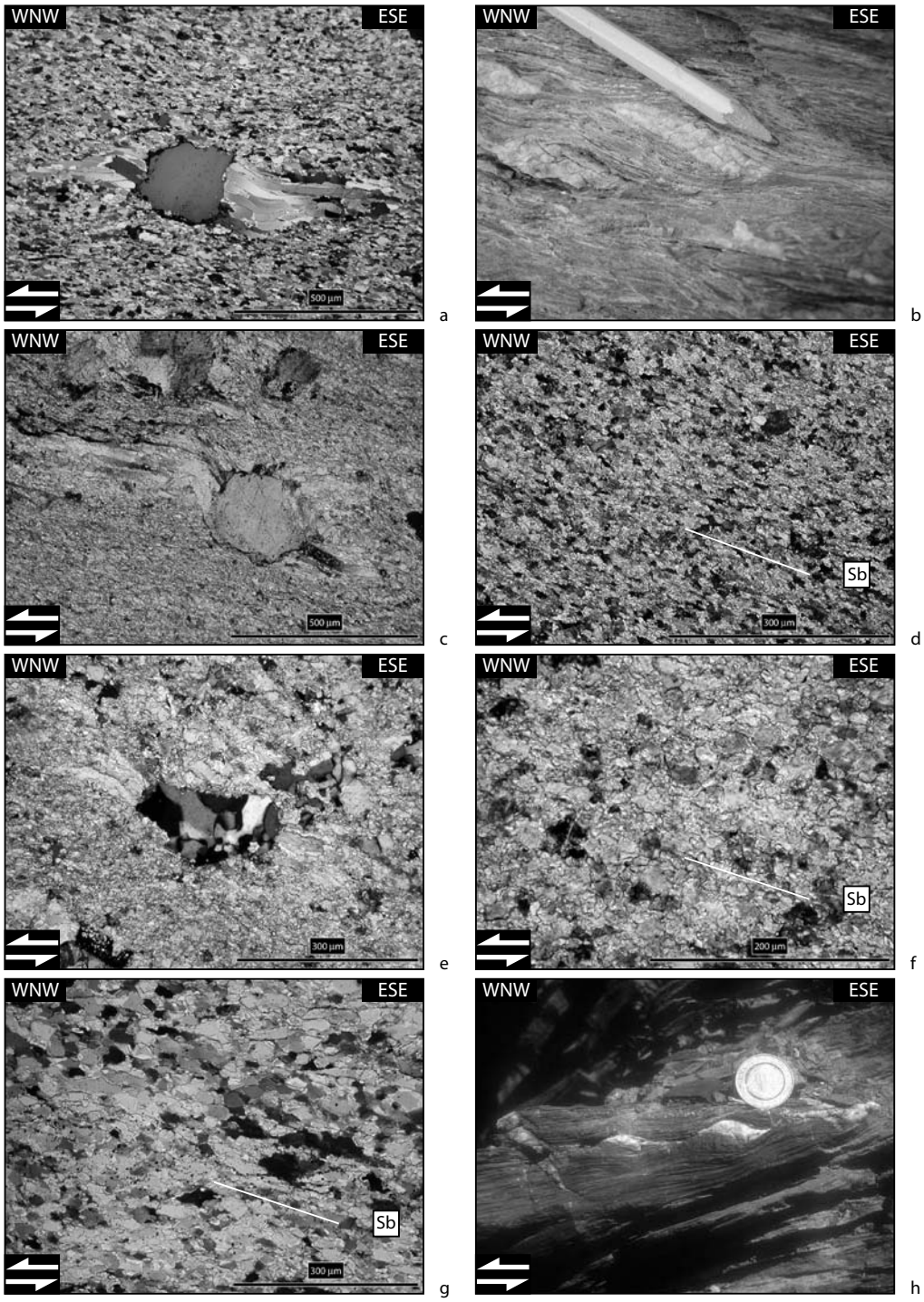


**Figure 1.5:** Meso- and microscopic shear sense indicators found along strike of the Roselend thrust and indicating top-WNW directed movements (samples and outcrops from the Rocher de l'Yret shear zone (a and b), the Oréac massif (c and d), the Briançonnais front south of the Réotier locality (e and f) and the Subriançonnais front at the rear of the Argentera massif (g and h), respectively). Normal thin sections (30 micrometers thickness) observed under crossed polarizers. The macroscopic foliation Sa is horizontal.
A detailed view of asymmetrically boudinaged calcite veins is given in b) and h).
Photomicrographs of different calcitic marbles, showing asymmetric calcite pressure fringes developed at the rim of detrital quartz grains (a, c and e) and oblique grain shape preferred orientation (Sb) within the dynamically recrystallised matrix (d, f and g).

layering to have resulted from pressure solution and re-deposition processes developed during the D1 deformation phase.

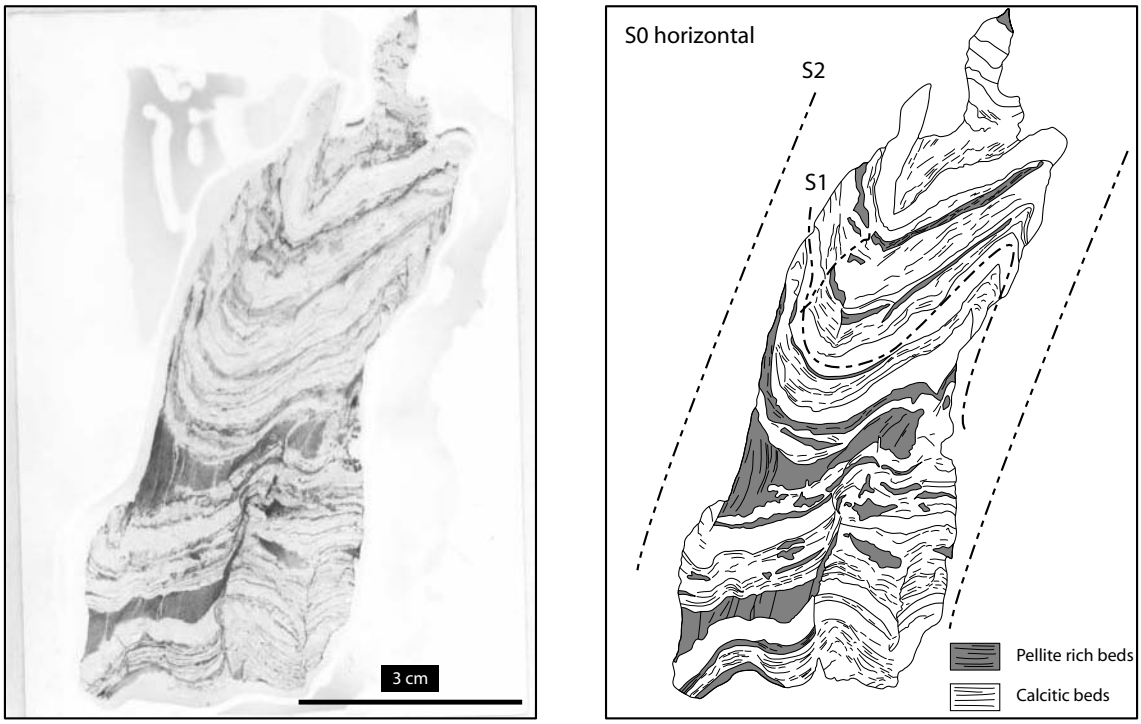


**Figure 1.6:** Photomicrographs of a hand specimen taken from the globigerina marls level in the Fournel valley. Overprinting relationships of a D1 foliation related to the top-WNW directed thrusting phase by D2 folding linked with top-SW directed transports are observed.

Hence, this confirms the hypothesis proposed by Ceriani et al. (2001) proposing that the RT joins the Briançonnais front (BF), as defined by Tricart (1980, 1986) further to the south and at the rear of the Embrunais Ubaye nappe stack, given the impressive amount of deformation of the frontal Briançonnais units, such as, for example, at the Réotier locality (fig 1.2 and see chapter 3). All shear sense indicators found in close vicinity of the Briançonnais front south of the Réotier locality are consistent with WNW-ESE directed transport (fig 1.5).

Further to the south, we propose that the RT propagates into the "complexe de base" (Kerckhove 1969) unit of the Embrunais Ubaye flysch series in the overturned limb of a megafold which formed the immediate footwall of the RT in order to finally join again the front of the Briançonnais and Subriançonnais units at the northeastern rim of the Argentera massif (see figure 1.3). Indeed, shear bands, dissecting a calcareous flysch unit of the Subriançonnais domain, indicate WNW-directed sense of transport, a feature confirmed by asymmetrically boudinaged calcitic veins found in mylonites of Subriançonnais origin (fig 1.5). As seen on the stereoplots presented in figure 1.3, all measured D1 stretching

lineations are nearly horizontal. The corresponding foliation planes are, however, always found in a steep orientation. This indicates that the displacement along this structure predominantly took place by sinistral strike slip within a deformation zone at the rear of the Argentera massif, as already documented by Laubscher (1971), Guillaume (1980), Ricou (1981), Lefevre (1983), so-called "Couloir de la Stura" of Ricou and Siddans 1986, Giglia 1996. This sinistral sense of shear has been independently confirmed by microfabric analysis of calcite ultramylonites of Briançonnais origin, presented in chapter 3.

1.3.3 D2 structures.

This second major deformation phase recorded within the investigated area results in SW-directed movements that overprint the top-WNW D1 deformation features and which are missing north of the Pelvoux massif. Going southward, evidence of top-SW deformation is found for the first time in the eastern slopes of the Montbrison massif 8 kilometres south of the Rocher de l'Yret (fig 1.2). Here the external Penninic units are clearly dissected by two sub-vertical tectonic contacts, that bring the entire Subriançonnais and Briançonnais domains into direct contact with the Priabonian detrital flysch. These structures, evidenced by Gidon (1965, 1979), Bravard and Gidon 1979, clearly represent dextral strike slip faults that offset the RT and which die out in the Champsaur flysch (fig 1.2). Further south, another dextral offset has also been recognized at the entrance of Dormillouse valley. Given the NE-SW orientation of these strike slip faults and the dextral offset of the internal units induced by their activity, they indicate a southward increasing amount of top-SW directed displacements. In summary, this area documents a later overprint of the Roselend thrust formed during the D1 deformation phase by D2 structures related to top-SW directed transport.

SW-directed thrusting, associated with the above described strike-slip movements, is recorded within the basal decollement level of the Tertiary cover, nicely exposed in Fournel and Dormillouse valleys (fig 1.2). Unambiguous top-SW directed shear bands (B3 structures of Bürgisser 1998) are widespread (fig 1.7) and a strong SW-NE oriented mineral lineation is developed within the planes of a penetrative foliation affecting the globigerina marls. In thin section, asymmetric calcite and/or quartz filled pressure shadows developed around pyrite crystals, clearly indicate a top to SW directed shear (fig 1.7).

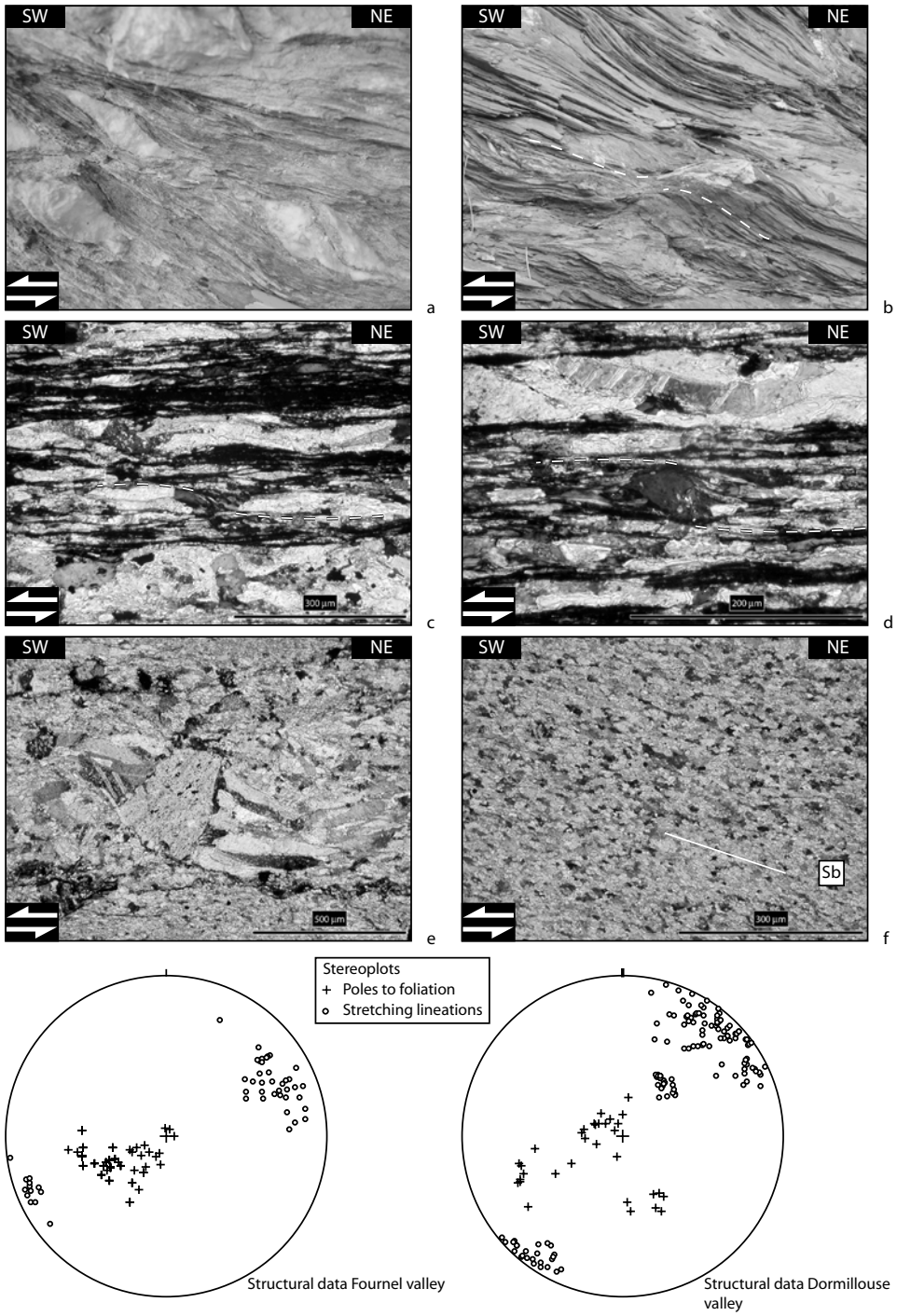


**Figure 1.7:** Meso- and microscopic shear sense indicators found within the basal decollement level of the Tertiary sedimentary succession in both the Fournel (c, d) and Dormillouse (a, b, e and f) valleys. The inferred sense of transport is top-SW (see stereoplots). All thin sections are cut perpendicular to the macroscopic foliation (horizontal in figures c, d, e and f) and observed under crossed polarizers.
a): asymmetrically boudinaged calcitic veins.
b): top-SW directed shear bands dissecting the globigerina marl formation.
c), d) and e): asymmetric calcite pressure fringes developed at the rim of detrital quartz grains.
f): oblique grain shape preferred orientation (Sb) observed within an entirely recrystallized nummulitic limestone specimen.

Evidences for SW-directed movements, overprinting earlier top-NW directed D1 structures, have been found at the contact between globigerina marls and Champsaur flysch. Figure 1.8 provides microstructural evidence regarding such overprinting structures: relicts of calcite pressure fringes developed at the rim of pyrite crystals materialize an old NNW-SSE oriented D1 lineation overprinted by later D2 NE-SW oriented striations. A

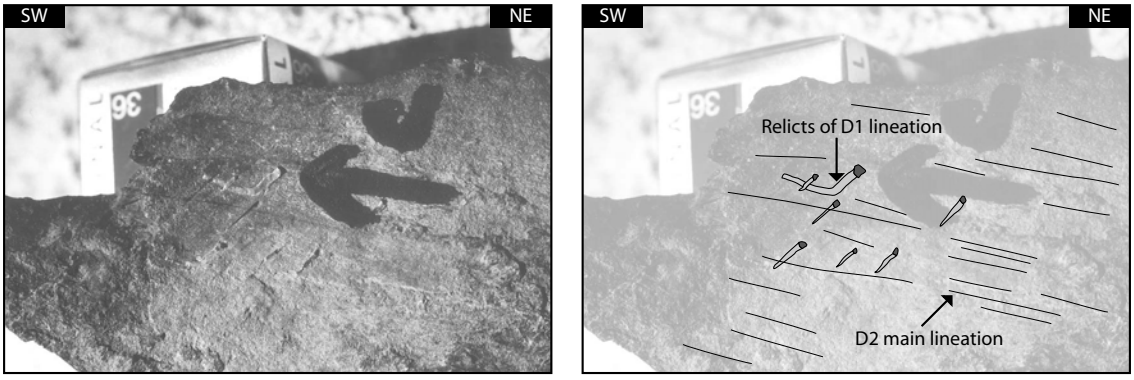


**Figure 1.8:** D1-related calcite pressure fringes overprinted by D2 NE-SW oriented striations.

superposition of D2 deformation features on earlier D1 structutes is also observable in figure 1.6. The S2 axial planar cleavage of chevron-type folds, such as those found in the Fournel valley, clearly overprints an earlier composite S0/1 foliation, related to D1 thrusting.

We conclude that the folding of the Champsaur flysch cover at the southeastern rim of the Pelvoux massif was induced by the onset of SW-directed shearing. The amounts of displacement accommodated by folding of the Tertiary cover increase from north to south. This is reflected by an evolution of folding style from open-type folds at the eastern slopes of the La Blanche massif 8 kilometres east of Montbrison massif to chevron-type folds in the Fournel and Dormillouse valleys (fig 1.2). This increase in shortening is compatible with and induced by the activity of the dextral strike slip zones dissecting the RT (see above). This strike slip network therefore acts as a transfer zone, allowing for decoupling of the domain north of the Pelvoux area from a domain south of this massif.

Structures related to SW-directed movements have only been found within the Dauphinois domain. They post-date the thrusting of the Briançonnais and Subriançonnais units along the RT.

Except for strike slip faulting affecting the Roche Charnière and Champcella Briançonnais external nappes, no evidence of D2 has been found within the Briançonnais domain. Instead, the internal Briançonnais south of Pelvoux is affected by major backfolds and backthrusts that play an important role in the overall structure of this domain. They

correspond to the late "Tectonique IV" phase described by Tricart (1980, 1986). According to the model of Tricart (1980, 1986), these backfolds and backthrusts indicate overall NE-directed shortening. It is important to note that the amounts of NE-directed shortening within the internal Briançonnais domain also increase from the north and towards the area south of the Pelvoux massif. These movements progressively die out in the Dauphinois domain. They are responsible of kink-type structures formation found along strike of the RT (see figure 1.9). In summary, both D2 and this "Tectonique IV" backfolding phase show the following characteristics: 1) amounts of top-SW displacement increase towards the south and are not recorded north of the Pelvoux massif, 2) D2 structures exhibit opposite senses of transport, 3) D2 post-dates the activity along the RT that was active during Oligocene (Fügenschuh and Schmid 2003).

It is tempting to relate part of the "Tectonique IV" phase (Tricart 1980, 1986) structures to the ones formed during D2 at least in the immediate vicinity of the RT. Eastward directed movements are indeed mechanically necessary at the rear of the accretionnary prism associated with D2 top-SW transport, the divide between fore-and retro-shearing being centered along the former RT.

### 1.3.4 D3 structures.

Normal faults related to the Durance fault system (High Durance Faulted Zone, Tricart 2004) are the latest deformation features found in the investigated area. These structures, first described by Debelmas 1955, have been later intensively studied by Sue et al. (1999), Sue and Tricart (1999, 2003), Tricart (2004), Tricart et al. (1996, 2001). These normal faults are notably responsible from a strong geothermal gradient and seismicity recorded along the Durance valley.

The timing of the onset of normal faulting, also recorded north of Pelvoux, remains a matter of debate in literature. Fügenschuh et al. (1999), Fügenschuh and Schmid (2003), based on results from fission track analysis, argue that this normal faulting phase is very recent in age (i.e. post 5 my) and that it is linked to the final exhumation of the external crystalline massifs. Tricart et al. (2001), on the other hand, propose that normal faulting is active since Early Miocene times and corresponds to an inversion of the Penninic front (i.e. RT), possibly induced by slab detachment processes below the Briançonnais domain (Sue et al. 1999).

We confirm the presence of impressive offsets found in the frontal Subriançonnais and Briançonnais units, as described by Tricart et al. (2001), Sue and Tricart (1999). These are also evidenced in the cross sections discussed later. However, we did not observe a complete inversion of the Penninic front (i.e. the RT) as proposed by Tricart (2004). All

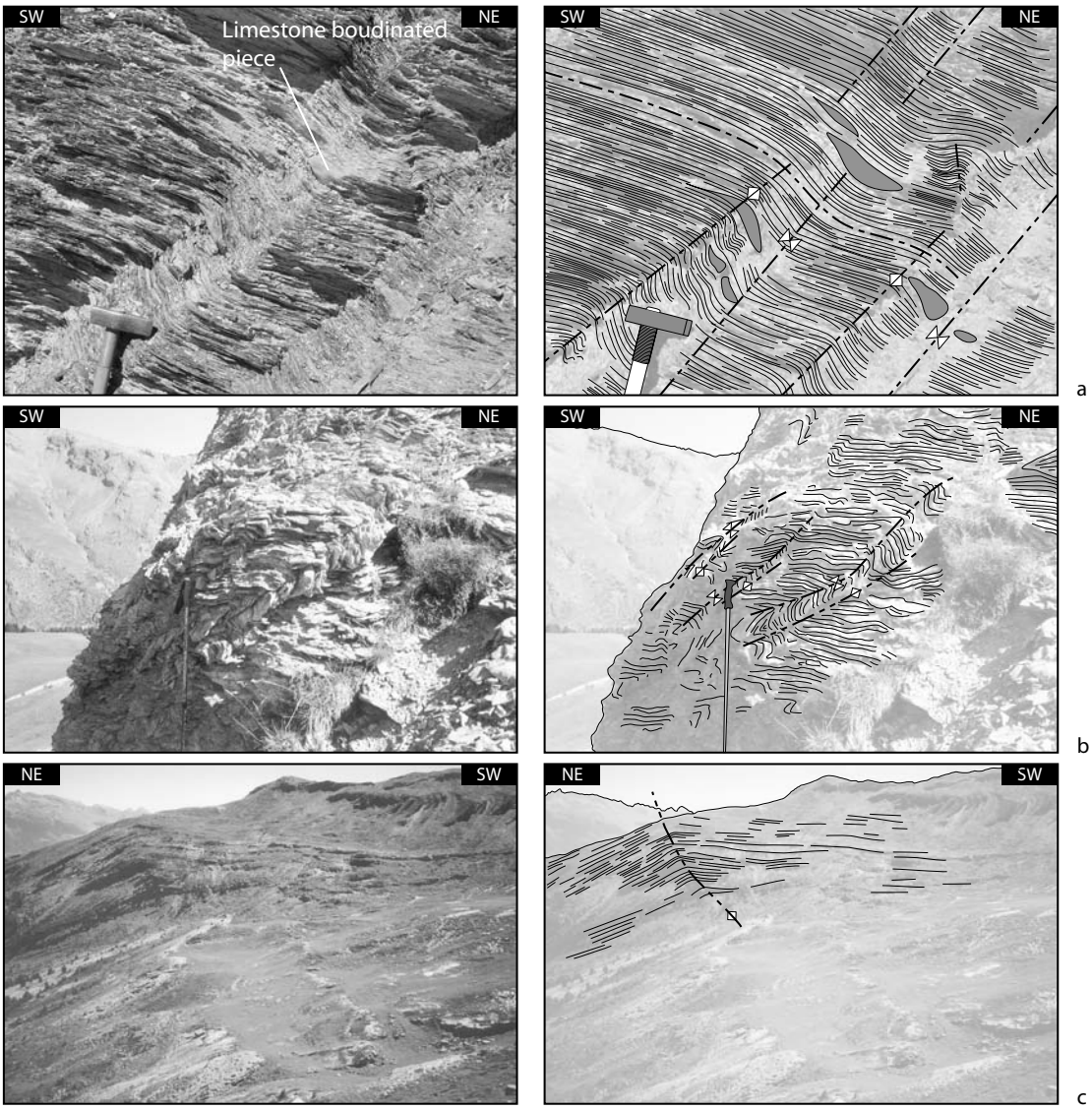


**Figure 1.9:** Examples of structures showing E to NE directed movements. Shown are kink band structures affecting a) schistose formations of the Subriançonnais calcareous flysch from the entrance of the Fournel valley, b) the external Briançonnais calcshists units below the Gaulent massif and c) the eastern termination of the Embrunais Ubaye nappe stack between Gaulent and Roche Charnière summits.

kinematic indicators along the RT consistently show WNW-directed sense of transport. Most of these normal faults are found to the east of the RT and hence they do not reactivate the RT directly. The stretch associated with this normal faulting is modest, amounting to about one kilometre, as inferred from the cross sections.

## 1.4 Tectonic evolution of the Embrunais Ubaye nappe stack.

In this paragraph we present a structural analysis of the "schistes à blocs" unit (Kerckhove 1969) found at the base of the Embrunais Ubaye nappes. This analysis aims to clarify the sense of emplacement of these internally derived nappes onto the Dauphinois domain since no general agreement is found in the literature. According to Lawson (1987), Fry (1989), Ritz (1991), Lickorish and Ford (1998), Bürgisser (1998), thrusting of these internally derived nappes onto the Dauphinois domain occurred in a top-SW direction. Merle and Brun (1984), based on an incremental strain analysis of quartz and calcite fibre growth in veins and pressure shadows, however, considered a progressive translation path from initial top-NW displacements towards top-SW displacements related to gravitational collapse. Early top-NW emplacement of the Embrunais Ubaye nappe stack has been proposed by Kerckhove (1978) as well. Our findings described below will be integrated into the description of cross sections in a later section that proposes a model for the tectonic evolution of the region.

We investigated the "schistes à blocs" formation in great detail at two different localities, namely at the Orcières locality (see figures 1.2 and 1.3) and at the Col de la Bonnette, about 50 kilometres further to the south (see figure 1.3). The "schistes à blocs" unit shows the typical characteristics of an olistostrome formation with plurimetric to centimetric blocks of different lithological composition and paleogeographic origin, embedded in a fine-grained black marly matrix. The embedded blocks are often striated at their surface or they carry calcitic precipitates, both WNW-oriented and kinematically related to the main macroscopic foliation (fig 1.10). Shear sense criteria are given by sigma clasts or centimetric shear bands found in the marly matrix. Both structures indicate top-WNW displacement.

At both localities investigated in detail, the "schistes à blocs" formation is dissected by a fault network which is clearly discordant to the main macroscopic foliation. The fault planes, commonly filled by white calcitic precipitates, carry striations indicating top-SW directed displacements (fig 1.10). These late brittle structures contrast with the overall ductile deformation regime recorded everywhere else in the "schistes à blocs" and they cannot be followed in continuity over distances of more than ten meters.

It is evident that the "schistes à blocs" unit underwent a first WNW-directed

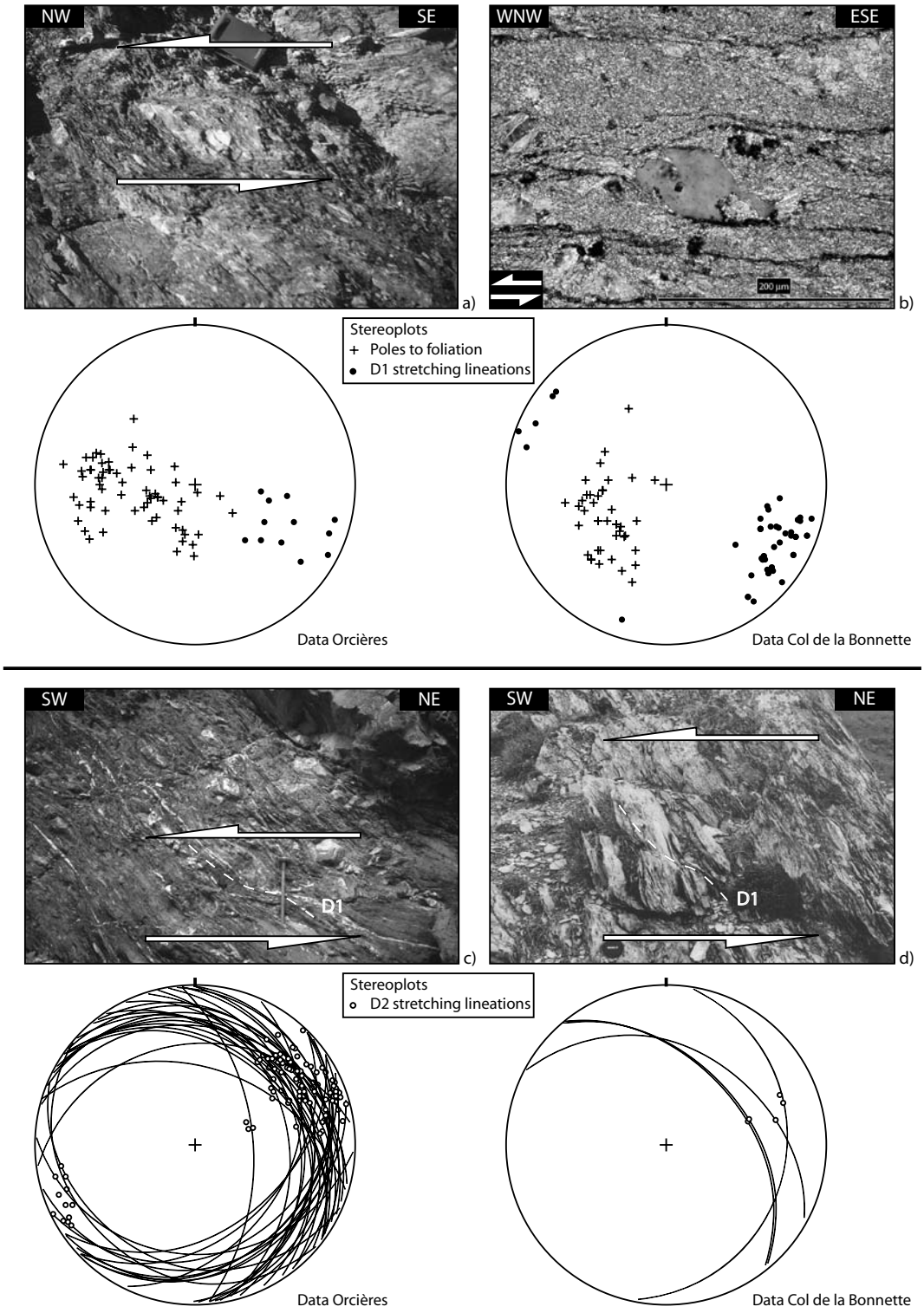


**Figure 1.10:** a), b): D1-related macro and microscopic shear senses indicators observed within the "schistes à blocs" formation (Kerckhove 1969) at the Orcières and Col de la Bonnette localities. The transport direction is top to WNW (see stereoplots). a): sigma clast structure developed at the rim of a calcareous boulder within a black marly matrix. b): asymmetric calcite pressure fringes developed at the rim a detrital quartz grain.
c), d): D2 related shear bands dissecting the whole "shistes à blocs" formation (Kerckhove 1969) at Orcières (c) and Col de la Bonnette (d) localities. All structural data indicate top-SW directed movements (see stereoplots).

thrusting episode, followed by top-SW directed movements. As a consequence, we propose that the initial emplacement direction of the Embrunais Ubaye nappe stack onto the Dauphinois domain was WNW-directed, as already proposed by Merle and Brun (1984) and Kerckhove (1978).

## 1.5 Description of cross sections.

Five cross sections, running from the external Briançonnais units to the Dauphinois domain, and including the eastern termination of the Embrunais Ubaye nappe stack, are presented in figure 1.11.

These sections will be used in order to better constrain the overall geometry of the investigated area and to visualize the superposition of the three main deformation phases presented above.

### 1.5.1 Cross sections A-A' and B-B'.

These two cross sections illustrate structures at the eastern rim of the Pelvoux massif previously investigated by Gidon (1954, 1965, 1979), Gidon and Vernet (1952), Bravard and Gidon (1979), Vernet (1950, 1951, 1952, 1966). As depicted in figure 1.2, these cross sections are perpendicular to the NE-SW strike of the so-called Peyron des Claux slice and the Ailefroide syncline structure. We will first describe profile A-A' since it represents a structurally deeper level in respect to cross section B-B' due to the axial plunge towards the south.

**Figure 1.11:** Detailed cross sections across the eastern rim of the Dauphinois domain and the most external Subriançonnais/Briançonnais units (see figure 2 for traces of profiles).
The difference in the orientation of cross sections A-A' and B-B' in respect to cross sections D-D' and E-E' is due to the fact that the main transport direction that predominantly shaped the cross sections within the Dauphinois domain changes from north (top-NW D1 thrusting) to south (top-SW D2 thrusting) of the investigated area.
a): cross section A-A'
b): cross section B-B'
c): cross section C-C'
d): cross section D-D'
e): cross section E-E'

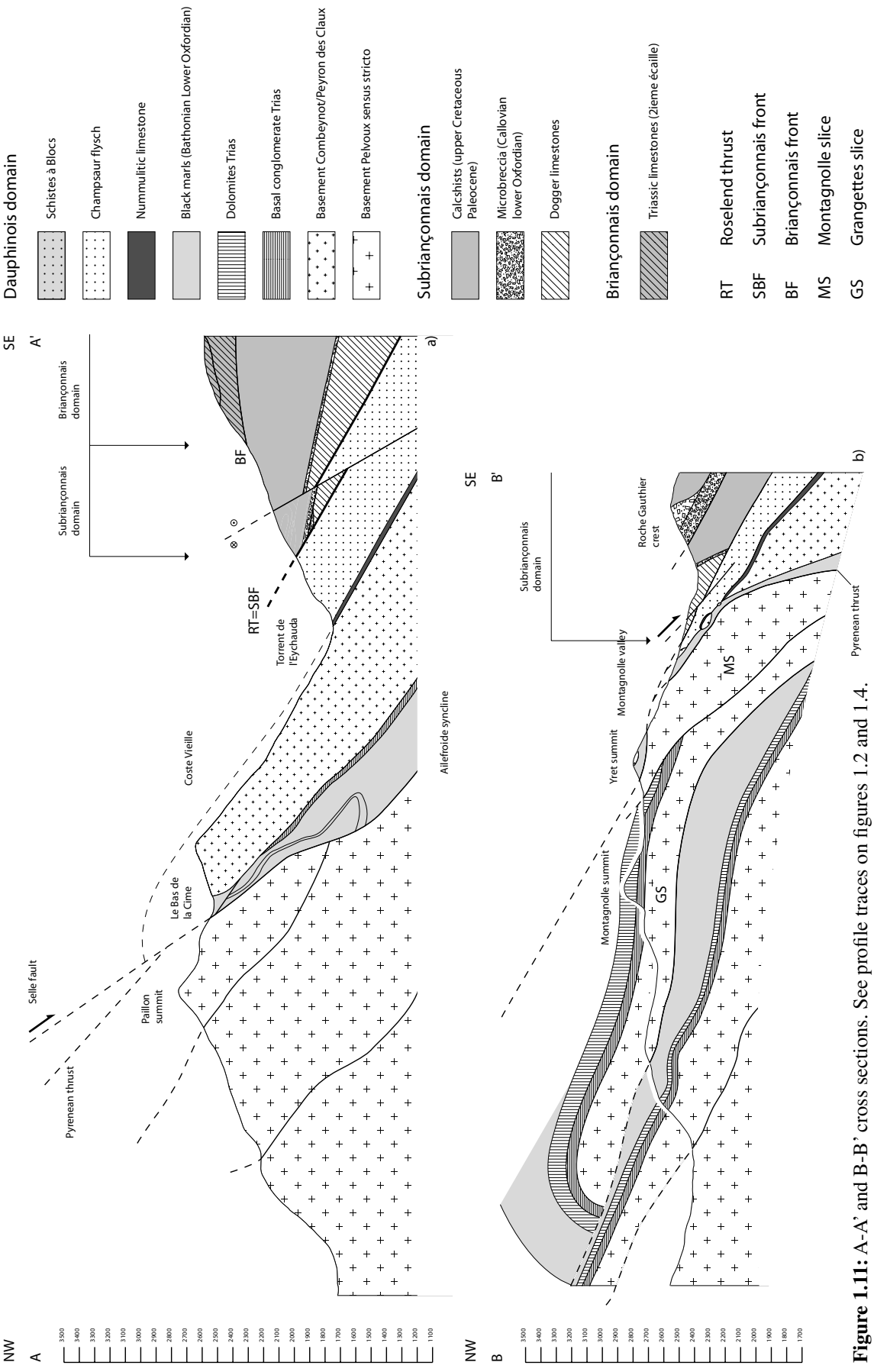


**Figure 1.11:** A-A' and B-B' cross sections. See profile traces on figures 1.2 and 1.4.

1.5.1.1 Cross section A-A' (fig 1.11a).

The northwestern part of this section represents the Mesozoic sedimentary series found within the Ailefroide syncline (figs 1.2 and 1.4) in detail. The western rim of this synform is largely overprinted by a steep late normal fault, that is part of the Selle fault system (Bürgisser 1998) dying out towards the north and increasing southwards with a total downthrow of about 870 metres according to Bürgisser (1998). The Mesozoic series are folded within a synclinal structure with Jurassic series in the core and Triassic conglomerates at the rim. These Triassic sediments lie on a preserved sedimentary contact below the Peyron des Claux basement slice, indicating that the eastern limb of the Ailefroide syncline is inverted. This inversion cannot be attributed to activity along the RT found immediately to the southeast, as is evidenced by intensively mylonitised strata that carry a N-S stretching lineation with top to the north kinematics, typical for the Pyrenean-Provencal phase, rather than for top-WNW thrusting associated with activity along the RT.

We propose that the Ailefroide syncline represents a former paleograben, inverted during this early alpine stage (i.e. before the nummulitic transgression). The map trace of the corresponding Pyrenean thrust is only preserved further north in the eastern slopes of the Rocher de l'Yret peak (figs 1.4 and 1.11b) and is down faulted within the Ailefroide structure by the Selle fault.

Further east, the RT coincides with the Subriançonnais front, as is evidenced by consistent WNW-directed transport found at the base of the Subbriançonnais slices and revealed by microfabric analysis of calcite ultramylonites derived from the "schistes à blocs" formation on top of the Dauphinois (see chapter 3). D2 strike slip structures (see figure 1.2) crossing this section dissect the Subriançonnais units and the Tertiary cover of the Dauphinois domain. The RT, separating these two domains, is offset by this D2 structure, which dies out further east within the Briançonnais domain.

1.5.1.2 Cross section B-B' (fig 1.11b).

This cross section is parallel to section A-A' and located 4 kilometres further north, i.e. at the northern termination of the Peyron des Claux basement slice and the Ailefroide structure (figs 1.2 and 1.4). From NW to SE, this cross section depicts a series of imbricates consisting of basement and cover found at the eastern rim of the Pelvoux massif, the Rocher de l'Yret massif and the external parts of the Subriançonnais domain.

The geometry found at the northwestern termination of this cross section consists of an imbricate between two slices of basement (Montagnolle and Grangettes slices) and

Mesozoic cover. Previously, the age of individualisation of these slices was considered as pre-Priabonian (Gidon 1979, Bravard and Gidon 1979). Our investigations from the basement slices basal contacts dipping towards SE again indicate a WNW-directed sense of transport. We therefore interpret these two contacts as subsidiary thrusts between the various basement slices on top of the Pelvoux massif sensu stricto, and related to the activity along the RT.

The Rocher de l'Yret massif again shows an imbricate between basement slices and sedimentary cover. Our structural data are consistent with findings of Butler (1992) who also described WNW-directed shearing in this area. Sense of movement is independently confirmed by microfabric analysis of Eocene nummulitic limestone intensively mylonitised (see chapter 2). The structural setting at the Rocher de l'Yret massif is, however, slightly different from the geometry found further NW, since part of the sedimentary cover of the basement slices is of Priabonian age. This Priabonian cover is found as a preserved sedimentary contact on top of boudinaged basement units. We interpret these boudin-type structures as remnants of the Peyron des Claux basement slice, tectonically reduced due to WNW-directed emplacement of the internal Subriançonnais and Briançonnais units onto the Dauphinois domain. We thus conclude that the Ailefroide syncline structure finds its northern termination in the Ravin de la Montagnolle valley (fig 1.4). Our interpretation differs from that depicted in the BRGM geological map Briançon (Barféty et al. 1996), where a tectonic contact is drawn at the base of these basement units. Instead, the underlying Mesozoic sediments lie on an inverted sedimentary contact found at the base of these boudinaged basement units. In our model, the Mesozoic series and basement boudins found at the Ravin de la Montagnolle are thrust on top of the Montagnolle basement slice along a former Pyrenean thrust that is pre-nummulitic in age, and totally reworked by later WNW-directed shearing.

These boudinaged basement units and their parautochtonous Eocene cover can be followed in map view below the Rocher de l'Yret summit and further north above the Mesozoic series from the "Grand Tabuc" valley (fig 1.4). According to Ceriani et al (2001), these boudinaged basement units represent the southern remnants of the Combeynot massif, tectonically reduced due to straining related to thrusting along the RT. This is confirmed by the microstructural analysis of basement cataclasites between Combeynot and Yret massifs showing a clear north-south deformation gradient (see Appendix A.2). It appears therefore that the Combeynot massif, lying in the hangingwall of the RT, represents the northern prolongation of the Peyron des Claux unit, which in turn lies in the footwall of the RT. The transition from a structurally lower Peyron des Claux unit to a structurally higher Combeynot unit occurs within the Rocher de l'Yret massif. At this place, however, the RT cannot be traced as a discrete structure (figs 1.4 and 1.11b). Rather, the top-WNW

directed displacement is accommodated within a 2 kilometres broad zone of deformation, that we refer to as the Rocher de l'Yret shear zone (RYSZ, see chapter 2). Further details of the geology of this massif are given in appendix A.3.

The southeastern part of the cross section depicts late-stage normal faulting along the Subriançonnais front, that is part of the RT in this area.

### 1.5.2 Cross sections C-C' and D-D'.

These two cross sections have been constructed along either side of the Fournel valley, about 17 kilometres south of the Rocher de l'Yret massif (fig 1.2). We also integrated results published by Bürgisser (1998) and Sue and Tricart (1999) into these sections.

The spectacular chevron-type folds affecting the Champsaur sandstone are a peculiar feature of the Fournel valley area. Bürgisser (1998) used the mean fold axial surface dip as a passive marker progressively rotating towards the shear direction with increasing shear (overshear model, Sanderson 1979). According to this author, a maximum value of the shear strain of $\gamma$=2.2 is recorded in the footwall of the Subriançonnais front. This corresponds to a minimum bulk shortening related to folding of 5 kilometers towards SW. The cross sections C-C' and D-D' of figure 1.11 will be used to describe structural relationships between Dauphinois, Subriançonnais and Briançonnais external domains in detail.

#### 1.5.2.1 Cross section C-C' (fig 1.11c).

Going from N to S, the Subriançonnais which forms the hangingwall of the RT further north is found in the immediate footwall of the RT for the first time along this section. Microfabric analysis of calcite ultramylonites from a Dogger limestone slice imbedded in the black flysch reveals a WNW-directed sense of transport (fig 1.5 and chapter 3).

Detailed mapping of the "Tête des Lauzières" summit revealed that the whole Champsaur flysch develops a major syncline at its eastern termination (see figures 1.2 and 1.11c). The orientation of the corresponding fold axis is similar to that of the chevron-type folds studied by Bürgisser (1998) in the Fournel valley, i.e. compatible with a top-SW phase of thrusting. Fault propagation folds are seen to develop within the Champsaur flysch, and they indicate a top to SW sense of transport.

The core of this synform, previously mapped as Champsaur flysch (Debelmas 1955 and Debelmas et al. 1966) lacks internal stratification. Based on sedimentological

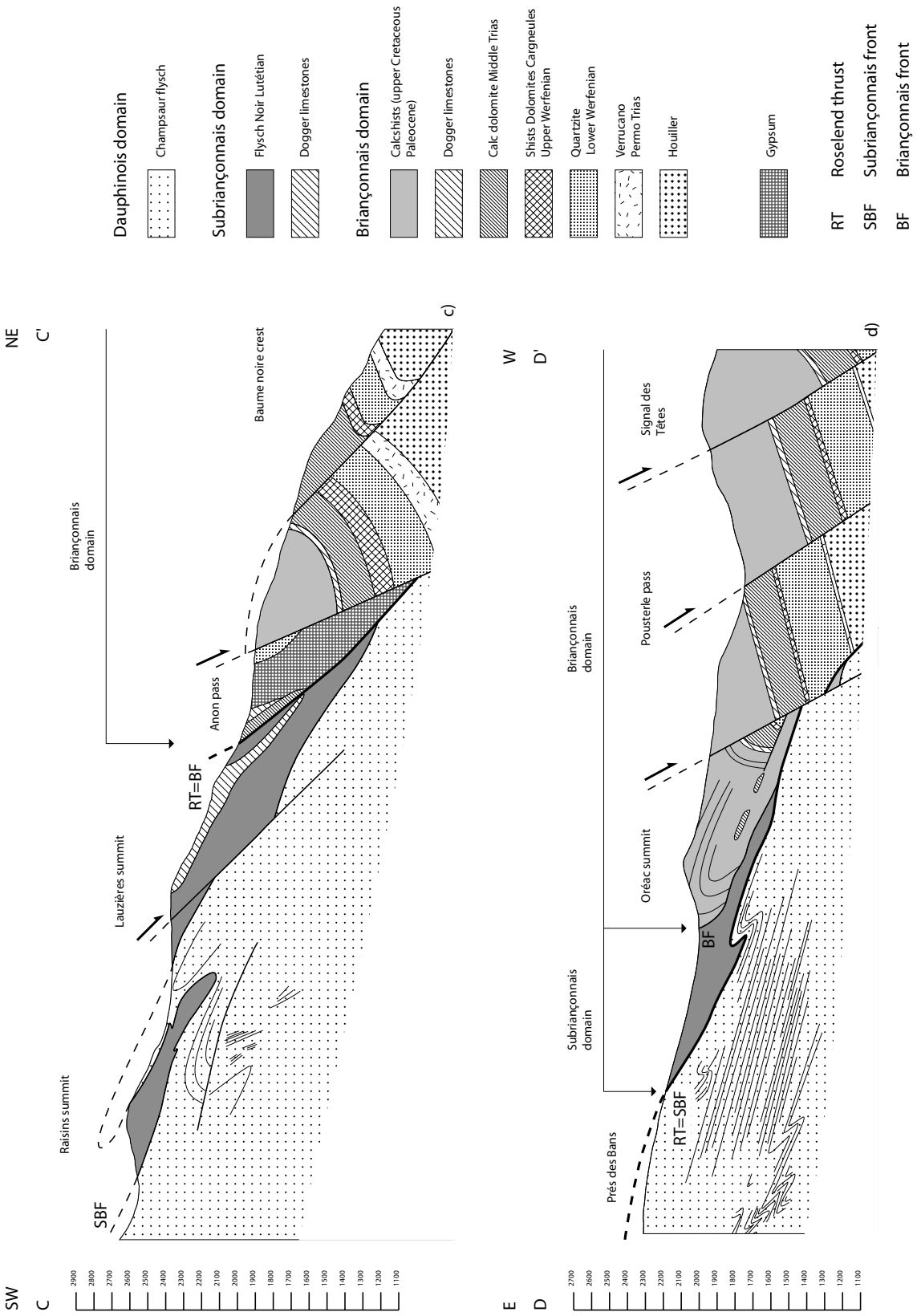


**Figure 1.11:** C-C' and D-D' cross sections. See profile traces on figure 1.2.

(lack of stratification, thickness) and structural arguments (mylonites found at the contact between this enigmatic unit and the underlying Champsaur flysch), we propose that this unit is made up of black flysch of the Subriançonnais unit found further east in the immediate footwall of the RT. Thus, this syncline folds the basal thrust of a Subriançonnais klippe, previously emplaced onto the Dauphinois domain. Figure 1.12a depicts a small-scale D2 fold found within this Subriançonnais domain. As shown in figure 1.12b, the S2 cleavage clearly overprints an S0/1 composite foliation related to early emplacement of Subriançonnais units onto the Dauphinois foreland.

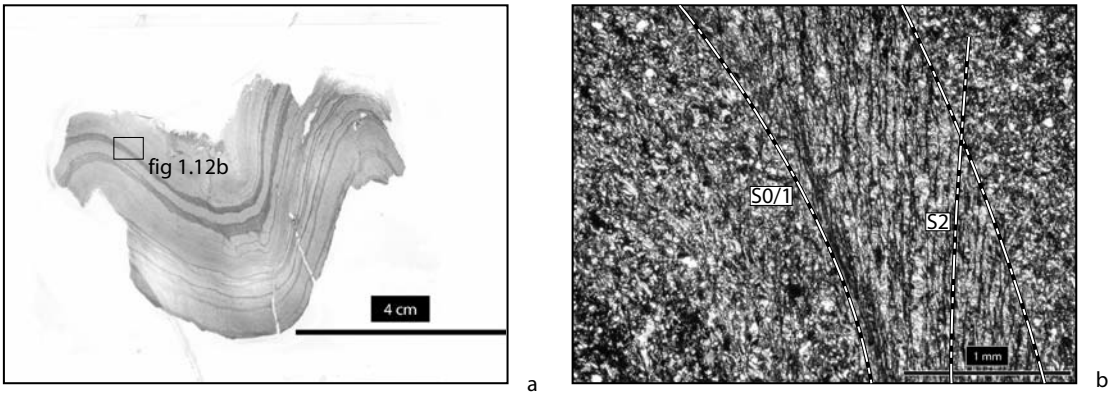


**Figure 1.12:** Evidence for top-SW D2 folding within the Subriançonnais units of the Fournel valley along profile C-C' of figure 1.11c.
a): small-scale D2 folding that affects Subriançonnais calcareous flysch at the entrance of the Fournel valley.
b): photomicrograph showing overprinting relationships between S2 (axial planar cleavage of the D2 fold shown in figure 1.12a) onto an earlier D1-foliation.

This Subriançonnais unit is also affected by late kink-type structures (fig 1.9a) possibly related to East-directed movements contemporaneous of D2 top-SW displacements (see section 1.3.3).

Finally, D3 normal faulting overprints the RT and underlying Subriançonnais and Dauphinois units. Large amounts of gypsum found at the "Col d'Anon pass" are related to this normal faulting phase.

1.5.2.2 Cross section D-D' (fig 1.11d).

The syncline with the core of inferred Subriançonnais material described in the previous section dies out towards the north but is still present in embryonic form at the front of the Oréac massif in this section. The RT (D1), which runs along the base of the Subriançonnais and outcrops along the "Prés des Bans" crest, is seen to dip underneath the

Oréac summit. There it merges with the basal thrust of the Roche Charnière Briançonnais unit (corresponding to the Briançonnais front of Tricart 1980). This directly shows that the RT is folded together with the underlying sedimentary cover of the Dauphinois domain during the later D2 phase. Hence, this cross section again confirms that SW-directed movements post-date earlier NW-directed transport.

Further east, the RT is clearly downfaulted by the Durance normal fault network. This D3 phase produces impressive offsets well visible in the Mesozoic sedimentary succession of the frontal Briançonnais units. These normal offsets, estimated to a minimum vertical component of 1000 metres, are achieved along steep E dipping contacts outlined by ultracataclasites (Sue and Tricart 1999).

1.5.3 Cross section E-E' (fig 1.11e).

This NE-SW trending section runs across the "Tête de Vautisse" summit, about 8 km south from the "Tête des Lauzières" peak (fig 1.2). It crosses the eastern termination of the Embrunais Ubaye nappe and runs through the frontal Roche Charnière and Champcella nappes of Briançonnais origin.

The geology of the Gaulent massif has first been described by Debelmas (1955) and later by Tricart (1980). Tricart (1980) individualized two generations of structures formed during the so-called "Tectonique II" and "Tectonique III" phases within this massif.

According to Tricart (1980), the "Tectonique II" phase corresponds to deformation within the Briançonnais domain and predates thrusting along the Briançonnais front (RT). This phase is responsible for early nappe stacking between Champcella and Roche Charnière nappes. The "Tectonique III" phase corresponds to our D1 thrusting along the RT. This later phase, which is the first one recorded within the Dauphinois units along this profile, clearly overprints the deformation features related to this earlier phase of nappe stacking, as is evidenced by the folding of the basal contact of the Champcella nappe (see figure 1.11e).

Thrusting of internal Briançonnais units onto the Dauphinois along the RT induced the formation of a major syncline at the rear of the Embrunais Ubaye nappe stack. This syncline can be followed further to the south, as depicted by the axial trace mapped in figure 1.2 and is, for example, spectacularly exposed in front of the Réotier village (so-called "Charnière synclinale de St Clément", Debelmas 1983).

D2 deformation features are clearly recognizable in the Gaulent massif area. The main structure developed during D2 consists of a flat lying thrust dissecting the frontal Roche Charnière nappe and offsetting the RT by about one kilometre. We name this

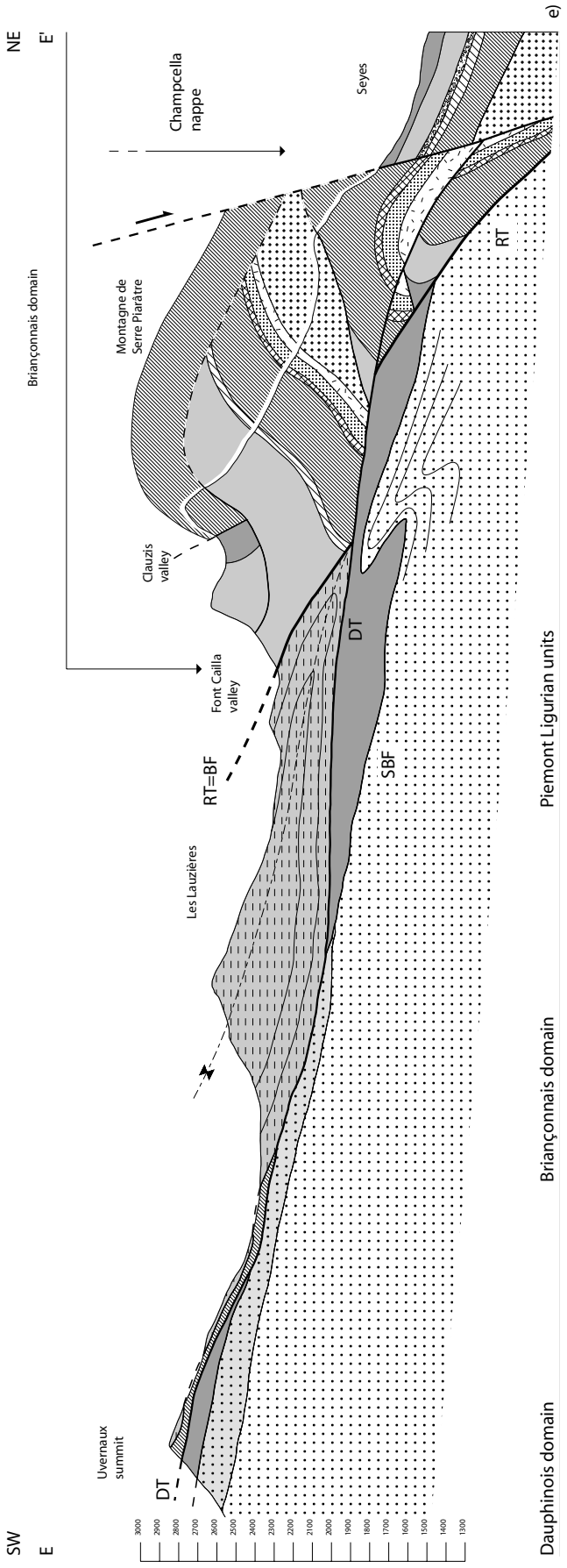


**Figure 1.11:** E-E' cross section. See profile trace on figure 1.2.

thrust, formed during D2, Dormillouse thrust (DT) after the type locality where it has first been recognized. The DT reactivates the basal contact of the Parpaillon nappe, as evidenced by shear band type structures found at the base of the "Pointe des Uvernaux" Briançonnais-related slice, which indicate top-SW directed movements (see figure 1.13). The southern termination of the Subriançonnais syncline described in section D-D' is found in the immediate footwall of the DT. The fold axes affecting both Subriançonnais and Champsaur flysch units are again consistent with top-SW directed displacements. In the eastern part of the cross section, the DT is downfaulted eastwards by D3 structures related to the Durance normal fault system. In map view, the DT is transformed into the steep strike slip fault at the southern entrance of the Dormillouse valley described earlier. This strike slip fault produces sinistral offsets of the front of both Roche Charnière and Champcella nappes above the Freissinière locality (fig 1.2). This again confirms that the amount of SW-directed deformation increases southwards because the strike slip network dissecting the RT south of Pelvoux transforms lateral movements into flat-lying thrusts within the Dauphinois. This D2 deformation pre-dates the onset of D3 normal faulting.

Finally, kink-type structures related to eastward-directed movements, can be observed in this profile. These structures have been recognized within the Gaulent massif (fig 1.9b) and induce a sudden steepening of the axial plane of the Embrunais

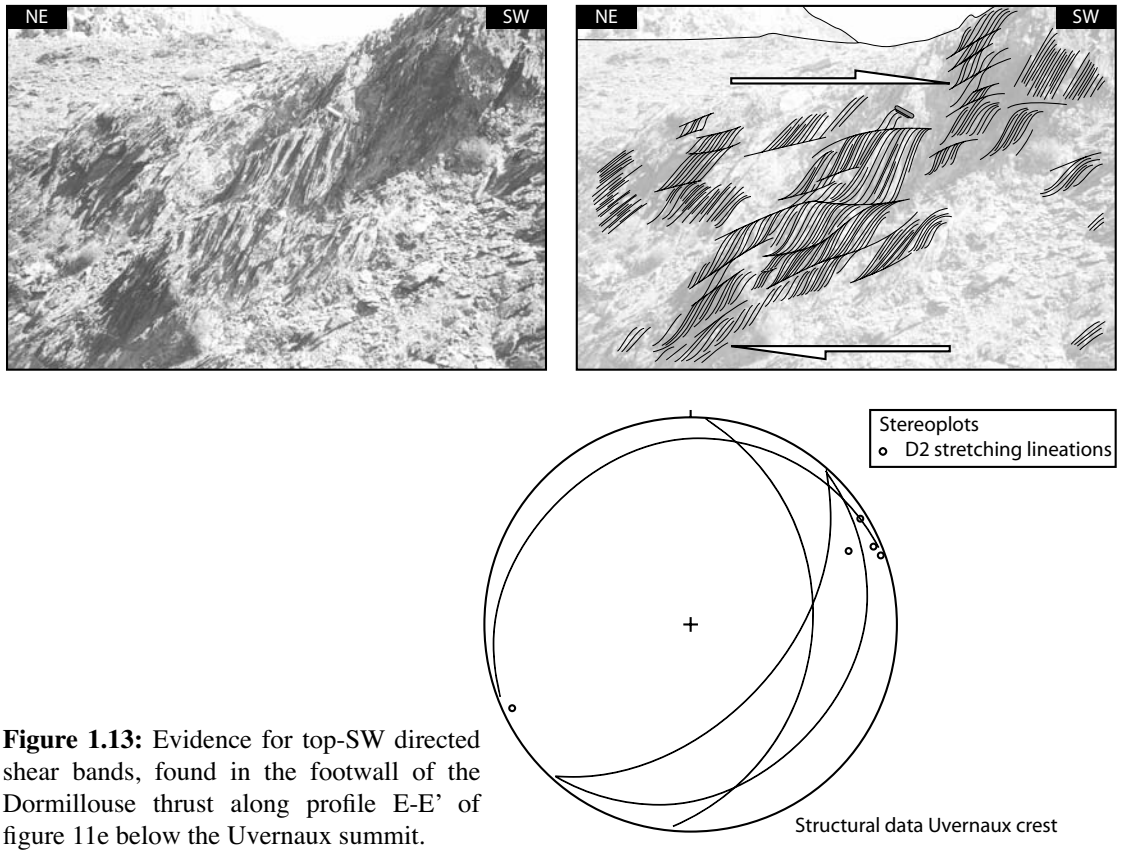


**Figure 1.13:** Evidence for top-SW directed shear bands, found in the footwall of the Dormillouse thrust along profile E-E' of figure 11e below the Uvernaux summit.

Ubaye syncline in the immediate footwall of the RT (fig 1.9c). Further south, i.e. at the Réotier locality, this steepening results in a dip of the RT of 60°. These eastward-directed movements have been interpreted to be responsible for the overall steepening of the Briançonnais front (i.e. the Roselend thrust) by Tricart (1980).

## 1.6 Summary and discussion.

Three major findings presented in this study will be summarized briefly and then used for proposing a new model of the geodynamic evolution of the investigated area.

Firstly, our data demonstrate the validity of the hypothesis formulated by Ceriani et al (2001). The RT, major tectonic structure found at the front of the arc of the Western Alps, partially reactivates the PBC (in the sense of Ceriani et al. 2001) to the north and immediately south of the Pelvoux massif. It joins the Briançonnais front (as defined by Tricart 1980, 1986) at the rear of the Embrunais-Ubaye nappe stack. Activity along the RT is kinematically linked to dextral activity along the Rhone Simplon line (Ceriani et al. 2001) and sinistral movements within a broad strike slip zone at the rear of the Argentera massif (fig 1.3 and Ceriani et al. 2001).

The second major finding concerns the early emplacement direction of the Embrunais-Ubaye nappe stack onto the Dauphinois domain. Evidences found within the "schistes à blocs" (Kerckhove 1969) units at the base of these nappes indicate a WNW-directed sense of transport shortly after deposition of the sediments, in accordance with findings by Merle and Brun (1984) and Kerckhove et al. (1978). The timing of emplacement of these nappes onto the Dauphinois domain is well constrained as Rupelian in age by Lickorish and Ford (1998). We attribute it to an event which corresponds to the earliest stage of our D1, immediately pre-dating thrusting along the Roselend thrust. D1 represents an Oligocene to Lower Miocene WNW-directed deformation phase related to the collision between the European and Adriatic microplates. WNW-directed thrusting along the RT postdates the emplacement of the Embrunais-Ubaye nappes as is evidenced by the large-scale syncline developed in the Helmenthoid flysch in the direct footwall of the RT. In summary, D1 starts with the emplacement of the Embrunais-Ubaye nappe stack onto the Dauphinois (early stage of D1 of this study) and is immediately followed in time by WNW-directed out of sequence thrusting along the RT. The early D1 and D1 phase sensus stricto correspond to the D3 structures of Ceriani 2001 and Ceriani et al. 2001.

Thirdly, we demonstrated that SW-directed movements (D2) are later than the WNW-directed (D1) emplacement of internally derived units onto the Dauphinois domain. Overprinting relationships have been found indeed within the frontal Subriançonnais/ Briançonnais units, the Priabonian cover of the Dauphinois domain and the "schistes à

blocs" (Kerckhove 1969) formation found at the base of the EU nappe stack.

We provided evidence that the WNW-directed movements south of Pelvoux and at the base of the internal Subriançonnais/Briançonnais units, including the Helmenthoid Flysch nappes of the Embrunais-Ubaye nappe stack, were overprinted by later top-SW directed movements. This asks for a revision of older concepts concerning the structural evolution of this area. "Radial" models (Vialon et al. 1989, Platt et al. 1989) clearly do not apply to the arc of the Western Alps since they imply the simultaneous activity of NW- and SW-directed thrust systems. The models of Bürgisser (1998), Lickorish et al. (2002), also implying simultaneous activity of these two systems do not apply to the working area either.

However, origin and significance of the younger SW-directed movements (D2), only observed south of the Pelvoux massif remain debatable and merit further discussion. Merle and Brun (1984) argued that the late-stage SW-directed emplacement of the Embrunais-Ubaye nappe stack could possibly be gravitationally driven. However, they did not exclude a possible push from the back. Push from the back is favoured by the fact that gravitational deformation cannot explain an increase in deformation amounts towards the back of the deformation front, as observed during top-SW thrusting in the Fournel valley for example and as pointed out by Bürgisser (1998). Furthermore, gravity-driven mechanisms are inadequate for explaining contemporaneous backward movements as suggested by this study. Hence, one has to look for a tectonic event which 1) postdates activity along the RT during Oligocene to Early Miocene times, 2) predates the onset of late-stage Neogene normal faulting and 3) affects the entire area between Pelvoux and Argentera massifs, but not areas along the RT further north.

A prominent large-scale tectonic event that fulfills these three conditions is the opening of the western Mediterranean basin (fig 1.14a, see reviews by Serranne 1999, Gueguen et al. 1998, Faccenna et al. 1997, Carminati et al. 1998b, Bonardi et al. 2001, Roca 2001, Cavazza et Wezel 2003 and Dèzes et al. 2004).

The combination of geophysical transects within the Mediterranean basin with on-land geological data (Cavazza et al. 2004, Carminatti et al. 2004, Faccenna et al. 2001a/b, Rollet et al. 2002, Blanco and Spakman 1993, Spakman et al. 1993) allow for a scenario briefly summarized below.

According to Burrus (1989), rifting within the western Mediterranean basin started during the Early Oligocene (fig 1.14b), i.e. at about 30 Ma (Odin and Odin 1990). NE-SW trending normal faults (fig 1.14c) started to dissect areas previously subjected to compressional deformation such as the Pyrenees and the Iberian chains. During Late Oligocene to Early Miocene times (fig 1.14c), the Valencia trough area is subjected to a major rifting phase (Bartrina et al. 1992, Watts and Torne 1992), which stops in the

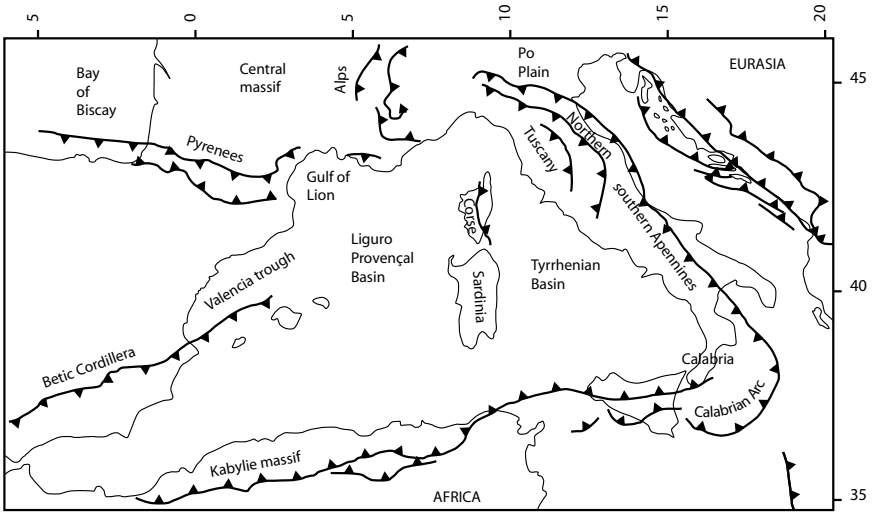
5
0
5
10
15
20
45
40
35
Bay of Biscay
Central massif
Alps
Po Plain
EURASIA
Pyrenees
Gulf of Lion
Tuscany
Northern
southern Apennines
Corse
Liguro Provençal Basin
Tyrrhenian Basin
Sardinia
Valencia trough
Betic Cordillera
Calabria
Calabrian Arc
Kabylie massif
AFRICA
a)

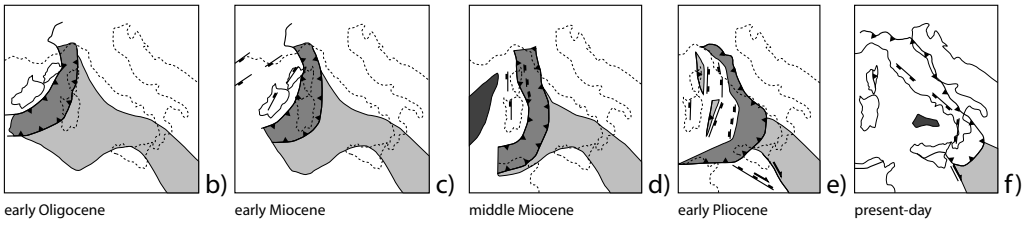
b)
c)
d)
e)
f)
early Oligocene
early Miocene
middle Miocene
early Pliocene
present-day

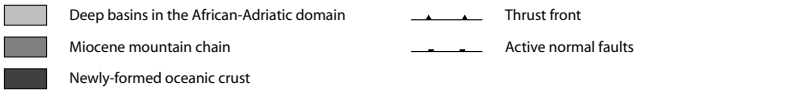
Deep basins in the African-Adriatic domain
Miocene mountain chain
Newly-formed oceanic crust
Thrust front
Active normal faults

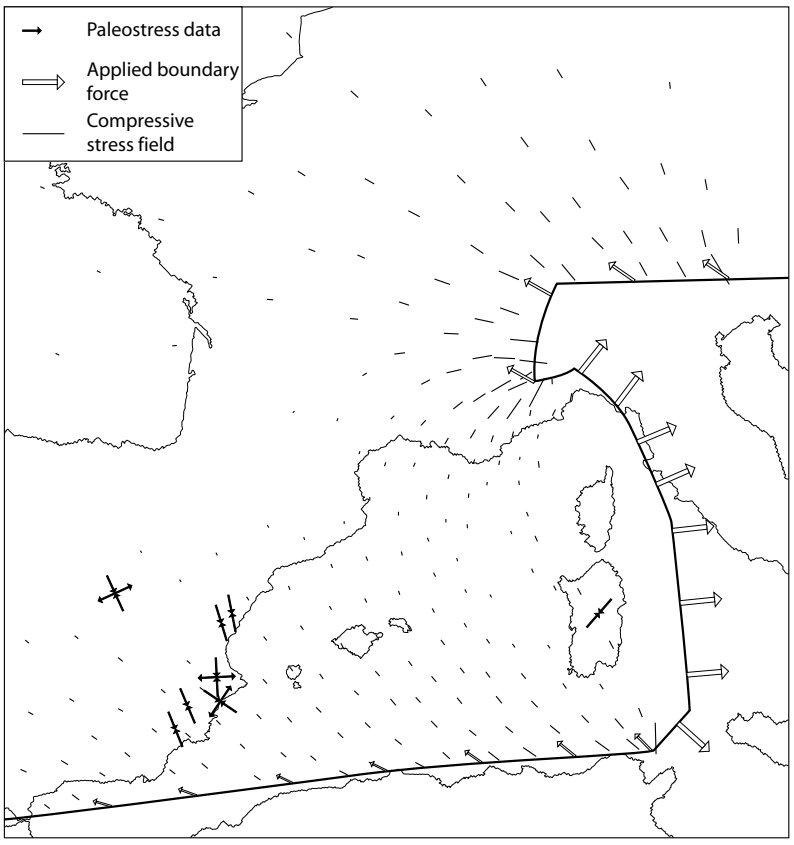
Paleostress data
Applied boundary force
Compressive stress field
g)

Burdigalian (Banda and Santanach 1992). This early extensional phase is responsible for the onset of displacement of Corsica-Sardinia block away from its initial position as shown in figures 1.14b, c and d (Burrus 1989). This in turn leads to the formation of an accretionary prism in the future northern appenines (Principi and Treves 1984).

Oceanization within the Liguro-Provençal basin taking place during the Early Miocene (Vigliotti and Langenheim 1995) starts in the Aquitanian and is responsible for most of the 30° counter-clockwise rotation of the Corsica-Sardinia-Calabria block (figs 1.14c and d). This oceanization (and related rotation of the Corsica-Sardinia-Calabria block) ceases in Mid-Miocene (fig 1.14d, Vigliotti and Langenheim 1995). Extensional deformation propagates further east at this time, as evidenced by a subsidence episode east of Corsica (Orszag Sperber and Pilot 1976).

The major episode of extension recorded within the Tyrrhenian basin however is of Tortonian to Middle Pliocene in age (Trincadi and Zitellini 1987). This extension is linked to compressional deformation within the Apennines (fig 1.14e) and continues until present, as is attested by continuous eastward shifting of the deformation front within this belt (Boccaletti et al. 1990).

Several models aiming to propose a possible origin for the opening in the western Mediterranean region are found in literature. They are briefly described in the following (see Jolivet and Faccenna 2000 for a complete review) in terms of the main geodynamic process that originated extension within the Mediterranean basin.

A first group of models dealing with extension in the Liguro-Provençal basin (Burrus 1984, Malinverno and Ryan 1986), the Tyrrhenian basin (Malinverno and Ryan 1986, Royden 1993, Serri et al. 1993, Faccenna et al. 1996) or the whole Mediterranean region and Middle East (Jolivet and Faccenna 2000) is based on slab rollback processes. The geodynamic mechanical evolution is as described by Dewey 1980, i.e. backarc extension occurs within a subduction zone system when the velocity of slab retreat is higher than that of the overriding plate.

A second group of models involves slab detachment processes (Wortel and Spakman 1992, Carminati et al. 1998b) in order to notably explain the dramatic eastward

**Figure 1.14:** a): simplified tectonic map of the central Mediterranean after Faccena et al. (2001).
b), c), d), e) and f): paleotectonic evolution of the western Mediterranean basin for early Oligocene, early Miocene, middle Miocene, early Pliocene and present day, respecticely (after Faccena et al. 1997).
g): Compressional intra-plate stress field for Langhian times along northern Africa. Black arrows refer to compilation of paleostress data (Bergerat 1987, Simon Gomez 1986, De Ruig 1990, Letouzey 1986, Ott d'Estevou 1988 and Galindo-Zaldivar et al. 1983) and white arrows represent the applied boundaries forces.

shift of extensional deformation from the Liguro Provençal to the Tyrrhenian basins in Langhian times. In these models, backarc extension finds its origin in the additional loading of the detached parts of the subducted slab onto the non-detached parts of this same slab. This pull favors the retreat of the subduction trench, which in turn induces backarc extension within the overidding plate. This group of models is similar to the simple rollback models. However, rollback is faster and leads to very arcuate structures, as observed in the western Mediterranean.

A third type of models found in literature is based on an increase of vertical stress within the Alpine orogen, either by crustal thickening within the Alpine belt itself (Le Pichon 1982, Platt and Vissers 1989) or by delamination of cold lithospheric roots by mantle convection (Platt and England 1994). In both cases, the Alpine orogen is subjected to extensional collapse resulting in opening within the Mediterranean region.

It is not the purpose of this session to discuss the validity of these models. Such models are either exclusively based on increased slab retreat velocities, or alternatively, they only involve an increase in vertical stress. This strict separation is unlikely, however. As argued by Jolivet and Faccenna (2000), the slab retreat models do not explain the sudden change from Alpine compression to extension and the vertical shear models are not appropriate for explaining the opening of the Liguro-Provencal basin, previously not strongly affected by Alpine collision. Models involving slab detachment processes are, however, successful in explaining the opening of local basins such as the Liguro Provencal and Tyrrhenean basins.

Carminati et al. (1998b) proposed that the late Oligocene to early Langhian extensional phase, responsible for the opening of the Liguro Provençal basin, resulted from rollback of the African slab. These authors proposed that the later opening of the Tyrrhenian basin, marking the eastward migration of extension within the Mediterranean domain, was due to a slab detachment episode along the northern margin of Africa. Carminati et al. (1998a) numerically modeled the mechanical effects induced by a slab detachment process using a thin shell model adapted to Mediterranean geodynamic setting (see Carminatti et al., 1998a, for details about the applied boundary conditions). Their simulation is achieved using a two step model with a first Oligocene-Burdigalian episode mechanically dominated by the effects of African slab rollback. A second step (Langhian to Present) investigates the effects of slab detachment on the mechanical evolution of the system and its influence in terms of the geodynamic evolution.

The numerical simulations applied to the Oligocene to Burdigalian (30-16 Ma) time interval reproduces the early rifting phase of the Mediterranean basin, starting in the Early Oligocene in the zone of the Valencia trough, Corsica, Sardinia and the Gulf of Lion. This opening phase progressively moves eastward and affects the Liguro-Provencal

basin from Aquitanian to Burdigalian.

The onset of slab breakoff along the northern margin of Africa during the Langhian drastically changes the stress field of the investigated area. The region east of the Corsica-Sardinia block is now subject to active extension marking the beginning of the opening of the Tyrrhenian basin. This opening will be active until present times and is kinematically linked to deformation within the Appennine chain.

Interestingly, the intra-plate stress field modeled for late Langhian times predicts that the foreland of the Alps in southeastern France is characterized by a strike slip stress field with a compression direction oriented NE-SW (fig 1.14g). This stress field dies out within the Mediterranean sea and is no more recorded further north in the Northern Subalpine chains where compression ranges from an E-W to a NW-SE direction.
It is tempting to correlate this NE-SW compression to top-SW directed thrusting during D2 in the area south of the Pelvoux massif since:

1) the compression direction is compatible with constant top-SW directed thrusting recorded in Dauphinois domain in this part of the Alpine chain (Lawson (1987), Fry (1989), Ritz (1991), Lickorish and Ford (1998), Bürgisser (1998), this study).
2) this compressional phase clearly postdates the D1 Roselend phase (Oligocene to Early Miocene according to Fügenschuh and Schmid 2003).
3) it explains why D2 related structures are only recorded south of the Pelvoux massif.

Carminati et al. (1998a) additionally show that the transport direction active during the same time period along the Appenine thrust front ranges from top-E to top-NE.

This direct comparison between our D2 top-SW thrusting event and the results of numerical modeling by Carminatti et al. (1998a) has, however, to be taken with a grain of salt. As outlined by these authors, the model is based on several assumptions in terms of rheology of the lithosphere, displacements vectors and local strain partitioning effects. The simulated stress field should therefore be regarded as a very simplified picture compared to reality. On a larger scale, however, the intraplate Langhian stress field closely matches with paleostress analysis from eastern Spain (fig 1.14g, Bergerat 1987, Simon Gomez 1986, De Ruig 1990, Letouzey 1986, Ott d'Estevou 1988 and Galindo-Zaldivar et al. 1983) indicating that the chosen model might be a reasonable approximation.

In summary, we propose that D2 top-SW deformation is linked to the formation of the Apeninnes, as a consequence of the opening of the Thyrrenian basin during the Langhian. This timing is in accordance with the model of Merle and Brun (1984) who propose a Miocene age for the late top-SW emplacement in the Embrunais Ubaye nappe stack. Top-SW directed thrusting within the southern subalpine chains, possibly guided by Hercynian structures at the border of Massif central (Gratier 1989) might be considered as

the response of the Dauphinois domain to orogeny in the Appenines.

## 1.7 Conclusions.

The present study has revealed that the area between the Pelvoux and Argentera massifs suffered the effects of several successive deformational events.

The first deformation features described in this contribution are related to the Pyrenean orogeny, i.e. the Pyrenean phase. They have been recognized in the Mesozoic sedimentary cover of the Dauphinois domain and within the external crystalline massifs, as evidenced by inverted paleo-grabens.

The structures related to this early phase have been intensively overprinted by Alpine deformation sensus stricto, linked to activity along the Roselend thrust (Ceriani et al. 2001). This last structure has been active during WNW-directed displacements of the Apulian indenter and is kinematically linked to dextral movements along the Rhone-Simplon line and sinistral movements at the rear of the Argentera massif.

Finally, SW-directed displacements, a peculiar feature only recorded in this portion of the Western Alps, are clearly later compared to activity along the Roselend thrust. It is proposed that SW-directed movements are linked to the opening of the western Mediterranean basin and formation of the Apennine chain.

This linkage between Western Alps and Appenines could partially explain the large amounts of Tertiary rotation revealed by paleomagnetic studies within the Briançonnais sedimentary cover in this area (Thomas et al. 1999, Collombet 2001, Colombet et al. 2002). In the absence of deep seismic data and detailed deformation phase correlation based on field studies between Appenine and Alpine chains (Ligurian knot, Laubscher et al. 1992), this model remains speculative and represents a working hypothesis for further research.

The latest deformation features are related to the presently still active orogenic collapse as revealed by geophysical studies (Sue et al. 1999, 2000, Delacou 2004).

## 1.8 Acknowledgments.

We thank our colleagues from the Geological Paleontological Institute of the Basel University, notably Stefan Bucher and Stefano Ceriani.
A special thank is given to Mary Ford, Thierry Dumont and Pierre Tricart for stimulative discussions.
Substantial funding by the Swiss National Science Foundation is gratefully acknowledged.

## 1.9 References.

Apps, G.M., Peel, F. and Elliott, T., 2004. The structural setting and palaeogeographical evolution of the Gres d'Annot Basin. Deep-water sedimentation in the Alpine Basin of SE France; new perspectives on the Gres d'Annot and related systems. Geological Society Special Publication 221: 65-96. 2004.

Bagnoud A., Wernli, R. and Sartori M., 1998. Decouverte de foraminiferes planctoniques paleogenes dans la zone de Sion-Courmayeur a Sion (Valais, Suisse). Eclogae Geologicae Helvetiae, 91(3): 421-429.

Banda, E. and Santanach, P., 1992. The Valencia Trough (western Mediterranean); an overview. Tectonophysics 208 (1-3): 183-202.

Barbier, R., Barféty, J.C., Bordet, P., Bulard, P.F., Debelmas, J., Fabre, J., Feys, R., Gréber, C., Gillot-Barbiéri, C., Lacombe, J.-C., Vialon, P., Le Fort, P., Mouterde, M., Pécher, A., Petiteville, J., Rivoirard, R., Tissot, B., Vernet, J. and Méloux, J., 1976. Carte géologique de la France (1/50000). Feuille La Grave. BRGM, Orléans.

Barféty, J.C., 1968. Importance des failles et des glissements superficiels dans le massif de Montbrison et ses environs (Briançon, Hautes-Alpes). Travaux du Laboratoire de Geologie de la Faculte des Sciences de Grenoble, 44: 49-54.

Barféty, J.C., Gidon, M. and Kerckhove, C., 1968. Sur l'importance des failles longitudinales dans le secteur durancien des Alpes internes francaises. Comptes Rendus Hebdomadaires des Seances de l'Academie des Sciences, Serie D: Sciences Naturelles, 267(4): 394-397.

Barféty, J.C., Gidon, M., Lemoine, M. and Mouterde, R., 1979. Tectonique synsedimentaire liasique dans les massifs cristallins de la zone externe des Alpes occidentales francaises; la faille du col d'Ornon. Comptes Rendus Hebdomadaires des Seances de l'Academie des Sciences, Serie D: Sciences Naturelles, 289(16): 1207-1210.

Barféty, J.-C., Pécher, A., Debelmas, J., Gidon, P., Gidon, M., Mouterde, R., Vernet, J., Le Fort, P., Pécher, A., Barbieri, A., Biju-Duval, J., Gillot-Barbieri, C., Bartoli, F.,

Ozocak, R. and Vernet J., 1984. Carte géologique de la France (1/50000). Feuille St-Christophe-en-Oisans. BRGM, Orléans.

Barféty, J.C., Tricart, P. and Jeudy de Grissac, C., 1992. La Quatrieme ecaille près de Briancon (Alpes francaises); un olistostrome précurseur de l'orogenese pennique eocene. Comptes Rendus de l'Academie des Sciences, Serie 2, Mecanique, Physique, Chimie, Sciences de l'Univers, Sciences de la Terre, 314(1): 71-76.

Barféty, J.-C., Lemoine, M., Mercier, D., Polino, R., Bertrand, J., Dumont, T., Aumadric du Chaffaut, S., Pêcher A., Monjuvent, G., Gidon, M., Debelmas, J., Vernet, J., Lami, A., Jaillard, E., Détraz, G., Landès, B., Jean, S. and Lavigne-Goldenberg, P., 1996. Carte géologique de la France (1/50000). Feuille Briançon. BRGM, Orléans.

Bartrina, M.T., Cabrera, L., Jurado, M.J., Guimera, J. and Roca, E., 1992. Evolution of the central Catalan margin of the Valencia Trough (western Mediterranean). Tectonophysics 203 (1-4): 219-247.

Bergerat, F., 1987. Stress fields in the European Platform at the time of Africa-Eurasia collision. Tectonics, 6(2): 99-132.

Bigi, G., Cosentino, D., Parotto, M., Sartori, R. and Scandone, P., 1983. Structural model of Italy, scale 1/500000.

Blanco, M.J. and Spakman, W., 1993. The P-wave velocity structure of the mantle below the Iberian Peninsula; evidence for subducted lithosphere below southern Spain. Tectonophysics 221 (1): 13-34.

Boccaletti, M., Ciaranfi, N., Cosentino, D., Deiana, G., Gelati, R., Lentini, F., Massari, F., Moratti, G., Pescatore, T., Ricci Lucchi, F. and Tortorici, L. 1990. Palinspastic restoration and paleogeographic reconstruction of the peri-Tyrrhenian area during the Neogene. Palaeogeography, Palaeoclimatology, Palaeoecology 77 (1): 41-42.

Bonardi, G., Cavazza, W., Perrone, V., Rossi, S., 2001. Calabria-Peloritani terrane and northern Ionian Sea. In: G.B.a.M.I.P. Vai (Editor), Anatomy of an orogen: the Apennines and adjacent Mediterranean basins. Kluwer Academic Publishers, Dordrecht, pp. 287-306.

Bravard, C. and Gidon, M., 1979. La structure du revers oriental du Massif du Pelvoux; observations et interpretations nouvelles. Geologie Alpine, 55: 23-33.

Bürgisser, J., 1998. Deformation in foreland basins of the Western Alps (Pelvoux massif, SE France); significance for the development of the Alpine arc., ETH, Zürich, 151 pp.

Bürgisser, J. and Ford, M., 1998. Overthrust shear deformation of a foreland basin; structural studies south-east of the Pelvoux Massif, SE France. Journal of Structural Geology, 20(11): 1455-1475.

Burrus, J., 1984. Contribution to a geodynamic synthesis of the Provencal Basin (north-western Mediterranean). Marine Geology, 55(3-4): 247-269.

Burrus, J., 1989. Review of geodynamic models for extensional basins; the paradox of stretching in the Gulf of Lions (Northwest Mediterranean). Compte rendu de la seance specialisée de la Societe geologique de France. Bulletin de la Societe Geologique de France, Huitieme Serie, pp. 377-393.

Butler, R.W.H., 1989. The influence of pre-existing basin structure on thrust system evolution in Western Alps. Geological Society Special Publications 44: 105-122.

Butler, R.W.H., 1992. Thrust zone kinematics in a basement-cover imbricate stack; eastern Pelvoux Massif, French Alps. Journal of Structural Geology, 14(1): 29-40.

Butler, R.W.H., Matthews, S.J. and Parish, M., 1986. The NW external Alpine thrust belt and its implications for the geometry of the western Alpine Orogen. Geological Society Special Publications 19: 245-260.

Carminati, E., Wortel, M.J.R., Meijer, P.T. and Sabadini, R., 1998. The two-stage opening of the western-central Mediterranean basins; a forward modeling test to a new evolutionary model. Earth and Planetary Science Letters, 160(3-4): 667-679.

Carminati, E., Wortel, M.J.R., Spakman, W. and Sabadini, R., 1998. The role of slab detachment processes in the opening of the western-central Mediterranean basins; some geological and geophysical evidence. Earth and Planetary Science Letters, 160(3-4): 651-665.

Carminati, E., Argnani, A., Carrara, G., Dabovski, C., Dumurdzanov, N., Gaetani, M., Georgiev, G., Mauffret, A., Nazai, S., Sartori, R., Scionti, V., Scrocca, D., Séranne, M., Torelli, L. and Zagorchev, I., 2004. TRANSMED Transect III: Massif Central - Provence - Gulf of Lion - Provençal Basin - Sardinia - Tyrrhenian Basin - Southern Apennines - Apulia - Adriatic Sea - Albanian Dinarides - Balkans - Moesian Platform, The TRANSMED Atlas The Mediterranean region from crust to mantle. Springer.

Cavazza, W. and Wezel, F.C., 2003. The Mediterranean region; a geological primer. International Union of Geological Sciences.

Cavazza, W., Roure, F. and Ziegler, P.A., 2004. The Mediterranean Area and the Surrounding Regions: Active Processes, Remnants of Former Tethyan Oceans and Related Thrustbelts. The TRANSMED Atlas The Mediterranean region from crust to mantle. Springer, pp. 1-29.

Ceriani, S., 2001. A combined study of structure and metamorphism in the frontal Penninic units between the Arc and Isère valleys (Western Alps): Implications for the geodynamic evolution of the Western Alps., University of Basel, Basel, 196 pp.

Ceriani, S., Fügenschuh, B. and Schmid, S.M., 2001. Multi-stage thrusting at the "Penninic Front" in the Western Alps between Mont Blanc and Pelvoux massifs. International journal of earth sciences 90: 685-702.

Ceriani, S. and Schmid, S.M., 2004. From N-S collision to WNW-directed post-collisional thrusting and folding: structural study of the Frontal Penninic Units in Savoie (Western Alps, France). Eclogae Geologicae Helvetiae, 97 in press.

Claudel, M.-E., 1999. Reconstitution paléogéographique du domaine Briançonnais au Mésozoique, Université Joseph Fourier Grenoble I, Grenoble, 236 pp.

Collombet, M., 2001. Cinématique et rotations des Alpes Occidentales. Approche paléomagnétique et modélisation analogique. Université Joseph Fourier, Grenoble, 207 pp.

Collombet, M., Thomas, J.C., Chauvin, A., Tricart, P., Bouillin, J P. and Gratier, J.P. 2002. Counterclockwise rotation of the Western Alps since the Oligocene; new insights from paleomagnetic data. Tectonics. 21 (4).

Coward, M.P., Gillcrist, R. and Trudgill, B., 1991. Extensional structures and their tectonic inversion in the Western Alps. Geological Society Special Publications 56: 93-112.

Delacou, B., 2004. Tectonique et géodynamique actuelle de l'arc alpin -Approche sismotectonique et modélisation numérique-, 249 pp.

Davies, V.M., 1982. Interaction of thrusts and basement faults in the French external Alps. Tectonophysics 88: 325-331.

De Ruig, M.-J., 1990. Fold trends and stress deviation in the Alicante fold belt, southeastern Spain. Tectonophysics 184 (3-4): 393-403.

Debelmas, J., 1955. Les zones Subriançonnaise et Briançonnaise occidentale entre Vallouise et Guillestre (Hautes-Alpes). Université de Grenoble, Grenoble, 169 pp.

Debelmas, J., Lemoine, M., Kerckhove, C., Fail, J.-P., Lavergne, M., Leduc, J., Legreneur, J., Ortollan, J., Robert, J.-P., Potié, R. and Gidon, M., 1966. Carte géologique de la France (1/50000). Feuille Guillestre. BRGM, Orléans.

Debelmas, J., Le Fort, P., Biju-Duval, J., Vernet, J., Monjuvent, G., Beuf, S., Debelmas, J., Kerckhove, C. and Pêcher, A., 1980. Carte géologique de la France (1/50000). Feuille Orcières. BRGM, Orléans.

Debelmas, J. and Kerckhove, C., 1980. Les Alpes franco-italiennes. Geologie Alpine 56: 21-58.

Debelmas, J., 1983. Alpes du Dauphiné. Guides géologiques régionaux. Masson, Paris,

198 pp.

Debrand-Passard, S., Courbouleix, S. and Lienhardt, M.-J., 1984. Synthèse géologique du Sud-Est de la France. Mémoire du Bureau de recherches géologiques et minières, 126.

Dewey, J.F., 1980. Episodicity, sequence, and style at convergent plate. In: The continental crust and its mineral deposits. Geological Association of Canada, pp. 553-573.

Dèzes, P., Schmid, S.M. and Ziegler, P.A., 2004. Evolution of the European Cenozoic Rift System: interaction of the Alpine and Pyrenean orogens with their foreland lithosphere. Tectonophysics, 389 (1-2): 1-33.
Dietrich, D. and Durney, D.W., 1986. Change of direction of overthrust shear in the Helvetic nappes of western Switzerland. Journal of Structural Geology 8: 389-398.

Faccenna, C., Becker, T.W., Lucente, F.P., Jolivet, L. and Rossetti, F., 2001a. History of subduction and Back-arc extension in the Central Mediterranean. Geophys. J. Int., 145: 809-820.

Faccenna, C., Davy, P., Brun, J.P., Funiciello, R., Giardini, D., Mattei, M. and Nalpas, T., 1996. The dynamics of backarc basins. An experimental approach to the opening of the Tyrrhenian Sea. Geophys. J. Int., 126: 781-795.

Faccenna, C., Funiciello, F., Giardini, D. and Lucente, P., 2001b. Episodic back-arc extension during restricted mantle convection in the central Mediterranean. Earth and Planetary Science Letters, 187(1-2): 105-116.

Faccenna, C., Mattei, M., Funiciello, R. and Jolivet, L., 1997. Styles of back-arc extension in the central Mediterranean. Terra Nova, 9(3): 126-130.

Flandrin, J., 1967. Sur l'age des principaux traits structuraux du Diois et des Baronnies. Bulletin de la Societe Geologique de France, 8(3): 376-386.

Ford, M., 1996. Kinematics and geometry of early Alpine, basement-involved folds, SW Pelvoux Massif, SE France. Eclogae Geologicae Helvetiae 89: 269-295.

Ford, M., Lickorish, H. and Kusznir, N.J., 1999. Tertiary foreland sedimentation in the Southern Subalpine Chains, SE France: a geodynamic appraisal. Basin Research, 11: 315-336.

Ford, M. and Lickorish, W.H., 2004. Foreland basin evolution around the western Alpine Arc. Geological Society Special Publication 221: 39-63.

Froitzheim, N., Schmid, S.M. and Frey, M., 1996. Mesozoic paleogeography and the timing of eclogite-facies metamorphism in the Alps; a working hypothesis. Eclogae Geologicae Helvetiae 89: 81-110.

Fry, N., 1989. Southwestward thrusting and tectonics of the Western Alps. Geological society special publications 45: 83-109.

Fügenschuh, B., Loprieno, A., Ceriani, S. and Schmid, S.M., 1999. Structural analysis of the Subbrianconnais and Valais units in the area of Moutiers (Savoy, Western Alps); paleogeographic and tectonic consequences. International Journal of Earth Sciences 88: 201-218.

Fügenschuh, B. and Schmid, S.M., 2003. Late stages of deformation and exhumation of an orogen constrained by fission-track data; a case study in the Western Alps. Geological Society of America Bulletin, 115(11): 1425-1440.
Galindo-Zaldivar, J., Gonzales-Lodeiro, F. and Jabaloy, A., 1993. Stress and Paleostress in the Betic-Rif cordilleras (Miocene to the present). Tectonophysics, 227: 105-126.

Gidon, M., 1965. Sur l'interpretation des accidents de la bordure meridionale du massif du Pelvoux. Travaux du Laboratoire de Geologie de la Faculte des Sciences de Grenoble, 41: 177-185.

Gidon, M., 1979. Le role des etapes successives de deformation dans la tectonique alpine du massif du Pelvoux (Alpes occidentales). Comptes Rendus Hebdomadaires des Seances de l'Academie des Sciences, Serie D: Sciences Naturelles, 288(9): 803-806.

Gidon, P., 1954. Les rapports des terrains cristallins et de leur couverture sedimentaire, dans les regions orientale et meridionale du massif du Pelvoux. Travaux du Laboratoire de Geologie de la Faculte des Sciences de Grenoble, 31: 1-199.

Gidon, P. and Vernet, J., 1952. Les accidents synclinaux de la haute vallee du Drac de Champoleon (Hautes-Alpes). Compte Rendu Sommaire des Seances de la Societe Geologique de France, 13-14: 269-270.

Giglia, G., Capponi, G., Crispini, L. and Piazza, M., 1996. Dynamics and seismotectonics of the West-Alpine arc. Tectonophysics, 267(1-4): 143-175.

Gignoux, M. and Moret, L., 1938. Description geologique du bassin superieure de la Durance. Travaux du Laboratoire de Géologie de la Faculté des Sciences de Grenoble, 21: 1-295.

Gignoux, M., Moret, L. and Schneegans D., 1933. Structure géologique de la fenêtre de L'Argentière au Sud de Briançon (Hautes-Alpes). Comptes Rendus de l'Academie des Sciences, 197(22): 1265-1267.

Gillcrist, R., Coward, M. and Mugnier, J.L., 1987. Structural inversion and its controls; examples from the Alpine Foreland and the French Alps. Geodinamica Acta, 1(1): 5-34.

Goguel, J., 1940. Tectonique de la chaine de Montbrison (feuille de Briancon au 1/ 50.000). Bulletin du Service de la Carte Geologique de la France, 203: 187-201.

Goguel, J., 1942. La chaine de Montbrison; essai de coordination tectonique (feuille de Briancon au 1/ 50.000). Bulletin du Service de la Carte Geologique de la France, 211: 109-118.

Goguel, J., 1963. Les problemes des chaines subalpines. [Fallot Memorial Vol.] (Soc. Geol. France), 2: 301-307.

Graham, R.H., 1978. Wrench faults, arcuate fold patterns and deformation in the southern French Alps. Proceedings of the Geologists' Association, 89 Part 2: 125-142.

Gratier, J.P., Menard, G. and Arpin, R., 1989. Strain-displacement compatibility and restoration of the Chaines Subalpines of the Western Alps. Geological Society Special Publications 45: 65-81.

Gueguen, E., Doglioni, C. and Fernandez, M., 1998. On the post-25 Ma geodynamic evolution of the western Mediterranean. Tectonophysics 298: 259-269.

Guillaume, A., 1980. Tectonophysics of the Western Alps. Eclogae Geologicae Helvetiae 73 (2): 425-436.

Gupta, S., 1997. Tectonic control on paleovalley incision at the distal margin of the early Tertiary Alpine foreland basin, southeastern France. Journal of Sedimentary Research, 67(6): 1030-1043.

Haug, E., 1894. Excursion géologique dans la haute vallée du Drac. Comptes Rendus des Séances de la Société Géologique de France, 22.

Huyghe, P. and Mugnier, J.L., 1995. A comparison of inverted basins of the southern North Sea and inverted structures of the external Alps. Geological Society Special Publications 88: 339-353.

Jolivet, L. and Faccenna, C., 2000. Mediterranean extension and the Africa-Eurasia collision. Tectonics, 19(6): 1095-1106.

Kerckhove, C., 1969. La 'zone du flysch' dans les nappes de l'Embrunais-Ubaye (Alpes occidentales). Geologie Alpine, 45: 5-190.

Kerckhove, C., Schneegans, D., Pairis, J.-L., Gidon, M. and Le Guernic, J., 1969. Carte géologique de la France (1/50000). Feuille Embrun. BRGM, Orléans.

Kerckhove, C., Debelmas, J. and Cochonat, P., 1978. Tectonique du soubassement parautochtone des nappes de l'Embrunais-Ubaye sur leur bordure occidentale, du Drac au Verdon. Geologie Alpine, 54: 67-80.

Kerckhove, C., Gidon, M., Malaroda, R., Barféty, J.-C., Bogdanoff, S., Lemoine, M., Carraro, F., Jorda, M. and Monjuvent, G., 1980. Carte géologique de la France (1/250000).

Feuille Gap. BRGM, Orléans.

Kerckhove, C., Gidon, M., Pairis, J.-L., Latreille, M. and Schneegans, D., 1988. Carte géologique de la France (1/50000). Feuille Chorges. BRGM, Orléans.

Laubscher, H., 1971. The large-scale kinematics of the Western Alps and the northern Apennines and its palinspastic implications. American Journal of Science, 271(3): 193-226.

Laubscher, H., 1991. The arc of the Western Alps today. Eclogae Geologicae Helvetiae, 84(3): 631-659.

Laubscher, H., Biella, G. C., Cassinis, R., Gelati, R., Lozej, A., Scarascia, S. and Tabacco, I., 1992. The collisional knot in Liguria. Geologische Rundschau, 81(2): 275-289.

Lawson, K., 1987. Thrust geometry and folding in the Alpine structural evolution of Haute Provençe., University of Wales, Swansea.

Lazarre, J., Tricart, P., Courrioux, G. and Ledru, P., 1996. Heritage tethysien et polyphasage alpin; reinterpretation tectonique du "synclinal" de l'aiguille de Morges (massif du Pelvoux, Alpes occidentales, France). Comptes Rendus de l'Academie des Sciences, Serie II. Sciences de la Terre et des Planetes, 323(12): 1051-1058.

Le Pichon, X., 1982. Land-locked oceanic basins and continental collision; the eastern Mediterranean as a case example. In: J. Hsue Kenneth (Editor), Mountain building processes. Acad. Press, London, United Kingdom, pp. 201-211.

Lefevre, R., 1983. La cicatrice de Preit; une discontinuite structurale majeure au sein de la zone brianconnaise interne entre Acceglio et l'Argentera (Alpes cottiennes meridionales). Comptes-Rendus des Seances de l'Academie des Sciences, Serie 2: Mecanique-Physique, Chimie, Sciences de l'Univers, Sciences de la Terre, 296(19): 1551-1554.

Lemoine, M., 1951. Donnees nouvelles sur la geologie du Brianconnais oriental et sur le probleme de la quatrieme ecaille. Bulletin de la Societe Geologique de France, 1: 191-204.

Lemoine, M., 1972. Rythme et Modalites des Plissements Superposes dans les Chaines Subalpines Meridionales des Alpes Occidentales Francaises. Geologische Rundschau, 61(3): 975-1010.

Lemoine, M., Bas, T., Arnaud-Vanneau, A., Arnaud, H., Dumont, T., Gidon, M., Bourbon, M., de Graciansky, P.-C., Rudkiewicz, J.-L., Megard-Galli, J. and Tricart, P., 1986. The continental margin of the Mesozoic Tethys in the Western Alps. Marine and Petroleum Geology, 3(3): 179-199.

Lemoine, M., Gidon, M. and Barféty, J.C., 1981. Les massifs cristallins externes des Alpes

Occidentales; d'anciens blocs bascules nes au Lias lors du rifting tethysien. Comptes-Rendus des Seances de l'Academie des Sciences, Serie 2: Mecanique-Physique, Chimie, Sciences de l'Univers, Sciences de la Terre, 292(12): 917-920.

Lemoine, M., Graciansky, P.-C., Tricart, P., 2000. De l'océan à la chaîne de montagnes. Tectonique des plaques dans les Alpes., 205 pp.

Letouzey, J., 1986. Cenozoic paleo-stress pattern in the Alpine Foreland and structural interpretation in a platform basin. Tectonophysics 132: 215-231.

Lickorish, W.H. and Ford, M., 1998. Sequential restoration of the external Alpine Digne thrust system, SE France, constrained by kinematic data and synorogenic sediments. Geological Society Special Publications 134: 189-211.

Lickorish, W.H., Ford, M., Buergisser, J. and Cobbold, P.R., 2002. Arcuate thrust systems in sandbox experiments; a comparison to the external arcs of the Western Alps. Geological Society of America Bulletin, 114(9): 1089-1107.

Maladora, R., Abiad, P.-L., Alesina, A., Blasi, A., Bortolami, Gc., Campanino Sturani, F., Cancelmo, C., Carraro, F., Crema, Gc., Cucchi, F., De Pol, C., Ezechieli, L., Fallot, P., Faure-Muret, A., Feltrin, F., Franceschetti, B., Francone, V., Gaiero, R., Govi, M., Grasso, F., Lorenzoni, S., Malaroda, R., Manzini Cucchi, A., Merlo, C., Perozzi, G., Ronco, P., Sacchi, R., Schiavinato, G., Sessa, N., Simonigh, A., Sodero, D., Sturani, C., Zanella, E., Zanettin Lorenzoni, E. and Zappi L., 1967. Carta Geologica del Massiccio dell' Argentera, scala 1/50000.

Malinverno, A. and Ryan, W.B.F., 1986. Extension in the Tyrrhenian Sea and shortening in the Apennines as result of arc migration driven by sinking of the lithosphere. Tectonics, 5(2): 227-245.

Merle, O. and Brun, J.P., 1984. The curved translation path of the Parpaillon Nappe (French Alps). Journal of Structural Geology, 6(6): 711-719.

Mosar, J., Stampfli, G.M. and Girod, F., 1996. western Prealpes Medianes Romandes; timing and structure; a review. Eclogae Geologicae Helvetiae 89 (1): 389-425.

Odin, G.S. and Odin, C., 1990. Echelle numérique des temps géologiques. Géochronique, 35: 12-21.

Orszag, S.F. and Pilot, M.D., 1976. Grands traits du Neogene de Corse. Bulletin de la Societe Geologique de France, 18(5): 1183-1187.

Ott d'Estevou, P., Montenat, C., Ladure, F. and D'Autrey, L.P., 1988. Evolution tectono-sedimentaire du domaine prébétique oriental (Espagne) au Miocène. C. R. Acad. Sci. Paris Série II, 307: 789-796.

Passchier, C.W., Trouw, R.A.J., 1996. Microtectonics, 289 pp.

Perriaux, J. and Uselle, J.P., 1968. Quelques donnees sur la sedimentologie des gres du Champsaur (Hautes-Alpes). Geologie Alpine, 44: 329-332.

Platt, J.P., Behrmann, J.H., Cunningham, P.C., Dewey, J.F., Helmann, M., Parish, M., Shepley, M.G., Wallis, S. and Weston, P.J. 1989. Kinematics of the Alpine arc and the motion history of Adria. Nature, 337(6203): 158-161.

Platt, J.P. and England, P.C., 1994. Convective removal of lithosphere beneath mountain belts; thermal and mechanical consequences. American Journal of Science, 294(3): 307-336.

Platt, J.P. and Vissers, R.L.M., 1989. Extensional collapse of thickened continental lithosphere; a working hypothesis for the Alboran Sea and Gibraltar Arc. Geology, 17(6): 540-543.

Principi, G. and Treves, B., 1984. Il sistema corso-appenninico come prisma di accrezione; riflessi sul problema generale del limite Alpi-Appennini. In: M. Vanossi (Editor), Atti del convegno sul tema Geologia delle Alpi Liguri. Memorie della Societa Geologica Italiana. Societa Geologica Italiana, Rome, Italy, pp. 549-576.

Ravenne, C., Vially, R., Riche, P. and Tremolieres, P., 1987. Sedimentation et tectonique dans le bassin marin Eocene superieur-Oligocene des Alpes du Sud. Revue de l'Institut Francais du Petrole, 42(5): 529-553.

Ricou, L.E., 1981. Glissement senestre des nappes penniques le long de la bordure nord de l'Argentera; son role dans le jeu de l'arc alpin. Comptes-Rendus des Seances de l'Academie des Sciences, Serie 2: Mecanique-Physique, Chimie, Sciences de l'Univers, Sciences de la Terre, 292(18): 1305-1308.

Ricou, L.E., 1984. Les Alpes occidentales; chaine de decrochement. Bulletin de la Societe Geologique de France, 26(5): 861-874.

Ricou, L.E. and Siddans, A.W.B., 1986. Collision tectonics in the Western Alps. Geological Society Special Publications 19: 229-244.

Ritz, F., 1991. Evolution du champ de contraintes dans les Alpes du Sud depuis la fin de l'Oligocène. Implications sismotectoniques., Montpellier.

Roca, E., 2001. The Northwest Mediterranean Basin (Valencia Trough, Gulf of Lions and Liguro-Provencal basins); structure and geodynamic evolution. In: A. Ziegler Peter, W. Cavazza, H.F. Robertson Alastair and S. Crasquin Soleau (Editors), Peri-Tethys memoir 6; Peri-Tethyan rift/ wrench basins and passive margins. Ed. du Museum National d'Histoire Naturelle. Paris, France. 2001.

Rollet, N., Déverchère, J., Beslier, M.-O., Guennoc, P., Réhault, J.-P., Sosson, M. and Truffet, C. 2002. Back arc extension, tectonic inheritance, and volcanism in the Ligurian Sea, western Mediterranean. Tectonics 21 (3).

Royden, L.H., 1993. Evolution of retreating subduction boundaries formed during continental collision. Tectonics, 12(3): 629-638.

Sanderson, D.J., 1979. The transition from upright to recumbent folding in the Variscan fold belt of Southwest England; a model based on the kinematics of simple shear. Journal of Structural Geology, 1(3): 171-180.
Schmid, S.M., Fügenschuh, B., Kissling E. and Schuster, R., 2004. Tectonic map and overall architecture of the Alpine orogen. Eclogae Geologicae Helvetiae, 97(1): 93-117.

Seranne, M., 1999. The Gulf of Lion continental margin (NW Mediterranean) revisited by IBS; an overview. Geological Society Special Publications 156: 15-36.

Serri, G., Innocenti, F. and Manetti, P., 1993. Geochemical and petrological evidence of the subduction of delaminated Adriatic continental lithosphere in the genesis of the Neogene-Quaternary magmatism of central Italy. Tectonophysics 223 (1-2): 117-147.

Seward, D. and Mancktelow, N.S., 1994. Neogene kinematics of the Central and Western Alps; evidence from fission-track dating. Geology, 22(9): 803-806.

Siddans, A.W.B., 1979. Arcuate fold and thrust patterns in the Subalpine chains of Southeast France. Journal of Structural Geology, 1(2): 117-126.

Simon Gomez, J.L., 1986. Analysis of a gradual change in stress regime (example from the eastern Iberian Chain, Spain. Tectonophysics, 124(1-2): 37-53.

Simpson, C. and Schmid, S.M., 1983. An evaluation of criteria to deduce the sense of movement in sheared rocks. Geological Society of America Bulletin, 94(11): 1281-1288.

Spakman, W.S., van der Lee and R. van der Hilst, 1993. Travel-time tomography of the European-Mediterranean mantle down to 1400 km. Physics of the Earth and Planetary Interiors 79: 3-74.

Spakman, W., and Wortel R., 2004. A Tomographic View on western Mediterranean Geodynamics., The TRANSMED Atlas The Mediterranean region from crust to mantle. Springer.

Spencer, S., 1992. A kinematic analysis incorporating incremental strain data for the frontal Pennine zones of the western French Alps. Tectonophysics, 206(3-4): 285-305.

Sue, C., Martinod, J., Tricart, P., Thouvenot, F., Gamont, J.-F., Fréchet, J., Marinier, D., Glot, J.-P., Grasso, J.R., 2000. Active deformation in the inner Western Alps inferred from

comparison between 1972-classical and 1996-GPS geodetic surveys. Tectonophysics, 320(1): 17-29.

Sue, C., Thouvenot, F., Frechet, J. and Tricart, P., 1999. Widespread extension in the core of the Western Alps revealed by earthquake analysis. Journal of Geophysical Research, B, Solid Earth and Planets, 104(11): 25,611-25,622.

Sue, C. and Tricart, P., 1999. Late Alpine brittle extension above the frontal Pennine thrust near Briancon, Western Alps. Eclogae Geologicae Helvetiae, 92(2): 171-181.

Sue, C. and Tricart, P., 2003. Neogene to ongoing normal faulting in the inner Western Alps; a major evolution of the late alpine tectonics. Tectonics, 22 (5).

Sue, C., Tricart, P., Dumont, T. and Pecher, A., 1997. Raccourcissement polyphase dans le massif du Pelvoux (Alpes occidentales); exemple du chevauchement de socle de Villard-Notre-Dame. Comptes Rendus de l'Academie des Sciences, Serie II. Sciences de la Terre et des Planetes, 324(10): 847-854.

Termier, P., 1903. Les montagnes entre Briançon et Vallouise. Mém. expl. Carte géol. Fr.: 182.

Thomas, J.C., Claudel, M.E., Collombet, M., Tricart, P., Chauvin, A. and Dumont, T., 1999. First paleomagnetic data from the sedimentary cover of the French Penninic Alps: evidence for Tertiary counterclockwise rotations on the Western Alps. Earth and Planetary Science Letters, 171: 561-574.

Tricart, P., 1980. Tectoniques superposées dans les Alpes occidentales au Sud du Pelvoux; évolution structurale d'une chaîne de collision., Université de Strasbourg, France, Strasbourg, 407 pp.

Tricart, P., 1986. Le Chevauchement de la zone brianconnaise au Sud-Est du Pelvoux; cle des rapports zone externe - zones internes dans les Alpes occidentales. Bulletin de la Societe Geologique de France, Huitieme Serie, 2(2): 233-244.

Tricart, P., Bouillin, J.P., Dick, P., Moutier, L. and Xing, C., 1996. Le faisceau de failles de haute-Durance et le rejeu distensif du front brianconnais au SE du Pelvoux (Alpes occidentales). Comptes Rendus de l'Academie des Sciences, Serie II. Sciences de la Terre et des Planetes, 323(3): 251-257.

Tricart, P., Bourbon, M., Chenet, P. Y., Cros, P., Delorme, M., Dumont, T., Graciansky, P.C., Lemoine, M., Megard, Galli J. and Richez, M., 1988. Tectonique synsedimentaire triasico-jurassique et rifting tethysien dans la nappe brianconnaise de Peyre-Haute (Alpes occidentales). Bulletin de la Societe Geologique de France, Huitieme Serie, 4(4): 669-680.

Tricart, P., Schwartz, S., Sue, C., Poupeau, G. and Lardeaux, J.M., 2001. La denudation

tectonique de la zone ultradauphinoise et l'inversion du front brianconnais au sud-est du Pelvoux (Alpes occidentales); une dynamique miocene a actuelle. Bulletin de la Societe Geologique de France, 172(1): 49-58.

Tricart, P., 2004. From extension to transpression during the final exhumation of the Pelvoux and Argentera massifs, Western Alps. Eclogae Geologicae Helvetiae, in press.

Trincardi, F., Zitellini, N., 1987. The rifting in the Tyrrhenian basin. Geo-Marine Lett., 7(1-6).

Vernet, J., 1950. Les limites SE du massif du Pelvoux et de l'anticlinal amygdaloïde des Ecrins. Bulletin de la Societe Geologique de France, 5(20): 275-287.

Vernet, J., 1951. Le Synclinorium de l'Aiguille de Morges et le style des déformations alpines du Cristallin du Pelvoux. Bulletin de la Societe Geologique de France, 6(1): 169-183.

Vernet, J., 1952. Les déformations d'âge alpin du Cristallin du Pelvoux, à la lumière d'observations nouvelles. Bulletin de la Societe Geologique de France, 6(2): 175-189.

Vernet, J., 1966. Observations nouvelles sur le synclinal d'Ailefroide et les bordures du massif du Pelvoux en Vallouise. Travaux du Laboratoire de Geologie de la Faculte des Sciences de Grenoble 42: 275-280.

Vialon, P., Rochette, P. and Menard, G., 1989. Indentation and rotation in the western Alpine arc. Geological Society Special Publications 45: 329-338.

Vigliotti, L. and Langenheim, V.E., 1995. When did Sardinia stop rotating? New palaeomagnetic results. Terra Nova, 7(4): 424-435.

Waibel, A.F., 1990. Sedimentology, petrographic variability, and very-low-grade metamorphism of the Champsaur sandstone (Paleogene, Hautes-Alpes, France). Evolution of volcaniclastic foreland turbidites in the external Western Alps., Université de Genève, Genève.

Watts, A.B. and Torne, M., 1992. Subsidence history, crustal structure, and thermal evolution of the Valencia Trough; a young extensional basin in the western Mediterranean. Journal of Geophysical Research, B, Solid Earth and Planets, 97(13): 20,021-20,041.

Wortel, M.J.R. and Spakman, W., 1992. Structure and dynamics of subducted lithosphere in the Mediterranean region. Proceedings of the Koninklijke Nederlandse Akademie van Wetenschappen (1990), 95(3): 325-347.

# 2. MICROFABRICS OF CALCITE ULTRAMYLONITES RECORDING COAXIAL AND NON-COAXIAL DEFORMATION KINEMATICS: EXAMPLES FROM THE ROCHER DE L'YRET SHEAR ZONE (WESTERN ALPS).

Ghislain Trullenque[a], Karsten Kunze[b], Renee Heilbronner[a], Holger Stünitz[a] and Stefan M. Schmid[a].

[a] Department of Geosciences, Basel University, CH-4056 Basel, Switzerland
[b] Geological Institute, ETH Zürich, CH-8092 Zürich, Switzerland

**Corresponding author:**

Ghislain Trullenque
Dept. of Geosciences
Basel University
Bernoullistr. 30-32
CH-4056 Basel
Switzerland

Tel. +41 - 61 - 267 3607
Fax. +41 - 61 - 267 3613
Email: ghislain.trullenque@unibas.ch

**Keywords:**
calcite, microstructure, crystallographic preferred orientation, shape preferred orientation, shear kinematics, coaxial and noncoaxial deformation, texture goniometry, CIP

## Abstract.

Microfabrics were analysed in calcite mylonites from the rim of the Pelvoux massif (Western Alps, France). WNW-directed emplacement of the internal Penninic units onto the Dauphinois domain has lead to intense deformation of an Eocene-age nummulitic limestone under lower anchizone metamorphic conditions (slightly below 300°C). Two types of microfabrics developed during deformation under coaxial or non-coaxial kinematics, respectively, primarily by dislocation creep accompanied by dynamic recrystallization in the absence of twinning. Coaxial kinematics are inferred for samples exhibiting grain shape fabrics and textures with orthorhombic symmetry. Their texture is characterized by two *c*-axis maxima at the periphery of the pole figure, symmetrically oriented at 15° from the normal to the macroscopic foliation. Non-coaxial deformation is evident in samples with monoclinic shape fabrics and textures characterized by a single oblique *c*-axis maximum tilted with the sense of shear by about 15°. From the analysis of suitably oriented slip systems for the main texture components under given kinematics it is inferred that the orthorhombic textures developed in coaxial kinematics favour activity of <10-11> and <02-21> slip along the *f*- and *r*-planes, respectively, with minor contributions of basal-<*a*> slip. In contrast, the monoclinic textures developed during simple shear are most suited for duplex <*a*> slip along the basal plane. The transition between orthorhombic and monoclinic microfabrics is interpreted to be due to the effects of dynamic recrystallization upon texture development. Calcite textures alone should not be used as unequivocal shear sense indicators, but need to be complemented by microstructural criteria such as shape preferred orientations, grain size estimates and amount of twinning.

## 2.1 Introduction.

Microfabrics, i.e. microstructures and textures, are important records of deformation conditions and kinematics in deformed rocks. The term texture is referred here particularly to crystallographic preferred orientations (CPO) as being used sensu stricto in materials sciences (Bunge, 1982). Calcite microfabrics are particularly used to characterize deformation under low-grade metamorphic conditions, where other minerals do not deform by ductile flow but show cataclastic deformation without dynamic recrystallization. Different texture types were distinquished for "high" or "low" temperature deformation of calcite (Wenk et al. 1987, Leiss et al. 1999).

There has been considerable debate about the interpretation of symmetry versus asymmetry of calcite textures and their kinematic significance as indicators for pure shear or simple shear deformation (Kern & Wenk 1983, Wenk et al. 1987, Erskine et al. 1993, Ratschbacher et al. 1991, Bestmann et al., 2000). Calcite textures in naturally and experimentally deformed rocks most often exhibit *c*-axis maxima rotated against the sense of shear (Schmid et al. 1981, 1987, Lafrance et al. 1994, Casey et al. 1998). However, there are also textures reported with *c*-axis maxima either oriented exactly normal to the shear direction (Pieri et al. 2001a, b, Barnhoorn et al. 2004), or even slightly rotated with the sense of shear (Lafrance et al. 1994, Bestmann et al. 2000). Because of such ambiguities, Lafrance et al. (1994) generally questioned the applicability of calcite textures as shear sense criteria. Further confusion arises from inconsistency in defining the sample reference frame, i.e. whether the foliation or the shear zone boundary are taken as the reference plane, which are approximately parallel only after large finite shear strain. Textures with *c*-axis maxima normal to the foliation or symmetrically inclined in two conjugate orientations with respect to foliation and lineation have been interpreted as indicating pure shear deformation (Kern & Wenk 1983, Wenk et al. 1987, Ratschbacher 1999). This interpretation is not unambiguous, as there are also textures reported with *c*-axis patterns of orthorhombic or even axial symmetry from shear zones that show convincing evidence for non-coaxial deformation (e.g. Bestmann et al., 2000). However, the inverse conclusion is certainly applicable, namely that pure shear deformation (of an initially isotropic aggregate) must lead to fabrics with at least orthorhombic symmetry. Analogously, simple shear must result in fabrics that possess at least monoclinic symmetry, but they may have higher (e.g. orthorhombic) symmetry. Torsion experiments (Pieri et al. 2001a, b, Barnhoorn et al., 2004) demonstrated that one and the same simple shear kinematics and identical deformation conditions result in calcite textures with monoclinic symmetry at low strain, which evolve into textures with either orthorhombic or monoclinic symmetry at high strain.

Apart from texture, a wide variety of microstructural features are potential kinematic indicators in deformed rocks (e.g. Passchier and Trouw, 1996). In monophase aggregates, it is particularly the grain shape fabric, here referred to as shape preferred orientation (SPO). Orthorhombic SPO are generally indicative of dominantly coaxial deformation whereas monoclinic SPO are indicative of dominantly non-coaxial deformation (for calcite see: Schmid et al. 1987, Lafrance et al. 1994, Bestmann et al. 2000, Pieri et al. 2001a, b). Torsion experiments (Barnhoorn et al., 2004) demonstrated that a monoclinic SPO establishes and remains stable under shear deformation up to very large strain.

This paper describes microstructures and textures analyzed in samples of naturally deformed limestone mylonites collected along two profiles across the Rocher de l'Yret shear zone at the rim of the Pelvoux massif (Western Alps). Microfabrics and field evidence clearly indicate distinguishable cases for simple and pure shear dominated deformation for the two sample series, respectively, which should have occurred simultaneously under the same temperature and comparable strain rates. It is concluded that the systematic differences observed in microstructure and texture are due to different deformation paths. Hence the two series of samples may serve as prototypes of distinct types of textures that are indicative of the kinematics of deformation.

## 2.2 Geological framework of the study area.

### 2.2.1 Regional Setting.

The Rocher de l'Yret Shear Zone (RYSZ), situated at the eastern rim of the Pelvoux massif (Western Alps, France; fig 2.1), separates the Dauphinois domain from the Penninic units and forms part of the Pennine/Penninic Front (Merle and Brun 1984, Mosar et al. 1986, Bagnoud et al. 1998) also referred to as Pennine/Penninic Frontal thrust (Spencer 1992, Seward and Mancktelow 1994, Bürgisser and Ford 1998). According to Ceriani et al. (2001), this thrust formerly represented a suture zone between Dauphinois and Briançonnais/Subriançonnais, active during Eocene times and related to the subduction of the Valaisan Ocean. The Valaisan oceanic domain was closed in sinistral transpression, associated with a top to the north sense of movement. During a second deformation stage (Oligo-Miocene), WNW-directed thrusting along the entire Western Alps on a major out-of-sequence thrust, the Roselend thrust, completely reworked the Penninic front. In particular, calcite mylonites were formed in Eocene sediments (nummulitic limestone) on top of a regional unconformity, which cuts across the Jurassic sediments into the basement and is defined by the deposition of a detrital calcitic conglomerate.

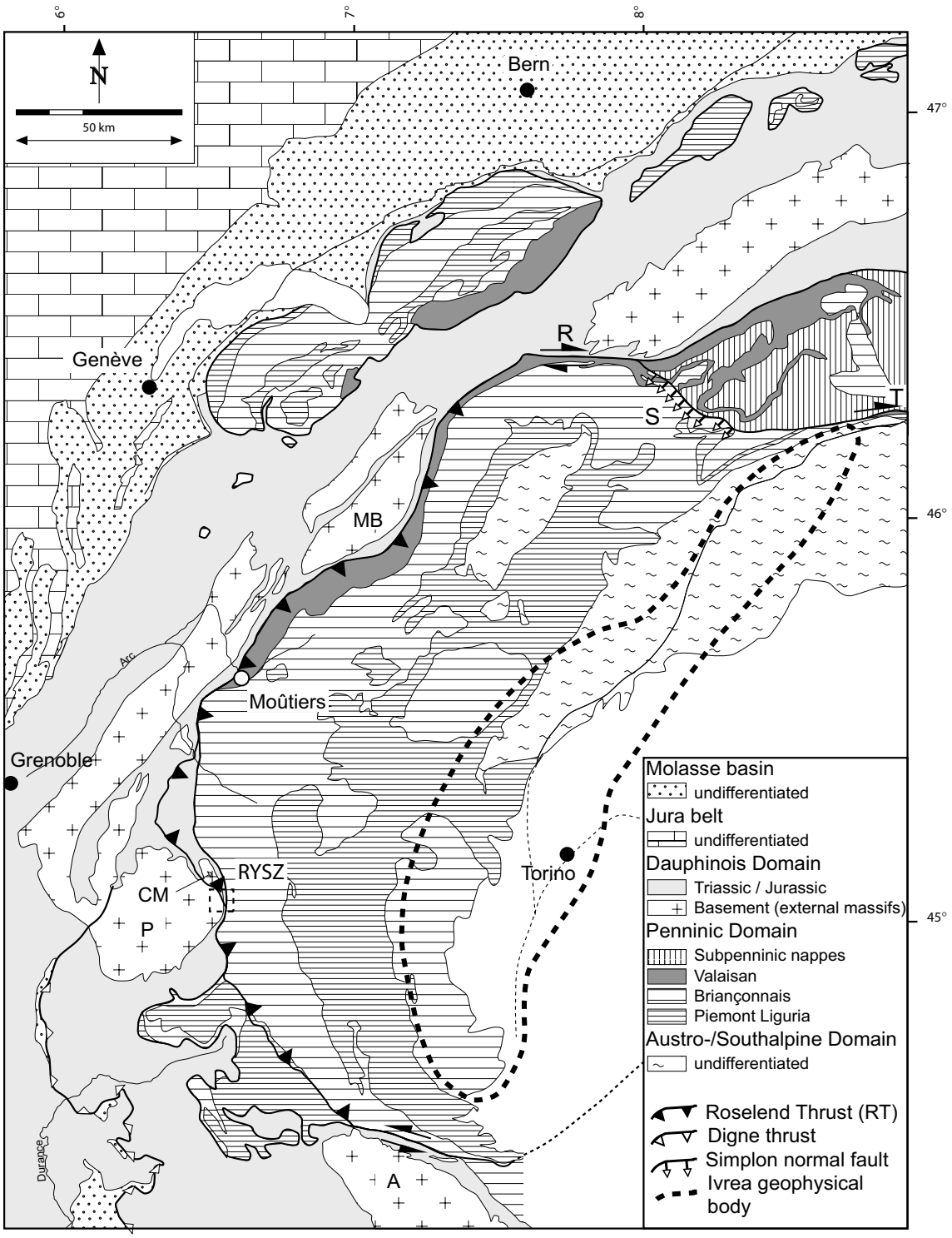


**Figure 2.1:** Simplified geological overview of the arc of the Western Alps (A: Argentera massif, CM: Combeynot massif, MB: Mont Blanc massif, P: Pelvoux massif, R: Rhone-Simplon line, S: Simplon normal fault, T: Tonale line, RYSZ: Rocher de l'Yret shear zone; after Ceriani et al. 2001 and Froitzheim et al. 1996).

### 2.2.2 Temperature conditions during deformation.

The degree of Alpine metamorphic overprint of the eastern rim of the Pelvoux massif, as estimated by Aprahamian (1974, 1988) by means of illite crystallinity (IC) measurements, occurred under epizonal conditions (IC < 2.8 for the RYSZ). Furthermore, temperatures can indirectly be derived from a contoured zircon fission track isochron map of the Western Alps compiled by Fügenschuh and Schmid (2003). The whole eastern rim of the Pelvoux massif is characterized by zircon fission track ages older than 60 My, indicating that the corresponding rocks had not been exposed to temperatures above the upper limit of the zircon partial annealing zone, i.e. 320°C (Tagami et al. 1998), for 60 My. Zircon fission track data from the Briançonnais and Dauphinois domains, immediately south of the RYSZ (Seward et al. 1999), yielded ages older than 100 My, which clearly excludes metamorphic temperatures above 320°C during the Tertiary. Hence, temperatures must have been around 300°C or even slightly below around the whole eastern rim of the Pelvoux massif. Preliminary results based on new IC data and fluid inclusion analyses indicate low anchizonal metamorphic conditions (Potel, pers. comm.), putting the epizonal conditions proposed by Aprahamian (1974, 1988) again under question.

### 2.2.3 Structural setting.

At the eastern rim of the Pelvoux massif, the Roselend thrust (RT) enters the Mesozoic cover of the external massifs. It thrusts the Combeynot massif together with its Eocene sedimentary cover over the Pelvoux massif (fig 2.1). Near the outcrop investigated in this study, the Combeynot massif wedges out into the RYSZ, which is a kilometre-wide shear zone that represents the RT in this area.

The RYSZ represents an imbricate structure consisting of two large slices of the Pelvoux massif, the lower "Grangettes" slice, and the upper "Montagnolle" slice (Gignoux and Moret 1938, Gidon 1954, Gidon 1979, Beach 1981, Ford 1996). Butler (1992) investigated the upper part of the "Crête de l'Yret" slice and has described WNW-directed shearing of nummulitic limestones in a basement/cover imbricate structure forming the Rocher de l'Yret summit (fig 2.2). According to own regional studies (see chapter 1), this summit consists of a third and very thin basement slice, which is a boudinaged slice of the Combeynot massif, together with its Eocene-age stratigraphic cover, which represents the calcite mylonites investigated by this study. Thrusting along the RT additionally led to local strike slip faults affecting these basement-cover boudins.

Most of the samples for this study were taken from an outcrop (locality 1 in fig

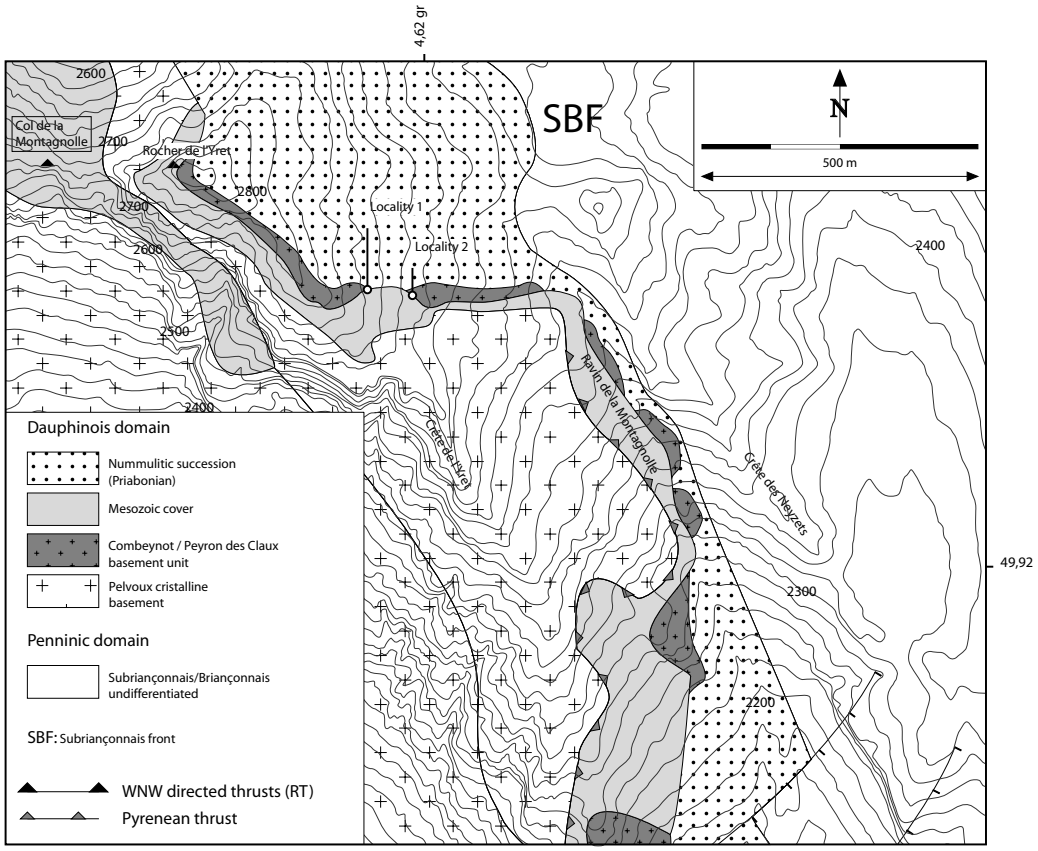


**Figure 2.2:** Detailed geological map of the sampling area around the Rocher de l'Yret shear zone (RYSZ) after field mapping (see chapter 1); sampling localities 1 and 2 are marked.

2.2) situated within the top-most parts of the RYSZ. It exposes a layer of mylonitized nummulitic limestone that was originally in stratigraphic contact with an isolated Combeynot basement boudin. At its northern edge, this basement-cover boudin is cut by a sinistral strike-slip zone (fig 2.3a). Lineations and associated shear sense criteria indicate top-WNW shearing over the entire area of the outcrop. Deformation inside the crystalline basement was accommodated by cataclastic faulting and/or flow (fig 2.4a, b), which is consistent with the low grade metamorphic conditions, while the nummulitic limestone underwent crystal-plastic deformation.

The main limestone layer is accessible over a horizontal distance of about 20 meters striking NNE-SSW. Its mylonitic to ultra-mylonitic foliation is parallel to internal bedding and to the original stratigraphic contact with the basement boudin. The layer reaches a maximum thickness of 110 centimeters at the southern termination of the outcrop. Abundant nummulites, several millimeters in size, are preserved in the bottom 30 centimeters of the sheared limestone layer. In the vicinity to the basal conglomerate it also contains a significant portion of detrital quartz. This quartz-calcite-mixture develops a strong stretching lineation. Progressive development of a mylonitic foliation parallel to

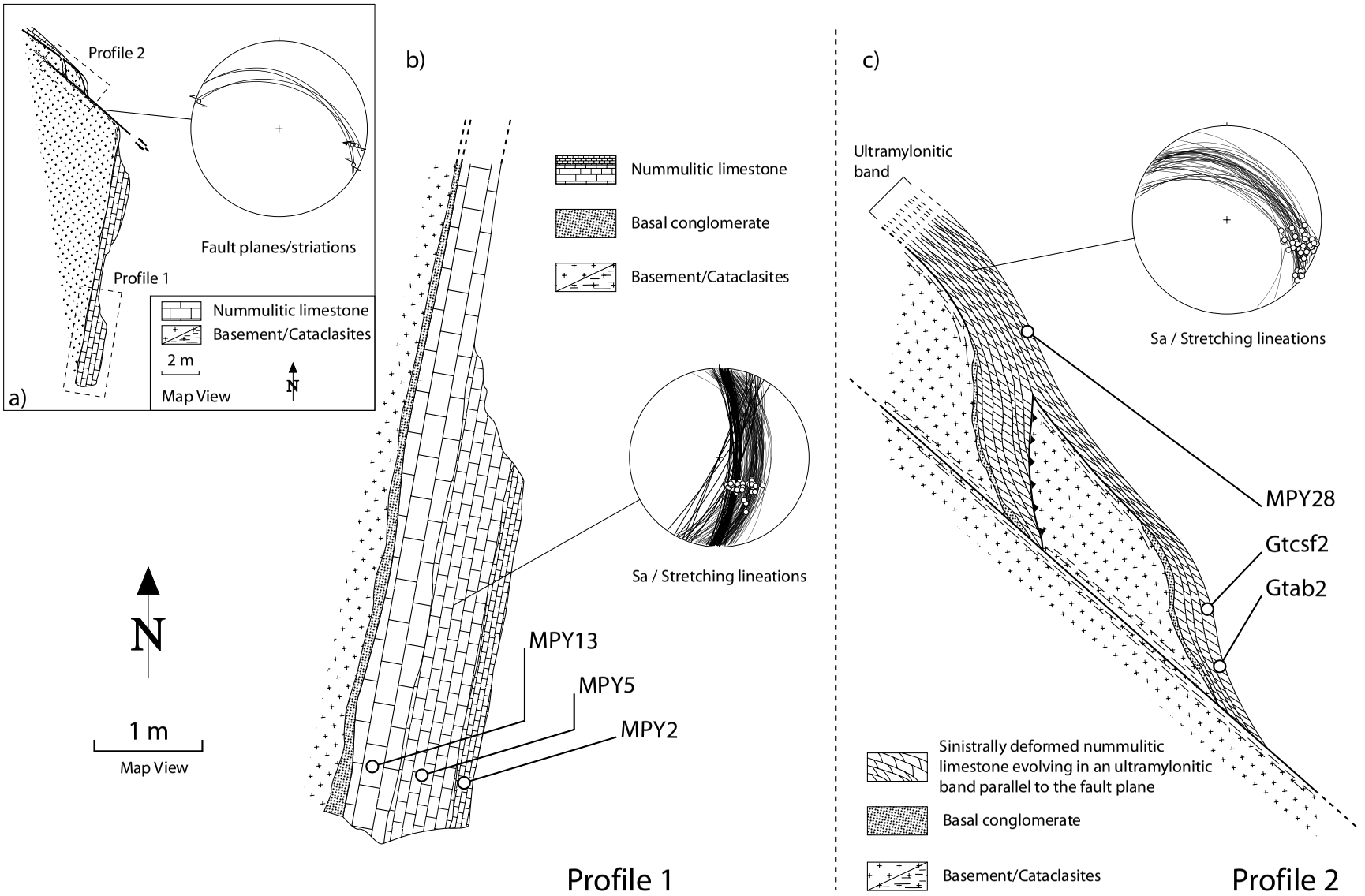
a)
Profile 2
Profile 1
Fault planes/striations
Nummulitic limestone
Basement/Cataclasites
2 m
Map View
N
b)
Nummulitic limestone
Basal conglomerate
Basement/Cataclasites
Sa / Stretching lineations
MPY13
MPY5
MPY2
N
1 m
Map View
Profile 1
c)
Ultramylonitic band
Sa / Stretching lineations
MPY28
Gtcsf2
Gtab2
Sinistrally deformed nummulitic limestone evolving in an ultramylonitic band parallel to the fault plane
Basal conglomerate
Basement/Cataclasites
Profile 2

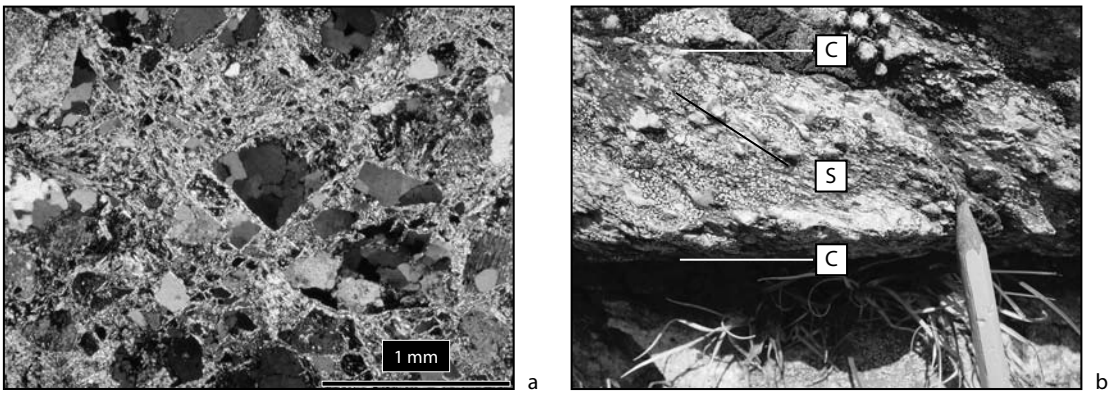


**Figure 2.4:**
a) Photomicrograph of the basement cataclastic rock.
b) Detailed view of the basement cataclasite along the main strike slip fault plane.

the bedding plane can be observed at increasing distance from the basement and towards the ESE. Decreasing amounts of recognizable nummulite shells correlate with increasing degree of dynamic recrystallisation in calcite, which is also interpreted as a strong gradient in finite strain directed normal to foliation. In this part of the outcrop sampling was carried out along a traverse normal to the foliation (profile 1, fig 2.3b).

The strike-slip zone exposed in the northern part of the outcrop is associated with the formation of a basement/cover imbricate structure. By approaching the strike-slip fault, which cataclastically dissects the basement units, the limestone is intensively sheared in a sinistral sense. The upper levels of the layer are progressively bent around the basement slice and form an ultramylonitic band parallel to the fault plane. This unit shows numerous isoclinal folds, together with a WNW oriented stretching lineation defined by quartz grains. We sampled the upper part of the limestone layers along strike, i.e. from their initial position on top of the basement slices towards the ultramylonitic band (profile 2, fig 2.3c).

The transition in orientation of both foliations and stretching lineations is rather gradual between the locations of profile 1 (steeply plunging stretching lineation) and profile 2 (mostly horizontal or shallowly plunging stretching lineation). This indicates that deformation of the limestone layer was coeval in profiles 1 and 2.

A paleostress analysis was performed for a set of 124 co-genetic fault planes

**Figure 2.3:**
a) Structural scheme of the investigated outcrop at sampling locality 1. Fault plane orientations with striations of the main strike slip zone are reported.
b) Map of profile 1 with location of samples MPY13, MPY5, MPY2; macroscopic foliations Sa with stretching lineations of nummulitic limestone.
c) Map of profile 2 with location of samples Gtab2, Gtcsf2 and MPY28; macroscopic foliations Sa with stretching lineations of nummulitic limestone.

dissecting basement boudins and their Eocene cover. This analysis was carried out using Tectonic VB software [1] including inversion methods (Angelier and Mechler 1977). The results (fig 2.5) show average orientations of σ1 at N264/10 and of σ3 at N154/60, which are considered to be representative for the orientation of the bulk stress tensor at a larger scale in the whole RYSZ. Throughout the outcrop, foliation planes roughly intersect in the intermediate stress axis σ2, while stretching lineations are about perpendicular to it

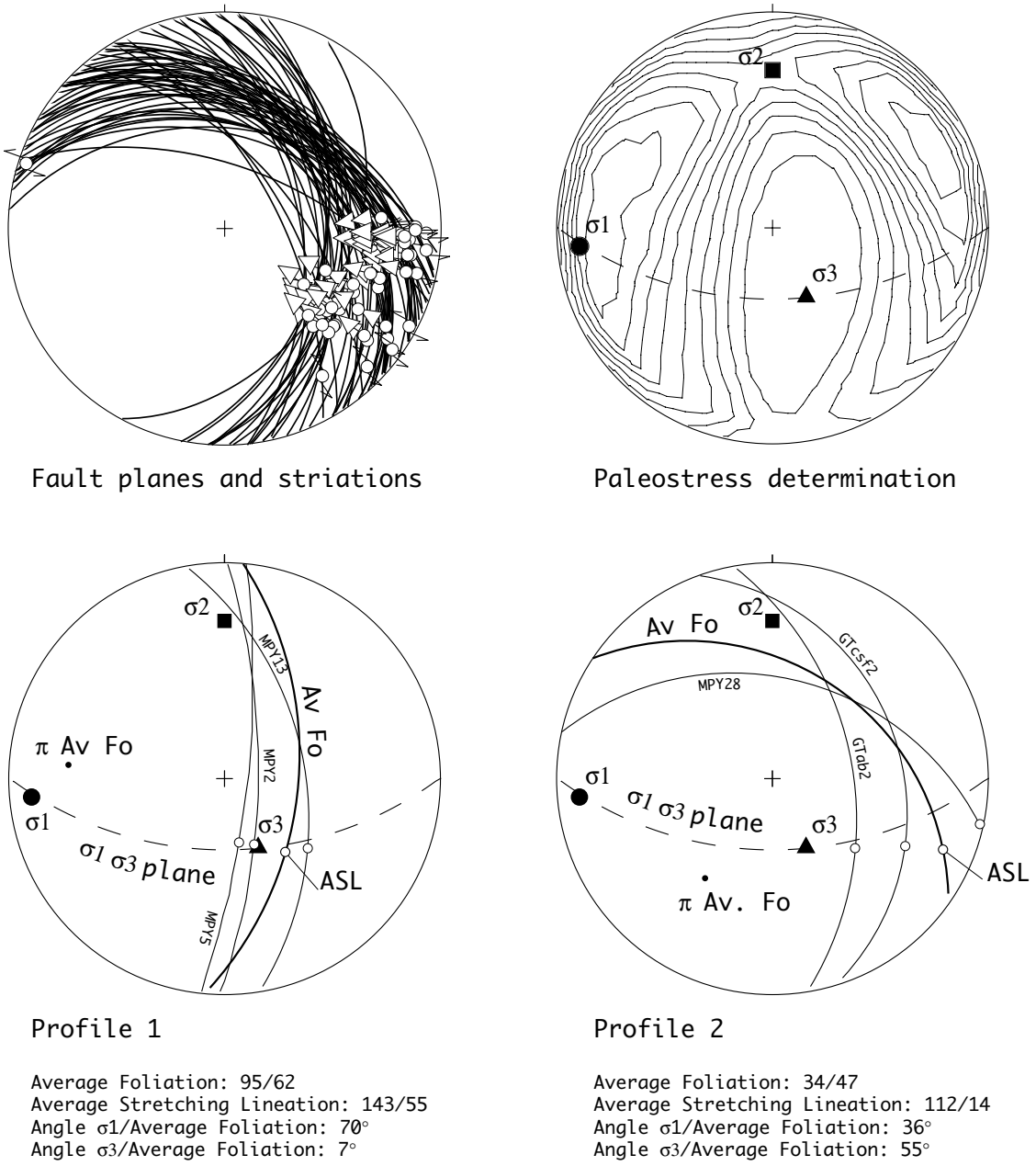


**Figure 2.5:** Paleostress analysis in the basement adjacent to limestone mylonites: P, B and T axes derived from 124 individual fault planes; average orientation of the principal stress axes σ1 (N264/10), σ2 (N0/27), σ3 (N154/60) are superposed over projections of macroscopic foliations (labeled great circles) and stretching lineations (open balls) from profiles 1 and 2 (on average and for the studied samples).
Contours of σ1, σ2 and σ3 are given in multiples of a uniform distribution with a contour interval of 0.3.

within the σ1-σ3 plane. For profile 1, the average stretching lineation falls close to σ3 while the average foliation is oriented subnormal to σ1. Such a kinematic framework is compatible with coaxial deformation. For the ultramylonic band of profile 2, σ1 and σ3 fall at intermediate (roughly 45°) angles to the average foliation and to the average stretching lineation of the mylonitic layer. This kinematic framework is indicative of non-coaxial deformation. If deformation were restricted to plane strain, for which we do not have ultimately decisive indications, then profiles 1 and 2 could be related to pure shear respectively simple shear dominated kinematics.

## 2.3 Methods of investigation.

Samples were cut normal to the macroscopic foliation (Sa) and parallel to the stretching lineation (XZ sections). Approximately 2 μm thick ultra-thin sections showing first order grey in calcite in crossed polarised light were prepared for microstructural analysis and for mapping of *c*-axis orientations by computer integrated polarization (CIP) microscopy (Panozzo Heilbronner and Pauli 1993, 1994). Vectorisation of grain boundaries was performed on digital micrographs using a combination of NIH Image [2] and own software. On average, about 3500 particles were evaluated per sample to determine their SPO and grain size distributions. The preferred orientation of the grain long axes was determined using the PAROR method, while the preferred orientation of grain boundary surfaces was analysed using the program SURFOR (Panozzo, 1983, 1984). The determination of particle grain sizes was performed using the program STRIPSTAR [3].

Pole figures were measured with a SIEMENS D5000 X-ray texture goniometer in reflexion and transmission modes for three crystallographic planes (*r* {10-14}, *a* {11-20} and *h* {20-22}) for each sample. Lattice planes and directions are designated here by Miller-Bravais hexagonal indices referring to the structural hexagonal unit cell with axial ratio c/a = 3.419 as classified by Wyckoff (1920). Empirical corrections for defocusing in reflection mode and for scattering volume in transmission mode were applied before merging into complete pole figures. The orientation distribution function (ODF) was calculated using both MENTEX (Schaeben, 1990) and BEARTEX-WIMV (Wenk et al., 1998) software, and selected ODF sections are displayed by intensity contour plots. The applied convention for Euler angles ($\psi_1$, $\Phi$, $\psi_2$) relates to the one ($\varphi_1$, $\Phi$, $\varphi_2$) defined by Casey, (1981, his Fig. 3) and Bunge (1982) by $\psi_1 = \varphi_1$ and $\psi_2 = \varphi_2 + 90°$, as the crystal coordinate axis $X_c$ is placed here parallel to +*a* instead of *m*. Pole figures were recalculated from the ODF for the three measured reflections and additionally for the basal (0001) and the *f* -planes {01-12}, for the inferred slip directions *sd1* <10-11> and *sd2* <02-21>, and

also inverse pole figures for particular specimen directions. All pole figures and inverse pole figures were treated with inversion symmetry except for the recalculated +*a*<-1-120> and –*a*<11-20> (non-reduced) pole figures. All figures are displayed using equal area projections of the upper hemisphere.

The measured orientation distributions were compared to idealised textures, which are modelled to be composed of a few components around fixed ideal crystal orientations using Gaussian standard distributions of constant and isotropic angular spread (half width of 40°; software package BEARTEX, Wenk et al., 1998). These model textures should be regarded only as first approximation for a complete component fit according to methods developed by Helming (1994). Pole figures, ideal pole figures and ODF sections of these model textures were displayed analogously to those of the corresponding samples.

## 2.4 Microstructure and texture of nummulitic limestone mylonites.

Microstructures and textures in limestone mylonites were quantitatively described for about 130 collected and analysed specimens along the Roselend Thrust (see chapter 3 and appendix B). In this huge data set, textural and microstructural characteristics are largely repetitive and cluster around two similar but distinct types, which are represented here by samples from profiles 1 and 2 of locality 1. Some other cases are exemplified here by one sample (Sa1a4) from locality 2. The protolith prior to shear zone formation is characterised by one weakly deformed sample (245a), which contains the sedimentary components still preserved.

Texture strength and degree of fabric anisotropy generally increase with distance from the basement, which will be interpreted also as gradients in finite strain and amount of recrystallisation. The three samples selected for each of the two profiles characterize these gradients.

### 2.4.1 Protolith.

***Sample 245a*** (fig 2.6a): The sample was collected south of the investigated shear zone and preserves an association of nummulites, echinoderma fragments and red algae. Two types of components were observed in the thin section. The first type consists of nummulite and echinoderm fragments whose size varies between 0.4 and 3.2 millimetres. Nummulite species *N. garnieri and N. fabianii* were identified. The shell of these organisms is made up of several rims of fibrous calcite showing a typical radial *c*-axis pattern. The echinoderm fragments are rounded calcite single crystals and constitute 20% of the rock. The second type of components consists of red algae mats. They appear as

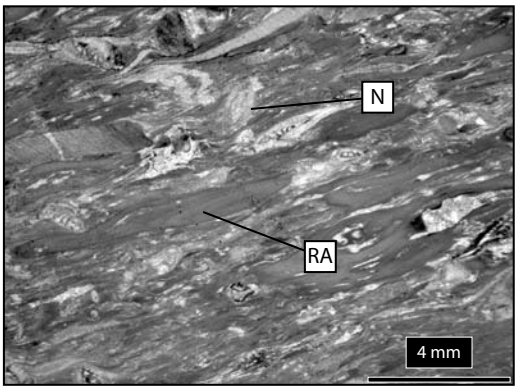


a

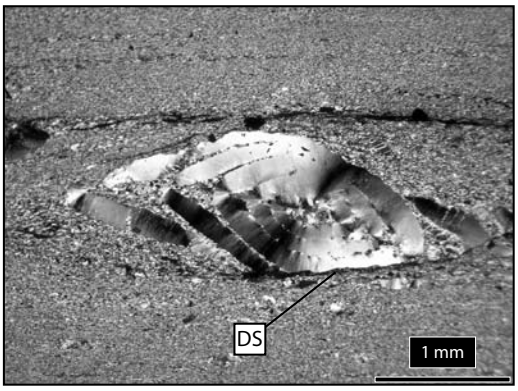


b

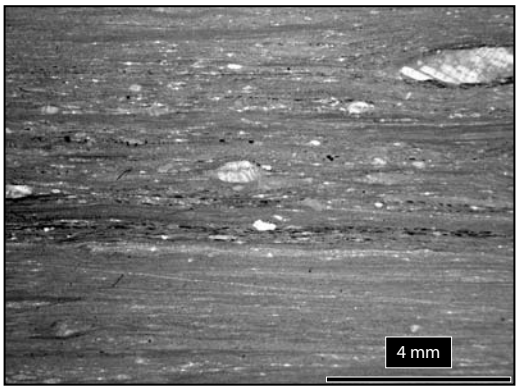


c

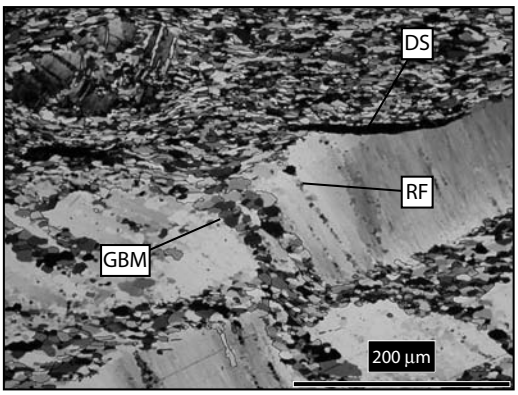


d

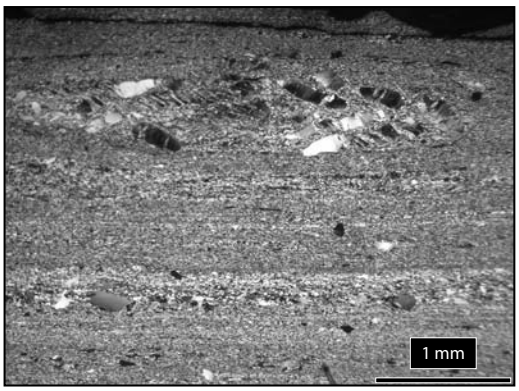


e


f

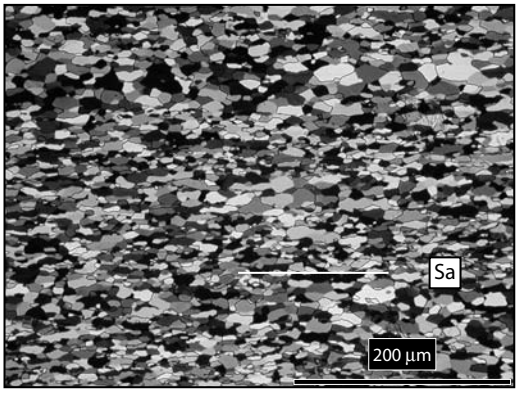


g

elongated patches with an average aspect ratio higher than 10:1. Their internal structure shows micritic calcite grains with very lobate boundaries and grain size ranging between 2 and 4 micrometres. These algae mats form between 50 and 60% of the rock. The rest of the rock consists of calcitic matrix material, as well as of detrital mica, quartz, or mud pellets.

Most of the clearly visible shape fabric anisotropy is attributed to primary sedimentary processes including compaction, but not to tectonic deformation during thrusting. Thus sample 245a is considered a typical protolith for the mylonites described below. It shows a texture that is very close to uniform, with faint preferred orientations of *a*-axes perpendicular to and *c*-axes within the bedding plane (fig 2.8, top). A very similar texture was observed in micritic Solnhofen limestone and attributed to passive alignment of calcite grains with their *c*-axes slightly preferred into the bedding plane (Wenk et al., 1973; Casey et al., 1998).

### 2.4.2 Profile 1.

Below we describe progressive deformation in three samples collected along profile 1 across the southern part of locality 1 (fig 2.3b).

***Sample MPY13*** (figs 2.6b, c)***:*** This sample shows a protomylonitic fabric, and dynamic recrystallisation affected all the biogenic components. The recrystallisation microstructures are heterogeneous, because the extent of their development is sensitive to the initial structure of the components.

Nummulites and echinoderm fragments typically show a "core and mantle" structure. New grains were produced by progressive subgrain rotation in echinoderm porphyroclasts. The internal structure in some nummulites is well preserved and still shows the radial *c*-axis pattern. Echinoderms are more competent than the surrounding fine-grained matrix and were fragmented by fracturing as well as deformed by twinning.

**Figure 2.6:** Photomicrographs of different limestone samples indicating mostly coaxial deformation (profile 1). Photomicrographs were taken from standard thin sections (30 μm thick) in transmitted light without polarizers (a, c), and from ultra-thin sections (2 μm thick) in cross polarized transmitted light (b, d, e, f, g). All sections are oriented normal to foliation and parallel to lineation (horizontal).
a) Nummulitic limestone protolith (sample 245a), weakly deformed prior to shear zone formation. Note the association of nummulites (N) and red algae (RA).
b, c) Sample MPY13 shows a strong horizontal Sa foliation and dissolution surfaces (DS) subparallel to Sa. The original radial *c*-axis distribution around the nummulite shell is still preserved.
d, e) Sample MPY5 shows a horizontally elongated nummulite shell. Microstructural features indicate grain boundary migration (GBM), rotation recrystallisation and pressure solution processes been active simultaneously. Recrystallisation festoons (RF) normal to the nummulite rim.
f, g) Sample MPY2 is an entirely recrystallised limestone with a grain shape preferred orientation horizontal (parallel to Sa) and symmetric calcite pressures fringes developed at the rim of detrital quartz grains.

Some 10% of the area contains nummulites and echinoderms that are still preserved.

The outer surfaces of nummulites are commonly oriented parallel to foliation. Dark outlines marked by relatively insoluble fine grained minerals (hematite, chlorite, micas) are interpreted as remnants of dissolved material indicating that pressure solution has also contributed to the deformation of these calcite rocks. Some external rims of the nummulites are fragmented during progressive deformation. Where fragmentation occurs, the internal parts of the nummulite shells show a greater degree of dynamic recrystallisation.

***Sample MPY5*** (figs 2.6d, e): The microstructure of this sample is characterized by further reduced volume fraction of initial components due to progressive deformation accompanied by dynamic recrystallisation. Pressure solution was also active, evident by locally dissolved nummulite and echinoderm fragments. Deformation affected the entire nummulite shells. The calcite fibres of the nummulite shells show lobate boundaries with bulges into neighbouring crystals, indicating grain boundary migration. Usually, bulges evolve into festoons of new grains along the fragments. Some of the fibres and their radial *c*-axis patterns are partially preserved. Nummulite shell aggregates are elongated parallel to lineation. The boundaries of primary twins in echinoderms are lobate indicating twin boundary migration. In some places, such twins are bent or overprinted by a second set of deformation twins. The percentage of nummulite and echinoderm fragments has been estimated at no more than 6%, the red algae mats constitute 20% of the rock.

***Sample MPY2*** (figs 2.6f, g): The main microstructural difference with respect to sample MPY5 is the lack of any relict nummulite shells. The grains of the dynamically recrystallised matrix are completely free of deformation twins and show slightly lobate boundaries. They occupy more than 90% of the rock. Pressure shadows filled with calcite fibres around detrital quartz grains are symmetrically developed with respect to the foliation.

***SPO analysis*** (fig 2.7): The SPO of the recrystallised matrix is similar in all three samples, therefore it is shown here only for sample MPY2. X-Z-sections of the matrix grains show a strong SPO parallel to the foliation with an average aspect ratio of 0.59 and a grain size mode of 12 μm. Y-Z-sections show SPO with the average long axis also parallel to foliation, an average aspect ratio of 0.81 and a grain size mode of 8 μm. In combination, the average grain shape ellipsoid is aligned parallel to the structural reference system XYZ and would plot near the diagonal in a Flinn-type diagram with K ~ 1.1 indicating a slightly prolate grain shape. The microstructure of the dynamically recrystallized matrix displays an orthorhombic symmetry with respect to foliation and lineation.

***Texture analysis*** (fig 2.8): X-ray texture analysis reveals a similar texture type for

all three samples of profile 1, but with strength increasing in the series ordered according to increasing distance from the basement. Even the weak texture of sample MPY13 is already significantly different from that of the protolith sample 245a. The pole figures display roughly maxima of *c*-axes normal to foliation and *a*-axes distributed along girdles parallel to the foliation.

In closer detail, pole figure maxima are elongated with some preference of rotations around the foliation normal, indicated by girdles and small circles in some pole figures. The *c*-axis pole figure of the most recrystallised sample (MPY2) shows two distinct maxima (cα and cβ) at the periphery of the pole figure, symmetrically oriented at 15° from Z. The CIP *c*-axis pole figure of the dynamically recrystallised matrix shows a similarly shaped but stronger maximum normal to the foliation (fig 2.9a). All textures are characterized by an orthorhombic sample symmetry, and the non-reduced +*a* and –*a* pole figures are approximately identical. The overall patterns are slightly asymmetric relative to the structural reference system by some minor rotations around the lineation, which may be attributed to misalignments with respect to the foliation plane during specimen collection and preparation.

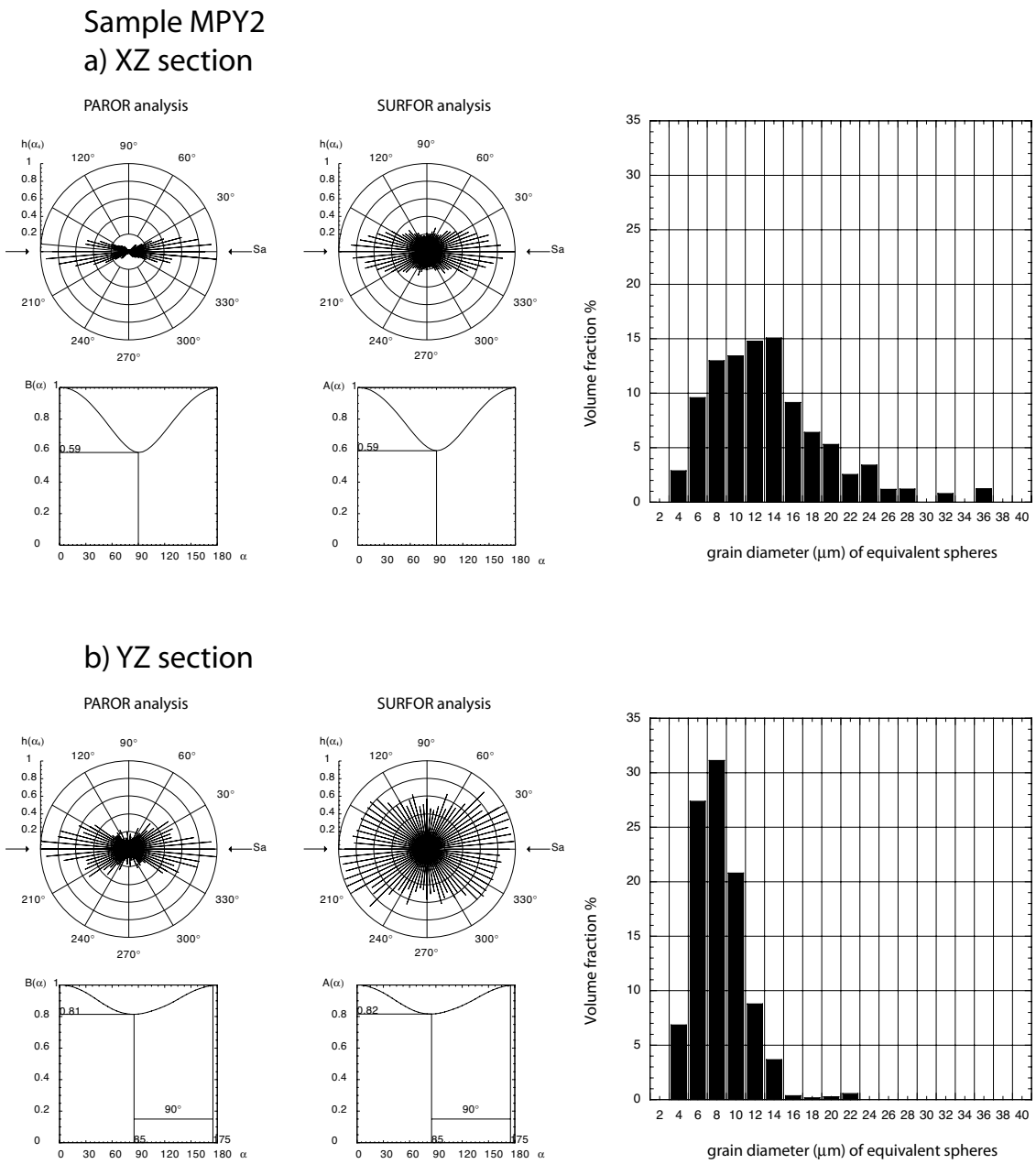


**Figure 2.7:** Microstructural analysis of mylonite sample MPY2 indicating coaxial deformation: The average grain shape ellipsoid is triaxial and parallel to the structural reference frame.
Rose diagrams for orientation distributions of particle long axes (PAROR) and of grain boundaries (SURFOR). Histograms of volume-weighted grain size distributions.
a) XZ-section, i.e. perpendicular to foliation and parallel to stretching lineation.
b) YZ-section, i.e. perpendicular to both foliation and stretching lineation.

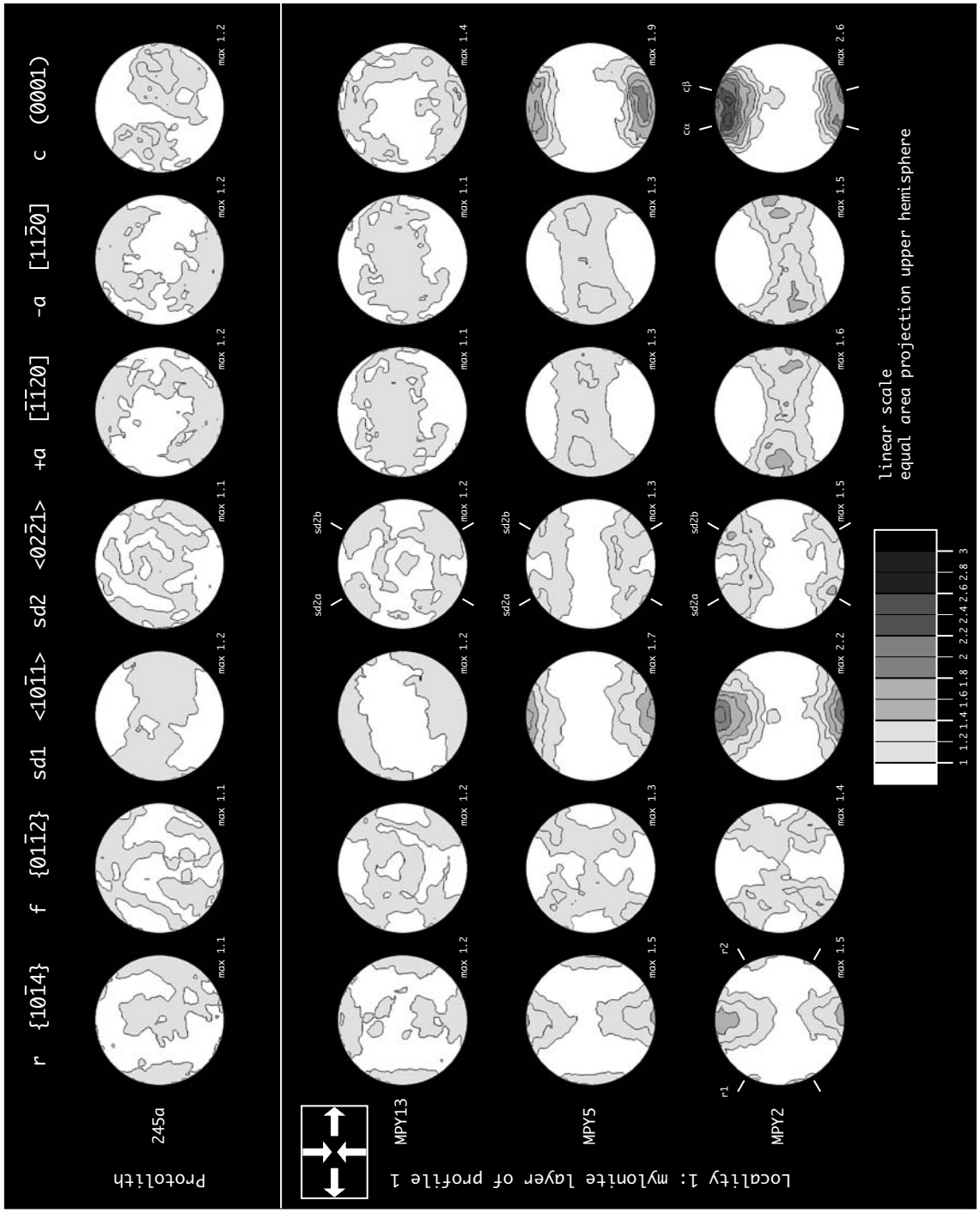


**Figure 2.8:** Texture evolution from the protolith (sample 245a) to mylonites across the limestone layer (profile 1). The protolith shows nearly uniform distributions, which are axial symmetric with faint maxima of *a*-axes perpendicular and of *c*-axes parallel to the bedding plane (S0). The three samples from profile 1 show similar textures of increasing strength with increasing degree of mylonitization (sorted from top to bottom). Bulk textures obtained by X-ray texture goniometry, all pole figures calculated from the ODF. Pole figure contours are given in multiples of a uniform distribution with a contour interval of 0.2. Intensities below 1 are neglected. The projection is perpendicular to the macroscopic foliation and the stretching lineation is horizontal in the projection plane, equal area projection of upper hemisphere.

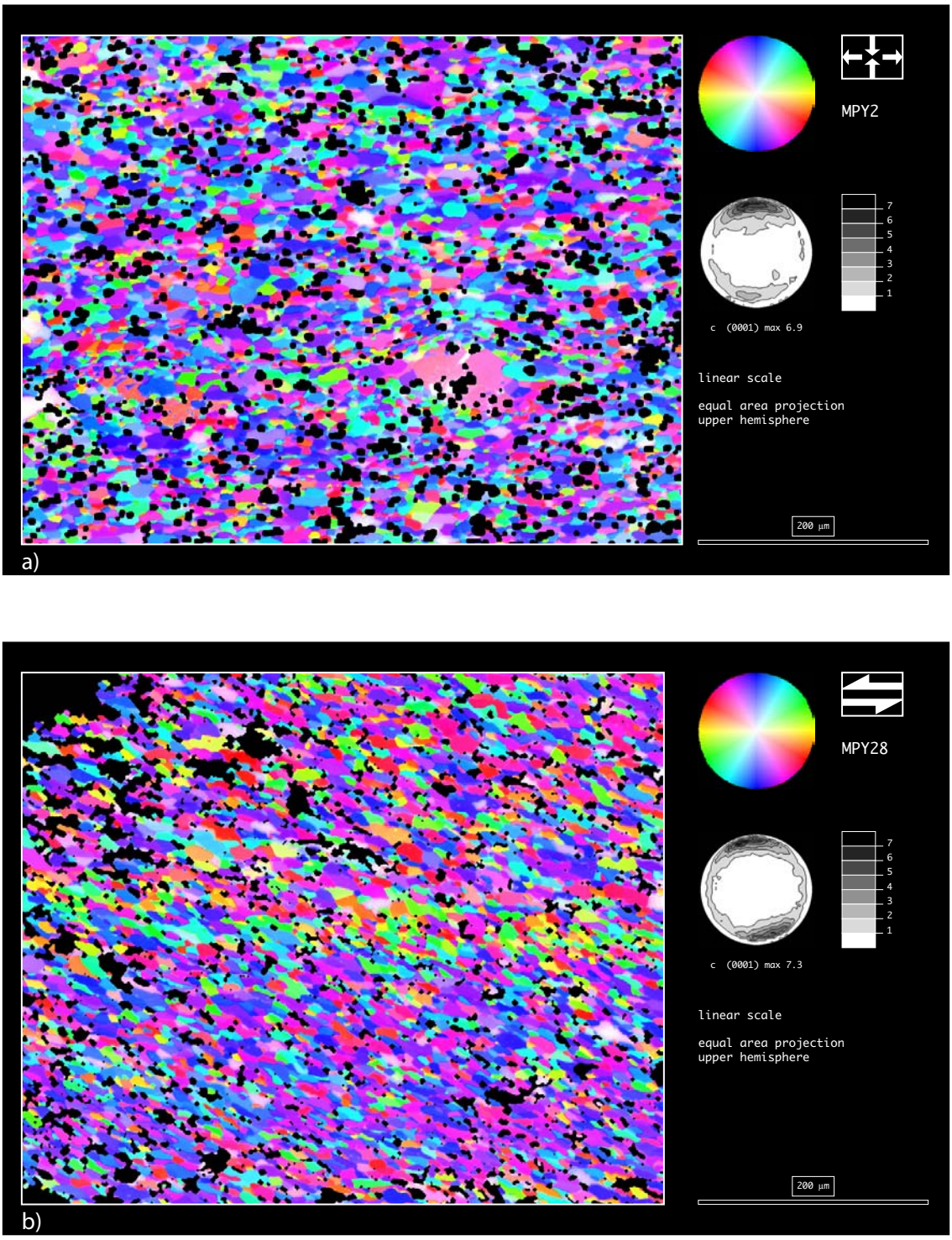


**Figure 2.9:** Computer Integrated Polarization (CIP) images and derived *c*-axis distributions. Color look-up table stereogram at upper right. Contours of the *c*-axis pole figure given in multiples of uniform distribution with intervals of 1. Specimen orientation as above perpendicular to macroscopic foliation Sa, stretching lineation is horizontal.
a) sample MPY2; b) sample MPY28, sinistral sense of shear.

2.4.3 Profile 2.

Below we describe progressive deformation along profile 2 across the sinistral shear zone in the northern part of the outcrop at locality 1 (fig 2.3c). These rocks were deformed under similar conditions as the ones from profile 1, and similar processes of dynamic recrystallization and/or pressure solution are inferred. The specific samples were selected to match pairwise those from profile 1 in terms of the extent of dynamic recrystallization and of texture strength.

***Sample Gtab2*** (fig 2.10a): The dynamically recrystallised matrix possesses an inhomogeneous grain size distribution, where diffuse patches of very fine grain size result from red algae remnants. While the grain size distributions are comparable between this sample and sample MPY13 from profile 1, the SPO of their dynamically recrystallised grains are different. This sample shows an asymmetric SPO oblique to the macroscopic foliation and consistent with sinistral shearing of the rock, which is further confirmed by asymmetric calcite pressure shadows developed at the rim of detrital quartz grains.

***Sample Gtcsf2*** (fig 2.10b, c): In this sample the volume fraction of recrystallized grains, and presumably also strain intensity, is similar to that of sample MPY5 from profile 1. The matrix of this sample shows a clearly oblique SPO compatible with sinistral shearing, further confirmed by asymmetric calcite pressure shadows developed at the rim of detrital quartz grains.

***Sample MPY28*** (fig 2.10d, e): The microstructure is dominated by S-C-structures. The secondary foliation Sb is at 30° to the primary foliation Sa, and calcite fibers at the rim of detrital quartz grains show a clear asymmetry consistent with sinistral shearing of the rock. There are no deformation twins in the recrystallised matrix.

***SPO analysis*** (fig 2.11): The SPO of the recrystallised matrix is similar in all three samples, therefore it is shown here only for sample MPY28. In the X-Z section grains have an average aspect ratio of 0.53 with preferential elongation at 15° to the foliation. This SPO angle is only half the angle of Sb to Sa, which was intuitively estimated from the micrographs of fig 2.10. This indicates some bias towards grain boundaries instead of grain long axes in the visual determination of Sb. The grain size distribution has a mode of 12 μm. The measurements in the Y-Z-section indicate flattening of the grains parallel to the foliation with average aspect ratio of 0.81. In combination, the average grain shape ellipsoid is rotated around Y by 15° with respect to the structural reference system XYZ. It would plot near the diagonal in a Flinn-type diagram with K ~ 1.2 indicating a slightly prolate grain shape.

***Texture analysis*** (fig 2.12): Like in the sample series of profile 1 (fig 2.8), the three samples possess textures of similar type, but with increasing strength. The weakest

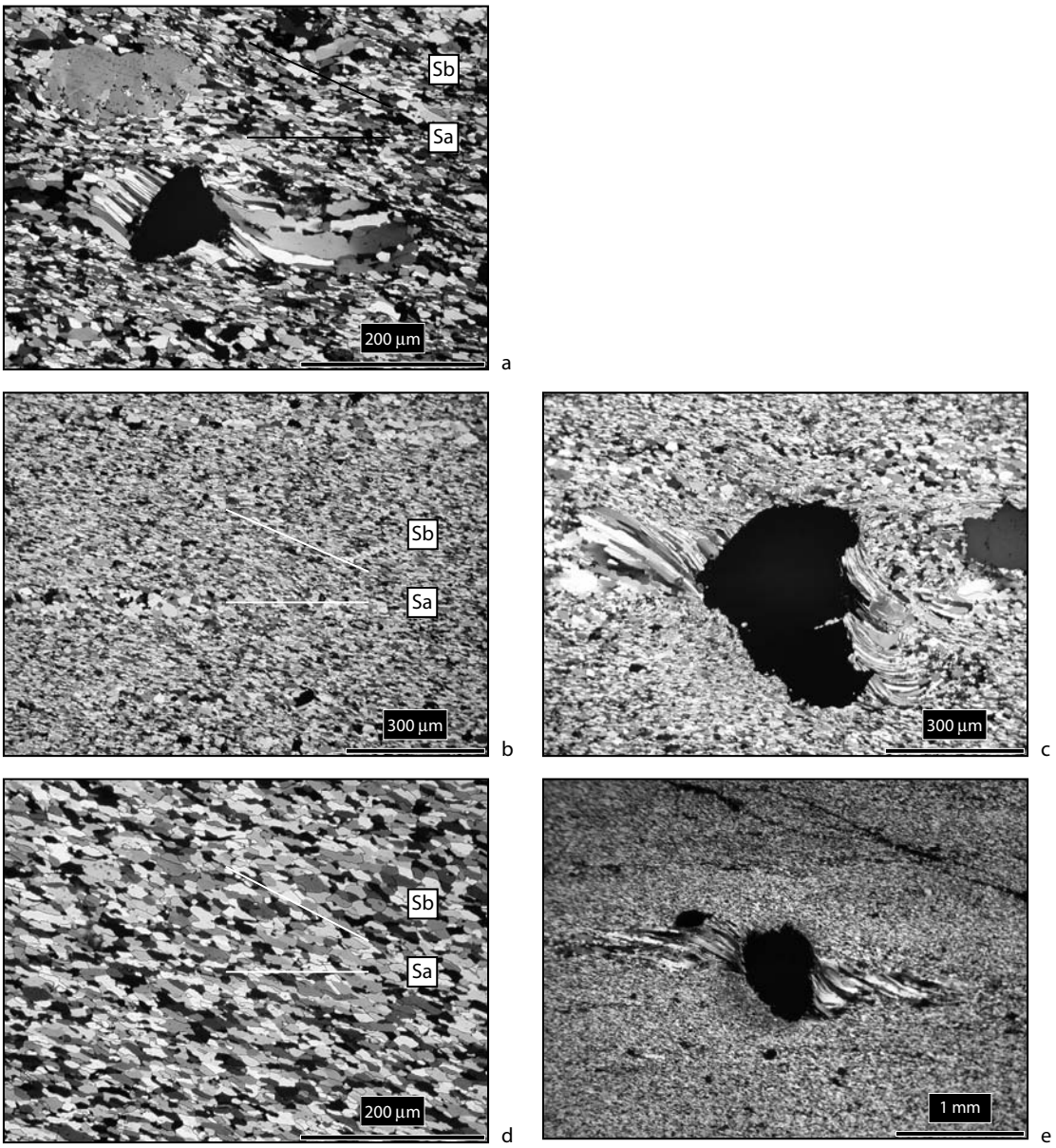


**Figure 2.10:** Photomicrographs of samples indicating non-coaxial deformation, taken from ultra-thin sections in cross polarized light.
a) sample Gtab2; b, c) sample Gtcsf2; d, e) sample MPY28.
Asymmetric calcite pressure fringes developed at the rim of detritical quartz grains (a, c and e). Oblique grain shape preferred orientation (Sb) consistent with sinistral sense of shearing in the rock (a, b and d).

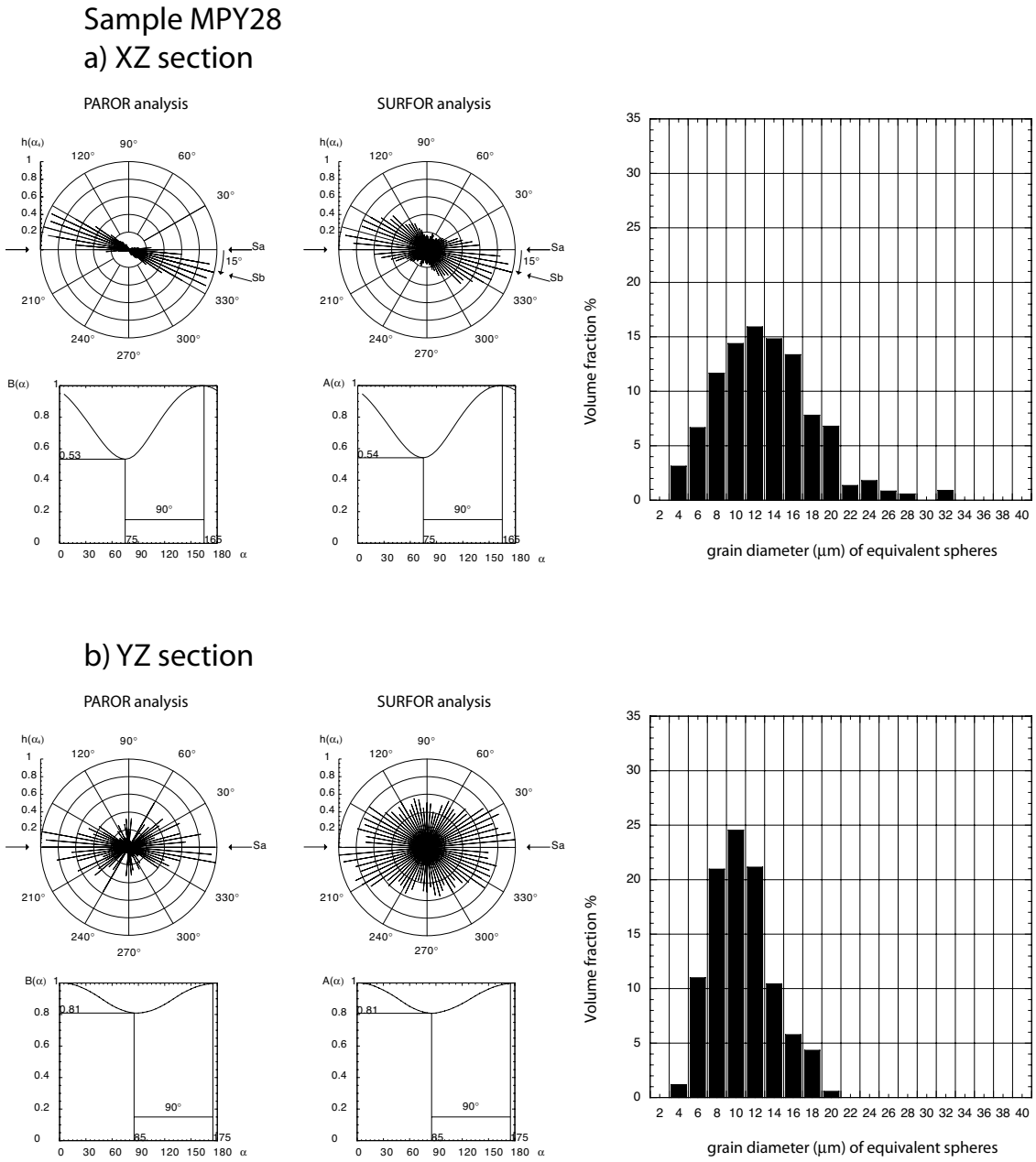


**Figure 2.11:** Microstructural analysis of mylonite sample MPY28 indicating non-coaxial deformation: The average grain shape ellipsoid is triaxial and oblique to the structural reference frame. Same representation as fig 2.7. The grain size distributions show no major differences compared to sample MPY2.
a) XZ section, i.e. perpendicular to foliation and parallel to lineation. Average grain long axis inclined by 15° to Sa, compatible with sinistral shearing.
b) YZ section, i.e. perpendicular to both foliation and lineation. Note the slight flattening of the grain shape.

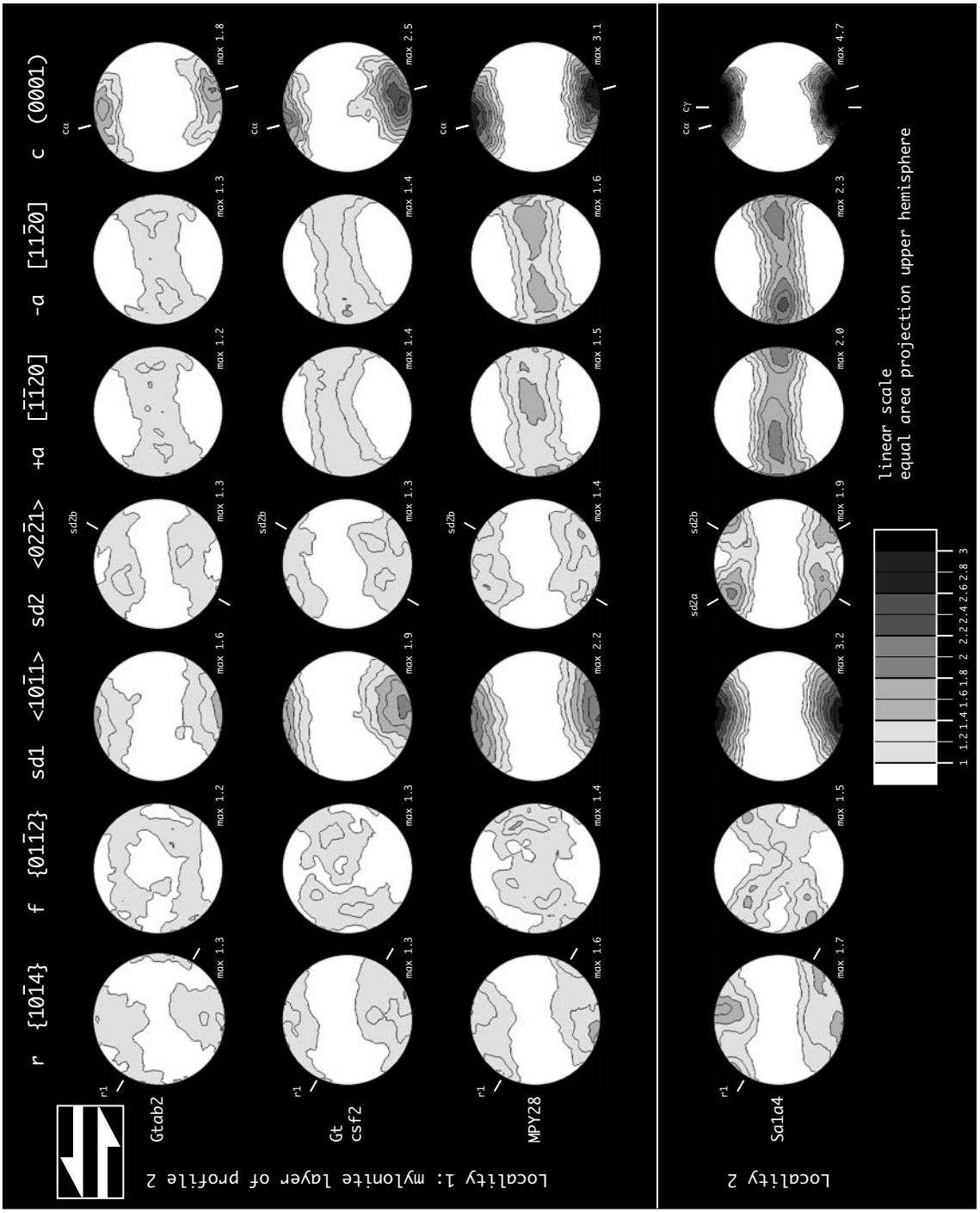


**Figure 2.12:** Texture evolution in the ultramylonitic band (profile 2). Foliation and stretching lineation are horizontal, sinistral sense of shear. Same representation as in fig 2.8.
Sample Sa1a4 originates from locality 2 (fig 2.2) and represents intermediate strain kinematics.

texture of sample Gtab2 has similarly low maxima as sample MPY13, though they are strong enough to distinguish it from MPY13 as well as from the protolith sample 245a. In difference to profile 1, the textures of profile 2 are asymmetric with reference to foliation and lineation, i.e. *c*-axis maxima are at 15° from the foliation normal towards the lineation, and girdles of *a*-axes are similarly inclined to the foliation by counter clockwise rotation of 15° about the structural Y-axis. Corresponding asymmetries are particularly visible in the *r*- and the *sd2*-pole figures. In reasonable approximation, all pole figures contain a two-fold rotational symmetry about the structural Y-axis.

The pole figures of the most recrystallized sample MPY28 show considerably stronger maxima compared to the other two samples of profile 2. The poles to the *r*-planes show one maximum close to Z and another one at position labelled "r1". The pole figure for the *sd2*-slip direction shows two maxima symmetrically oriented with respect to the foliation but with different intensities. Along the girdle distributions of the *a*-axes, the +*a*-direction has the maximum in the projection center, while the –*a*-direction shows two maxima oppositely inclined at 60° from it. The *c*-axis is tilted by 15° in the sense of shear, which is confirmed by the CIP pole figure (fig 2.9b).

Both microstructure and texture of the dynamically recrystallized matrix indicate a monoclinic symmetry, with the structural Y-direction as the two-fold symmetry axis.

### 2.4.4 Ultramylonite sample with symetric characteristics.

Sample Sa1a4 was taken at locality 2 (fig 2.2), which is east of and along-strike from the outcrop of the two profiles at locality 1. It originates from the hinge of a fold that re-deformed previously formed calcite mylonites and separates two basement boudins including their Eocene cover. The grain size distribution is very similar to those found in samples MPY2 and MPY28, and likewise the dynamically recrystallised matrix covers more than 90% of the volume. The microstructure shows a clear grain shape foliation Sb oriented at 25° to the foliation (fig 2.13a). The grains show sharp extinction and no deformation twinning. Incipient S-C type structures are locally recognizable. Calcite pressure shadows at the rims of detrital quartz grains show an asymmetry and confirm a sinistral sense of shearing (fig 2.13b). Quantitative analysis (fig 2.13c) on the X-Z section yields an average aspect ratio of 0.59 with preferred elongation at 25° to the lineation, and a grain size mode of about 12 $\mu$m.

This sample Sa1a4 shows a texture that is intermediate between that of samples MPY2 and MPY28 (fig 2.12, bottom): the *c*-axes form a broad and strong maximum roughly normal to the foliation. The *r* planes and *a*-directions are fairly similarly oriented as in MPY28, whereas *sd1* and *sd2* are similar to the patterns in MPY2. The symmetry

of the pole figures deviates visibly from monoclinic about the Y-axis of the structural reference frame, but could be brought into approximate orthorhombic symmetry after rotating the reference axes X and Y within the foliation plane by 30°.

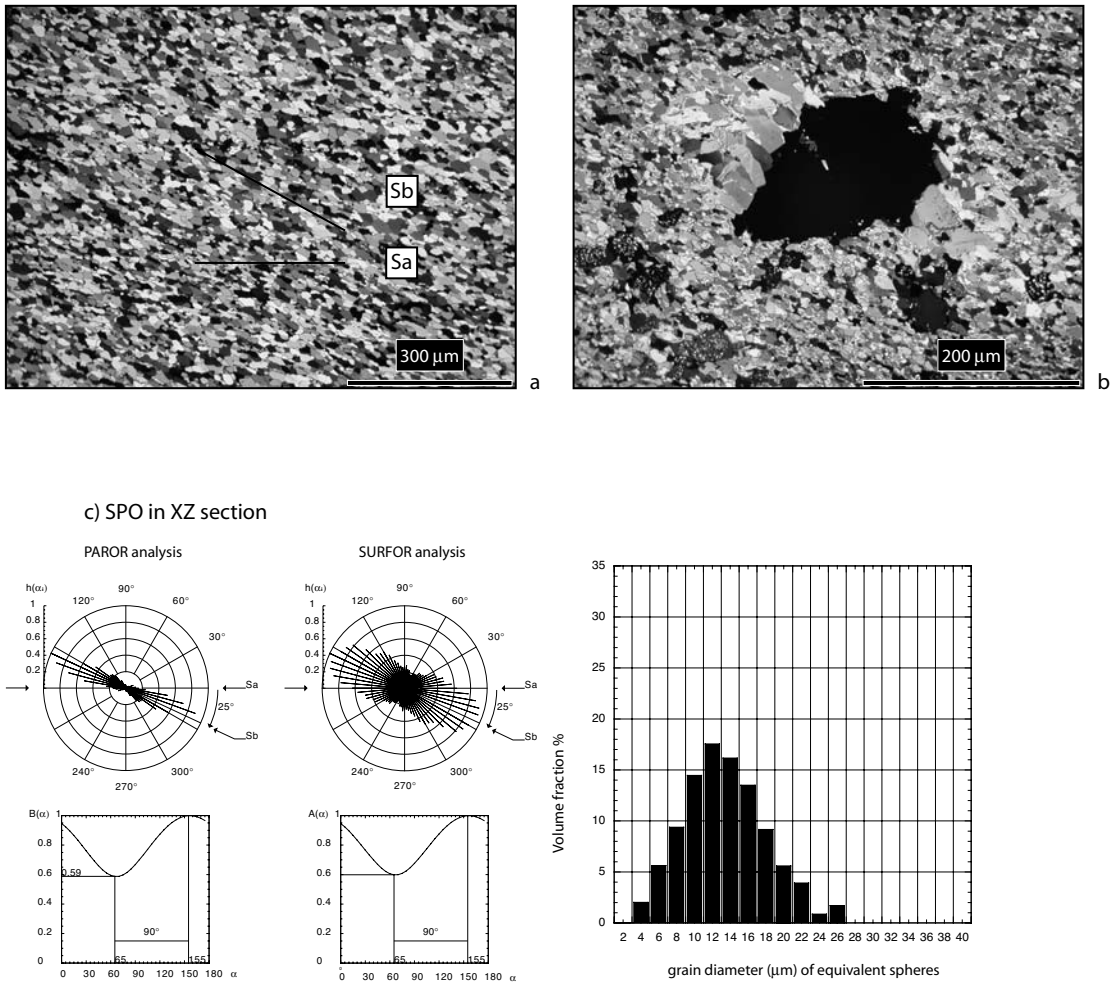


**Figure 2.13:** Microstructure of sample Sa1a4 from locality 2.
a, b) Photomicrographs of thin sections in cross polarized light. Oblique grain shape preferred orientation and asymmetric calcite pressure fringes developed at the rim of detrital quartz grain are both indicative of sinistral shear.
c) Microstructural analysis. Grain shape preferred orientation is oblique to Sa by 25° compatible with sinistral shearing of the rock. Grain size distribution is similar to that in XZ sections of samples MPY2 and MPY28.

2.4.5 ODF sections and ideal crystal orientation models.

In the following, the different texture types found in profiles 1 and 2 and at locality 2 will be discussed. Samples MPY2 and MPY28 are used to represent profiles 1 and 2, respectively, since they exhibit the most strongly developed textures in the two series of samples. Sample Sa1a4 from locality 2 represents a third texture type found repeatedly along the RYSZ.

All textures observed for the limestone mylonites have in common, that the *c*-axes are preferentially oriented towards directions at the pole figure periphery and nearly normal to the foliation plane. Consequently, the ODF sections displayed in fig 2.14 are restricted to sections between $\Phi = 60°$ and 120°, where the highest ODF densities occur along fibres for fixed Euler angles close to $\Phi = 90°$ and $\psi_1 = 90°$ and variable $\psi_2$.

Apart from this general similarity, the three sample textures occupy several orientations with different frequency. In an attempt to highlight these differences, model textures are constructed from a set of five ideal crystal orientation components M1, M2, M3, M4 and M4'. The orientations (defined in fig 2.15) and width (40°) of the components were fixed, and only their volume fraction, i.e. there relative weight, was varied, until a satisfying match to the sample textures was found by manual trial-and-error (Table 1). It is emphasized that all three model textures contain between 50 and 75% volume of grains with orientations drawn from a uniform distribution, which means that the visible ODF maxima are actually built of comparatively small volume portions of the sample. In all three cases, M1 is the strongest component, while the second strongest component is either M2 (profile 1) or M3 (profile 2) or M4 (locality 2).

Orientation M1 places the *c*-axis at an angle of 15° counterclockwise from the Z-direction of the sample. Two single poles of *r* and *f*-planes are located at the periphery of the pole figure at angles of about 60° and 50° from Z in a conjugate geometry, respectively. These *r* and *f*-planes contain a *sd2*- or a *sd1*-direction at the periphery of the pole figure. A second *sd2* direction in the *f* plane is not far off the periphery of the pole figure.

Orientation M2 results from M1 by a rotation of 180° around either the X or Z-axis. Its projection looks like the mirror image of M1 with respect to either the Y-Z or X-Y plane, but with the sign of the *a*-axes inverted.

Orientation M3 is related to M1 by a 60° rotation around the *c*-axis at c$\alpha$. Both orientations place the basal plane at an angle of 15° counter clockwise from the plane normal to Z (foliation). Their projections appear as mirror positions with respect to the basal plane, again with sign inversion for the *a*-axes.

The orientations M1, M2 and M3 have a two-fold symmetry axis (crystal *a*-axis) parallel to Y. Thus a texture that only consists of any amount of these components has

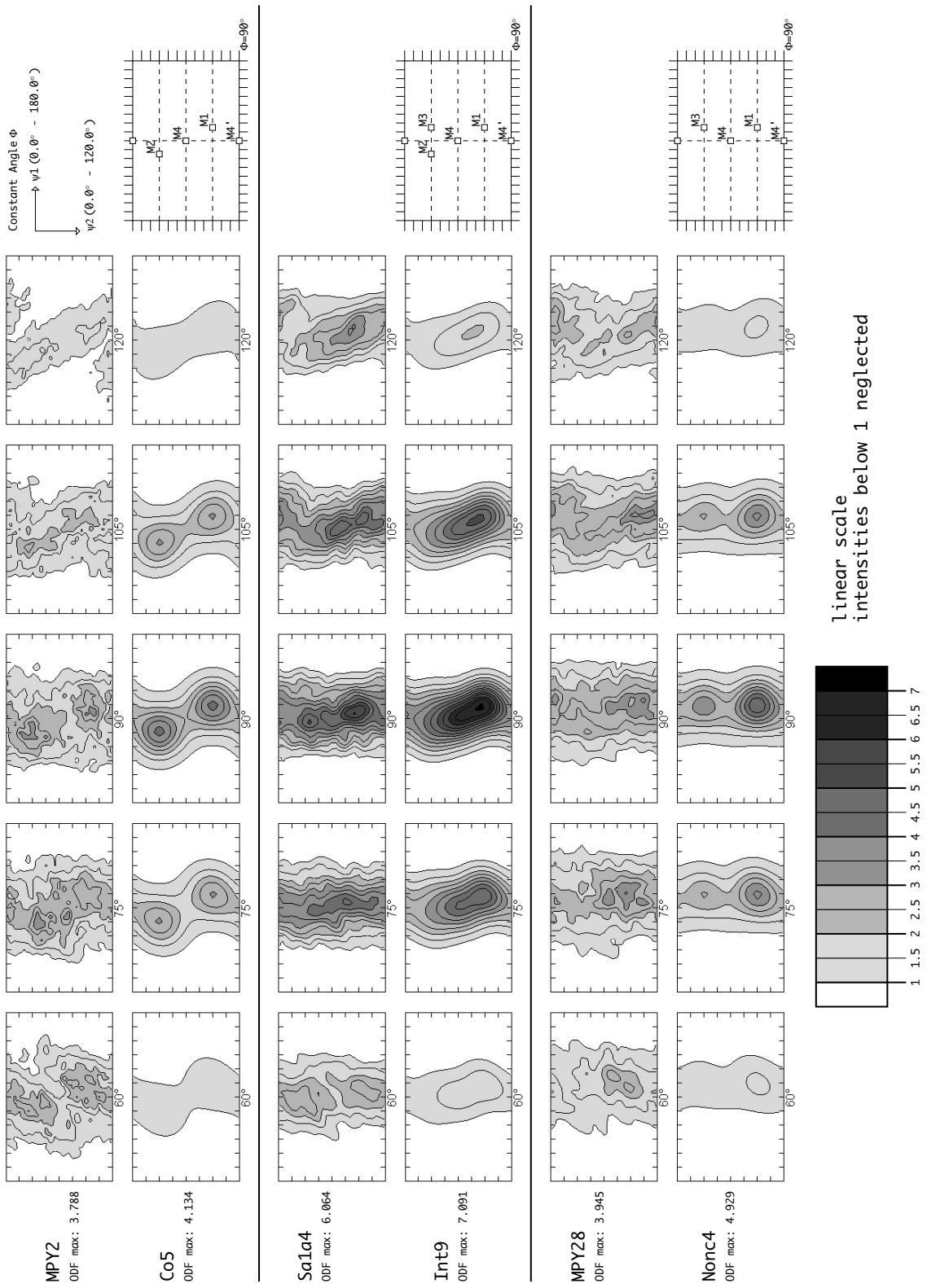


**Figure 2.14:** ODF sections for constant Φ between 60° and 120° for the three most recrystallized samples (MPY2 from profile 1, Sa1a4 from locality 2, MPY28 from profile 2) and for three corresponding idealized model distributions (co5, int9 and nonco4). The ideal crystal orientations M1, M2, M3, M4, M4' at Φ = 90° are illustrated in fig 2.15.

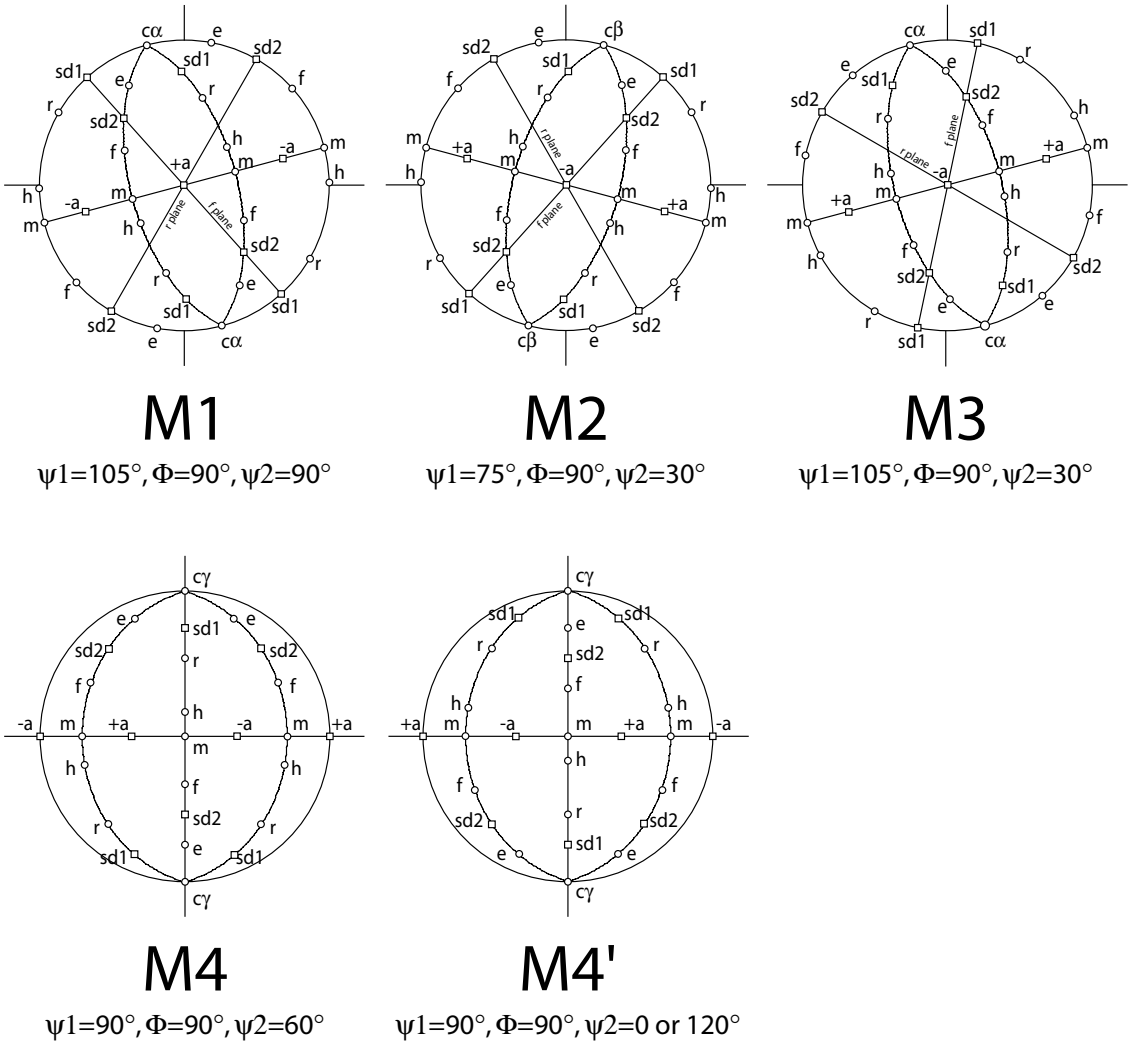


**Figure 2.15:** Equal area projections (upper hemisphere) of ideal crystal orientations used as centers for model distributions. Relevant crystal directions (squares) and poles (circles) are marked.

| Texture components (%) / Model | Random | M1 | M2 | M3 | M4 | M4' |
|---|---|---|---|---|---|---|
| Co5 | 75 | 10 | 10 | 0 | 2.5 | 2.5 |
| Int9 | 50 | 17.5 | 7.5 | 5 | 15 | 5 |
| Nonco4 | 75 | 12.5 | 0 | 7.5 | 2.5 | 2.5 |

**Table 1:** Volume fractions of orientation components in the three model distributions.

at least monoclinic symmetry with symmetry axis Y. A texture only with M1 and M2 in equally large portions possesses orthorhombic sample symmetry. If only M1 and M3 would be present in equal shares, then the texture would resemble hexagonal crystal (and sample) symmetry with respect to the crystal *c*- and *a*-axes.

The orientations M4 and M4' have their *c*-axis parallel to Z, and an *a*-axis parallel to X. They are mutually related by a 180° rotation around Y. If they are equally present then the texture preserves monoclinic symmetry, otherwise the two-fold symmetry around Y is broken.

The pole figures for the three models are shown in fig 2.16 to be compared with those for the samples of profile 1 (fig 2.8), profile 2 (fig 2.12) or locality 2 (fig 2.12, bottom). They resemble particularly the symmetry of the three texture types, which is orthorhombic for profile 1 (model co5), monoclinic for profile 2 (model nonco4), and asymmetric for locality 2 (model int9).

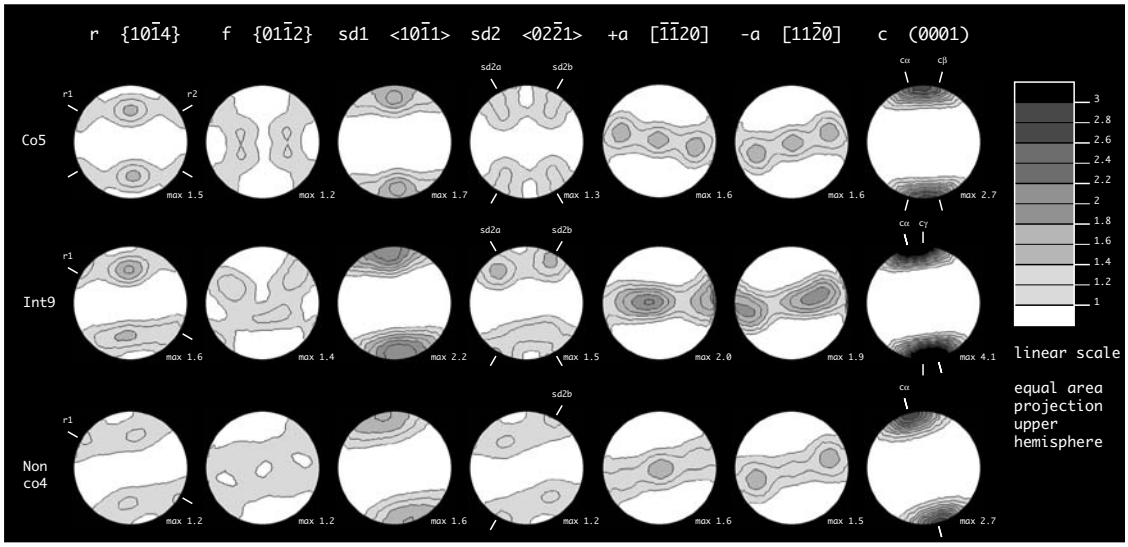


**Figure 2.16:** Pole figures for the three idealized model distributions (co5, int9 and nonco4); same cases as in fig 2.14. Same representation as for the studied samples (figs 2.8 and 2.12).

### 2.4.6 Inverse pole figures.

Inverse pole figures (IPF) were calculated in order to show the preferential orientation of crystal planes and directions with respect to certain sample directions (fig 2.17). These are foliation normal (Z=FoN), stretching lineation (X=StLin), intermediate direction (Y=IntDir), two conjugate directions at 45° between X and Z (45°CCW and 45°CW), directions 15° counter clockwise (cα) and 75° clockwise (cαN) from Z around Y, directions 15° clockwise (cβ) and 75° counter clockwise (cβN) from Z around Y.

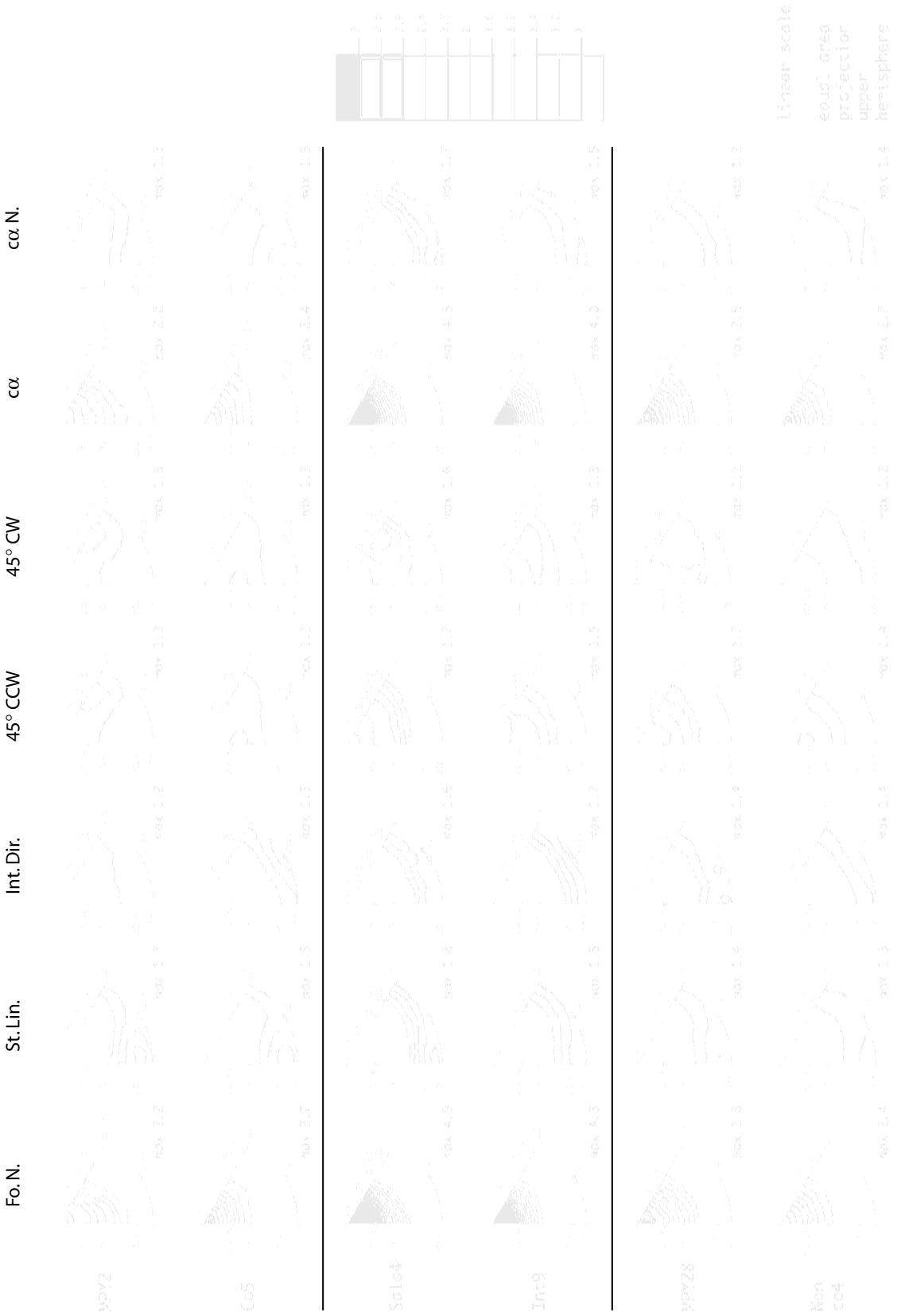
Fo. N.
St. Lin.
Int. Dir.
45° CCW
45° CW
cα
cα N.

Like the ODF and pole figures, the IPF show similar general characteristics. The IPF for Z and cα have the sharpest concentrations, which are towards the *c*-axis. The IPF for X and Y show girdle distributions along directions in the basal planes, where the lineation (and similarly cαN) is preferentially aligned normal to poles of *m*-prisms or *h*-rhomboeders, and the intermediate direction has a somewhat higher concentration of *a*-axes. The IPF for the two conjugate directions (45° CCW, 45° CW) show maxima near *r*- and *f*-rhomboeder planes and *sd1* and *sd2*-directions. Subtle differences are noticed, as only samples from profile 1 and locality 2 show some shoulder towards *r* in the IPF for Z, and only for profile 1 the two IPF for 45°CCW and 45°CW are identical, as expected for symmetry reasons.

## 2.5 Discussion.

### 2.5.1 Deformation mechanisms.

The microfabric evolution shows the following characteristics with increasing distance to the basement along both profiles 1 and 2: (1) The extent of dynamic recrystallisation increases. (2) The dynamically recrystallised grains show an increasing degree of shape preferred orientation. (3) Increasingly stronger textures develop. These observations lead to the interpretation that the spatial gradient across the profiles also maps gradients in finite strain, and that deformation has most likely occurred by dominant dislocation creep accompanied by dynamic recrystallisation. While there is some evidence also for pressure solution and re-precipitation, grain boundary sliding and/or diffusion creep were presumably not the dominant deformation mechanisms in our samples, because those are expected to result in rocks with isotropic fabrics (Edington 1976, Schmid et al. 1977, Padmanabhan & Davies 1980, Schmid et al. 1987, Rutter & Brodie 1988).

### 2.5.2 Kinematics of deformation: coaxial vs. non-coaxial.

The samples from profile 1 exhibit microfabric characteristics, notably in terms of SPO and texture measurements, which possess orthorhombic sample symmetry with respect to the structural reference frame, defined by lineation X, foliation normal Z and

**Figure 2.17:** Inverse pole figures for the three most recrystallized samples (MPY2 from profile 1, Sa1a4 from locality 2, MPY28 from profile 2) and for three idealized model distributions (co5, int9 and nonco4), same cases as in fig 2.14. Sample reference directions are foliation normal (Fo. N.), stretching lineation (St. Lin.), intermediate direction (Int. Dir.), two conjugate directions at 45° between lineation and foliation normal, the directions of *c*-axis maxima (cα and cβ) and perpendicular to them (cαN and cβN) along the pole figure periphery. Contouring as in fig 2.8, equal area projection of upper hemisphere.

intermediate strain axis Y. Fabrics are approximately symmetric with respect to rotations by 180° around these three axes, which is almost equivalent to mirror symmetries perpendicular to them. They do not indicate any preferred sense of shearing, i.e. do not contain any record of dominant non-coaxial (simple shear) deformation. We interpret these rocks to be deformed under a coaxial deformation path, where all three principal axes are distinct, which is presumably close to plane strain, i.e. pure shear. The inferred principal stress axes nearly coincide with the axes of the structural reference frame of profile 1, i.e. σ1 is oriented about normal to the macroscopic foliation and σ3 falls near the stretching lineation, which independently demonstrates conditions of coaxial strain.

The samples from profile 2 possess microstructures and textures that have no more than monoclinic sample symmetry with a single two-fold symmetry axis around the intermediate strain axis Y. It is emphasized that the fabric symmetry could not be raised just by redefinition of the reference frame, but that there are distinct features oriented relative to each other that break orthorhombic symmetry. These are S-C fabrics and asymmetric pressure fringes in the microstructures, and the position and weight of orientation components relative to each other as well as relative to primary and secondary foliation planes in the textures. Only the intermediate axes σ2 of the inferred principal stress tensor roughly coincides with an axes (the Y-axis) of the structural reference frame of profile 2, while σ1 and σ3 are oriented at equally large angles to foliation and lineation. All this is clear evidence that deformation of these samples must have occurred on a non-coaxial deformation path with vorticity axis towards Y, i.e. simple shear in the idealized case of plane strain deformation.

The samples of the two profiles exhibit different types of fabrics, which developed in the same lithology through simultaneous deformation under the same PT-conditions. Therefore the deformation mechanisms and internal conditions (like ratios between critical resolved shear stresses for activating different slip systems) should have been identical. Hence, the differences in texture evolution relate to different kinematics of deformation.

### 2.5.3 Asymmetric fabrics.

The microstructure of sample Sa1a4 indicates that this rock was deformed by a significant amount of rotational deformation. Its texture shows similarities with the textures of sample MPY2 (profile 1, coaxial) as well as of sample MPY28 (profile 2, non-coaxial). It differs from both as it does not equally balance the orientation components around M4 and M4'. This means, none of the three structural reference axes is actually a two-fold symmetry axis anymore, and the strain path must have deviated from plane

strain. It remains puzzling that the texture resembles nearly orthorhombic symmetry with respect to axes rotated by about 30° relative to X and Y within the foliation plane, because those apparent symmetry directions have no pendant in the field when back-projected into geographic coordinates.

2.5.4 Suitably oriented slip systems.

The following slip systems have been confirmed as dominant slip systems for calcite in experiments of Turner et al. (1954), Griggs et al. (1960), Turner & Heard (1965), Weiss & Tuner (1972, Braillon & Serughetti (1976), Spiers & Wenk (1980), and De Bresser & Spiers (1990, 1993, 1997):

| | |
|---|---|
| *r* {10-14} *sd2* <02-21> | Turner et al., 1954<br>Griggs et al., 1960<br>Turner and Heard, 1965<br>Weiss and Turner, 1972<br>Braillon and Serughetti, 1976<br>Spiers and Wenk, 1980<br>De Bresser and Spiers, 1990<br>De Bresser and Spiers, 1993 |
| *f* {01-12} *sd2* <02-21> | Turner et al., 1954<br>Griggs et al., 1960<br>Spiers and Wenk, 1980 |
| *f* {01-12} *sd1* <10-11> | De Bresser and Spiers, 1990<br>De Bresser and Spiers, 1993<br>De Bresser and Spiers, 1997 |
| *c* {0001} <*a*> | De Bresser and Spiers, 1997 |

Assuming ideal plastic rheology of an isotropic material, the maximum shear stress is resolved on two conjugate planes oriented at 45° between the two extreme principal stress directions, where the normal to one plane is also the shear direction on the other plane. In coaxial deformation, the principal directions of stress fall together with those of strain rate as well as finite strain, thus the maximum shear stress is expected on planes at 45° to X and Z. In simple shear as a special case of non-coaxial deformation, the principal directions are identical for stress and strain rate, but those of finite strain rotate with progressive deformation around the Y axis and converge to a position, where σ1 and σ3 make equal angles of 45° both to X and Z. Given that deformation was dominated by simple shearing and has reached high shear strain, the angle between the shear zone boundary and the macroscopic foliation is very small, and it can be assumed that the σ1

direction lies for sinistral shear near the upper-right/lower-left corners of the XZ-plane. In other words, the maximum shear stress is then resolved on the foliation plane and on the plane perpendicular to the lineation. While both positions are equally suited at a local scale, only shear on the foliation plane along lineation is geometrically feasible at the larger scale of a shear zone.

For any given crystal orientation, those slips systems are most likely to be activated on which the highest shear stress is resolved, i.e. which are closest to the above planes and directions of maximum resolved shear stress. Our paleostress analysis may have given some indications for the principal directions of stress, but there is hardly any knowledge on the magnitudes of the principal stresses. Therefore we restrict the following discussion on qualitative arguments instead of attempting to quantify the resolved shear stress by means of the Schmidt factor, which would require further assumptions on the complete stress tensor.

For coaxial deformation (e.g. pure shear) as inferred for the samples from profile 1, their ideal crystal orientations M1 and M2 both have a *r*[*sd2*] and a *f*[*sd1*] slip system suitably oriented, and to a lesser extent also a *f*[*sd2*] system. The *a*-direction that is parallel to the Y-axis is geometrically disabled to slip, and the other two basal [*a*] slip systems are rather unsuitably oriented. For the orientations M4 and M4', the resolved shear stress vanishes for all three basal slip systems, but slip on conjugate pairs of *r*[*sd2*] and *f*[*sd2*] is possible.

For non-coaxial deformation (e.g. simple shear) as inferred for the samples from profile 2, their main orientations M1 and M3 have *r*- and *f*-planes oriented at 60° and 50° to the foliation, which thus are not well oriented slip planes. The basal plane, inclined at 15° to the foliation "with the sense of shear", is the only potential slip plane that is close to the orientation of the bulk shear plane, and which could have been activated by duplex slip along the two *a*-directions that are not parallel to Y. However, given the angle of 15° between basal plane and foliation, it appears that antithetic slip along the *f* or *r* planes would also be needed in order to maintain homogeneous simple shear deformation (Mancktelow 1987, Schmid 1994). Basal [*a*] slip systems are perfectly oriented for the orientations M4 and M4', which, however, do not constitute the primary orientation components in the textures along profile 2.

### 2.5.5 Textures in experimentally deformed samples.

The pure shear textures are similar to the "high temperature type" textures obtained in pure shear experiments of micritic limestones performed by Wagner et al. (1982) in a testing apparatus with three independent stress actuators at 400°C. This experimentally

produced texture consists of two stronger maxima at the periphery of the pole figure, 30° on either side of the sigma 1 direction and a third weaker maximum parallel to the sigma 3 direction. Except for the weaker maximum, our textures resemble the HT-type textures of Wagner et al. (1982), for which slip on the *r*- and *f*-planes was inferred to be the dominant deformation mechanism. The corresponding microstructures (Kern and Wenk 1983) show a strong SPO consistent with the imposed coaxial strain path and no twinning or dynamic recrystallisation. Also in case of our natural samples at Rocher de l'Yret no twinning is observed. Hence the absence of twinning at higher temperatures appears to be an important criterion of distinction between "low" and "high temperature" deformation in the sense of Wagner et al. (1982), especially in the texture evolution (see also Schmid et al. 1987 their "twinning" vs. their "intracrystalline slip" regime). Twinning activity is further suppressed due to the small grain size in the limestone and in our mylonites, while a coarse grained marble would still easily twin under the same conditions. Model simulations of the texture evolution by dislocation glide are consistent with the observed textures in the absence of twinning (Wagner et al 1982, Kern & Wenk 1983, Wenk et al. 1987).

Since the pure shear experiments have not been carried out to high enough strains the role of dynamic recrystallization for texture evolution could not be assessed experimentally. It is likely that recrystallization by subgrain rotation and local boundary migration processes do not alter the texture type but strengthen the texture with progressive deformation similarly as observed in the RYSZ samples of profile 1.

None of the studies of texture evolution in experimental simple shear (Schmid et al., 1987, Pieri et al., 2001a,b) has produced exactly the same textures as those observed in the RYSZ. Schmid et al. (1987) observed similar textures in their 800°C "grain boundary migration regime" experiments with a distinct *c*-axis maximum rotated with the sense of shear relative to foliation, which they also inferred due to a dominating contribution of slip in the basal plane. Preferred orientations similar to M3 with *c*-axes inclined with the sense of shear developed in torsion experiments of Carrara marble at 500°C and 600°C after very large shear strain ($\gamma \geq 10$). Twinning of the initially coarse grained marble controlled the texture formation at small strain and caused a *c*-axis maximum opposite to the sense of shear. Twinning was less important in the fine grained mylonite at large strain, which then caused the texture transition.

### 2.5.6 Texture evolution in naturally deformed limestones.

One geometric assumption often made for texture interpretation is that during progressive simple shear deformation accompanied by dynamic recrystallization, one or

several distinct slip planes tend to align parallel or at small angles to the bulk shear plane and corresponding slip directions tends to align with the bulk shear direction of the rock (Nicolas et al. 1971, 1972, 1973, 1976, 1977, Bouchez 1978, Schmid 1994, Etchecopar 1977). This so-called 'easy slip' implies that the microscopic deformation (simple shear by crystal plastic slip on one slip system) coincides with the macroscopic deformation, which is exclusively possible for simple shear kinematics. In any other strain regime, particularly in coaxial deformation including pure shear, homogeneous deformation of an aggregate requires simultaneous activation of several slip systems and causes continuous rotation of the crystal lattice.

The previous discussion revealed that there seems to be a gradual shift from predominant rhomb slip (*r* and *f*-slip) in pure shear to predominant basal slip in simple shear. This seems to imply that the kinematics of deformation has an influence on the activity of the slip systems. At first sight this appears intriguing, since the critical resolved shear stresses of the various slip systems should not be influenced by the kinematics of deformation. However, the texture evolution is also influenced by dynamic recrystallisation (see review by Schmid 1994). In the case of simple shear grains with their *c*- axis orientations inclined against the sense of shear are unsuitably oriented for basal slip and may hence be eliminated by nucleation and preferential growth of grains that are suitably oriented in terms of basal slip. Provided that grains with orientations that are not suitably oriented for basal slip act as local stress raisers during simple shearing, they will be preferentially consumed by dynamic recrystallisation. Dynamic recrystallisation results in a stationary cycle of newly formed small grains (through subgrain rotation and/or bulging), which grow and deform by slip until they will be consumed again by their neighbours. While individual grains permanently change their size, shape and orientation, the microstructure and texture on average remain constant with strain after a certain initialisation. The rate of these recrystallisation cycles is largely affected by the impurity content at the micro- and nanoscale (Herwegh and Kunze, 2002). The nummulitic limestone of RYSZ must be considered a rather impure calcite rock in that sense, as it contains enough impurities to prevent grain growth and to decelerate the microstructural resetting. The latter might also be a reason for the general observation that the microfabrics in calcite mylonites from pure shear and simple shear dominated strain paths are actually more similar to each other than what should be expected from the different kinematics themselves, which have their principal axes for incremental strain (and stress) rotated by 45° relative to each other. When microfabric resetting is not immediate but retarded, lattice rotations due to deformation by slip bring the textures in closer relation to the finite strain coordinates at least for a longer interval, i.e. to a reference system defined by foliation and lineation. Dynamic recrystallisation has also been incorporated into models of texture formation

through slip accompanied by grain growth and nucleation, where the resulting textures are dominated by 'easy slip' orientations, if nucleation is assumed to dominate over grain growth, which is a reasonable proposition for mylonitic deformation (Pieri et al., 2001, and references therein).

In summary of our empirical observations, a texture transition as function of strain path is schematically depicted in fig 2.18, following ideas proposed for quartz by Schmid and Casey (1986). We emphasize, however, that in case of calcite the simple-shear end-member does not involve slip along one single slip system only, namely the basal plane, but antithetical slip on *r* and *f* also contributed to deformation. Slip along a single slip system is only possible if this slip system is perfectly aligned with the shear zone boundary. The obliquity between basal plane and foliation is too high (15°) in case of the ultramylonites, for which the foliation is expected to nearly coincide with the shear zone boundary.

To our knowledge all published oblique calcite *c*-axis textures (see for example Behrmann 1983, Dietrich and Song 1984, Schmid et al. 1987, Ratschbacher et al. 1991) exhibit maxima oriented "against the sense of shear", as expected when calcite *e*-twinning is responsible for texture evolution (Schmid et al. 1987). In our samples, however, twinning was suppressed by the small grain size and elevated temperatures. The *c*-axis maxima oriented "with the sense of shear" correspond to what is consistently found for quartz mylonites (Schmid and Casey, 1986), which are similarly attributed to dominant basal slip.

Two conditions need to be satisfied if the interpretation of the texture transition discussed so far is correct: (1) The slip systems involved (*r*, *f* and basal plane) need to have comparable critical resolved shear stresses at the temperature conditions of deformation, and (2) there must be very subordinate twinning during deformation. Condition (1) appears to be satisfied for the high temperature deformation regime (De Bresser & Spiers 1997). Condition (2) appears to be satisfied in many experimentally and naturally deformed samples where dynamic recrystallization dominates (Pieri et al. 2000a,b, Schmid et al. 1987, Wagner et al. 1982, Lafrance et al. 1994, Bestmann et al. 2000).

Whether calcite textures and their asymmetry can be used as unequivocal shear sense criteria remains an open question and microstructural criteria such as oblique SPO are certainly more reliable criteria. If no twinning occurs, it appears that either *c*-axis maxima normal to foliation or maxima rotated synthetically with the sense of shear may form. If twinning is dominant during deformation, the *c*-axis maximum will be rotated antithetically to, i.e. "against" the shear sense and an asymmetry opposite to that observed for the samples from Rocher d'Yret, is expected. Thus, for all practical purposes, calcite textures should only be used in conjunction with shape fabric analyses and microstructural

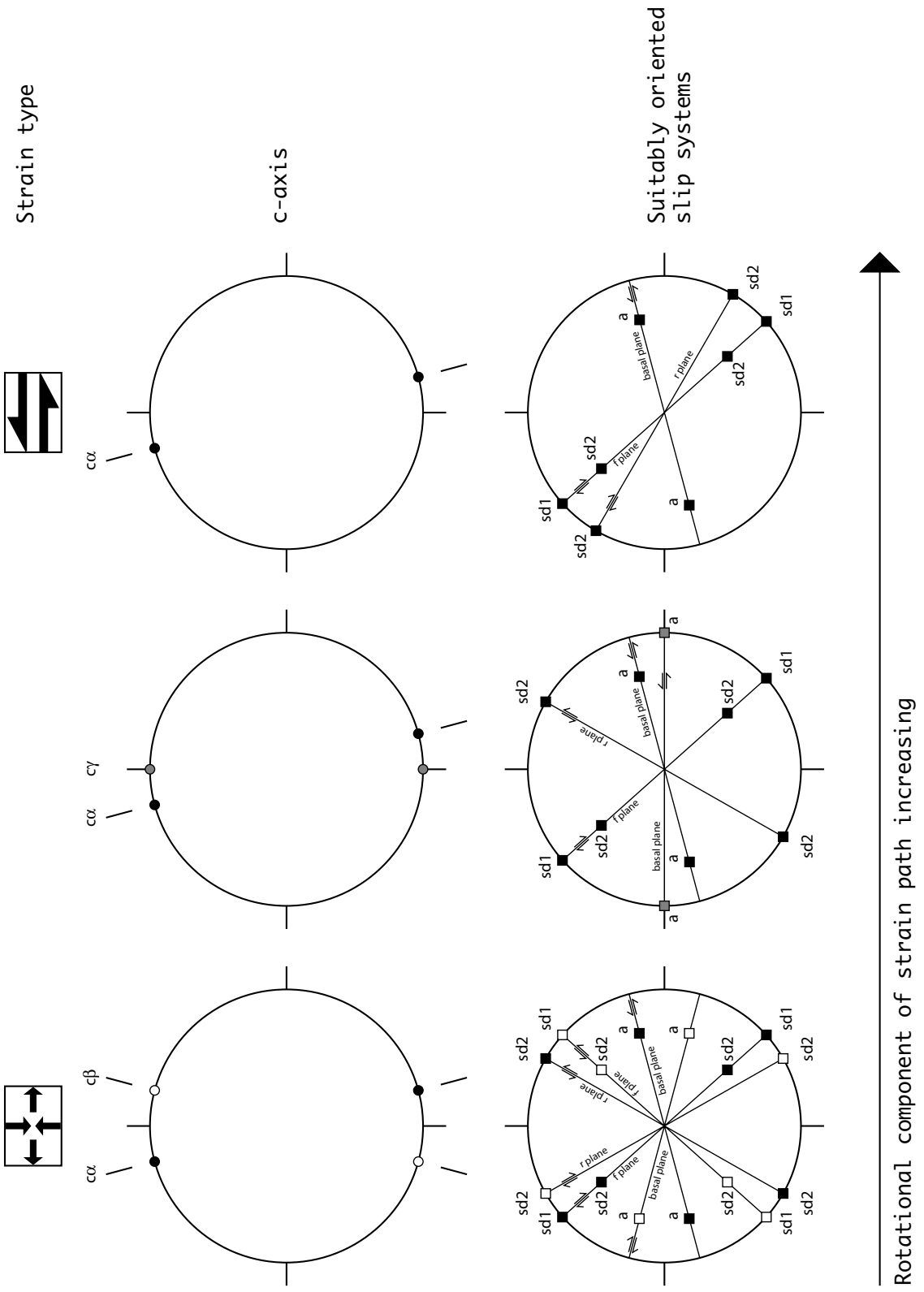


**Figure 2.18:** Sketch summarizing the evolution of the calcite *c*-axis distribution during the transition from coaxial dominated to non-coaxial dominated deformation under conditions supressing twinning. Poles and projections of slip planes and slip directions are reported for the main ideal orientation components, which are suitably oriented for slip under the assumed kinematics. Black symbols belong to orientations with *c*-axis at cα (M1, M3), white symbols at cβ (M2), grey symbols at cγ (M4, M4').

studies of twinning and dynamic recrystallization.

## 2.6 Summary and Conclusions.

Two sample series from the Rocher de l'Yret shear zone were studied, which deformed at the same time under conditions of low anchizone metamorphic conditions. From the fabric analysis of both zones it is concluded that orthorhombic SPO symmetry is indicative of pure shear dominated deformation while monoclinic SPO symmetry is indicative of simple shear dominated deformation. The textures of these samples also show orthorhombic and monoclinic symmetries, respectively, and confirm the conclusion that the two profiles represent cases that are close to the pure and simple shear end members.

In general, the SPO and texture analysis of samples from the Rocher de l'Yret deformation zone indicates that the symmetry of calcite fabrics appears to indicate simple shear deformation for monoclinic fabrics. Orthorhombic fabric symmetry, however, may but does not necessarily has to indicate pure shear deformation, because the latter may also be produced by simple shear strain paths as documented in the literature (Schmid et al. 1987, Lafrance 1994, Pieri et al. 2000a,b). The type of *c*-axis patterns observed in the simple shear samples shows some deviation from textures reported from other naturally deformed calcitic rocks, where an oblique *c*-axis maximum typically occurs opposite to the sense of shear due to *e*-twinning. The *c*-axis maximum rotated synthetically with the sense of shear may be also used as a shear sense indicator provided that it can be demonstrated that twinning in calcite is of subordinate importance compared to basal slip, which is likely the case for fine grained calcite mylonites.

## 2.7 Acknowledgments.

The first author wishes to thank all the colleagues from the tectonic group at the institute of geology and paleontology of the Basel University for stimulating discussions.
Pierre Dèzes and Konrad Leu are greatly acknowledged for assistance in computer programming.
A special thank is given to Willy Tschudin for preparing excellent ultrathin sections.
This study was funded by the Swiss National Science Foundation.

## 2.8 Software used.

[1] Tectonic VB 1.5a Ortner, H., 2001. http://geopal.uibk.ac.at/tvb/front.html.

[2] NIH image public domain software http://rsb.info.nih.gov/nih-image/download.html.

[3] Stripstar http://www.unibas.ch/earth/micro/software/grainsize/grainsize.html.

## 2.9 References.

Angelier, J. and Mechler, P., 1977. Sur une methode graphique de recherche des contraintes principales egalement utilisables en tectonique et en seismologie : la methode des diedres droits. Bulletin de la Societe Geologique de France, 19(6): 1309-1318.

Aprahamian, J., 1974. La cristallinite de l'illite et les mineraux argileux en bordure des massifs cristallins externes de Belledonne et du Pelvoux (variations et relations possibles avec des evenements tectoniques et metamorphiques alpins). Geologie Alpine, 50: 5-15.

Aprahamian, J., 1988. Cartographie du metamorphisme faible a tres faible dans les Alpes francaises externes par l'utilisation de la cristallinite de l'illite. Geodinamica Acta. Volume 2(1): 25-32.

Bagnoud, A., Wernli, R. and Sartori, M., 1998. Decouverte de foraminiferes planctoniques paleogenes dans la zone de Sion-Courmayeur a Sion (Valais, Suisse). Eclogae Geologicae Helvetiae, 91(3): 421-429.

Barnhoorn, A., Bystrichy, M., Burlini, L., Kunze, K., 2004. The role of recrystallisation on the deformation behaviour of calcite rocks: large strain torsion experiments on Carrara marble. Journal of Structural Geology, 26(5): 885-903.

Beach, A., 1981. Thrust structures in the eastern Dauphinois Zone (French Alps), north of the Pelvoux Massif. Journal of Structural Geology, 3(3): 299-308.

Behrmann, J.H., 1983. Microstructure and fabric transitions in calcite tectonites from the

Sierra Alhamilla (Spain). Geologische Rundschau, 72(2): 605-618.

Bestmann, M., Kunze, K. and Matthews, A., 2000. Evolution of a calcite marble shear zone complex on Thassos Island, Greece; microstructural and textural fabrics and their kinematic significance. Journal of Structural Geology, Vol. 22(11-12): 1789-1807.

Bouchez, J.L., 1978. Preferred orientations of quartz <a> axes in some tectonites; kinematic inferences. Tectonophysics, 49(1-2): T25-T30.

Braillon, P.a.S., J., 1976. Deformation plastique de monocristaux de calcite en compression suivant <001>. Physica Status Solidi (a), 36: 637-646.

Bravard, C. and Gidon, M., 1979. La structure du revers oriental du Massif du Pelvoux; observations et interpretations nouvelles. Geologie Alpine, 55: 23-33.

Brodie, K.H. and Rutter, E.H., 1987. The role of transiently fine-grained reaction products in syntectonic metamorphism; natural and experimental examples. Canadian Journal of Earth Sciences. 24(3): 556-564.

Bürgisser, J. and Ford, M., 1998. Overthrust shear deformation of a foreland basin; structural studies south-east of the Pelvoux Massif, SE France. Journal of Structural Geology, 20(11): 1455-1475.

Bunge, H.J., 1982. Texture Analysis in Material Science - Mathematical Methods. Butterworth, London.

Butler, R.W.H., 1992. Thrust zone kinematics in a basement-cover imbricate stack; eastern Pelvoux Massif, French Alps. Journal of Structural Geology, 14(1): 29-40.

Casey, M., 1981. Numerical analysis of X-ray texture data; an implementation in Fortran allowing triclinic or axial specimen symmetry and most crystal symmetries. Tectonophysics, 78(1-4): 51-64.

Casey, M., Kunze, K. and Olgaard, D.L., 1998. Texture of Solnhofen Limestone deformed to high strains in torsion. Journal of Structural Geology. 20(2-3): 255-267.

Ceriani, S., Fuegenschuh, B. and Schmid, S.M., 2001. Multi-stage thrusting at the „Penninic Front“ in the Western Alps between Mont Blanc and Pelvoux massifs. International Journal of Earth Sciences. 90(3): 685-702.

De Bresser, J.H.P. and Spiers, C.J., 1990. High-temperature deformation of calcite single crystals by r (super +) and f (super +) slip. Geological Society Special Publications, 54: 285-298.

De Bresser, J.H.P. and Spiers, C.J., 1993. Slip systems in calcite single crystals deformed at 300-800 degrees C. Journal of Geophysical Research, 98(4): 6397-6409.

De Bresser, J.H.P. and Spiers, C.J., 1997. Strength characteristics of the r, f, and c slip systems in calcite. Tectonophysics, 272(1): 1-23.

Dietrich, D. and Song, H., 1984. Calcite fabrics in a natural shear environment, the Helvetic nappes of western Switzerland. Journal of Structural Geology, 6(1-2): 19-32.

Edington, J.W., Melton, K.N., Cutler, C.P., 1976. Superplasticity. Prog. Mat. Sci., 21: 61-170.

Erskine, B.G., Heidelbach, F. and Wenk, H.R., 1993. Lattice preferred orientations and microstructures of deformed Cordilleran marbles; correlation of shear indicators and determination of strain path. Journal of Structural Geology, 15(9-10): 1189-1205.

Etchecopar, A., 1977. A plane kinematic model of progressive deformation in a polycrystalline aggregate. Tectonophysics, 39(1-3): 121-139.

Ford, M., 1996. Kinematics and geometry of early Alpine, basement-involved folds, SW Pelvoux Massif, SE France. Eclogae Geologicae Helvetiae, 89(1): 269-295.

Friedman, M. and Higgs, N.G., 1981. Calcite fabrics in experimental shear zones. Geophysical Monograph. 24: 11-27.

Froitzheim, N., Schmid, S.M. and Frey, M., 1996. Mesozoic paleogeography and the timing of eclogite-facies metamorphism in the Alps; a working hypothesis. Eclogae Geologicae Helvetiae. 89(1): 81-110.

Fuegenschuh, B. and Schmid, S.M., 2003. Late stages of deformation and exhumation of an orogen constrained by fission-track data; a case study in the Western Alps. Geological Society of America Bulletin, 115(11): 1425-1440.

Gidon, M., 1979. Le role des etapes successives de deformation dans la tectonique alpine du massif du Pelvoux (Alpes occidentales). Comptes Rendus Hebdomadaires des Seances de l'Academie des Sciences, Serie D: Sciences Naturelles, 288(9): 803-806.

Gidon, P., 1954. Les rapports des terrains cristallins et de leur couverture sedimentaire, dans les regions orientale et meridionale du massif du Pelvoux. Travaux du Laboratoire de Geologie de la Faculte des Sciences de Grenoble, 31: 1-199.

Gignoux, M. and Moret, L., 1938. Description geologique du bassin superieure de la Durance. Travaux du Laboratoire de Géologie de la Faculté des Sciences de Grenoble, 21: 1-295

Gillcrist, R., Coward, M. and Mugnier, J.L., 1987. Structural inversion and its controls; examples from the Alpine Foreland and the French Alps. Geodinamica Acta, 1(1): 5-34.

Gonzalez, C.J.M. and Garcia, C.C., 1999. Calcite twins from microveins as indicators of

deformation history. Journal of Structural Geology, 21(7): 875-889.

Griggs, D.T., Turner, F.J. and Heard, H.C., 1960. Deformation of rocks at 500 degrees to 800 degrees C. Geological Society of America. Geological Society of America, pp. 39-104.

Heilbronner, R.P. and Pauli, C., 1993. Integrated spatial and orientation analysis of quartz c-axes by computer-aided microscopy. Journal of Structural Geology, 15(3-5): 369-382.

Heilbronner, R.P. and Pauli, C., 1994. Orientation and misorientation imaging: integration of microstructural and textural analysis. In: H.J. Bunge, Siegesmund, S., Skrotzki, W., Weber, K. (Editor), Texture of Geological Materials. DGM Informationsgesellschaft Verlag, Oberursel, pp. 147-164.

Helming, K., Geier, St., Heinitz, J., Leiss, B., Rauschenbach, B., Schwarzer, R.A., Ullemeyer, K., Wenk, H.-R., 1994. Texture Estimates by Means of Components. Z. Metallkd., 85: 545-553.

Herwegh, M. and Kunze, K., 2002. The influence of nano-scale second-phase particles on deformation of fine grained calcite mylonites. Journal of Structural Geology, 24(9): 1463-1478.

Kern, H. and Wenk, H.R., 1983. Calcite texture development in experimentally induced ductile shear zones. Contributions to Mineralogy and Petrology, 83(3-4): 231-236.

Lafrance, B., White, J.C. and Williams, P.F., 1994. Natural calcite c-axis fabrics; an alternate interpretation. Tectonophysics, 229(1-2): 1-18.

Leiss, B., Siegesmund, S., Weber, K., 1999. Texture asymmetries as shear sense indicators in naturally deformed mono- and poly-phase carbonate rocks. Textures Microstruct., 33: 61-74.

Mancktelow, N.S., 1987. Quartz textures from the Simplon fault zone, Southwest Switzerland and North Italy. Tectonophysics, 135(1-3): 133-153.

Merle, O. and Brun, J.P., 1984. The curved translation path of the Parpaillon Nappe (French Alps). Journal of Structural Geology, 6(6): 711-719.

Mosar, J., Stampfli, G.M. and Girod, F., 1996. western Prealpes Medianes Romandes; timing and structure; a review. Eclogae Geologicae Helvetiae, 89(1): 389-425.

Nicolas, A., 1976. Flow in upper-mantle rocks; some geophysical and geodynamic consequences. Tectonophysics, 32: 93-106.

Nicolas, A., Bouchez, J.L., Blaise, J. and Poirier, J.P., 1977. Geological aspects of deformation in continental shear zones. Tectonophysics, 42(1): 55-73.

Nicolas, A., Bouchez, J.L. and Boudier, F., 1972. Interpretation cinematique des deformations plastiques dans le Massif de lherzolite de Lanzo (Alpes piemontaises); comparaison avec d'autres massifs. Tectonophysics, 14(2): 143-171.

Nicolas, A., Bouchez, J.L., Boudier, F. and Mercier, J.C., 1971. Textures, structures and fabrics due to solid state flow in some European lherzolites. Tectonophysics, 12(1): 55-86.

Nicolas, A., Boudier, F. and Boullier, A.M., 1973. Mechanisms of flow in naturally and experimentally deformed peridotites. American Journal of Science, 273(10): 853-876.

Padmanabhan, K.A., Davies, G.J., 1980. Superplasticity. Springer, 312 pp.

Panozzo, R.H., 1983. Two-dimensional analysis of shape-fabric using projections of digitized lines in a plane. Tectonophysics, 95(3-4): 279-294.

Panozzo, R.H., 1984. Two-dimensional strain from the orientation of lines in a plane. Journal of Structural Geology, 6(1-2): 215-221.

Passchier, C.W., Trouw, R.A.J., 1996. Microtectonics. Springer, 289 pp.

Pieri, M., Burlini, L., Kunze, K., Stretton, I. and Olgaard, D.L., 2001. Rheological and microstructural evolution of Carrara Marble with high shear strain; results from high temperature torsion experiments. Journal of Structural Geology, 23(9): 1393-1413.

Pieri, M., Kunze, K., Burlini, L., Stretton, I., Olgaard, D.L., Burg, J.P., Wenk, H.R., 2001. Texture development of calcite by deformation and dynamic recrystallization at 1000 K during torsion experiments of marble to large strains. Tectonophysics, 330(1-2): 119-140.

Ratschbacher, L., Wenk, H.R. and Sintubin, M., 1991. Calcite textures; examples from nappes with strain-path partitioning. Journal of Structural Geology, 13(4): 369-384.

Rutter, E.H. and Brodie, K.H., 1988. The role of tectonic grain size reduction in the rheological stratification of the lithosphere. Geologische Rundschau. 77(1): 295-308.

Schaeben, H., Siemes, H., Hoefler, S. and Will, G., 1990. Practical application of entropy optimization in quantitative texture analysis. Geological Society Special Publications. 54: 375-381.

Schmid, S.M., 1982. Microfabric studies as indicators of deformation mechanisms and flow laws operative in mountain building. In: J. Hsue Kenneth (Editor), Mountain building processes. Acad. Press, London, pp. 95-110.

Schmid, S.M., Boland, J.N. and Paterson, M.S., 1977. Superplastic flow in finegrained limestone. Tectonophysics, 43(3-4): 257-291.

Schmid, S.M. and Casey, M., 1986. Complete fabric analysis of some commonly observed quartz c-axis patterns. Geophysical Monograph. 36: 263-286.

Schmid, S.M., Casey, M. and Starkey, J., 1981. The microfabric of calcite tectonites from the Helvetic Nappes (Swiss Alps). Geological Society of London Special Publication. 9: 151-158.

Schmid, S.M., Panozzo, R. and Bauer, S., 1987. Simple shear experiments on calcite rocks; rheology and microfabric. Journal of Structural Geology. 9(5-6): 747-778.

Schmid S.M., 1994. Textures of geological materials: computer model predictions versus empirical interpretations based on rock deformation experiments and field studies. In: H.J. Bunge, Siegesmund, S., Skrotzki, W., Weber, K. (Editor), Texture of Geological Materials. DGM Informationsgesellschaft Verlag, Oberursel, pp. 279-301.

Seward, D., Ford M., Bürgisser, J., Lickorish, H., Williams, E.A., Meckel L.D., 1999. Preliminary results of fission-track analyses in the southern Pelvoux area, SE France. In: G. Gosso, F. Jadoul, M. Sella and I. Spalla Maria (Editors), 3rd workshop on Alpine geological studies. Memorie di Scienze Geologiche, 51(1): 25-31.

Seward, D. and Mancktelow, N.S., 1994. Neogene kinematics of the Central and Western Alps; evidence from fission-track dating. Geology, 22(9): 803-806.

Spencer, S., 1992. A kinematic analysis incorporating incremental strain data for the frontal Pennine zones of the western French Alps. Tectonophysics, 206(3-4): 285-305.

Spiers, C.J. and Wenk, H.R., 1980. Evidence for slip on r and f in the positive sense in deformed calcite single crystals. American Geophysical Union; 1980 fall meeting. Eos, Transactions, 61(46): 1128.

Tagami, T., Galbraith, R.F., Yamada, R., and Laslett, G.M., 1998. Revised annealing kinetics of fission tracks in zircon and geological implications. In: P. Van den Haute, and De Corte, F. (Editor), Advances in fission-track geochronology. Dordrecht, Kluwer Academic Publishers, pp. 99-112.

Turner, F.J., Griggs, D.T. and Heard, H.C., 1954. Experimental deformation of calcite crystals. Geological Society of America Bulletin, 65(9): 883-933.

Turner, F.J.a.H., H.C., 1965. Deformation in calcite crystals at different strain rates. Univ. Calif. Publ. Geol. Sci., 46: 103-126.

Wagner, F., Wenk, H.R., Kern, H., Houtte, P.V. and Esling, C., 1982. Development of preferred orientation in plane strain deformed limestone; experiment and theory. Contributions to Mineralogy and Petrology, 80(2): 132-139.
Weiss, L.E. and Turner, F.J., 1972. Some Observations on Translation Gliding and Kinking in Experimentally Deformed Calcite and Dolomite, Flow and Fracture of Rocks.

Geophysical Monograph. 16: 95-107.

Wenk, H.R., Matthies, S., Donovan, J., Chateigner, D., 1998. BEARTEX, a Windows-based program system for quantitative texture analysis. Journal of Applied Crystallography, 31: 262-269.

Wenk, H.R., Takeshita, T., Bechler, E., Erskine, B.G. and Matthies, S., 1987. Pure shear and simple shear calcite textures; comparison of experimental, theoretical and natural data. Journal of Structural Geology. 9(5-6): 731-745.

Wenk, H.R., Venkitasubramanyan, C.S., Baker, D.W. and Turner, F.J., 1973. Preferred Orientation in Experimentally Deformed Limestone. Contributions to Mineralogy and Petrology, 38(2): 81-114.

Wyckoff, R.W.G., 1920. The crystal structures of some carbonates of the calcite group. American Journal of Science, 50: 317-360.

# 3. MICROFABRIC ANALYSIS OF CALCITIC MARBLES FROM THE AREA INVESTIGATED IN THE WESTERN ALPS AND THE GAVARNIE BASAL CONTACT (CENTRAL PYRENEES).

## 3.1 Introduction.

In the previous chapter, a model of microfabric evolution of calcite ultramylonites, plastically deformed at temperatures lower than 350°C, has been presented. The very specific setting of the outcrop investigated in great details at the "Rocher de l'Yret" shear zone (RYSZ) allowed for the recognition of both coaxial and non-coaxial deformation kinematics. The samples deformed with a dominant component of rotational deformation show a *c*-axis distribution tilted synthetically with the sense of shear. In the absence of twinning, this feature, commonly observed for quartz tectonites, can be used as a reliable shear sense indicator. Additionally, the model allows for the recognition of incipient rotational deformation in the bulk flow accomodated in the rock.

The structural data presented in chapter 1 will now be completed by means of a microfabric analysis of a series of calcitic marbles, found in abundance in the investigated area.

The results of investigations on calcite ultramylonites found along the Roselend Thrust (RT) are presented first. Four localities along the RT have been investigated between the eastern rim of the Pelvoux massif in the North and the rear of the Argentera massif in the South (sites BFY, Lauz, Reot and Arg in fig 3.1). This study aims to 1) independently confirm the overall WNW-directed sense of transport along the RT, 2) deduce the type of strain along this structure and its possible variations using the model of microfabric evolution presented in chapter 2.

In a second step, the basal decollement of the Dauphinois parautochtonous cover from the southeastern rim of the Pelvoux massif will be investigated. Such decollement occurred within the nummulitic limestone layer intensively mylonitised in the Dormillouse valley (site Dorm, see fig 3.1 and 3.2). This study confirms the overall top-SW overprinting deformation recorded in this domain and documents important bulk flow partionning within the basal decollement level of the Eocene stratigraphic series.

Finally, the results of investigations on samples from the Gavarnie thrust from the central Pyrenees (courtesy J.H.P. de Bresser) will be presented (see fig 3.37). The results are in accordance with the overall top-S directed emplacement of the Gavarnie nappe during Pyrenean orogeny and give evidence for strain variations within the shear zone developed along the Gavarnie basal thrust.

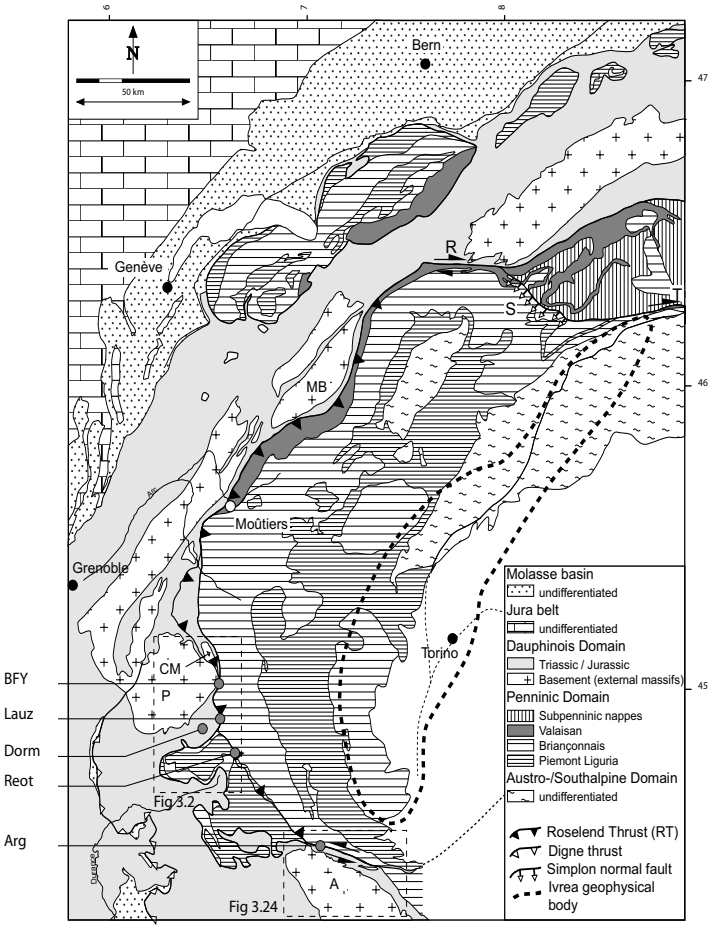


**Figure 3.1:** Simplified geological overview of the arc of the Western Alps (A: Argentera massif, CM: Combeynot massif, MB: Mont Blanc massif, P: Pelvoux massif, R: Rhone-Simplon line, T: Tonale line; after Froitzheim et al. 1996 and Ceriani et al. 2001). BFY, Lauz, Dorm, Reot and Arg refer to the different sampling sites investigated in this study.

## 3.2 Methodology.

For each locality, at least three samples have been studied for statistically reliable representation. Microstructure analysis has been performed on ultra-thin sections of about 2 to 3 micrometers thickness (samples BFY and R10, see fig 3.4 and 3.16) or normal thin sections (30 micrometers thickness). All sections are observed under crossed polarizors.

Crystallographic preferred orientation (CPO), referred to as texture, was measured with an X-ray texture goniometer. In the following, Miller-Bravais hexagonal indices are used in order to designate the lattice planes and directions, as well as the classifications from Wyckoff (1920). All pole figures are displayed using equal area stereoplots, upper hemisphere. The pole figure contours are given in multiples of a uniform distribution, with a contour interval of 0.2. Intensities below 1 are not subdivided.

In the large majority of cases (unless mentioned), the microstructural characteristics of the samples presented in the following are those of ultramylonites. The dynamically recrystallised matrix is often very homogeneous and occupies more than 90% of the surface of the thin section. The grains exhibit a sharp extinction and remain unaffected by mechanical twinning. Their average grain size is comparable to that found in the samples of nummulitic limestone analyzed in chapter 2, namely MPY2 (coaxially deformed), Sa1a4 (so-called "intermediate" strain regime) and MPY28 (non-coaxially deformed), i.e. smaller that 50 micrometers. A strong grain shape preferred orientation (SPO) is often observed in thin section. This feature indicates a substantial contribution of intracrystalline deformation. Pressure solution deformation mechanisms outlined by seams of insoluble minerals along dissolution surfaces have also been recognized. All samples collected in the structural units derived from the Dauphinois, Subriançonnais and Briançonnais domains were deformed at temperatures between 220°C ± 10°C and 260°C ± 10°C (Potel, pers. com.). The Pyrenean samples presented in the last paragraph were exposed to P/T conditions of about 1.6 kbar and 200°C during mylonitisation (DeBresser, 1989). The strong similarities in terms of microstructural characteristics and P/T conditions during deformation allow for direct comparison of textural characteristics between these samples and the ones presented in chapter 2. The positions r1, r2, *sd2*a, *sd2*b, cα, cβ and cγ refer to the orientation of *r* crystallographic planes, *sd2* slip directions and *c* axes as defined for samples MPY2, Sa1a4 and MPY28 (see chapter 2). These notations are superposed to the textures obtained in the following session in order to facilitate pole figures description.

The results of the texture analysis are presented in three steps:

1) The pole figures of recalculated *r* and *h* crystallographic planes, reduced *a* and *sd1* slip directions plus *c*-axis are presented first.
2) For each locality, at least one more complete texture analysis is presented. A distinction is then made between the non-reduced *+a* and *–a* directions. The *f* crystallographic plane and *sd2* slip direction pole figures are calculated from the orientation distribution function. These detailed analyses allow for direct comparison with data presented in chapter 2.
3) Finally, the above analysis is completed by calculations of the following inverse pole figures for the corresponding sample: foliation normal (Fo. N., i.e. Z sample direction), stretching lineation (St. Lin, i.e. X sample direction), intermediate direction (Int. Dir., i.e. Y sample direction), directions at 45° counter-clockwise (45° CCW) and 45° clockwise (45° CW) from the foliation normal, cα direction (see chapter 2) and normal to cα within the XZ plane (cα N), cβ direction (see

chapter 2) and normal to cβ within the XZ plane (cβ N).

## 3.3 Microfabric analysis of samples collected along the Roselend thrust.

3.3.1 The Subriançonnais front at the eastern rim of the Pelvoux massif (sampling locality BFY indicated in fig 3.1 and 3.3).

Several evidences in favor of the hypothesis of Ceriani et al. (2001). which proposes that the RT joins the Subriançonnais front (SBF) south of the "Rocher de l'Yret" peak (cf fig 3.2 and 3.3), have been given in chapter 1. The overall WNW transport direction recorded along the SBF is confirmed by microstructural analysis of calcite ultramylonites found in the footwall of this structure. Samples from locality BFY have been taken from a calcitic marble block embedded in the "schistes à blocs" formation (Kerckhove 1969) found in the upper part of the "Ravin de la plaine de St Jean" canyon (see fig 3.3).

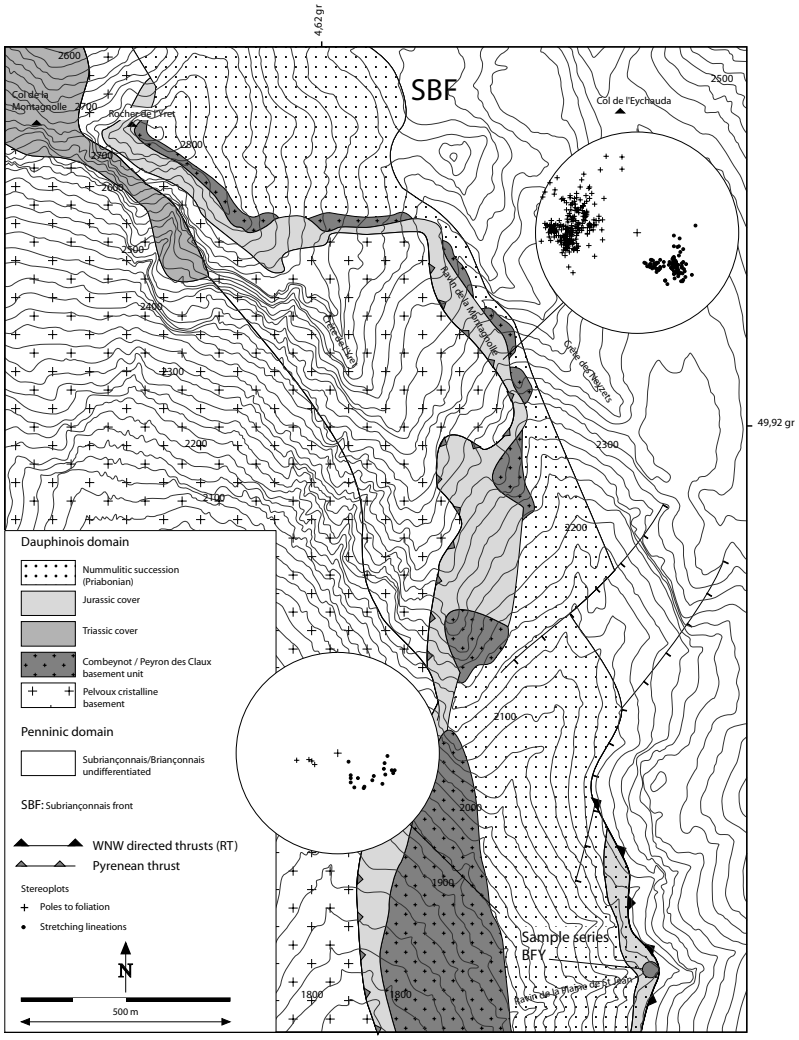


**Figure 3.3:** Detailed geological map of the "Rocher de l'Yret" shear zone according to new field mapping. Localisation of samples from the BFY series (4 samples) is shown.

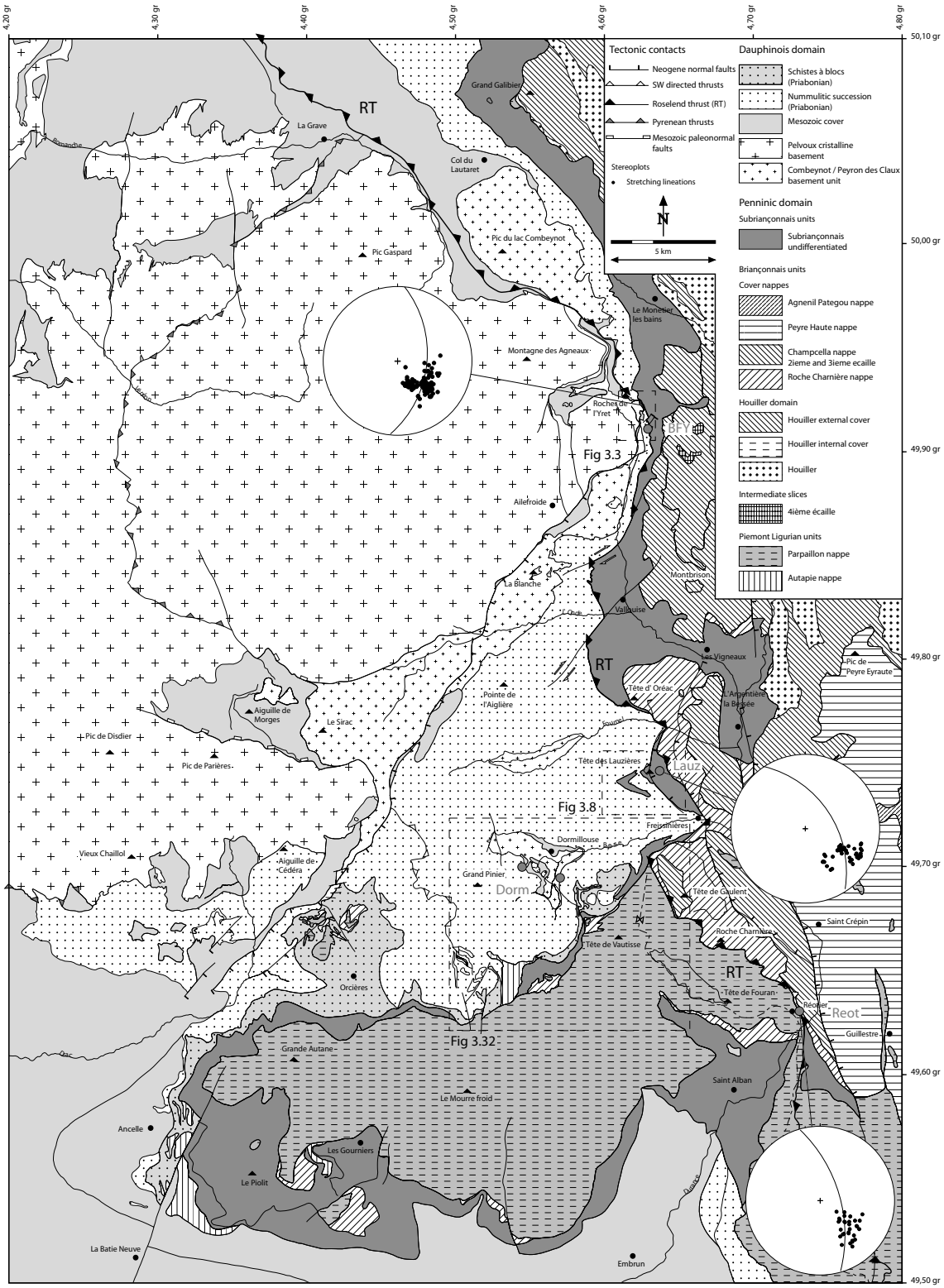


**Figure 3.2:** Structural map of the eastern rim of the Pelvoux massif. Points BFY, Lauz, Reot and Dorm refer to samples series presented in the text. These were collected at the eastern rim of the Pelvoux massif, the Subriançonnais units at the entrance of the Fournel valley, the frontal Briançonnais units at the village of Réotier and the basal decollement level of the Eocene cover in the Dormillouse valley, respectively. See text for details of sampled geological formations.
Stereoplots indicate the average foliation and stretching lineations of the different formations sampled at BFY, Lauz and Reot localities.

In hand specimens, the corresponding rocks are affected by a penetrative foliation. They show numerous evidence of isoclinal folding affecting former calcitic veins. A strong WNW-oriented stretching lineation is observable on surfaces of the macroscopic foliation plane, indicating that the mylonitisation process undoubtly developed during the activity along the RT.

A pronounced SPO Sb at about 20° from the macroscopic foliation Sa is observable in thin section and indicates an overall sinistral sense of shear, i.e. compatible with thrusting along the RT (cf fig 3.4a). Twins were only found in the relicts of initial porphyroclasts (see fig 3.4b).

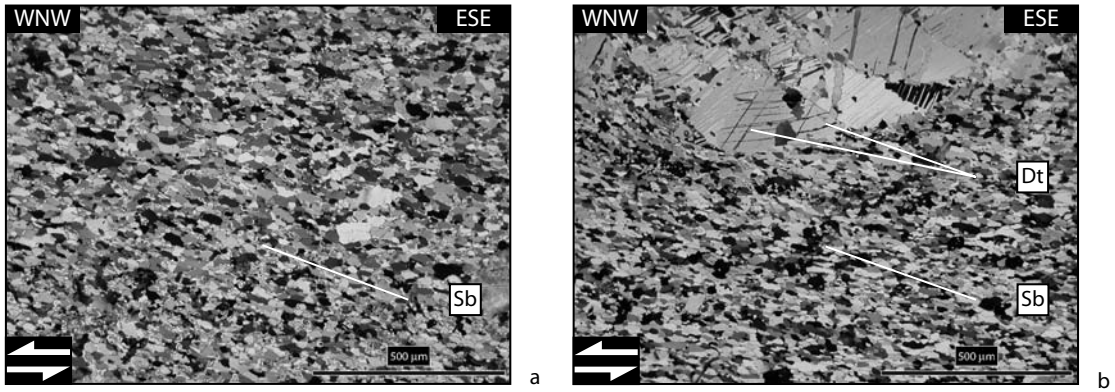


**Figure 3.4:** Photomicrographs of samples from the BFY series, taken from ultra-thin sections (2 micrometers thickness) under crossed polarizors, transmitted light. All sections are oriented normal to foliation Sa and parallel to lineation (horizontal).
a) note the strong SPO Sb indicating a sinistral sense of shear.
b)relicts of calcite porphyroclasts affected by numerous mechanical twins (Dt: deformation twins).

Four samples have been collected for texture analysis at the locality BFY and all measurements indicate a clear monoclinic symmetry (see fig 3.5 and 3.6). The *r* pole figure shows a maximum close to the foliation normal but slightly inclined in a clockwise sense by a few degrees and a second maximum at position r1. *h*, *f* and *a* pole figures show girdle distributions inclined at different angles from the XY plane in a clockwise sense. The non-reduced +*a* and –*a* directions show different distributions: the –*a* pole figure shows two maxima symmetrically disposed at 60° from Y while one maximum at Y is observed in the +*a* pole figure. This last feature confirms the monoclinic symmetry of the texture (Bestmann et al. 2000). The *sd2* pole figure shows a predominant maximum corresponding to the *sd2*a position (see chapter 2). The *sd1* slip direction pole figure is tilted in the sense of shear by an angle of about 20° and the *c*-axis orientation coincides with the cα position.

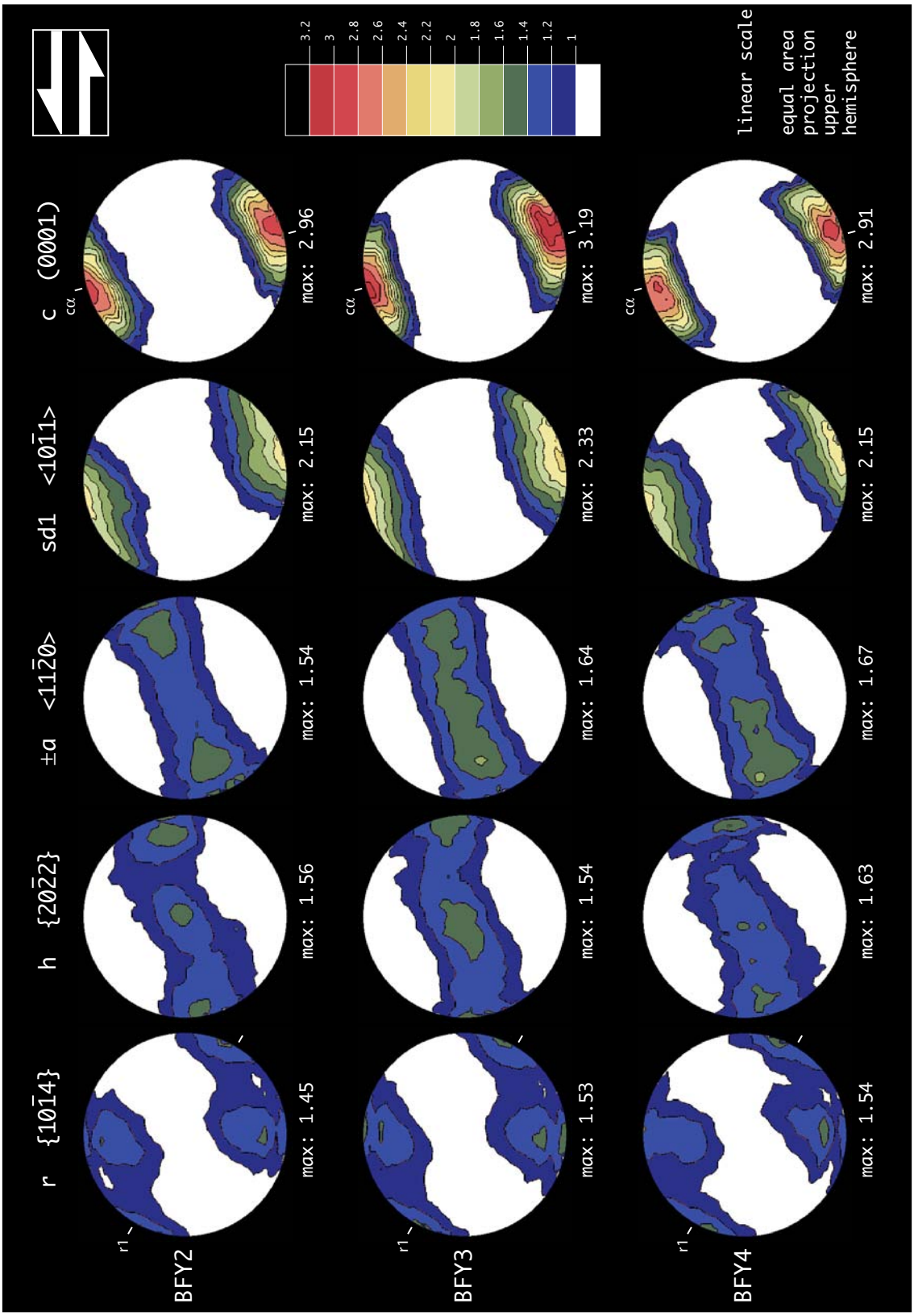


**Figure 3.5:** Crystallographic preferred orientation (CPO) of samples BFY2, BFY3 and BFY4. Note the clear monoclinic symmetry of the texture, indicative of sinistral simple shear deformation. See text for discussion.

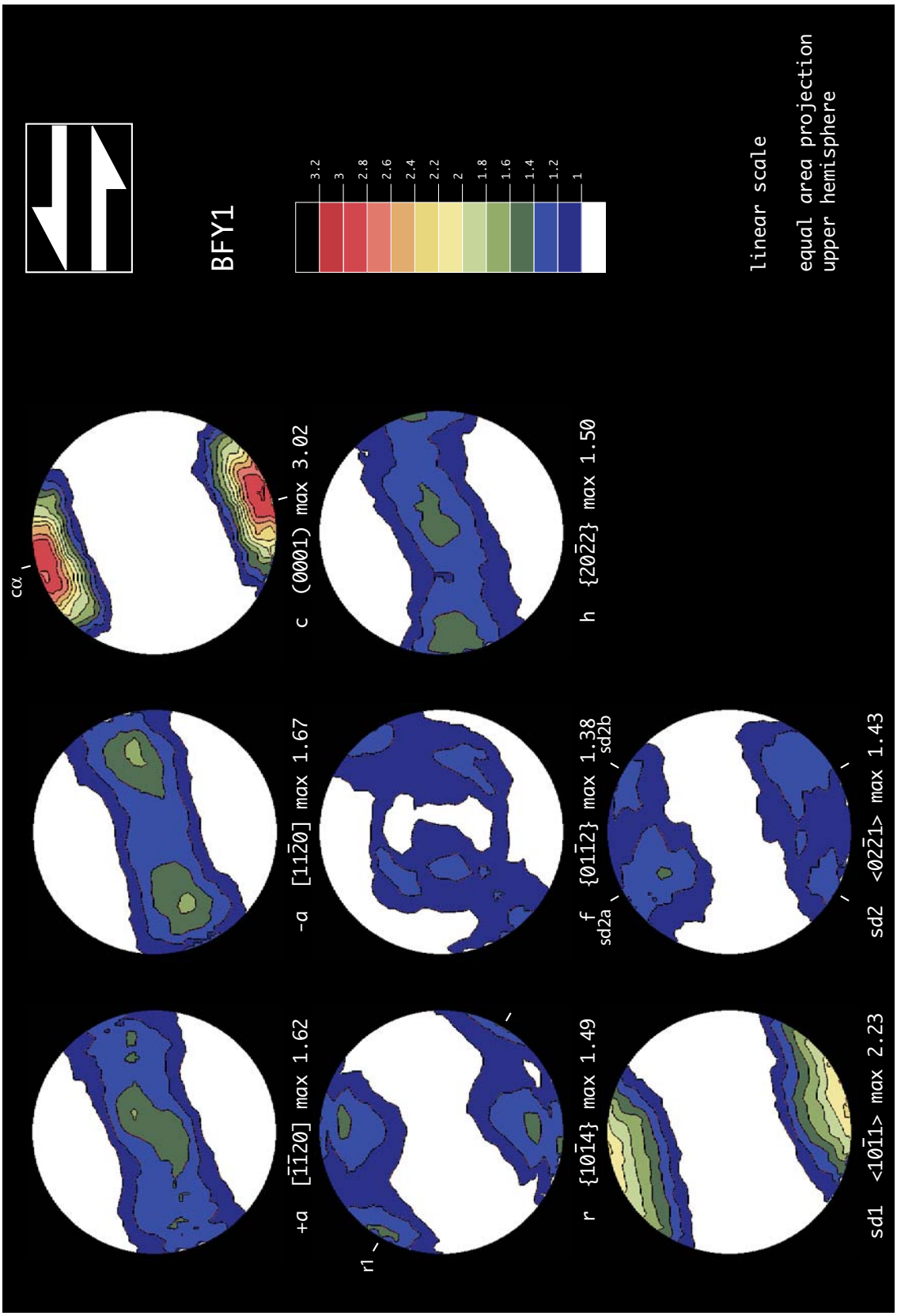


**Figure 3.6:** Complete texture analysis of sample BFY1. Note the different distribution of *+a* and *–a* directions on the non-reduced *a* pole figures.

The inverse pole figure for the cα position shows a strong maximum at *c* (intensity of about 3 mrd) while the position for cαN shows a girdle distribution with a weak maximum at *m* (fig 3.7). In chapter 2, these features have been interpreted as an indication for dominant slip on the basal plane in two conjugate *a* directions.

Given the similarities in the microfabric of sample MPY28 from the RYSZ (chapter 2) and the samples collected at locality BFY, it is proposed that the samples from locality BFY have been deformed in a dominant non-coaxial strain regime. The tilting of the *c*-axis in the sense of shear independently confirms the WNW directed sense of thrusting related to activity along the RT.

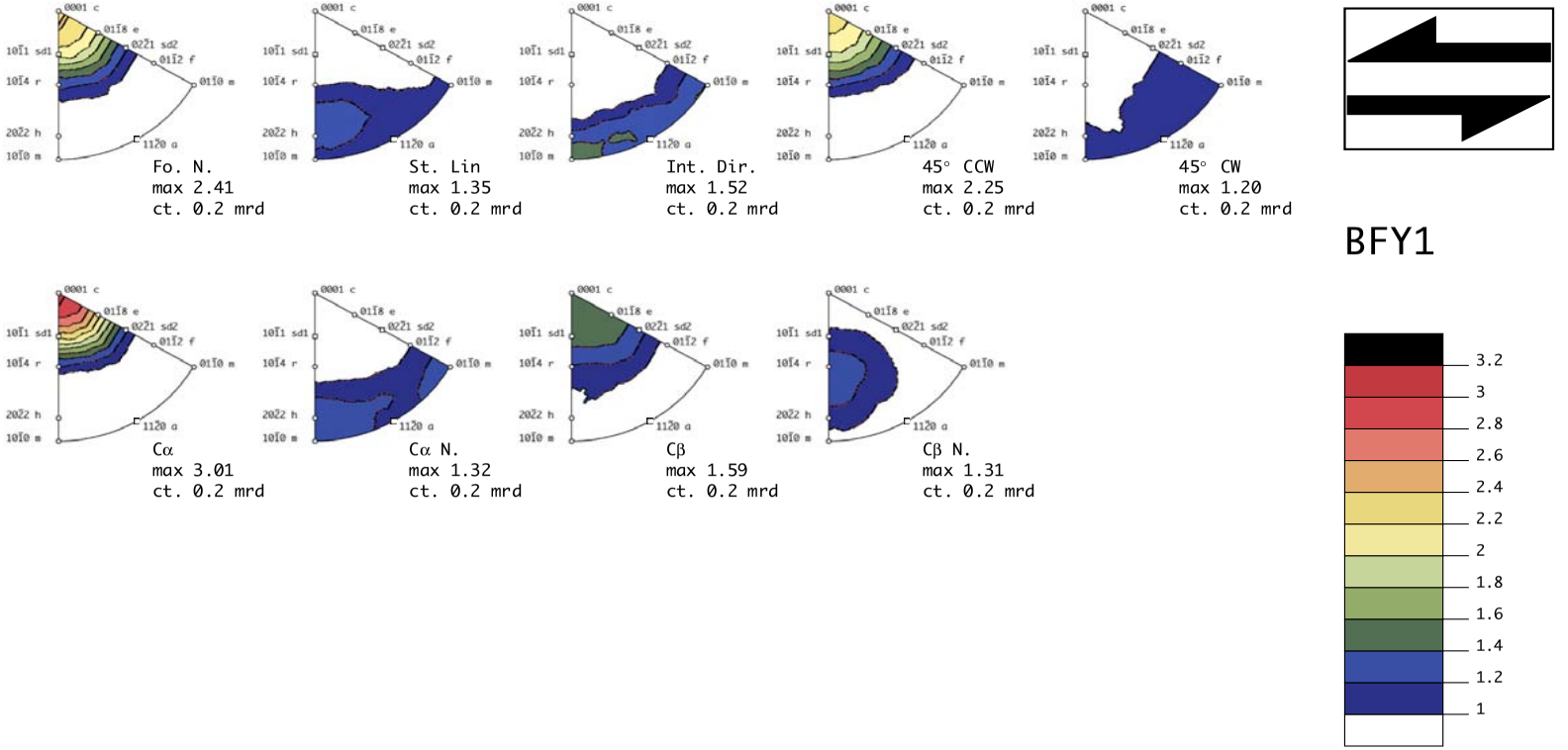


**Figure 3.7:** Inverse pole figures calculated for sample BFY1.
Note the different distributions between: both directions at 1) 45° from Z, 2) cα and cβ and 3) cαN and cβN reflecting the non-orthorhombic symmetry of the texture.

3.3.2 The Subriançonnais front at the entrance of the Fournel valley (sampling locality Lauz).

The investigated rocks were taken from the Dogger limestone found as an isolated slice embedded within the Subriançonnais black flysch series at the southern entrance of the Fournel valley (cf locality Lauz in figs 3.2 and 3.8). This slice is found in a steeply E-dipping orientation and develops a penetrative foliation carrying a strong WNW-oriented stretching lineation.

The results of a microfabric analysis of five samples (TL2 to TL6b: series Lauz 1), collected at the northern termination of this slice and along the path leading to the "Vallon de Crouzet" valley, are presented first. Then, three samples (TL1a, TL1al and TL1b: series Lauz 2), taken from the southern part of this slice at the "Pointe des casses de la Font de lance" locality, will be presented.

3.3.2.1 Samples from locality Lauz 1.

From a microstructural point of view, incipient S-C structures are locally developed, with the C planes oriented parallel to the macroscopic foliation Sa. A pronounced SPO Sb at about 30° from Sa is noticed and consistent with sinistral shearing of the rock (cf fig 3.9a, b, d, f and h). This last feature is compatible with WNW-directed movements along the RT and is confirmed by asymmetric calcite pressure shadows developed at the rim of detritical quartz grains (cf fig 3.9c, e and g).

The corresponding textures are similar to those of the samples from locality BFY (previous paragraph) and present a monoclinic symmetry (cf fig 3.10 and 3.11). However, some differences are noticed when comparing the two series. First of all, the tilting of the *c*-axis and *sd1* slip direction in the sense of shear is less pronounced compared to the BFY samples series, and samples TL2 to TL6b show a strong *c*-axis density near the normal to the foliation. The *a*, *f* (fig 3.11) and *h* pole figure again show a girdle distribution tilted at small angles from the XY plane in a counterclockwise sense. Calculations of the non-reduced pole figures for the +*a* and –*a* directions do not show a clearly different distribution as observed in the BFY samples. Instead, a girdle distribution is observed for +*a* and –*a* (fig 3.11). Another difference to the BFY sample series concerns the *r* and *sd2* (fig 3.11) pole figures. In the *r* pole figure, the maximum close to Z is clearly represented but the second maximum r1 is not well defined. It is more appropriate to describe a shoulder extending from the maximum close to Z in the direction of r1, instead of postulating two individual maxima. The degree of symmetry of the *sd2* pole figure (fig

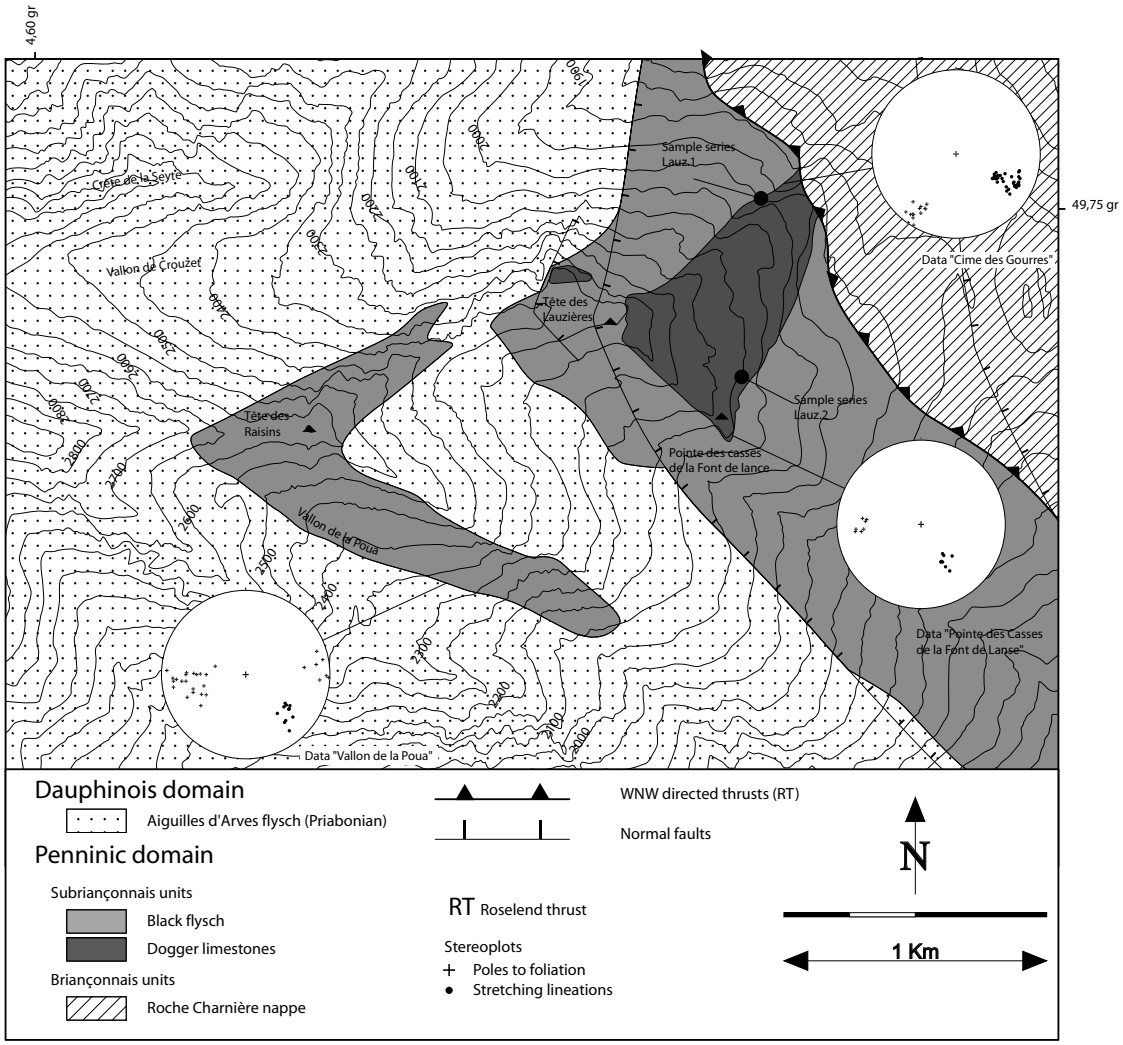


**Figure 3.8:** Detailed geological map from the southern entrance of the Fournel valley.
Samples sites Lauz 1 (5 samples) and Lauz 2 (3 samples) are shown.
Note the constant ENE-WNW transport direction along the RT.

3.11) is close to orthorhombic since 2 maxima of similar intensities at about 30° degrees from Z are observed. Only a slight predominance of the position at *sd2*a over the position at *sd2*b is noticed. To some extent, such a level of symmetry is reached by the *f* pole figure as well (fig 3.11).

The inverse pole figures calculated for samples TL3ne and TL6b are presented in figure 3.12. The non-similarity between the inverse pole figures at 45° counterclockwise and 45° clockwise from Z in the XZ plane confirms the non-orthorhombic symmetry of the texture. The inverse pole figures for the foliation-normal and the cα direction present similar intensities.

The microfabric characteristics of the Lauz 1 sample series are very close to those of sample Sa1a4 from the RYSZ (chapter 2). The *c*-axis distribution is interpreted as a combination between two orientations, namely cα and cγ. It is therefore likely that these

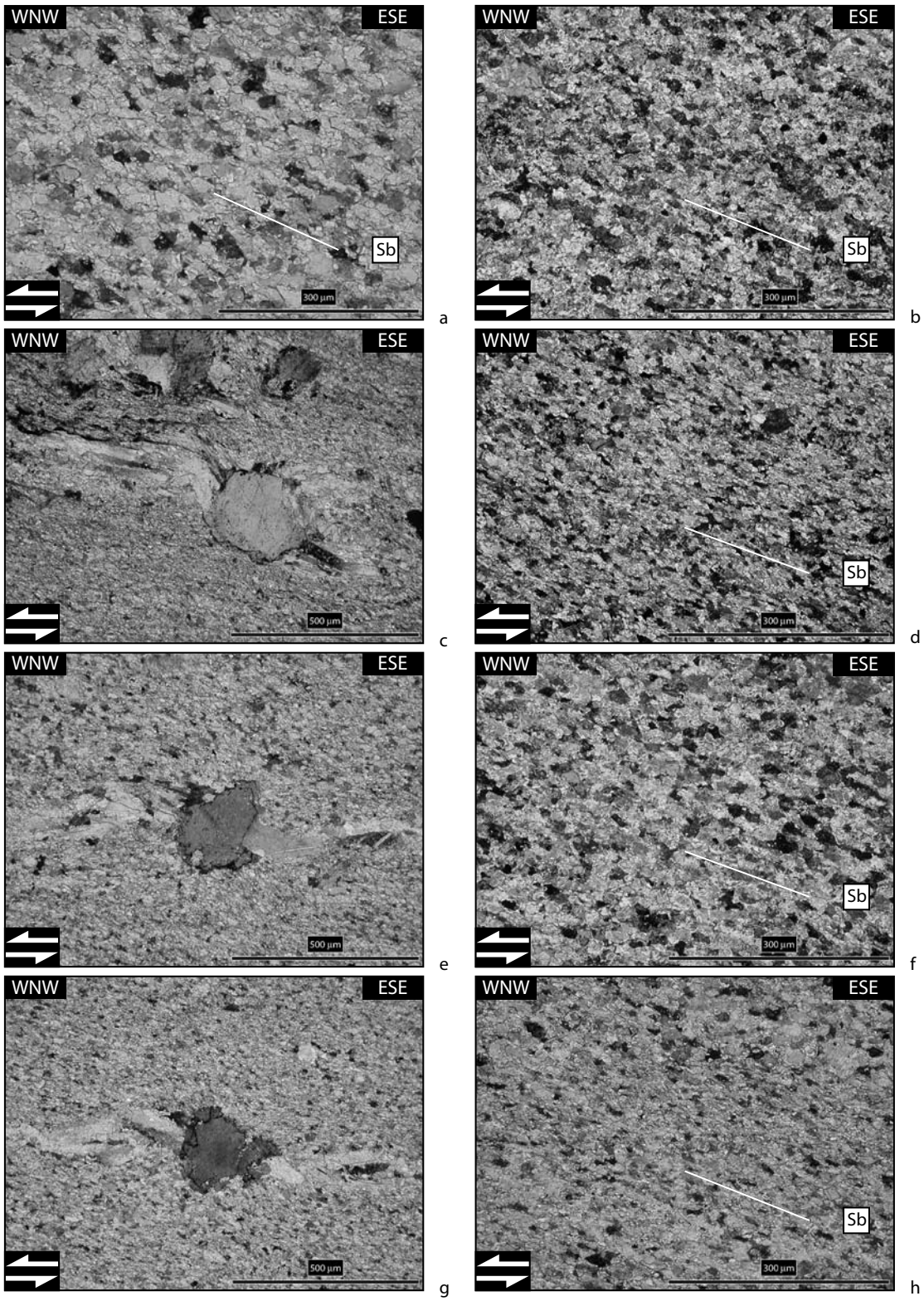


**Figure 3.9:** Photomicrographs of different calcitic marbles from the Lauz 1 series.
Normal thin sections (30 micrometers thickness) observed under crossed polarizors.
a, b, d, f and h: oblique GSPO Sb in samples TL2, TL3, TL4, TL5 and TL6.
c, e and g: asymmetric calcite pressure fringes developed at the rim of detritical quartz grains.
The sinistral sense of shear is compatible with activity along the RT. The macroscopic foliation Sa is horizontal.

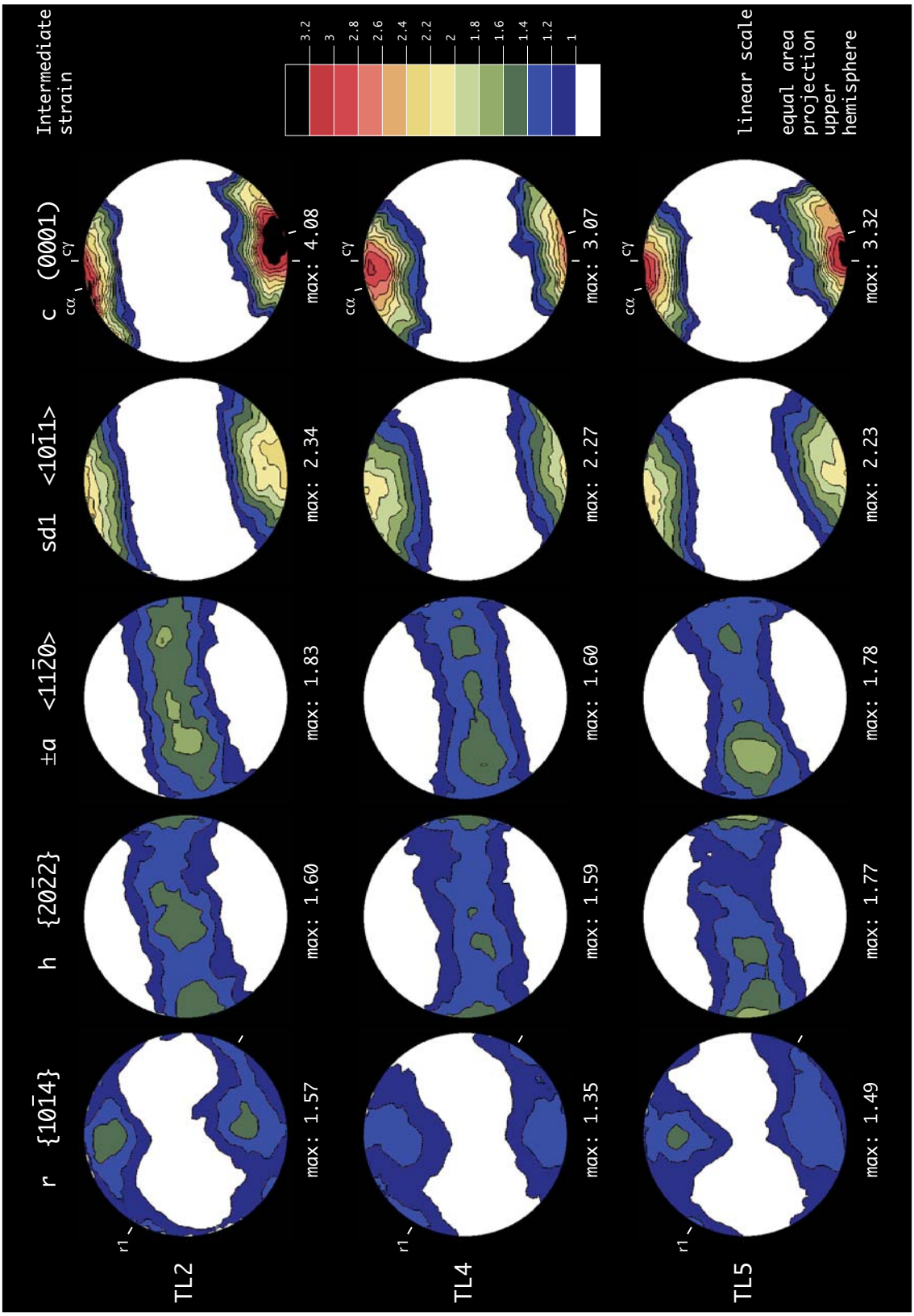


**Figure 3.10:** Texture analysis of samples TL2, TL4 and TL5.

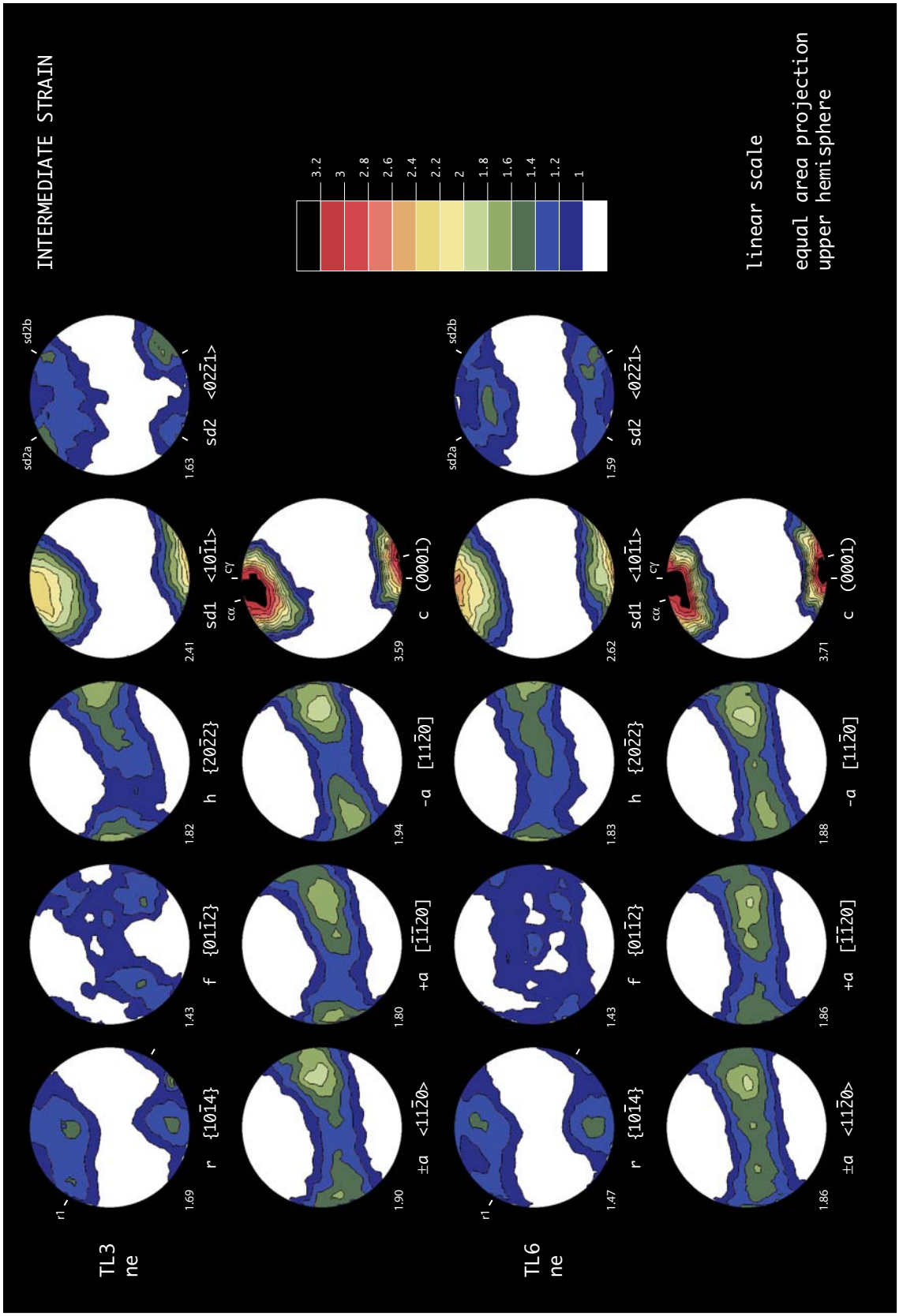


**Figure 3.11:** Complete texture analysis of samples TL3ne and TL6ne. Note the slight monoclinic symmetry of the texture.

samples have been deformed under the conditions of the so-called "intermediate" strain regime, as defined in chapter 2.

3.3.2.2 Samples from locality Lauz 2.

The thin sections from this series of samples are presented in figure 3.13. The macroscopic foliation is outlined by insoluble minerals (hematite, micas). The dynamically recrystallized matrix presents a SPO parallel to the macroscopic foliation (see fig 3.13c). Calcite pressure fringes developed at the rim of detrital quartz grains do not show clear evidence for an asymmetry (cf fig 3.13a and b). Additionally, calcite porphyroclasts symmetrically boudinaged within the foliation have been found (cf fig 3.13c).

The corresponding textures, presented in figure 3.14, show a symmetry that is close to orthorhombic. This is notably observed in the *r* pole figure showing a strong maximum close to Z and two weaker positions at r1 and r2. In detail, slight departures from orthorhombic symmetry are observed, as shown by the slight tilt in the sense of shear recorded by the *sd1* slip direction and *c*-axis pole figures (see TL1b, notably). *h* and *a* pole figures show a girdle distribution slightly inclined from the XY plane in the sense of shear. Two individualized maxima at 60° from Y are recorded in the *a* pole figure.

The Lauz 2 sample series therefore show microfabric characteristics close to those observed in sample MPY2 from the RYSZ (chapter 2). The *c*-axis distribution is therefore interpreted as a combination between the two cα and cβ orientations. The slight departures from orthorhombic symmetry in both microstructural and textural characteristics imply that the rock suffered a minor component of non-coaxial strain.

In summary, the above microfabric analysis shows that the samples collected in the Subriançonnais limestone slice from the "Têtes des Lauzières" locality have suffered a component of top-WNW shear (sinistral in figs 3.9 to 3.14). However, the proportion of non-coaxial strain is apparently more important at the northern termination of the limestone slice than along its southern continuation. The sense of shear deduced from this microfabric analysis is compatible with a southern continuation of the RT along the Briançonnais front at the entrance of the Fournel valley.

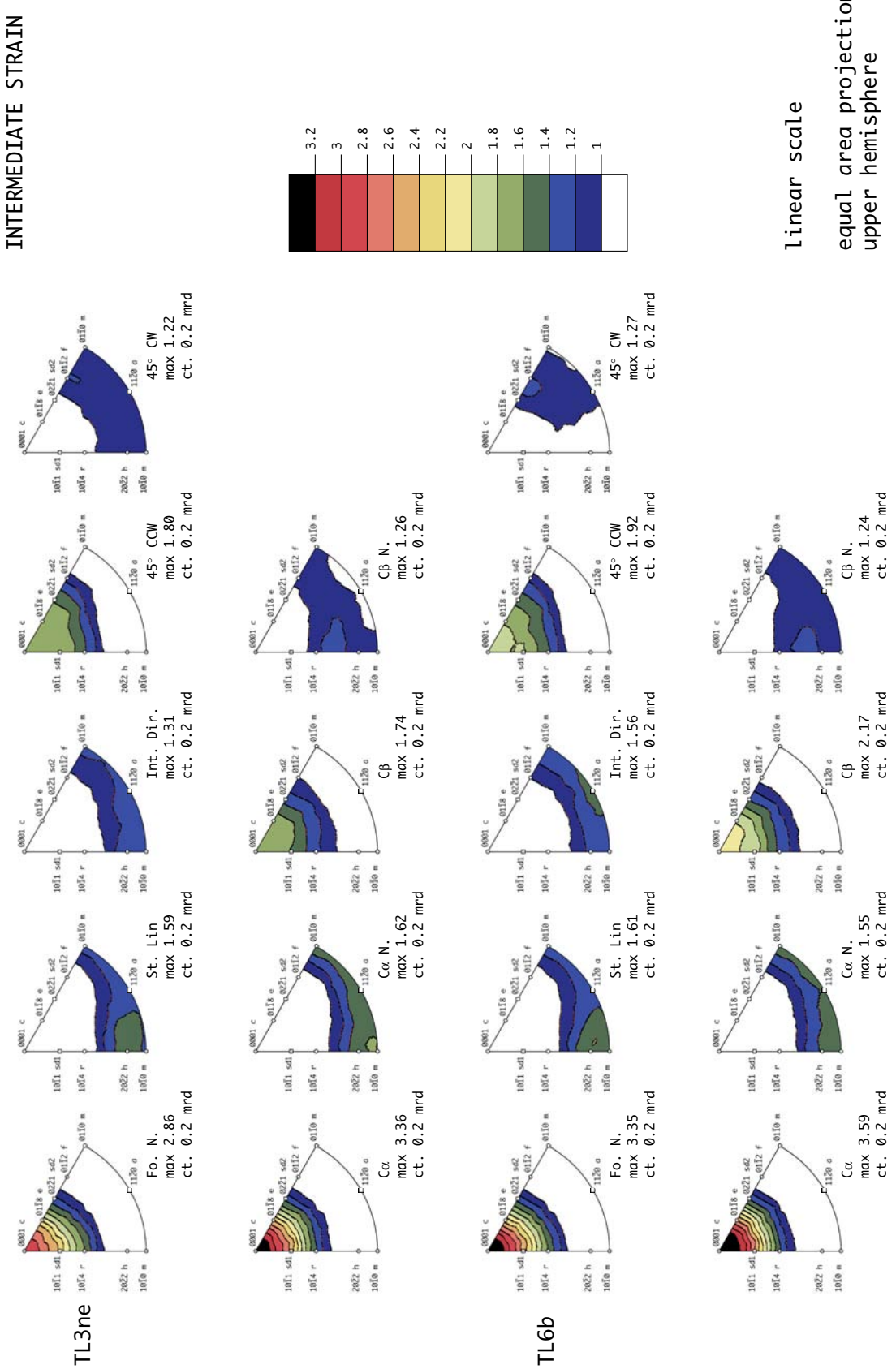


**Figure 3.12:** Inverse pole figures calculated for samples TL3ne and TL6ne. See text for discussion.

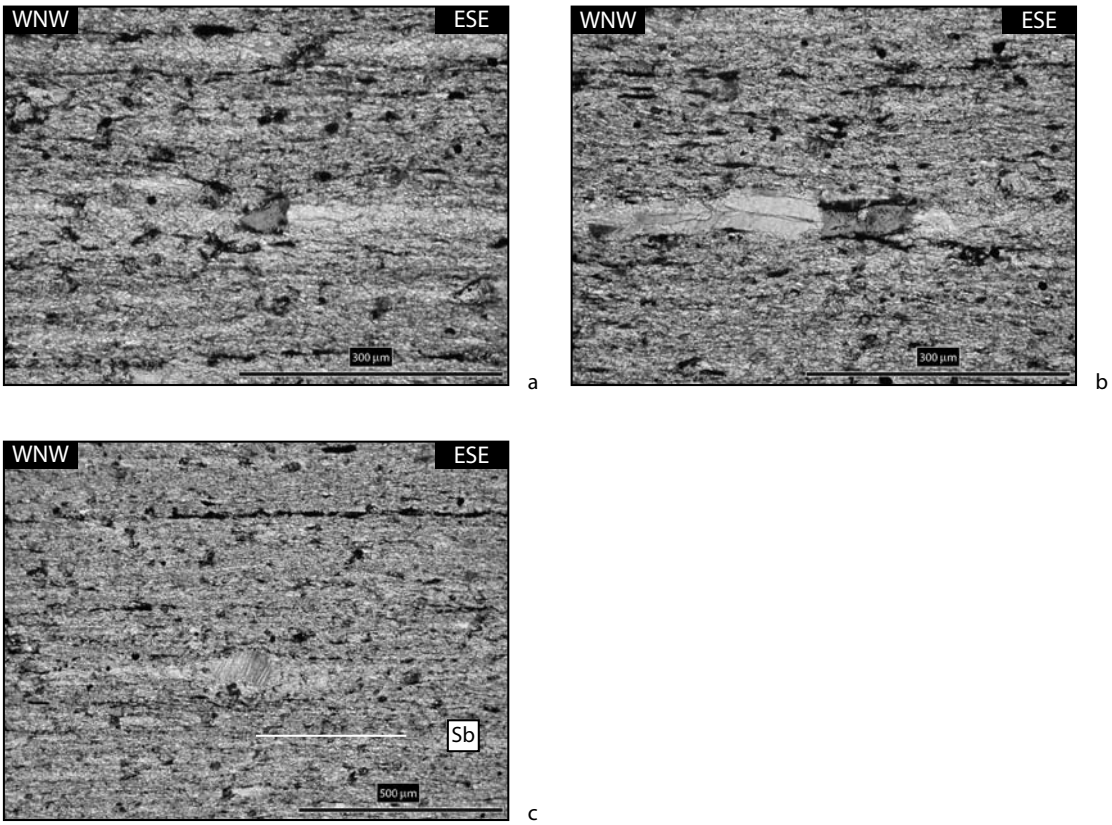


**Figure 3.13:** Photomicrographs of sample TL1. The thin section presents a thickness of 30 micrometers and is observed under crossed polarizors. The macroscopic foliation Sa is horizontal.
a) and b): symmetric calcite pressure fringes.
c): boudinaged calcite clasts; note the horizontal SPO Sb.

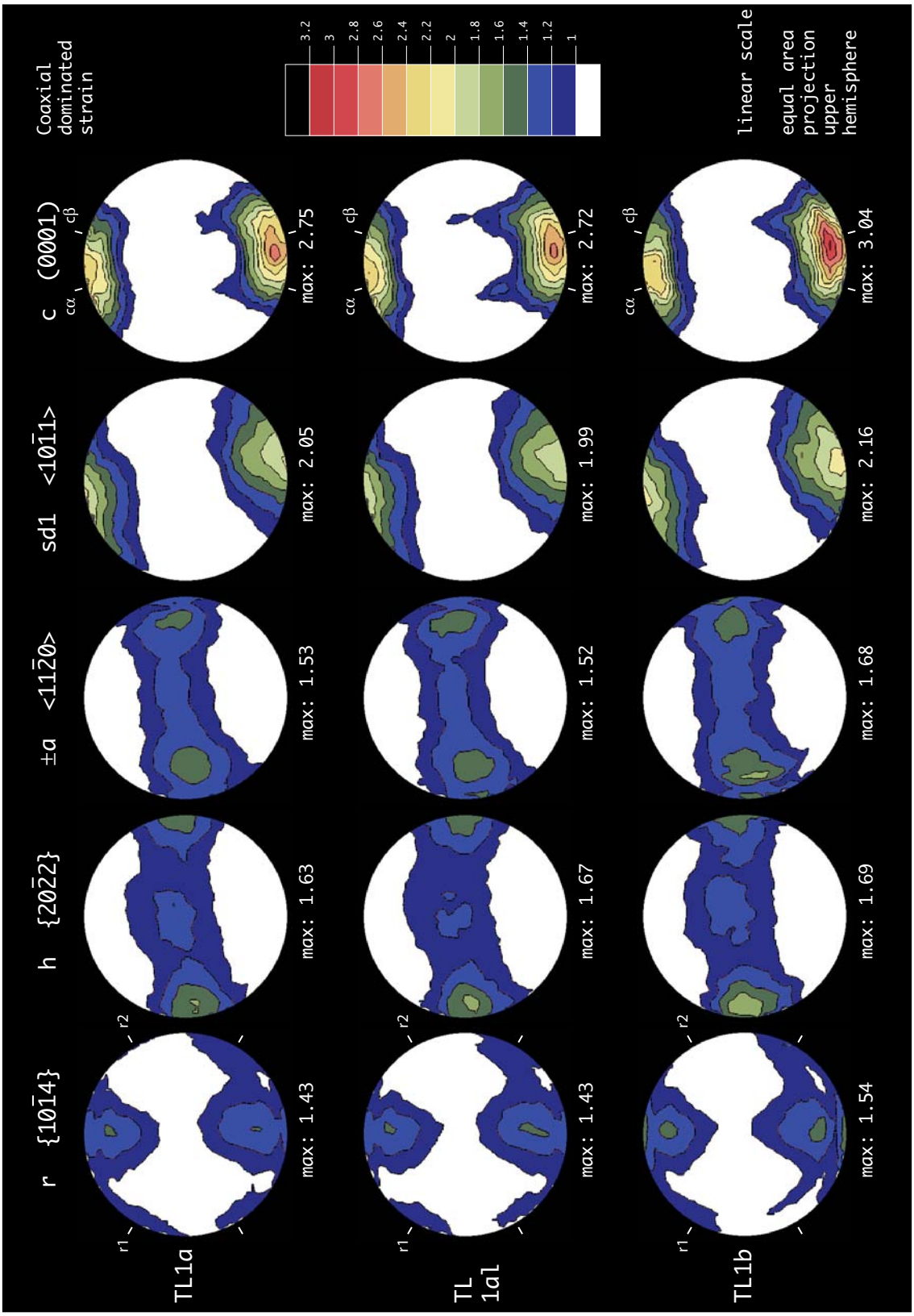


**Figure 3.14:** Texture analysis of samples TL1a, TL1al and TL1b. Note the nearly orthorhombic level of symmetry recorded by each pole figure.

3.3.3 The Briançonnais front at the village of Réotier (locality Reot).

A detailed description from the cross section at the village of Réotier is found in Debelmas (1955) and Debelmas (1983) who individualized 18 rock units when going from the inverted limb of the syncline developed at the back of the Embrunais-Ubaye nappe stack through the southern remnants of the Roche-Charnière and Champcella external Briançonnais nappes (cf fig 3.2 and 3.15).

This analysis was completed by Tricart (1980) who argued that the overall steep orientation of the different units was the result of late eastwards movements (so-called Tectonique IV phase).

Deformation features are widespread within this cross section, as attested by impressive mylonitisation phenomena developed in the calcareous formations from the Briançonnais units. All kinematic indicators are consistent with activity along the RT, i.e. WNW-directed movements.

Two different layers appeared of primary interest for microfabric analysis, namely:

1) the rock unit RC1 (corresponding to the rock unit number 4 of Debelmas 1955), middle Triassic in age, consisting in a 25 meters thick alternance between dolomite and calcitic marble layers (see fig 3.15a and 3.15b). A very intense foliation (see fig 3.15c), about N-S striking is developed and carries a strong WNW-ESE stretching lineation. Hand specimens show a strong mylonitic foliation outlined by yellowish millimetric levels of dolomitic nature (see below). The competence contrast between calcitic marbles and dolomitic layers is expressed in well-developed metric-scale “pinch and swell” structures (see fig. 3.15d). The samples taken from this unit are R6, R7, R9, R10, R10b, GT202, Bar1, Bar2, Bar2b and Bar3. They are grouped into the so-called Reot 1 series.
2) the rock unit Ch4 (corresponding to the rock unit number 18 of Debelmas 1955), consisting of a ten meters thick Dogger marble layer (cf fig 3.15a). These rocks again carry a pronounced stretching lineation outlined by macroscopically recognizable calcite pressure fringes developed at the rim of pyrite crystals. Five samples have been taken in this layer (R1, R2a, R2b, R3 and R4). They correspond to the Reot 2 series.

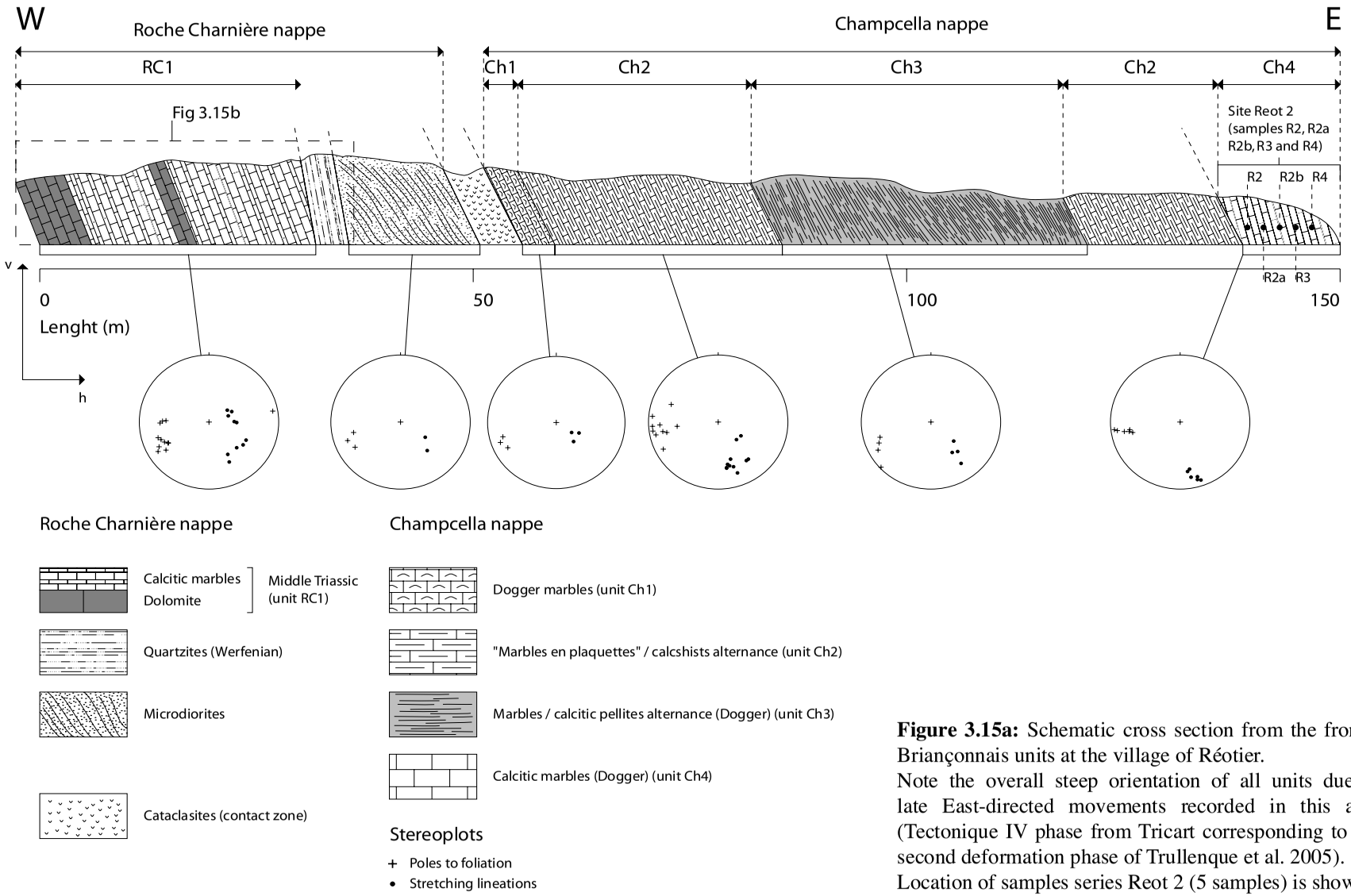


**Figure 3.15a:** Schematic cross section from the frontal Briançonnais units at the village of Réotier.
Note the overall steep orientation of all units due to late East-directed movements recorded in this area (Tectonique IV phase from Tricart corresponding to the second deformation phase of Trullenque et al. 2005).
Location of samples series Reot 2 (5 samples) is shown.

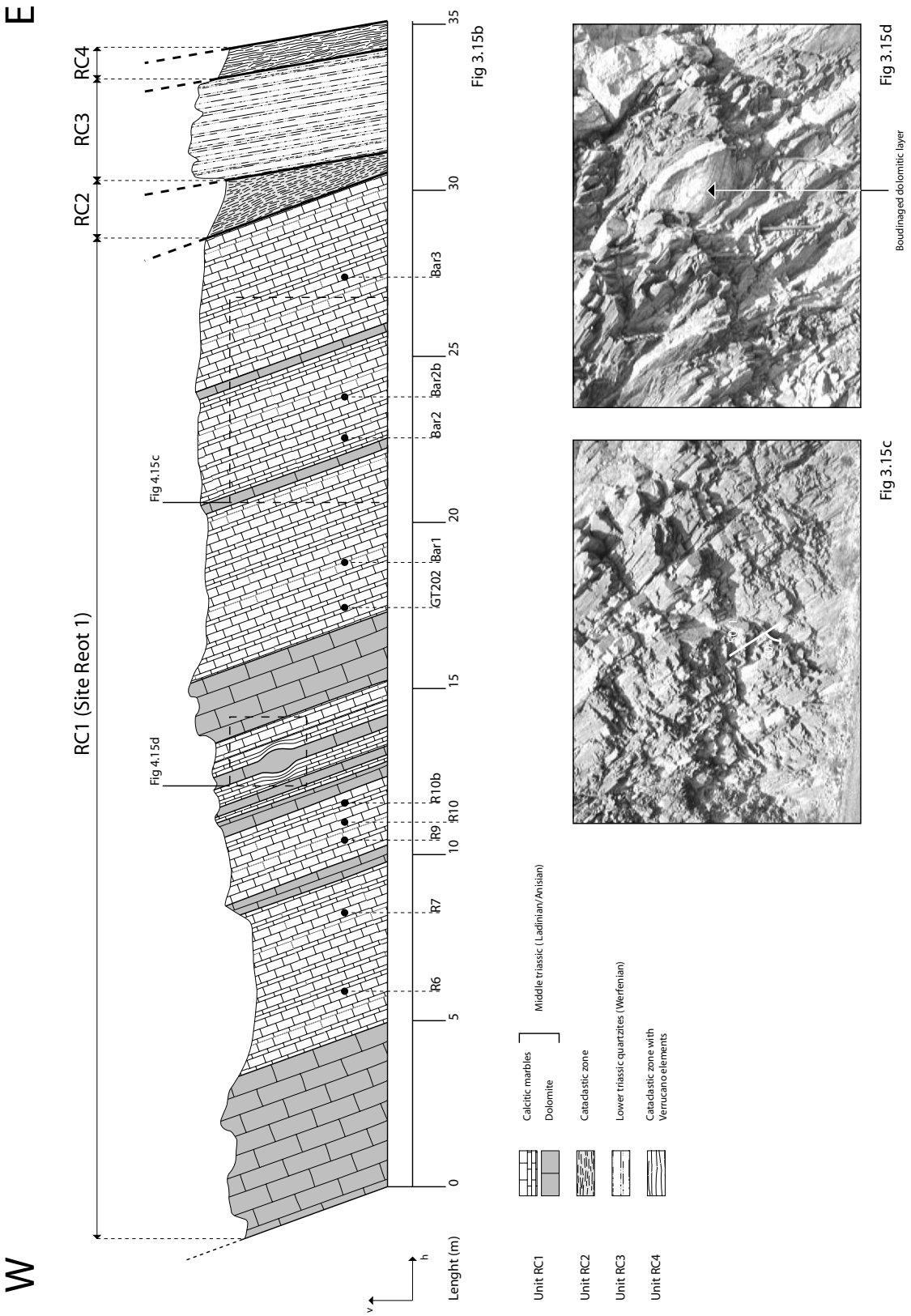
E
W
RC4
RC3
RC2
RC1 (Site Reot 1)
Fig 4.15c
Fig 4.15d
Fig 3.15b
Bar3
Bar2b
Bar2
Bar1
GT202
R10b
R10
R9
R7
R6
35
30
25
20
15
10
5
0
Lenght (m)
h
v
Calcitic marbles
Dolomite
Middle triassic ( Ladinian/Anisian)
Catadastic zone
Lower triassic quartzites (Werfenian)
Catadastic zone with Verrucano elements
Unit RC1
Unit RC2
Unit RC3
Unit RC4
Fig 3.15d
Boudinaged dolomitic layer
Fig 3.15c

**Figure 3.15 (continued)**
**b:** Detailed representation of the frontal units of the Roche Charnière nappe. Note that the overall stratigraphic sequence is inverted. Localisation of samples series Reot 1 (10 samples) is shown. WNW oriented stretching lineations measured on the macroscopic foliation plane indicate that the mylonitisation process is related to activity along the RT.
**c:** penetrative foliation developed within the middle Triassic marbles series.
**d:** metric-scale boudin type deformation features indicating a WNW-ESE direction of stretching.

3.3.3.1 Samples from profile Reot 1.

In thin section, the rocks from locality Reot 1 appear intensively recrystallised. The grains show a very slight shape preferred orientation parallel to the macroscopic foliation (cf fig 3.16).

A few dolomitic clasts are preserved from dynamic recrystallization. The nature of these clasts has been analyzed by cathodo-luminescence whereby dolomite appears in light orange color (cf fig 3.17). These clasts are often fragmented and show evidence of twinning deformation. The rock additionally contains an appreciable amount of detrital quartz grains.

From the textural point of view, the samples from the Reot 1 locality usually present weak pole figure maxima (cf fig 3.18a, 3.18b, 3.19a and 3.19b). A crystallographic preferred orientation is nonetheless recorded and presents an orthorhombic symmetry, most readily observed in sample R10 and R10b (see fig 3.18b). A broad maximum for the *c*-axis and *sd1* slip direction is measured in close vicinity with the foliation normal. *a* and *h* pole figures show a girdle distribution within the XY plane with two maxima symmetrically oriented at 60° for Y in the case of the *a* directions. One dominant maximum is recorded at Z for the *r* pole figure.

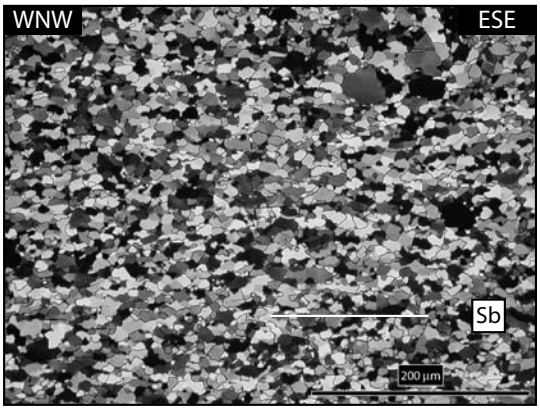


**Figure 3.16:** Photomicrographs of sample R10 (ultra-thin sections of 2 micrometers thickness observed under crossed polarizers).
Note the slight horizontal flattening of the grains (Sb). The macroscopic foliation Sa is horizontal.

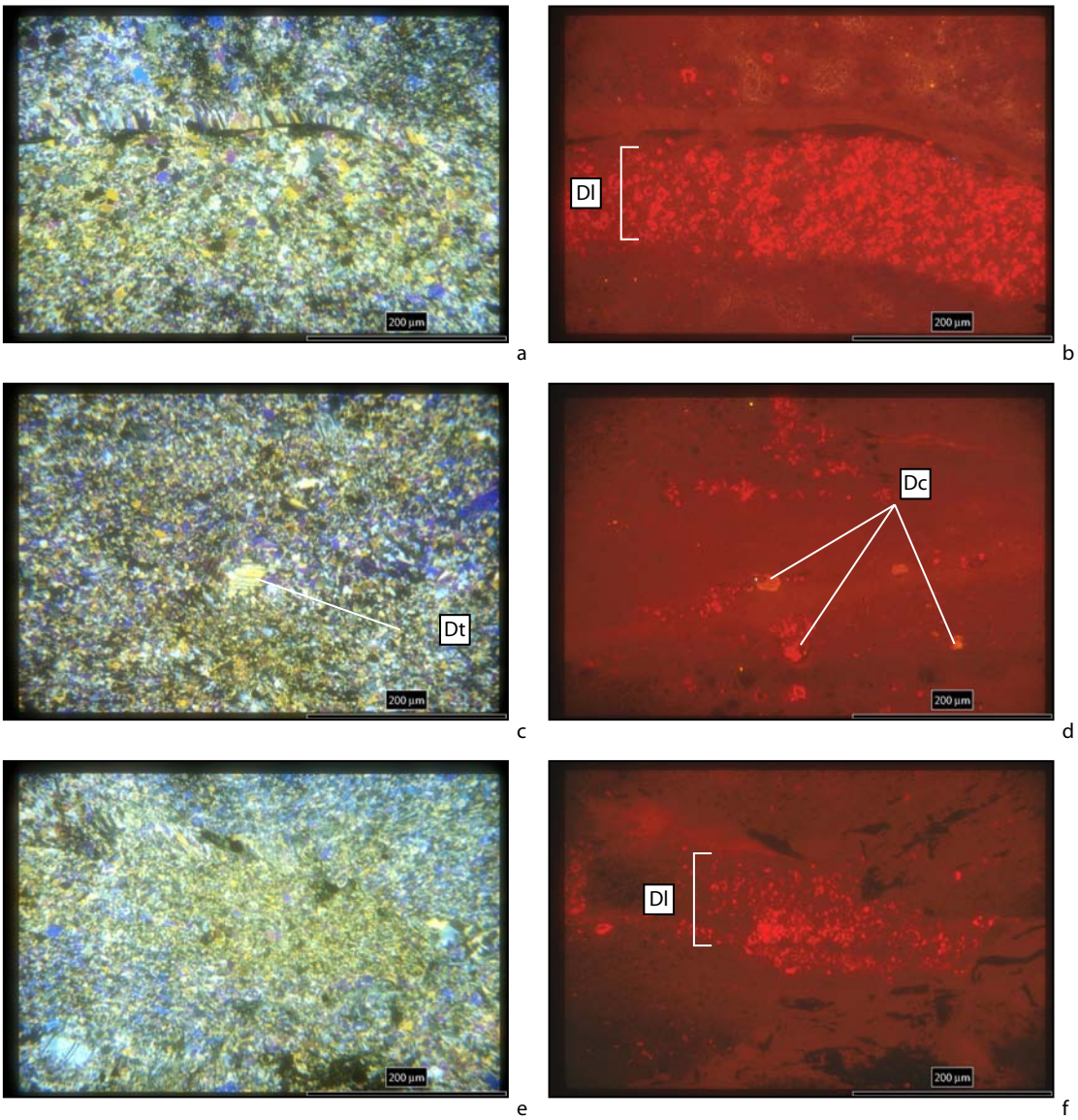


**Figure 3.17:** a, c and e: photomicrographs of sample GT202 taken from an ultra-thin section observed under crossed polarizors.
b, d and f: cathodoluminescence analysis of the corresponding photomicrographs.
Dl: dolomitic levels, Dc: dolomite crystals, Dt: deformation twins. The macroscopic foliation Sa is horizontal.

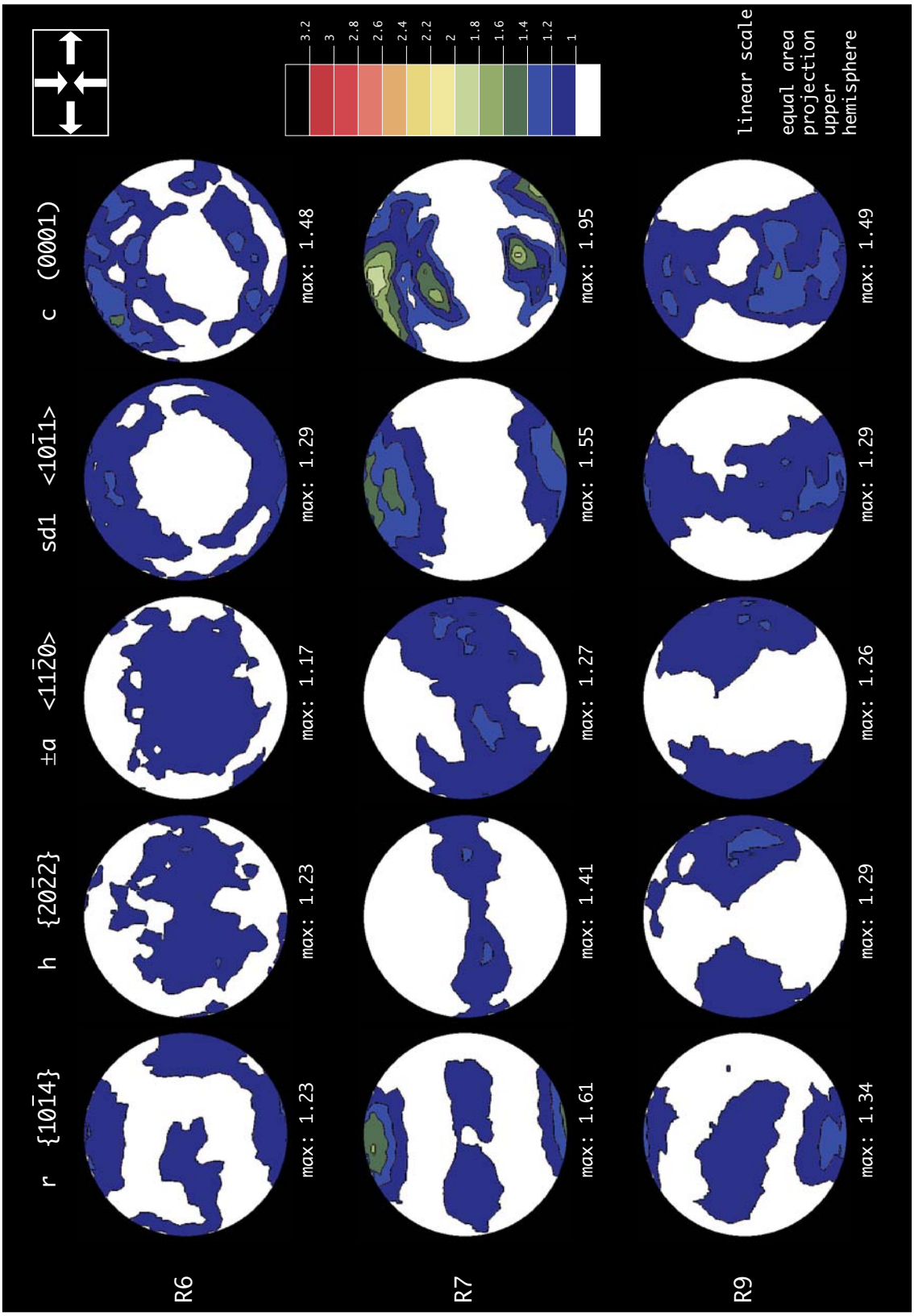


**Figure 3.18a:** Texture analysis of samples R6, R7 and R9.

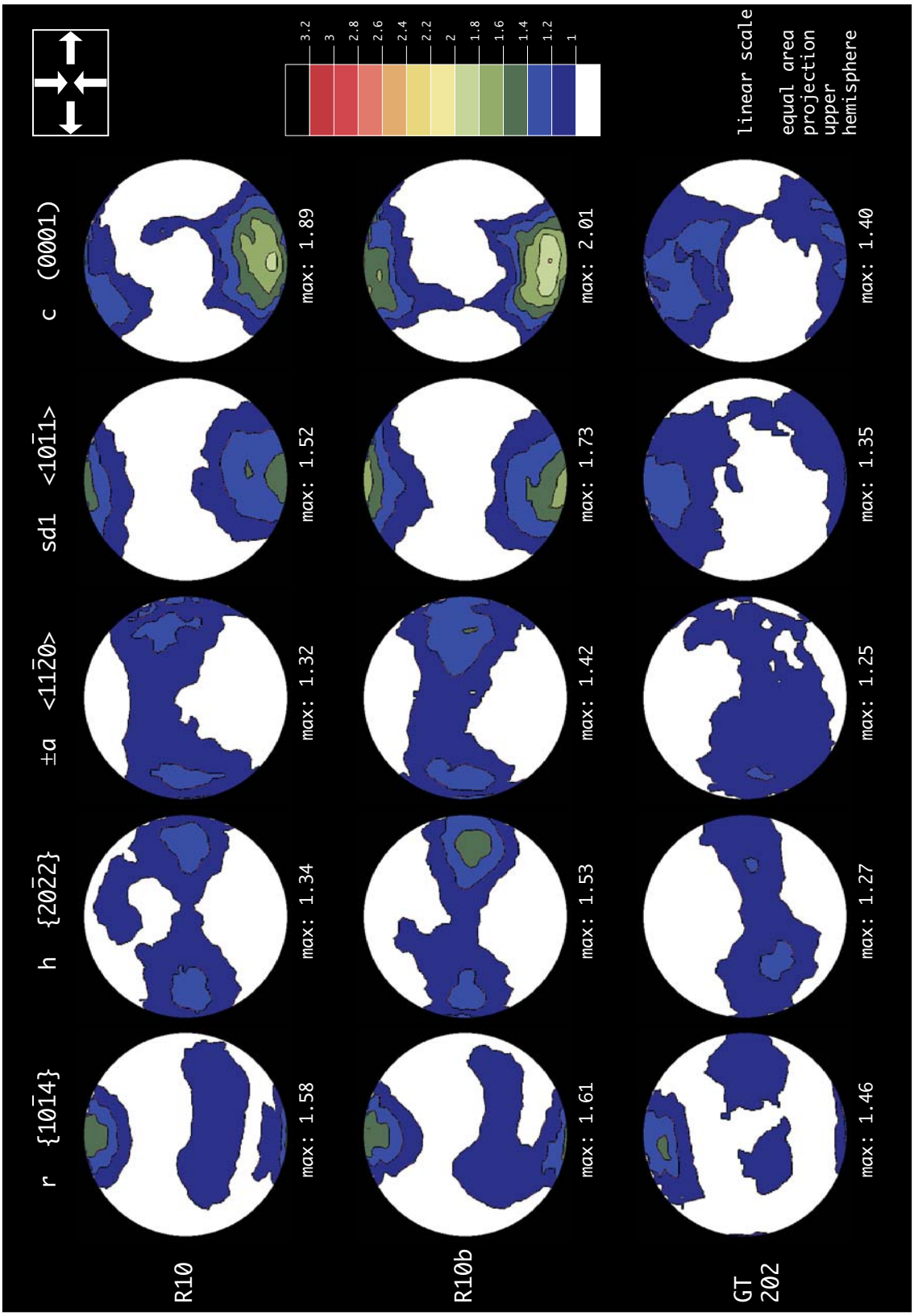


**Figure 3.18b:** Texture analysis of samples R10, R10b and GT202.

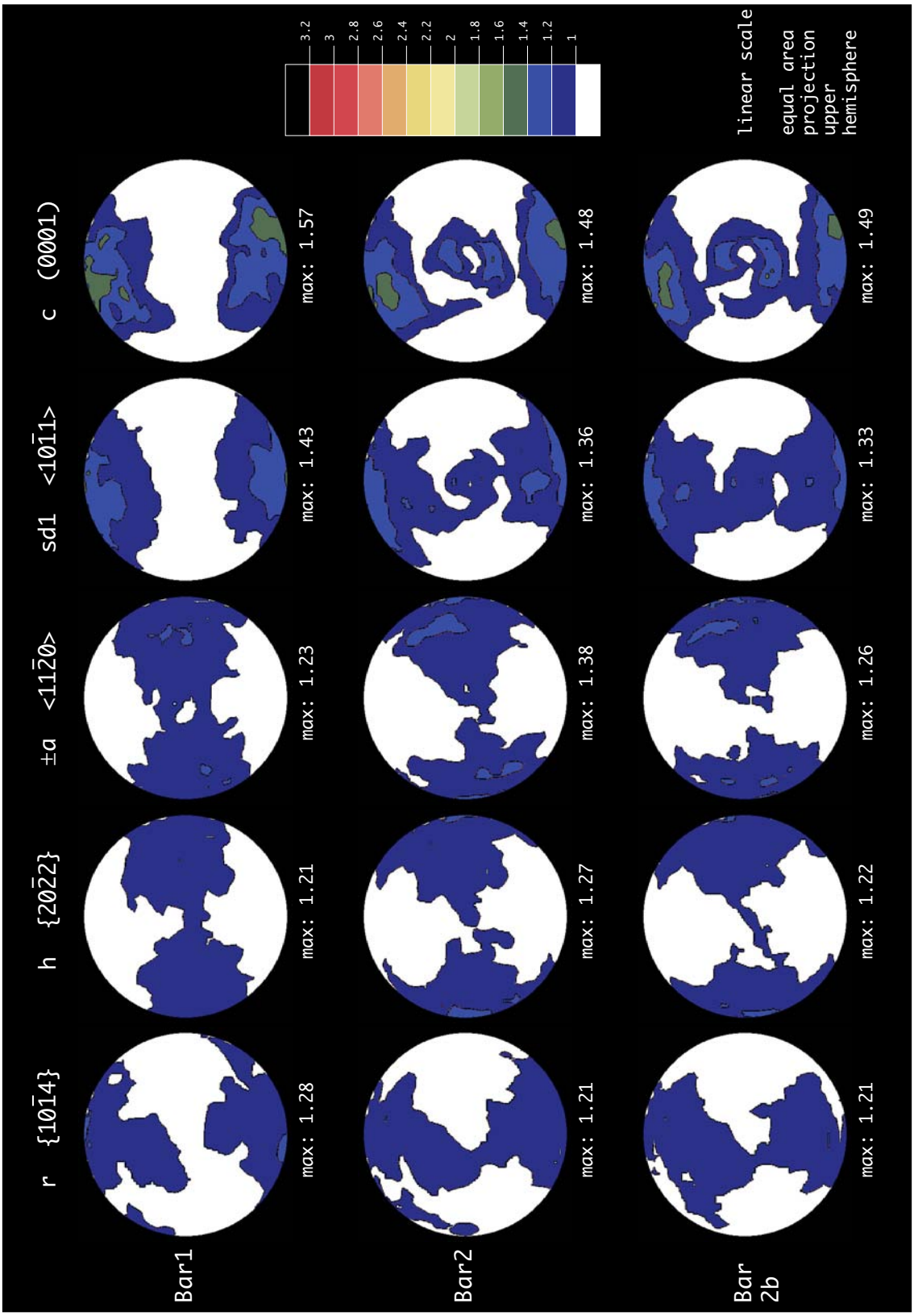


**Figure 3.19a:** Texture analysis of samples Bar1, Bar2 and Bar2b.

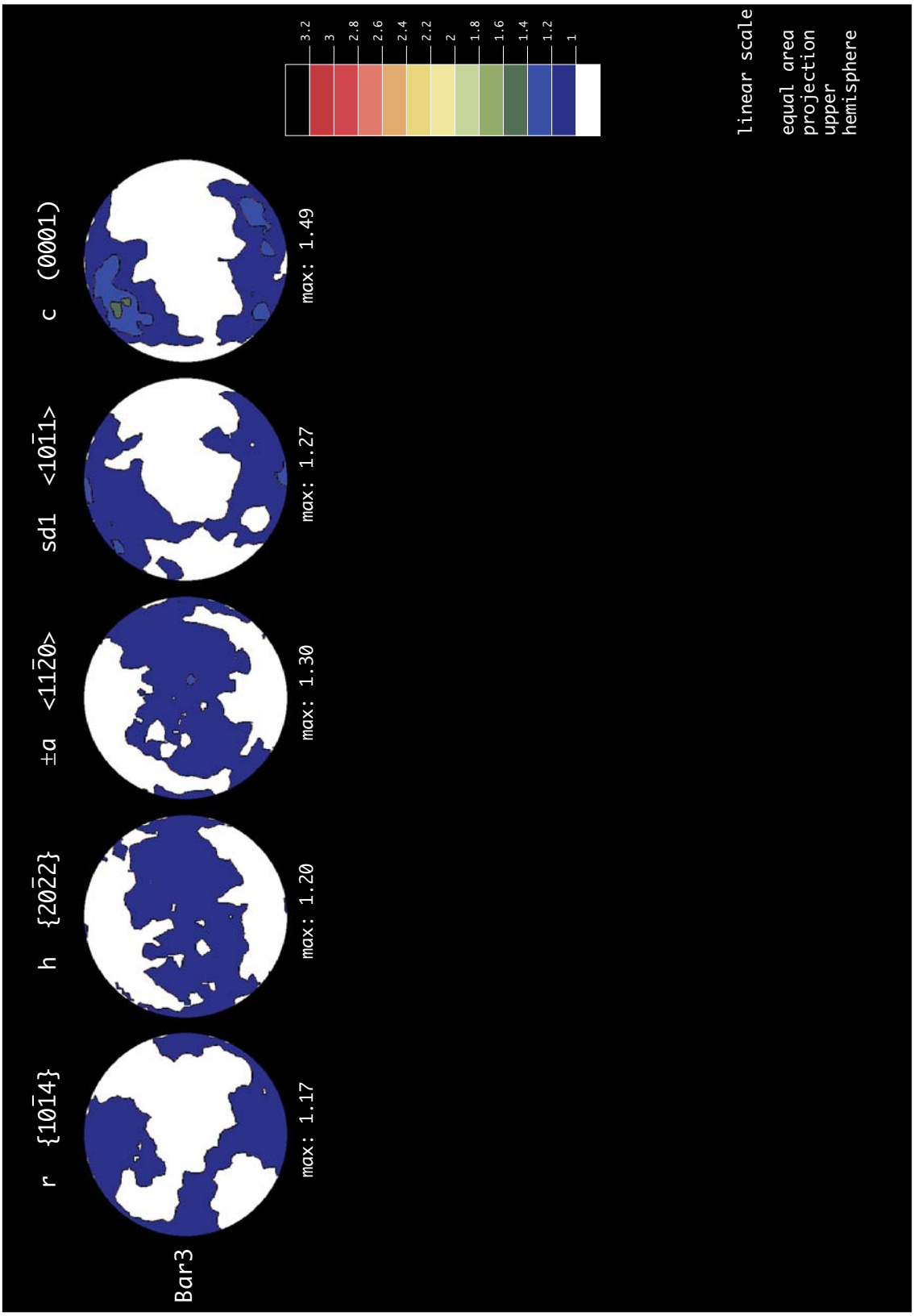


**Figure 3.19b:** Texture analysis of sample Bar3.

3.3.3.2 Samples from profile Reot 2.

Photomicrographs from samples R3 and R4 taken at different levels of magnification are presented in fig 3.20. Figures 3.20a, b and d present microboudinage deformation features of a former vein of dolomitic composition. The boudinaged pieces present angular shapes and are often internally fragmented (see fig 3.20b). Note that the dynamically recrystallized calcitic matrix flows around these boudinaged units, as a consequence of competence contrast. Calcite pressure fringes developed at the rim of detrital quartz grains do not show any evidence of asymmetry (see fig 3.20c). A strong grain shape preferred orientation parallel to the macroscopic foliation plane is observed (cf fig 3.20e).

From the textural point of view, the *c*-axis pole figures of samples from this series show a broad maximum at the periphery of the pole figure and around the foliation normal (cf fig 3.21 and 3.22). This broad maximum often shows a tendency to split into two sub-maxima corresponding to the cα and cβ positions defined in chapter 2. The *a* axis pole figure shows a girdle distribution within the XY plane with two weak maxima at 60° from Y. No differences have been noticed between the non-reduced +*a* and –*a* pole figures (cf fig 3.22). The *f* crystallographic planes are distributed on two small circles centered at X with an opening angle of about 40° (see fig 3.22). Finally, the *r* pole figure shows again a maximum close to the Z direction and a broad weaker maximum at X corresponding to positions r1 and r2.

It is concluded that these textures present an orthorhombic level of symmetry. This is confirmed by calculations of inverse pole figures for samples R3 and R4 showing similar distributions at 45° clockwise and 45° counterclockwise from the foliation normal, cα and cβ directions, cαN and cβN, respectively (see fig 3.23).

From the above analysis, it appears that both samples series taken from the Triassic and Dogger marbles from the Roche Charnière and Champcella nappes, respectively, present microfabric characteristics similar to the ones of sample MPY2 from the RYSZ and indicating a coaxial deformation regime (see chapter 2). The main difference is found in the average values of pole figures and inverse pole figures maxima, which are slightly lower at the Réotier locality.

It is therefore proposed that the whole Briançonnais external units found along the RT at the Réotier locality have been deformed under conditions of dominant coaxial strain. The inferred WNW-ESE oriented stretching direction is compatible with activity along the RT.

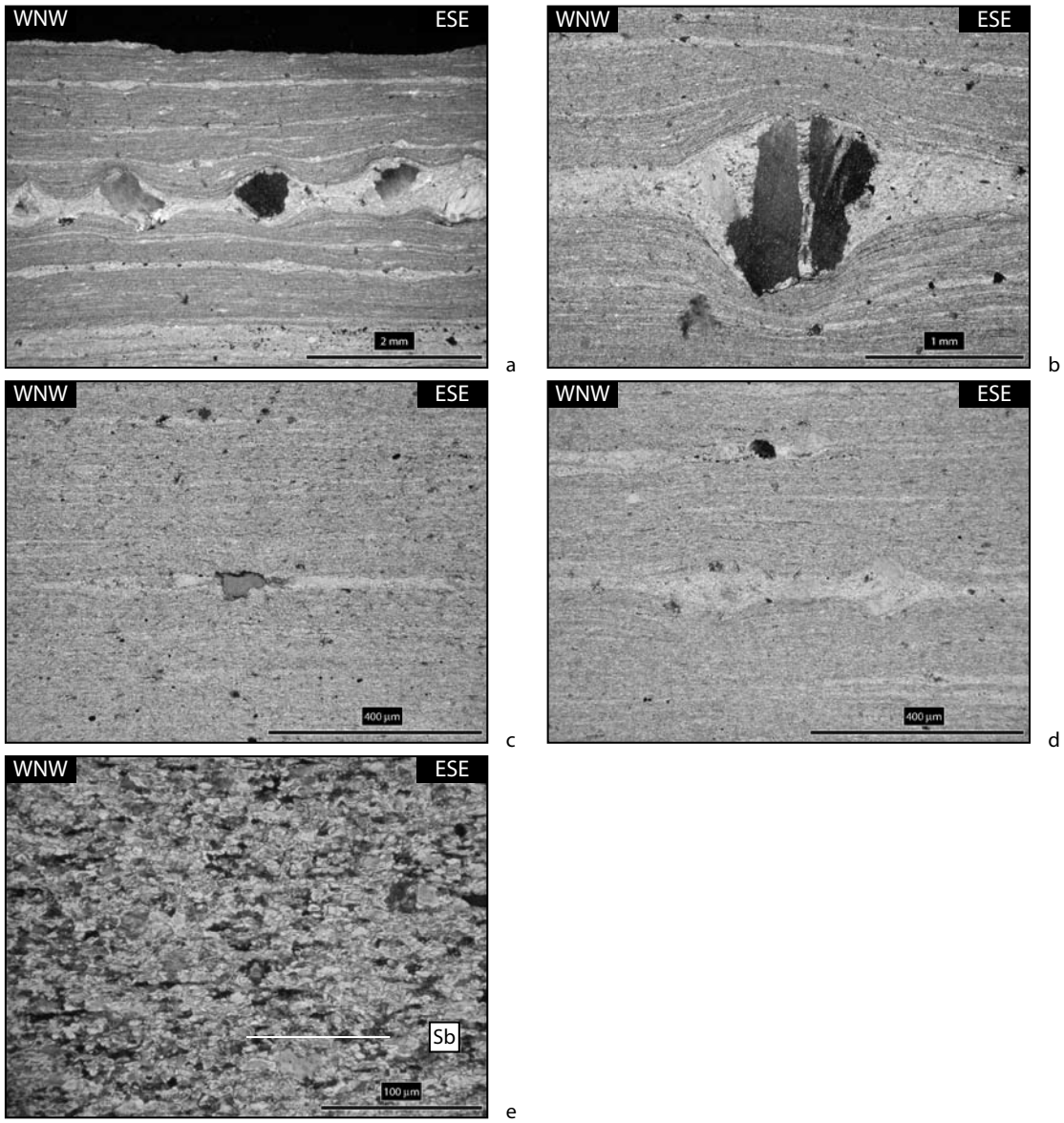


**Figure 3.20:** Photomicrographs of sample R3 (a, b and c) and R4 (d and e) observed in XZ sections (normal thin section 30 micrometers thickness observed under crossed polarizors).
a: boudinage of a former dolomitic vein. Note the flowing of the dynamically recrystallized calcitic matrix around the angular-shaped clasts.
b: details of a fragmented dolomitic clast.
c: symmetric calcite pressure fringes developed at the rim of a detritical quartz grain.
d: symmetrically boudinaged calcite clast.
e: SPO Sb developed within the homogeneous dynamically recrystallized matrix.

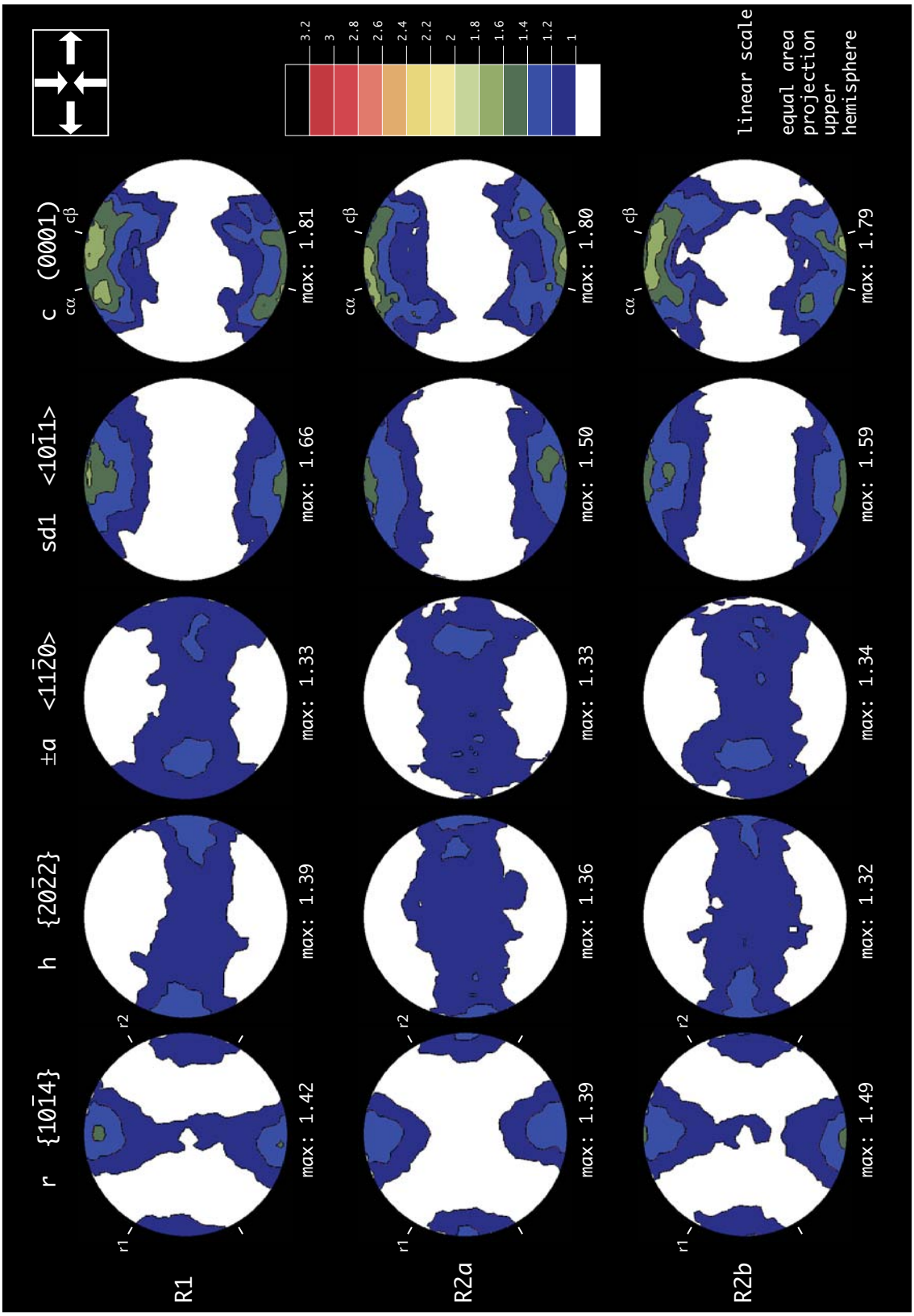


**Figure 3.21:** Texture analysis of samples R1, R2a and R2b.

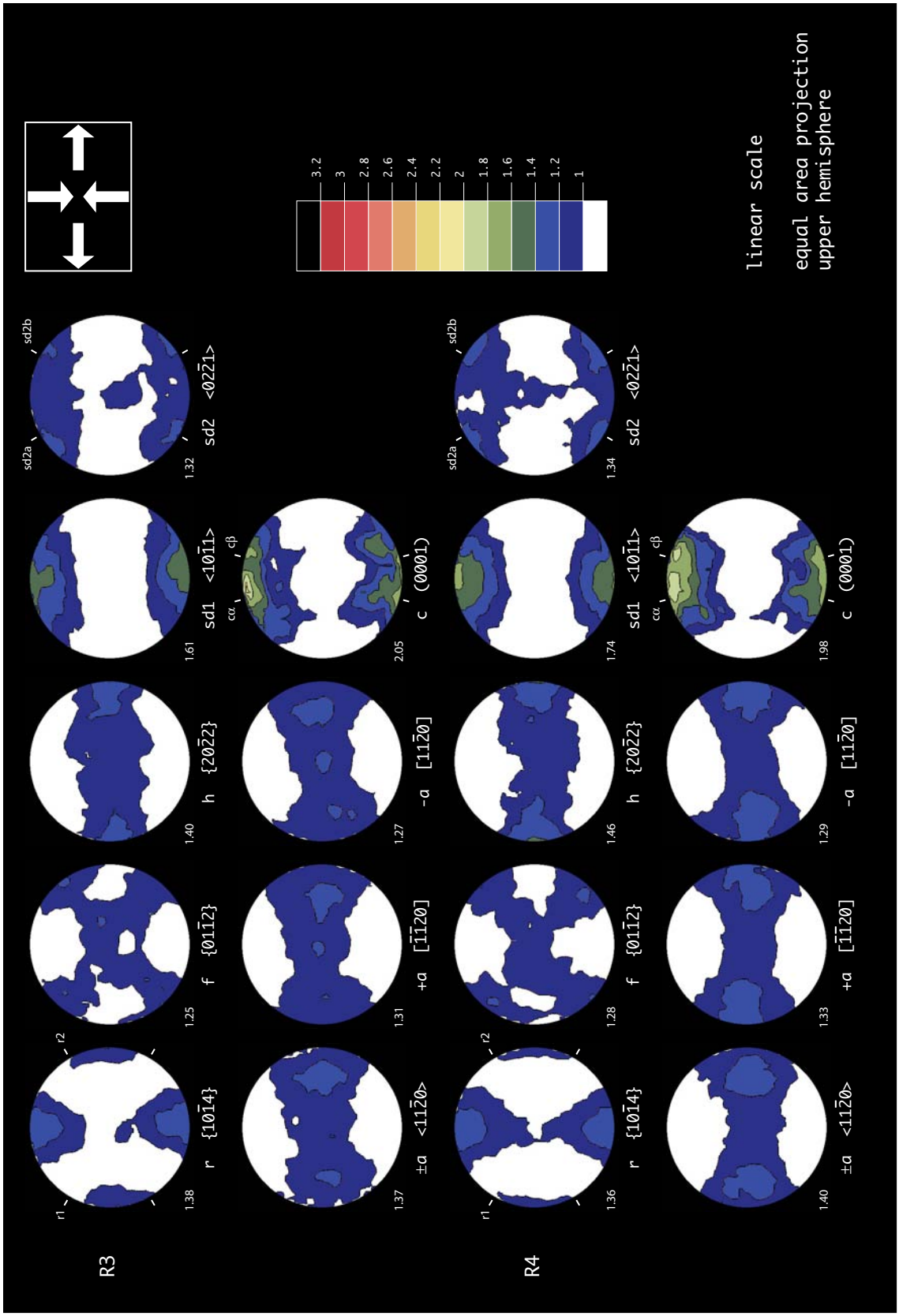


**Figure 3.22:** Complete texture analysis of samples R3 and R4. Note the splitting of the *c*-axis distribution at positions cα and cβ.

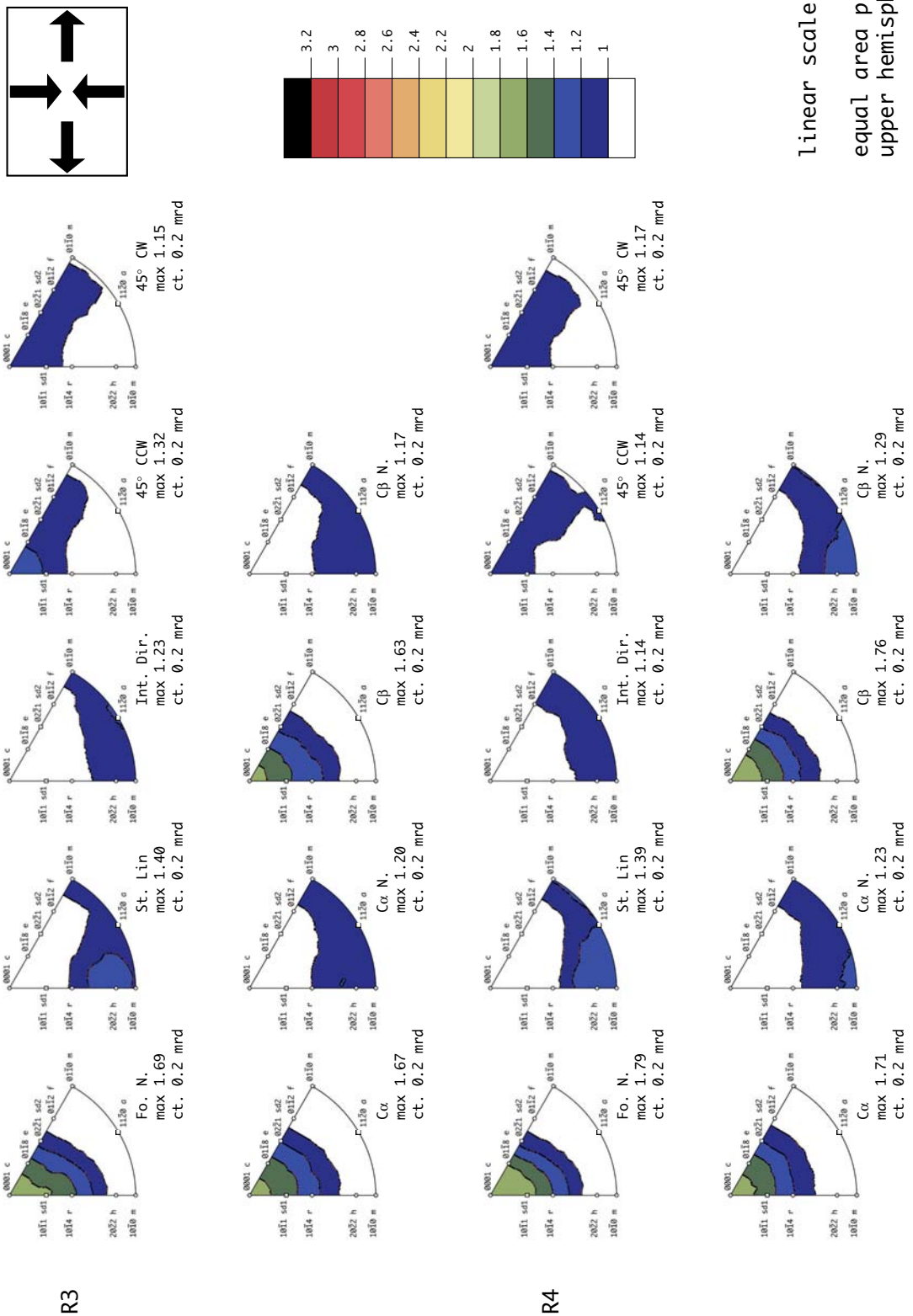


**Figure 3.23:** Inverse pole figures calculated for samples R3 and R4. See text for discussion.

3.3.4 The RT at the rear of the Argentera massif (locality “Vallone del Arma”).

This series of samples has been taken from the rear of the Argentera massif, as is shown in the map presented in figure 3.24. Numerous mylonitic bands are indeed found within the frontal units of Briançonnais origin, notably in the “Vallone del Arma” valley. Samples Gtsc2401, Gtsc2501 and GT901ne have been taken from Jurassic marbles intensively deformed. Sample Gtsc2901, of Subriançonnais origin, comes from a fine-grained calcitic mylonitic band affecting Malm-Dogger marbles pinched in between two thick dolomitic layers.

The deformation of these calcitic marbles is related to activity along the RT (see chapter 1), inducing sinistral strike slip deformation at the rear of this external crystalline massif.

At outcrop scale, the rocks present a typical mylonitic foliation outlined by white millimetric layers, possible remnants of initial calcitic veins.

3.3.4.1 Sample GT901ne (Jurassic marble of Briançonnais origin).

The following discussion focuses on sample GT901ne since only this sample presents a clear crystallographic preferred orientation (compare fig 3.26 with fig 3.27).

In thin section, the dynamically recrystallized matrix presents an oblique SPO consistent with top-WNW shearing of the rocks (cf fig 3.25). A significant proportion of second phase particles (hematite, pyrite and micas) is observed.

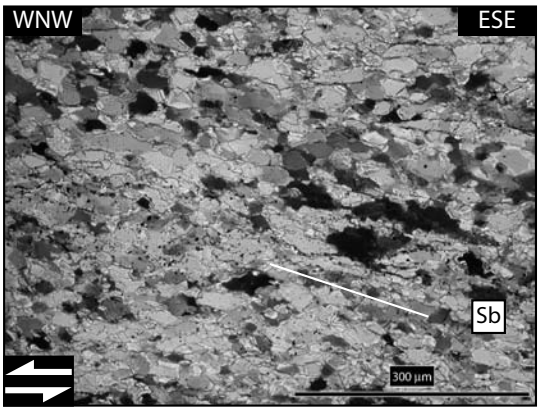


**Figure 3.25:** XZ section of sample GT901ne (30 micrometers thickness section observed under crossed polarizors).
Note the oblique GSPO Sb of the dynamically recrystallized matrix indicative of sinistral sense of shear and compatible with activity along the RT.

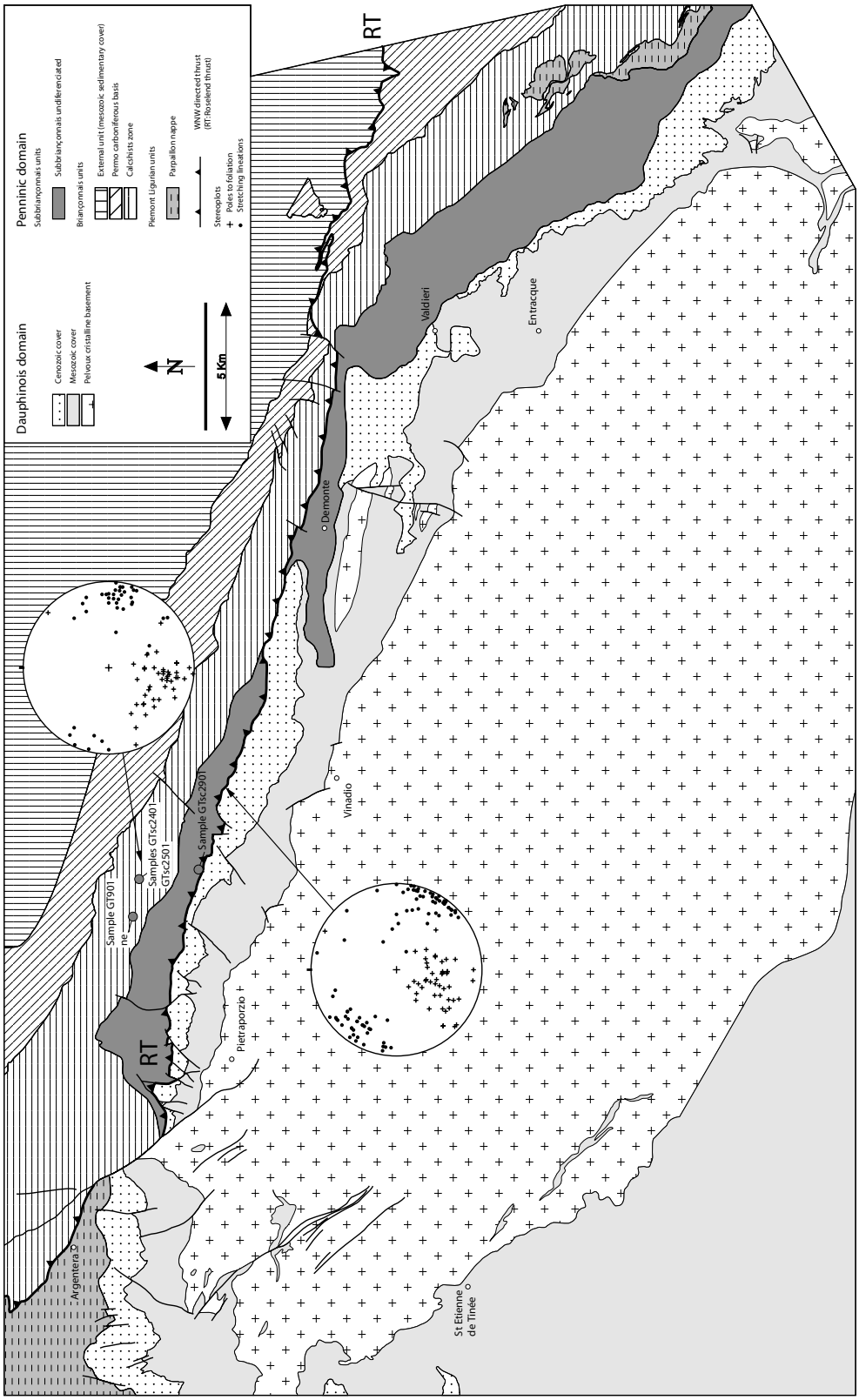


**Figure 3.24:** Structural map of the Argentera crystalline massif and external Briançonnais units after Malaroda et al. (1967). All kinematic indicators show an overall WNW-ESE orientation, i.e. compatible with activity along the RT. Localities of samples GT901, Gtsc2401, Gtsc2501 and Gtsc2901 are reported.

From the textural point of view, sample GT901ne presents a clear monoclinic symmetry in respect to the XYZ sample coordinate system (cf fig 3.27). Both *c*-axis and *sd1* slip direction are tilted in the sense of shear by an angle of about 20°. This tilting is accordingly found in the +*a* and –*a* girdle distributions rotated from the XY plane in a counterclockwise sense. The final *c*-axis orientation measured in this sample is interpreted as the cα position determined in chapter 2. The *r* pole figure shows a maximum close to the Z direction with a shoulder extending towards position r1. The *sd2* pole figure shows a dominant preferred orientation at *sd2*a.

The non-orthorhombic level of symmetry of sample GT901ne is reflected by the non-similarity in inverse pole figures between the directions at 45°CW and 45°CCW from Z, the position at cα and cβ, cαN and cβN respectively (cf fig 3.28). The strongest maximum is recorded in the cα inverse pole figure (2.70 mrd) while the cαN direction shows a nearly random girdle distribution. According to the conclusions drawn in chapter 2, it is proposed that the texture measured on sample GT901ne is the result of dominant slip on the basal plane in two conjugate *a* directions.

In summary, most of the microfabric characteristics reported in sample GT901ne are directly comparable to those described for sample MPY28 at the "Rocher de l'Yret" locality. It is therefore concluded that sample GT901ne has been deformed under a non-coaxial dominated deformation path within a broad sinistral shear zone found at the rear of the Argentera massif. The inferred sense of shear is again compatible with activity along the RT, i.e. WNW directed movements.

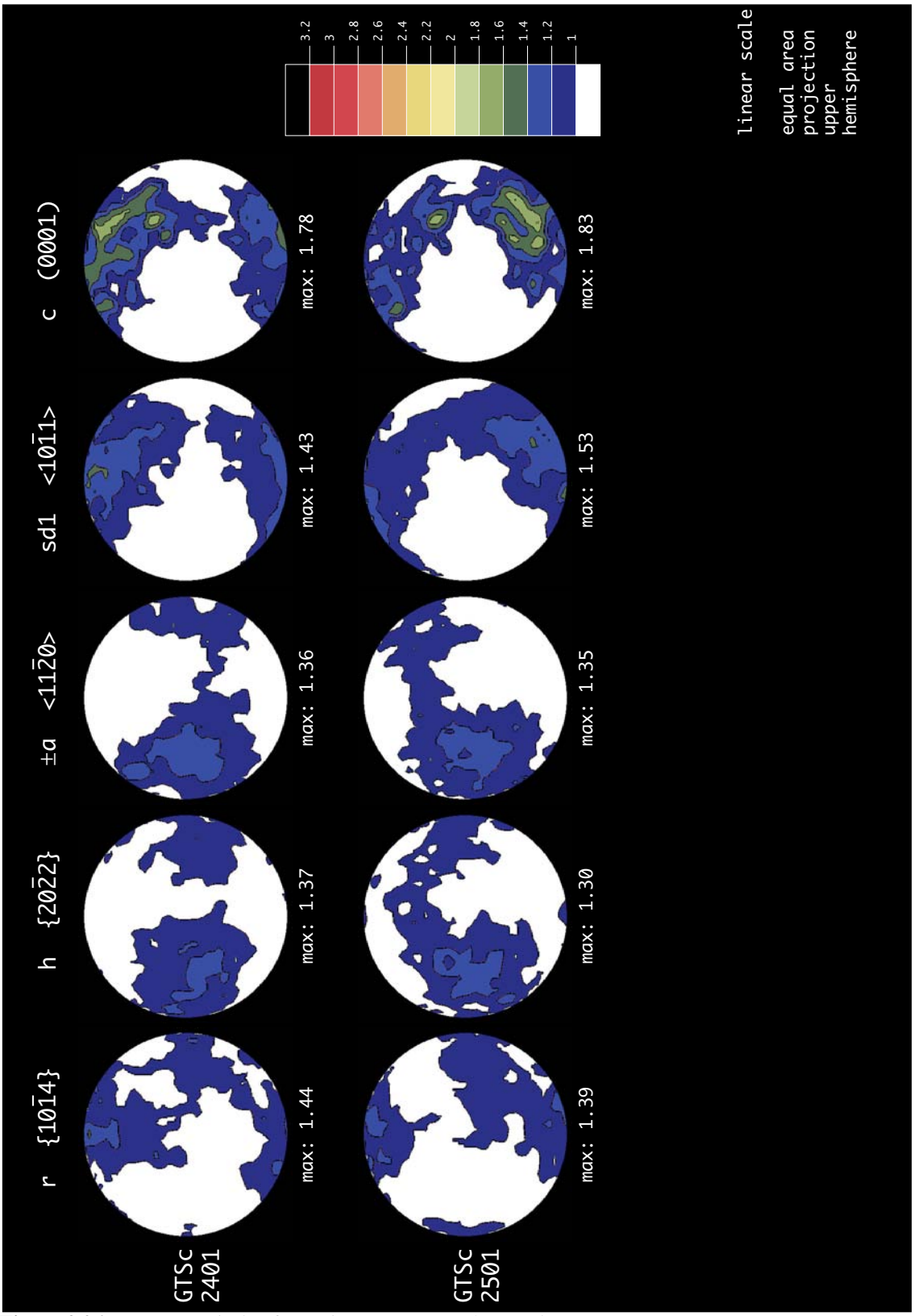


**Figure 3.26:** Texture analysis of samples Gtsc2401 and Gtsc2501.

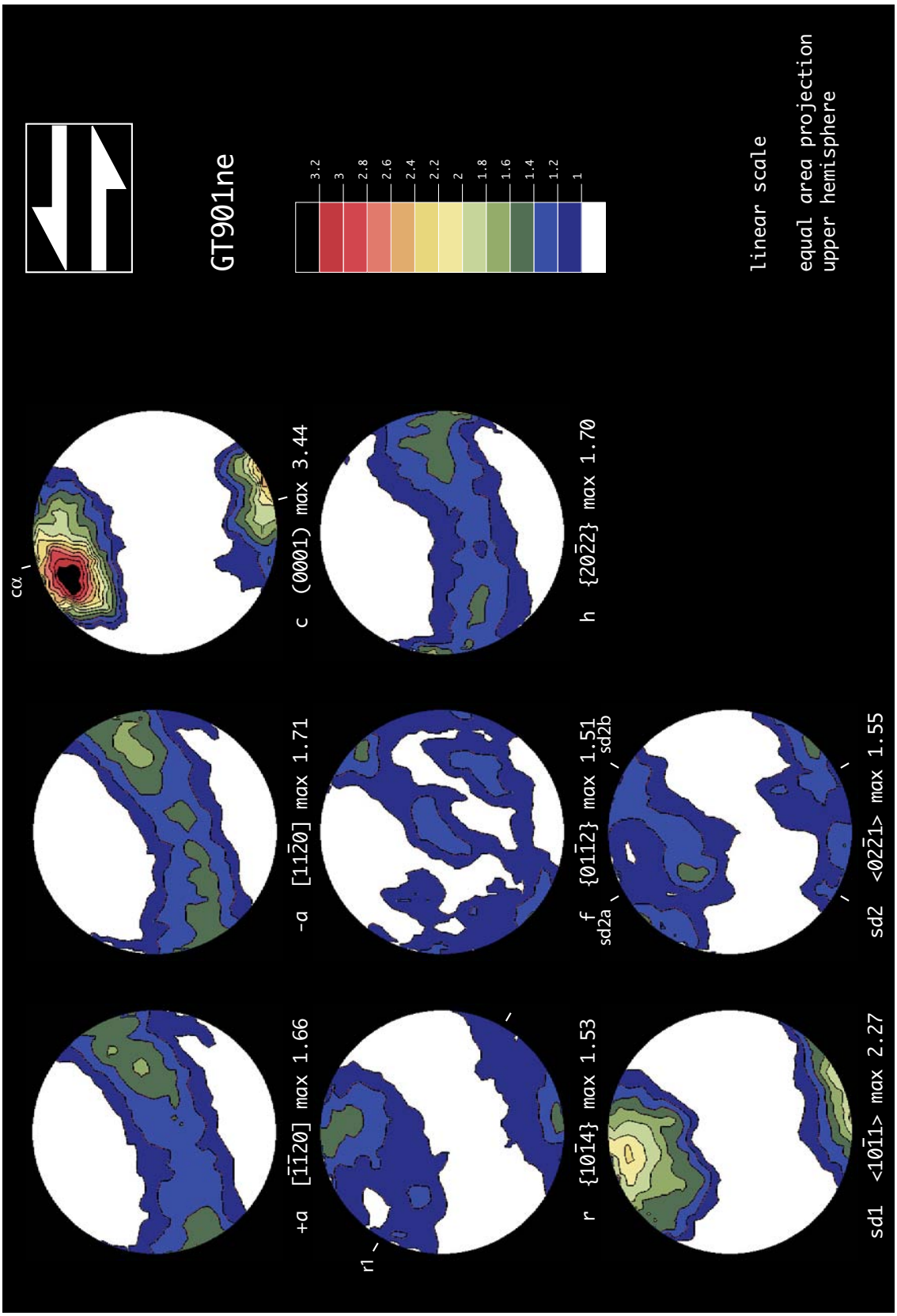


**Figure 3.27:** Complete texture analysis of sample GT901ne. Note the clear monoclinic symmetry of the texture developed under a non-coaxial strain path.

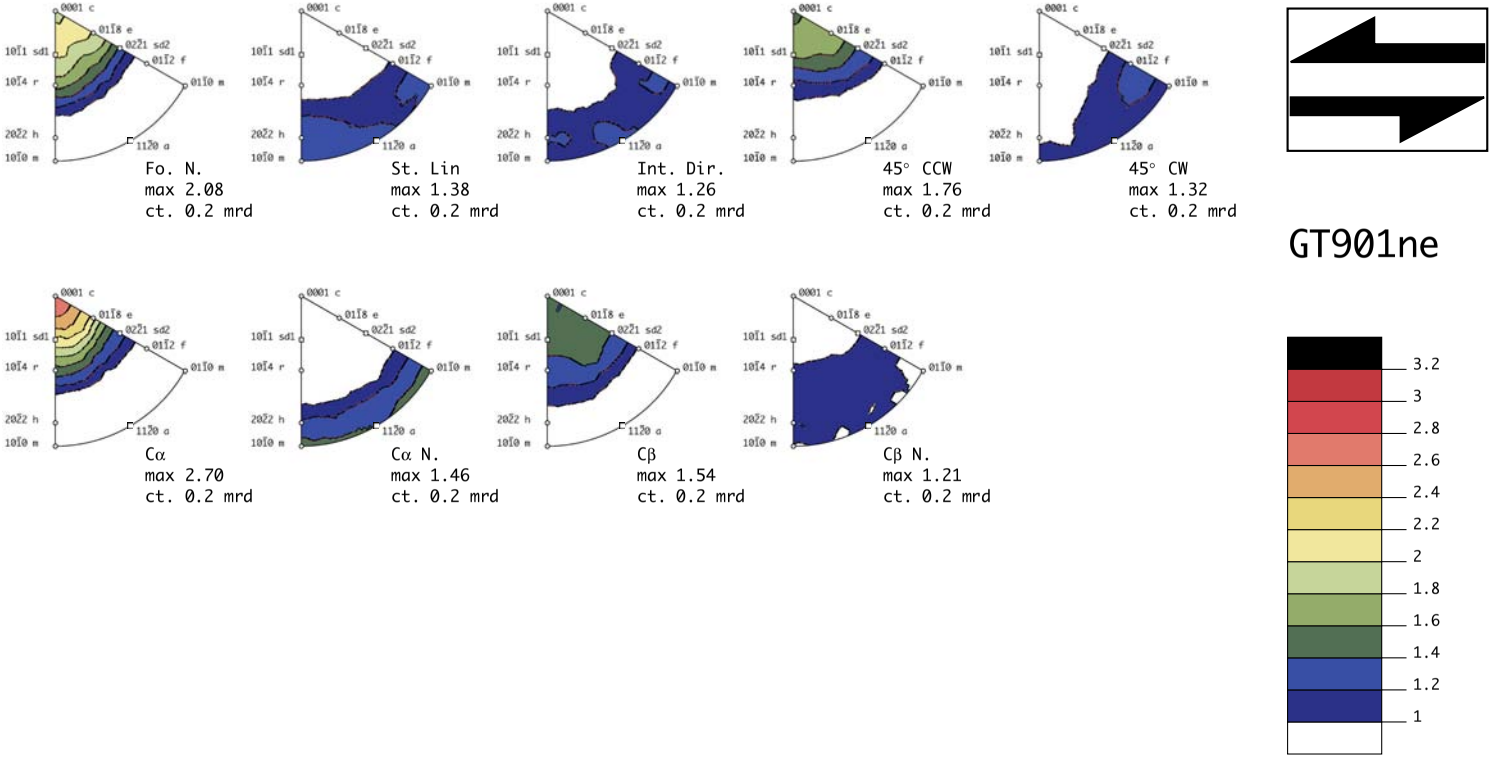


**Figure 3.28:** Inverse pole figures calculated for sample GT901ne.
The monoclinic level of symmetry for this texture is reflected by the non-similarity between the directions at 45° from Z, cα and cβ, cαN and cβN.

3.3.4.2 Sample Gtsc2901 (Malm-Dogger marbles of Subriançonnais origin).

In this section, this sample consists of calcitic marble that is again nearly completely recrystallised. From the microstructural point of view, calcite pressure fringes found at the rim of opaque crystals (probably hematite) do not show any asymmetry (cf fig 3.29a). The SPO of the dynamically recrystallized matrix is parallel to the macroscopic foliation (see fig 3.29b).

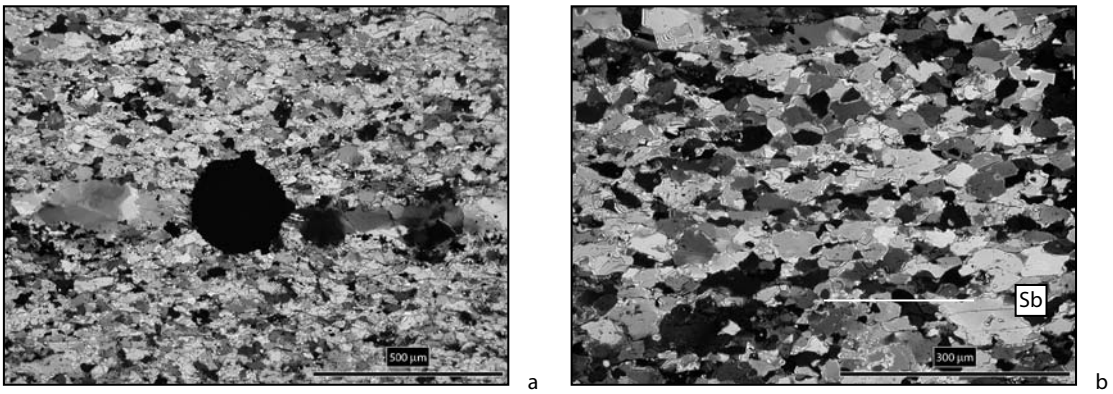


**Figure 3.29:** Photomicrographs of sample Gtsc2901 (30 micrometers thickness thin section observed under crossed polarized light). The macroscopic foliation Sa is horizontal.
a: symmetric calcite pressure fringes developed at the rim of hematite crystals.
b: horizontal SPO Sb observed in the dynamically recrystallized matrix.

The texture analysis, presented in figure 3.30, shows a clear orthorhombic symmetry. The *c*-axis and the *sd1* slip direction show a broad maximum normal to foliation. In detail, the *c*-axis pole figure shows a very slight tendency to be divided in two sub-maximums close to positions cα and cβ defined in chapter 2. The non-reduced *a* pole figures show a similar girdle distribution slightly rotated in a clockwise sense in the case of the *+a* direction and counterclockwise sense for the *–a* direction. The *sd2* slip direction pole figure shows two equivalent maxima at positions *sd2*a and *sd2*b.

The orthorhombic symmetry of the texture is confirmed by calculations of inverse pole figures showing similar distributions between the directions at 45°CW and 45°CCW, cα and cβ, cαN and cβN respectively (cf fig 3.31). Both directions at 45° from Z show a ridge distribution running from the *c*-axis to the *f* crystallographic plane with a shoulder extending to the *sd1* slip direction and *r* crystallographic plane. It is proposed that the texture of sample Gtsc2901 results from dominant activity on *r* and *f* planes and that the rock has experienced a dominant component of coaxial strain (see chapter 2).

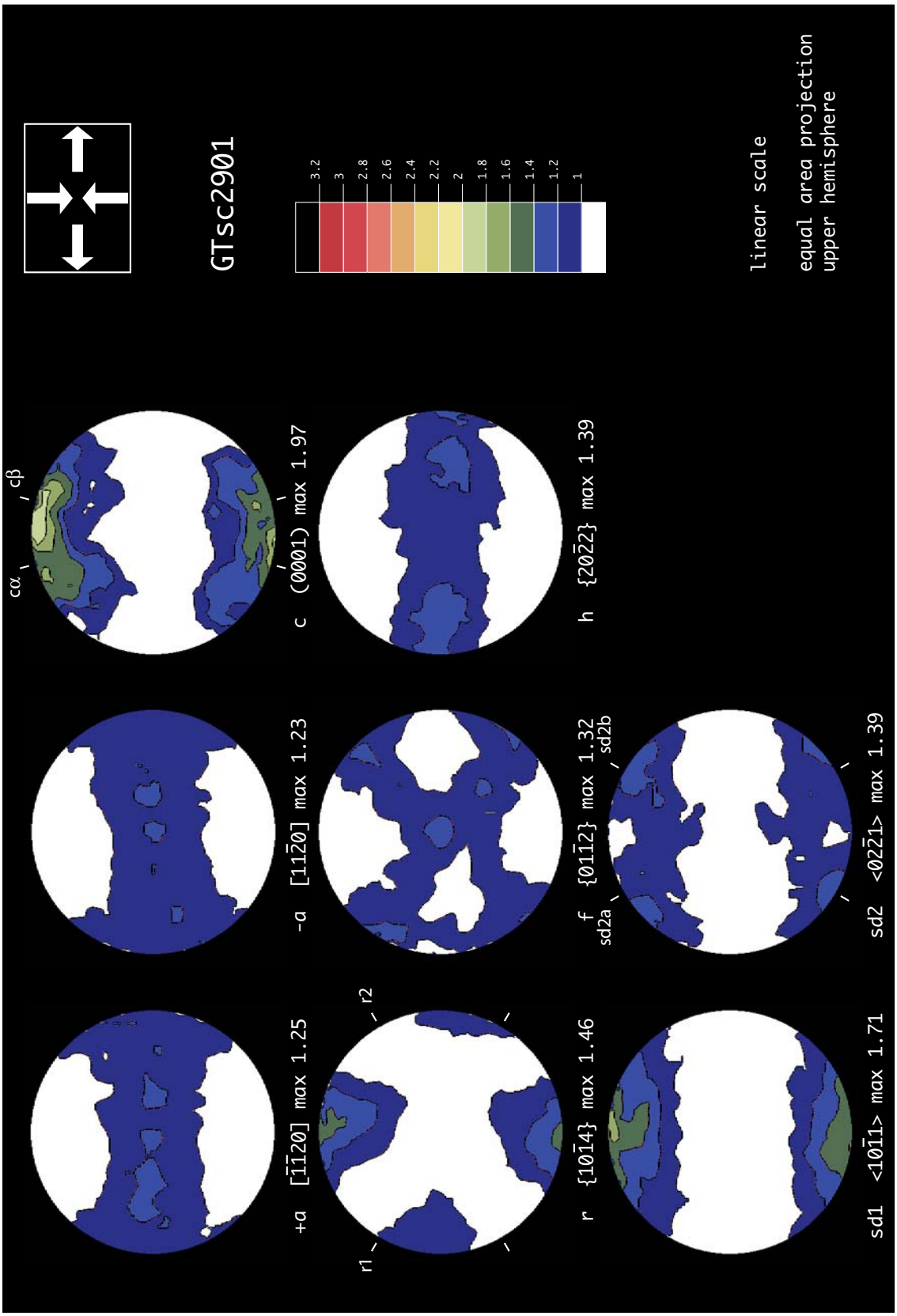


**Figure 3.30:** Complete texture analysis of sample Gtsc2901. Note the orthorhombic level of symmetry recorded in each pole figure.

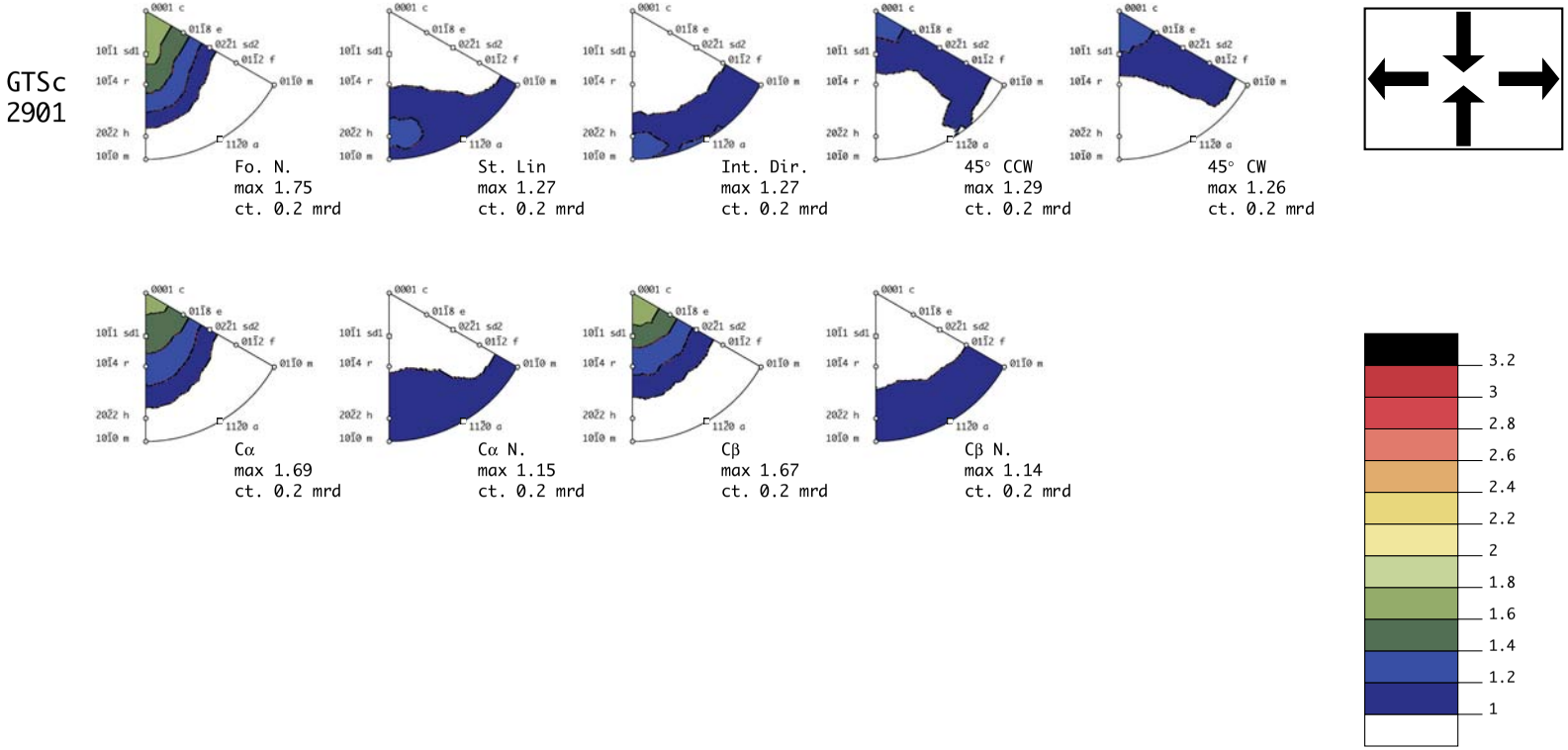


**Figure 3.31:** Inverse pole figure calculated for sample Gtsc2901.
The orthorhombic level of symmetry for this texture is reflected by the similarities between the directions at 45° from Z, cα and cβ, cαN and cβN.

3.3.5 Summary.

The microfabric characteristics of samples analysed in chapter 2 have been recognized in mylonitic layers developed during activity of the RT. The model of microfabric evolution presented in chapter 2 allowed for recognition of strain type variations within this structure. An increasing amount of non-coaxial deformation is for example noted when approaching the Pelvoux massif in the northern part of the investigated area.

The constant top-WNW oriented sense of transport along the RT deduced from microfabrics analysis presented here give further arguments confirming the model of Ceriani et al. (2001).

## 3.4 Microfabric analysis of samples collected along the basal decollement level of the Dauphinois, derived from the Eocene cover at the southeastern rim of the Pelvoux massif.

According to the structural analysis presented in chapter 1, two main deformation phases affected the Eocene cover of the eastern rim of Pelvoux massif (Dauphinois domain): a first phase D1, related to WNW-directed thrusting along the RT is clearly followed by a later D2 phase associated with SW-directed movements. Clear overprinting phenomena have also been described along the RT itself and within the Dauphinois domain.

Deformation features within the basal decollement level of the Tertiary Dauphinois cover and related to SW-directed displacement are widespread in both the Fournel and the Dormillouse valleys (cf fig 3.2 and 3.32). Intensity of deformation related to D2 is, however, much higher in the Dormillouse area. There, several outcrops analysed along the basal decollement level of the Tertiary cover do not preserve any deformation features related to D1, due to the very intense D2 overprint. The underlying nummulitic limestones are frequently mylonitised during D2, a feature not observed in the Fournel area. These differences in syn-D2 strain intensity between the two valleys are a mere consequence of strain localization due to the differences in the thickness of the basal shear zone. As estimated by Bürgisser (1998), this thickness is 22 meters in the Dormillouse area and 60 meters in the Fournel valley.

In the following, the results of microfabric analysis of nummulitic samples from the Palluel lake (Dormillouse valley), intensively deformed and carrying a strong NE-SW oriented stretching lineation (cf fig 3.32) will be presented (samples Do1, Do2 and Dorm1a). Sample Fan from the Fangeas lake (cf fig 3.32) is presented as well. This

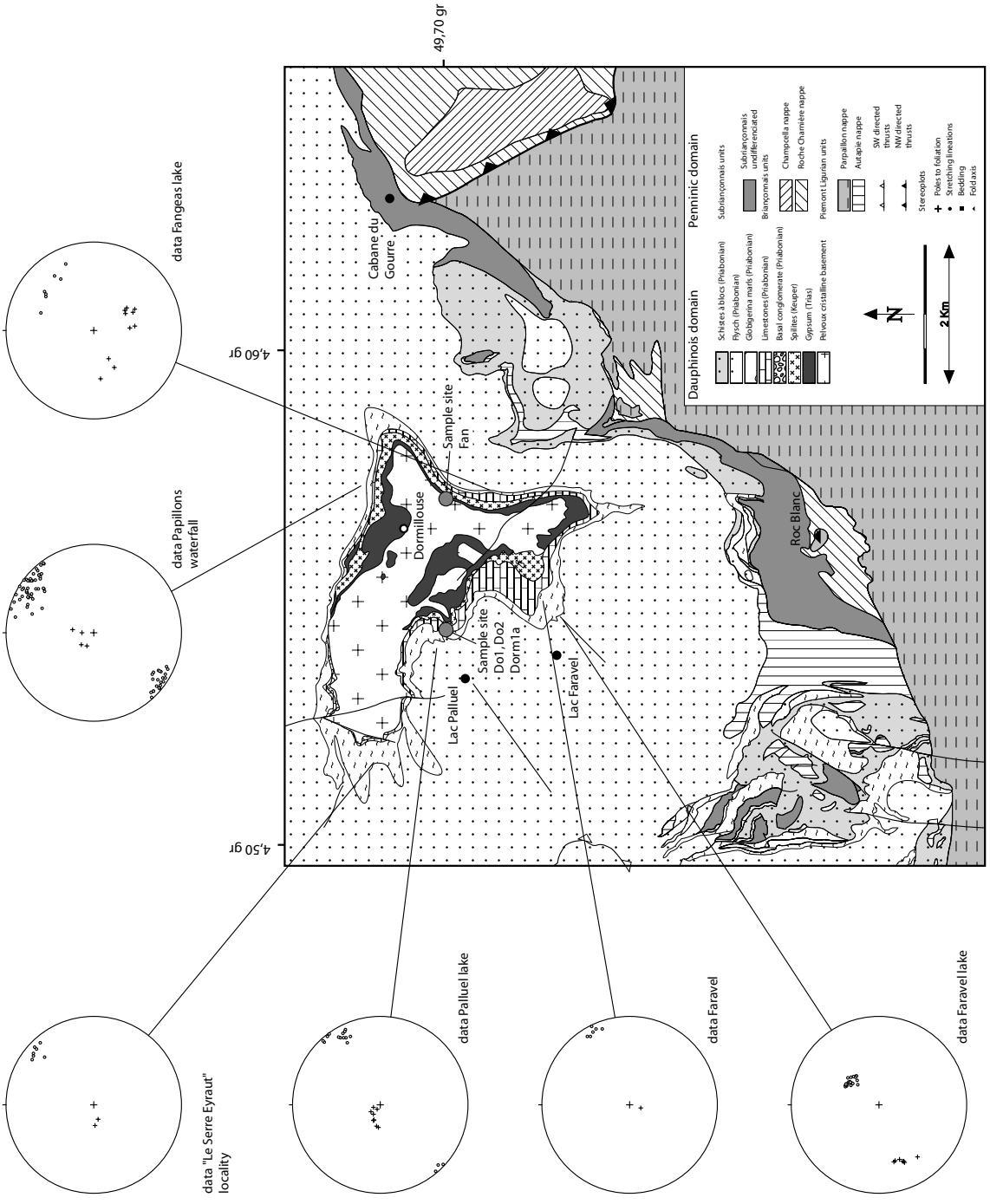


**Figure 3.32:** Structural map of the Dormillouse area. Note the overall NE-SW oriented sense of transport recorded in the basal decollement level of the Eocene para-autochtonous cover. Samples sites Do1, Do2, Dorm1a and Fan are shown.

sample revealed much weaker textures when compared to the samples from the Palluel locality and hence does not allow for accurate considerations in terms of texture analysis (cf fig 3.34).

Given the strong microfabric differences obtained between 1) sample Do1 and 2) samples Do2 and Dorm1a, the description is divided in two parts, sample Do1 being presented separately.

### 3.4.1 Sample Do1.

The thin sections presented in figure 3.33 show that both asymmetric calcite pressure fringes developed at the rim of detritical quartz grains and oblique SPO at about 20 to 30 degrees to the macroscopic foliation are consistent with top-SW shearing of the rock.

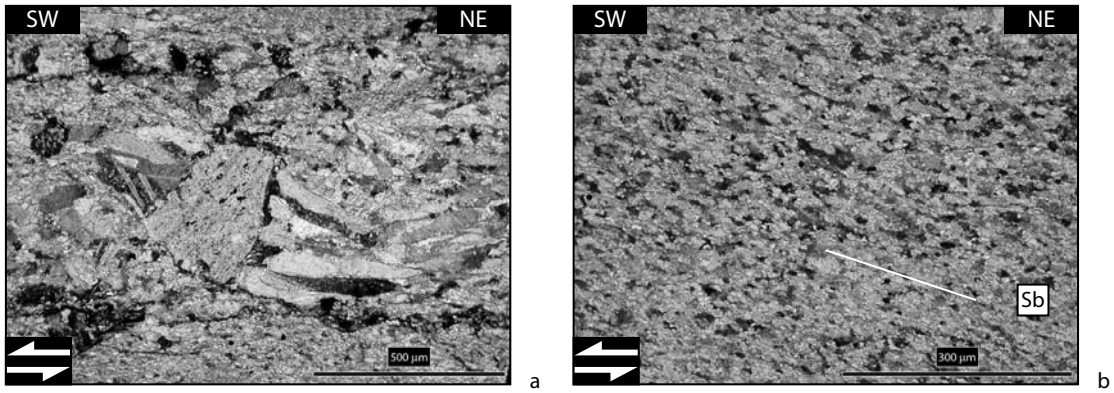


**Figure 3.33:** Photomicrographs of sample Do1 (normal thin section of 30 micrometers thickness observed under crossed polarizors). The macroscopic foliation Sa is horizontal.
a: asymmetric calcite pressure fringes developed at the rim of a detritical quartz grain.
b: oblique SPO Sb observed in the dynamically recrystallized matrix.
Both pictures indicate a sinistral sense of shear, compatible with top-SW directed movements.

From the textural point of view, the *c*-axis pole figure shows a strong maximum at the Z position with a strong shoulder in the direction of the cα position (cf fig 3.34). The *a* direction and *h* crystallographic planes show girdles distributions inclined from the XY plane in a counterclockwise sense. The *r* pole figure shows to maxima within the YZ plane and one maximum at the r1 position.

In summary, sample Do1 presents microfabric characteristics close to sample Sa1a4 from the RYSZ (chapter 2). The *c*-axis distribution is therefore interpreted as a combination between two positions at cα and cγ and it is proposed that this sample suffered a so-called “intermediate” strain regime. This microfabric analysis confirms the

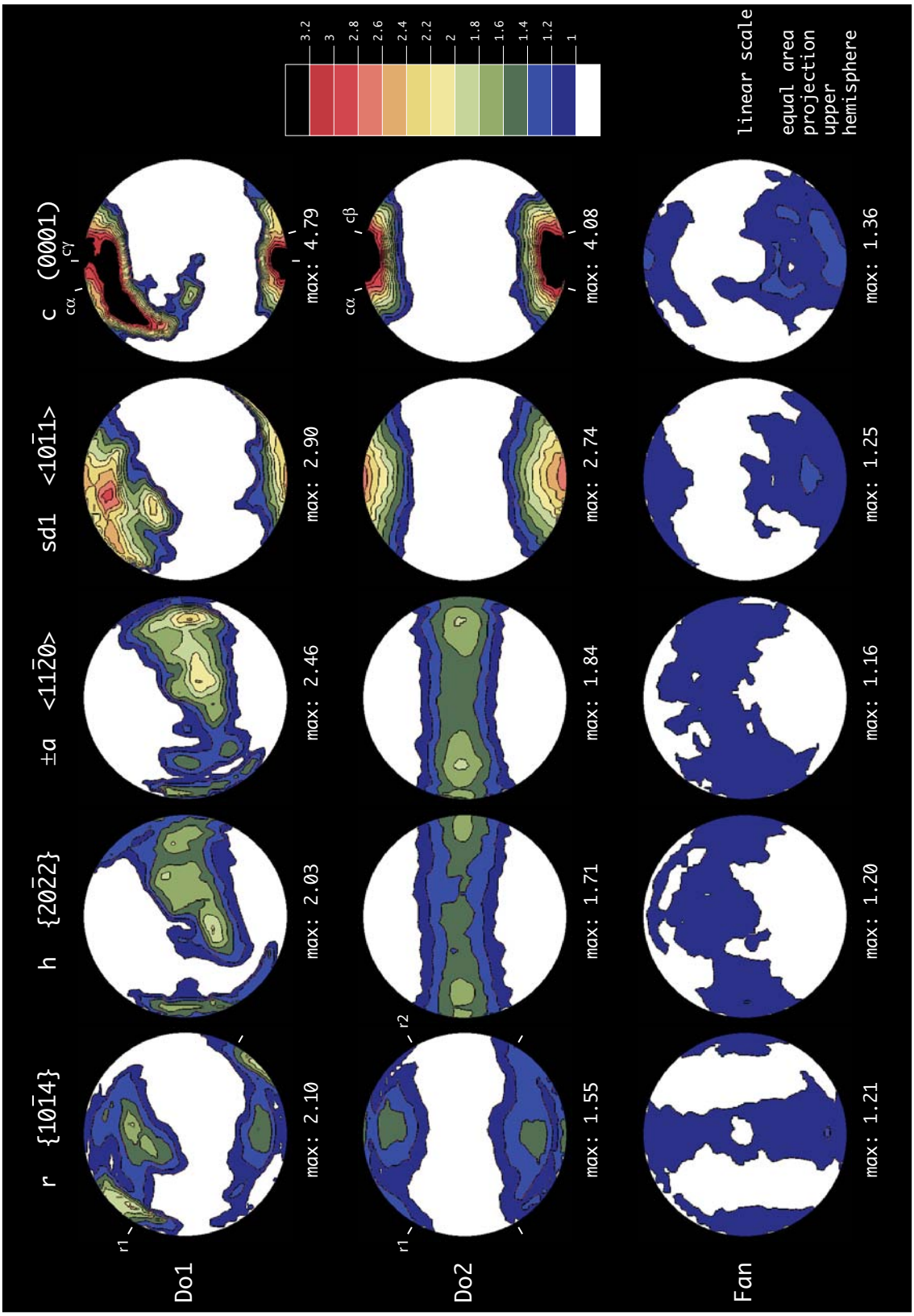


**Figure 3.34:** Texture analysis of samples Do1 and Do2 (Palluel lake) and Fan (Fangeas lake).

top-SW directed sense of shear recorded within the basal decollement of the Eocene cover.

### 3.4.2 Samples Do2 and Dorm1a.

These two samples have been taken from the same limestone layer, at about 10 meters from the Do1 sampling site. Given this close distance, it can be reasonably assumed that the microstructural characteristics between sample Do1 described above and the two samples described now should not be significantly different, notably in terms of grain size and amount of dynamic recrystallisation. The kinematic conditions accomodated in these rocks are therefore deduced based on the results of the texture analysis only.

From a textural viewpoint, the distribution of the *r* plane shows two maxima within the YZ plane and 2 maxima at positions r1 and r2. The *f* pole figure shows two small circles distribution centered at X and the *sd2* distribution shows two equal maxima at *sd2*a and *sd2*b (see fig 3.35). The textural characteristics of these two samples are therefore consistent with orthorhombic symmetry.

The orthorhombic symmetry of the texture of sample Dorm1a is also deduced from the common features noticed between the inverse pole figures calculated for the directions at 45°CW and 45°CCW, c$\alpha$ and c$\beta$, c$\alpha$N and c$\beta$N respectively (see fig 3.36).

Given their textural similarities with sample MPY2 from the RYSZ (see chapter 2), it is proposed that samples Do2 and Dorm1a have been deformed under conditions of coaxial strain.

In summary, it appears that a significant amount of coaxial strain is recorded within the basal decollement level of the Eocene cover. Partitioning of the bulk flow resulted in the formation of domains dominated by coaxial deformation within this basal shear zone. Such processes have previously been recognized in the Moine thrust zone in Scotland (Law et al. 1984), the Betic range in Spain (Platt and Behrmann 1986) and the Gavarnie thrust zone in the Pyrenees (J.H.P. DeBresser 1989).

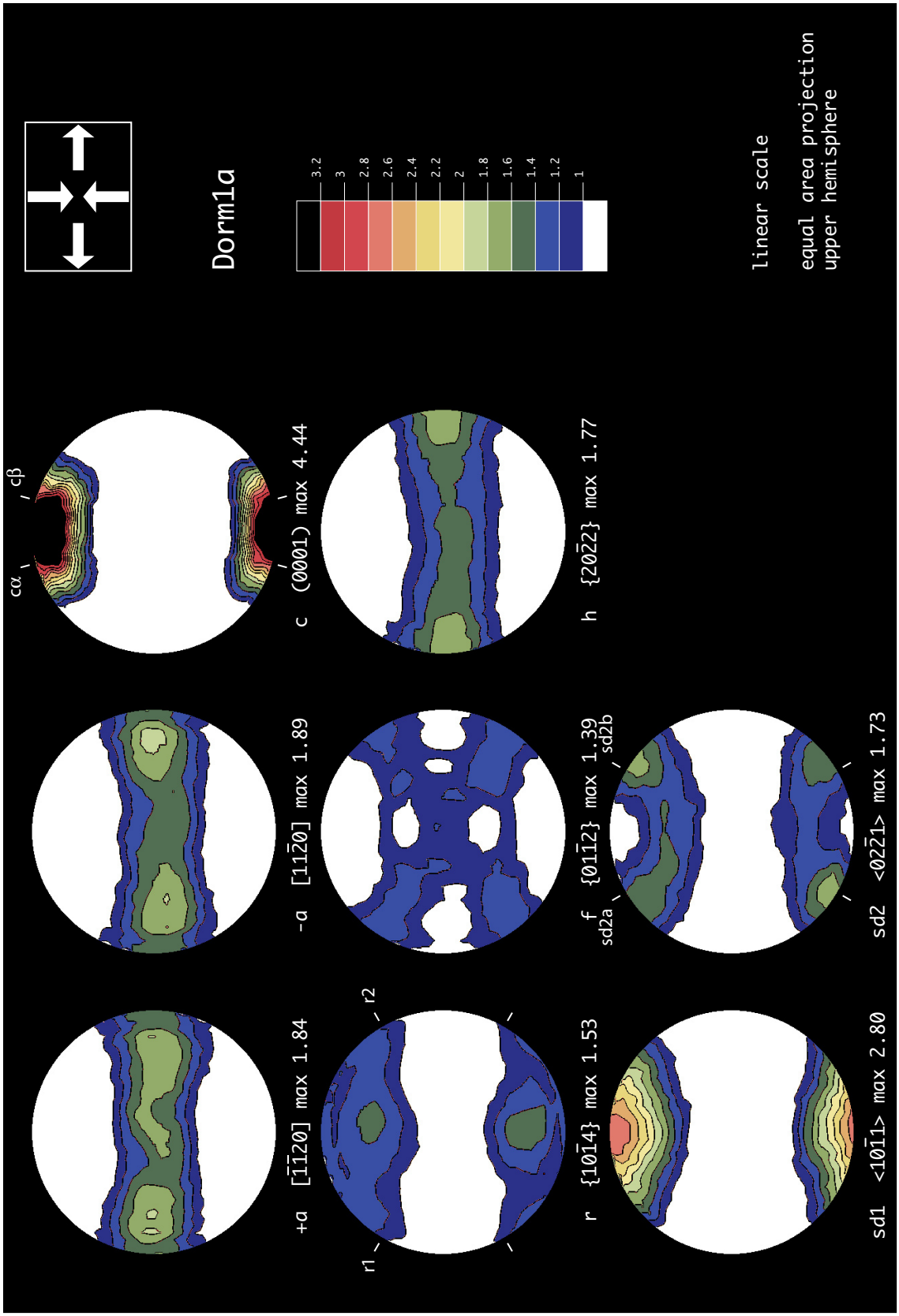


**Figure 3.35:** Complete texture analysis of sample Dorm1a. Note the orthorhombic level of symmetry recorded in each pole figure.

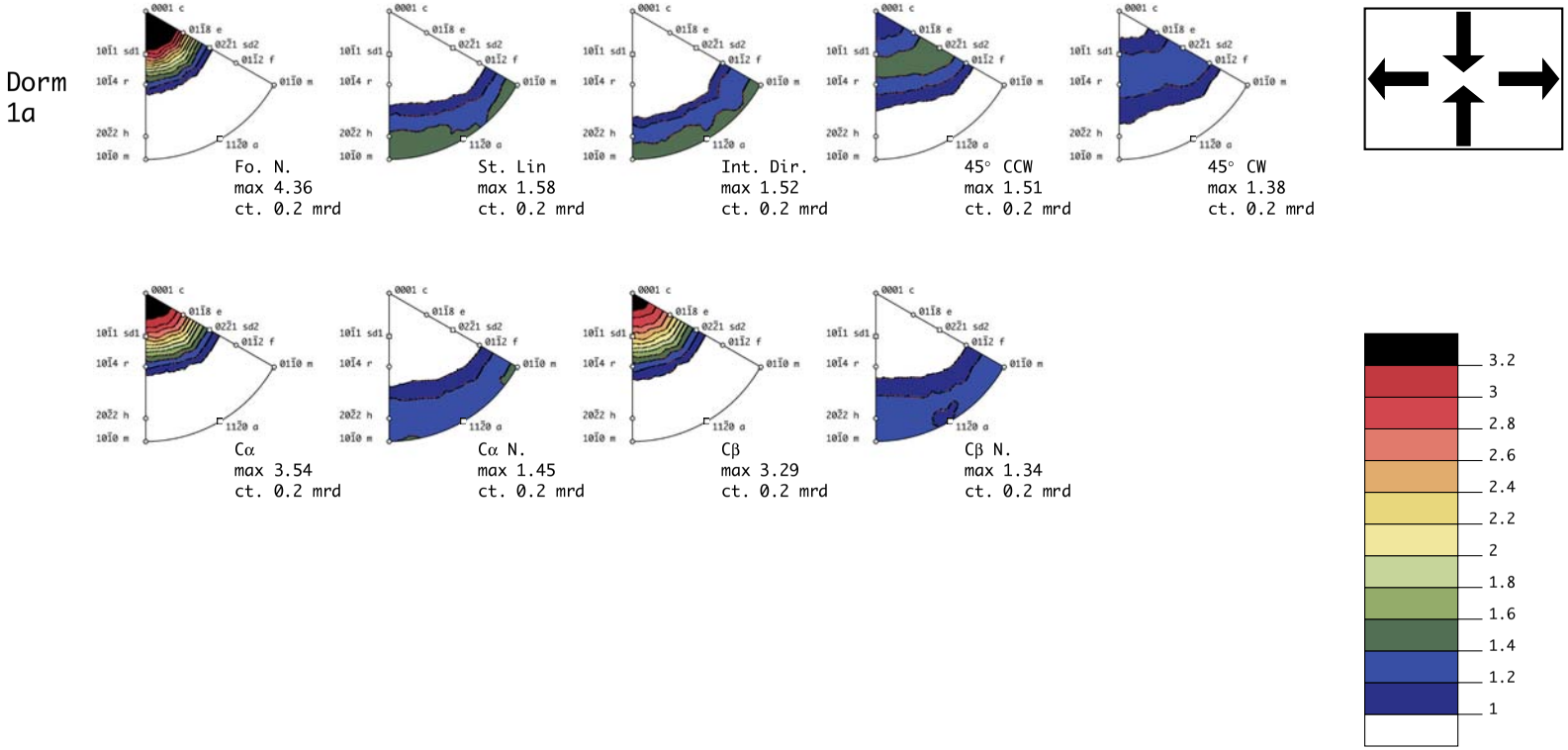


**Figure 3.36:** Inverse pole figure calculations for sample Dorm1a.
The orthorhombic symmetry of the texture is reflected by the similarities between the directions at 45° from Z, cα and cβ, cαN and cβN.

## 3.5 Microfabric analysis along the Gavarnie thrust zone, central Pyrenees.

An extensive description of the geology from the Gavarnie thrust zone is found in the PhD thesis of Majesté-Menjoulas (1979) and Roddaz (1977). Further insights are found in the description by DeBresser et al. (1986) and by Parish (1984).

From a general point of view, the geological setting found along the Gavarnie basal thrust zone is consistent with the thrusting of Devonian units onto Cambro-Ordovician basement during Pyrenean orogeny (see fig 3.37). The overall emplacement of this kilometric-scale nappe is towards the South.

The samples analysed in the present paragraph have been taken along strike of the Gavarnie basal thrust zone, east of the Gèdre village, between the Moudang and Louron rivers (see fig 3.37). These rocks are Silurian and Devonian mylonitic limestones and present a centimetric scale compositional and grain size layering. They are provided by J.H.P. DeBresser and the present study is aimed to complete the U-stage study of this author by means of X-ray textural goniometry.

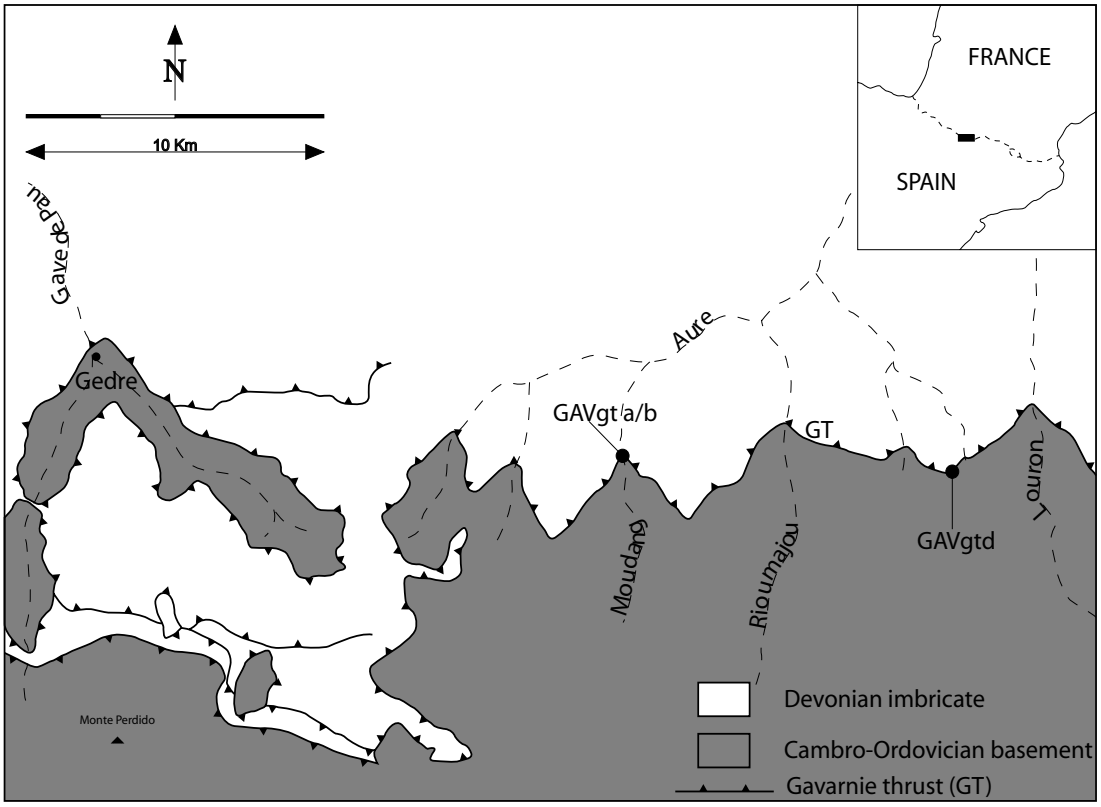


**Figure 3.37:** Structural map of the Gavarnie thrust zone redrawn after J.H.P DeBresser (1989).

The reader is referred to DeBresser (1989, p.369 to 371) for a complete microstructural description of this sample series. The most important points found in this presentation are:

1) twinning deformation is only of minor importance.
2) intracrystalline deformation and dynamic recrystallisation are dominant.
3) S-C type structures and porphyroclasts geometry confirm the top-S directed displacement along the Gavarnie thrust system.
4) an average grain size ranging between 30 and 100 micrometers for the fine-grained levels analysed by textural goniometry.

Apart from the slightly higher values of grain size, the microstructural characteristics of these samples are close to the ones analysed in chapter 2.

### 3.5.1 Samples GAVgta and GAVgtb.

The most obvious difference compared to all textures analysed so far is that the signal recorded on all pole figures is extremely noisy (see fig 3.38). Such artifacts are typically encountered in X-ray texture analysis when the grain size of the sample is too coarse.

Sample GAVgta shows one dominant *sd1* maximum tilted in the sense of shear. The *c*-axis distribution is consistent with a single maximum at cα.

Sample GAVgtb presents two clear *c*-axis maxima symmetrically disposed from Z. They correspond to the cα and cβ positions defined in chapter 2. In detail, it appears that cα is dominant on cβ. The *sd1* slip direction shows one dominant maximum at Z and two submaxima symmetrically disposed at around 20° from it.

The texture of sample GAVgta presents an overall monoclinic symmetry comparable to sample MPY28 from the RYSZ (chapter 2). The level of symmetry for the texture of sample GAVgtb is instead close to orthorhombic and strong similarities are found when comparing this sample to sample MPY2 from the RYSZ.

According to the model presented in chapter 2, it is concluded that samples GAVgta and GAVgtb have experienced various amounts of coaxial (resp. non-coaxial) strain.

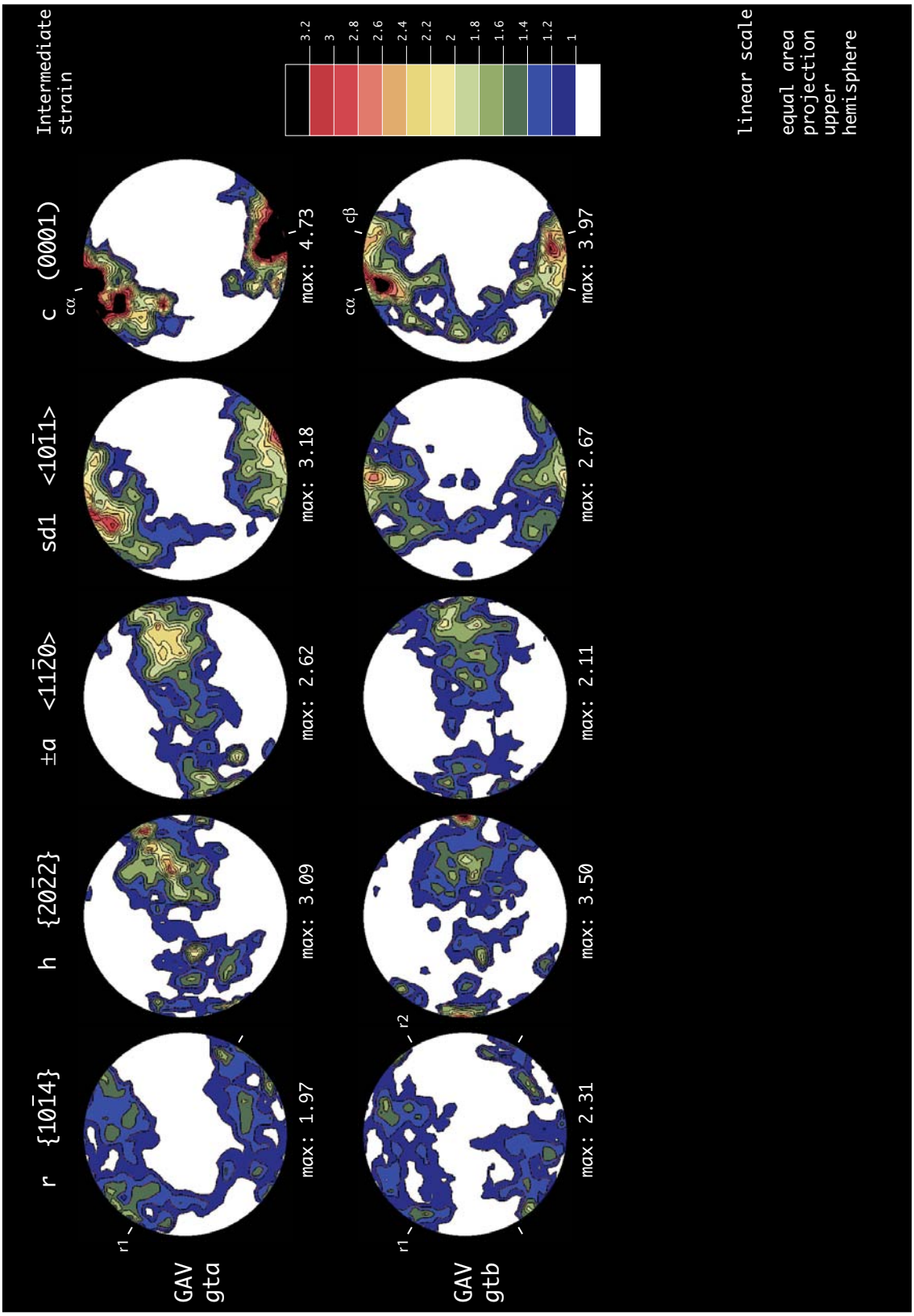


**Figure 3.38:** Texture analysis of samples GAVgta and GAVgtb. All pole figures show departure from orthorhombic symmetry. See text for discussion.

3.5.2 Sample GAVgtd.

The *c*-axis pole figure shows a very strong maximum slightly inclined in a counterclockwise sense from the foliation normal and presents an exceptionally high intensity of 5.51 mrd (cf fig 3.39). This texture presents a monoclinic symmetry evidenced by 1) the different distributions of *a* directions in the non-reduced pole figures, 2) the position at r1 on the *r* pole figure and 3) the asymmetric girdle distribution of the *f* crystallographic planes.

The non-orthorhombic symmetry is again confirmed by the non-identity between the directions at 45°CCW and 45°CW from Z, cα and cβ, cαN and cβN (see fig 3.40). Note that a signal concentration at *m* is recorded in the inverse pole figure for the cαN direction while the inverse pole figure for cα presents a strong maximum at *c*. According to the findings presented in chapter 2, this feature is indicative of a significant contribution of slip on the basal plane in two conjugate *a* directions during simple shear deformation. The main textural characteristics of this sample are strikingly similar to the ones observed for sample Sa1a4 from the RYSZ (chapter 2). It is therefore proposed that sample GAVgtd has been deformed under conditions of "intermediate" strain regime.

In his study J.H.P. DeBresser (1989) argued that the "*c*-axis textures of calcite rocks from the Pyrenean Gavarnie thrust zone indicate a considerable contribution of pure shear to the total strain". The analysis presented above gives further insights to these conclusions and it is argued that this pure shear component has been accommodated by dominant slip on the *r* and *f* planes (see chapter 2). The simple shear component of deformation induces in turn dominant slip on the basal plane (see chapter 2).

The situation found within the Gavarnie thrust zone is directly comparable to the one described within the nummulitic limestone formation found along the Priabonian cover basal decollement level. Bulk flow deformation is in both cases partioned in a component of coaxial and a component of non-coaxial strain. The sense of shear deduced from the more or less pronounced monoclinic symmetry confirms the top-S directed sense of transport along the Gavarnie basal thrust zone.

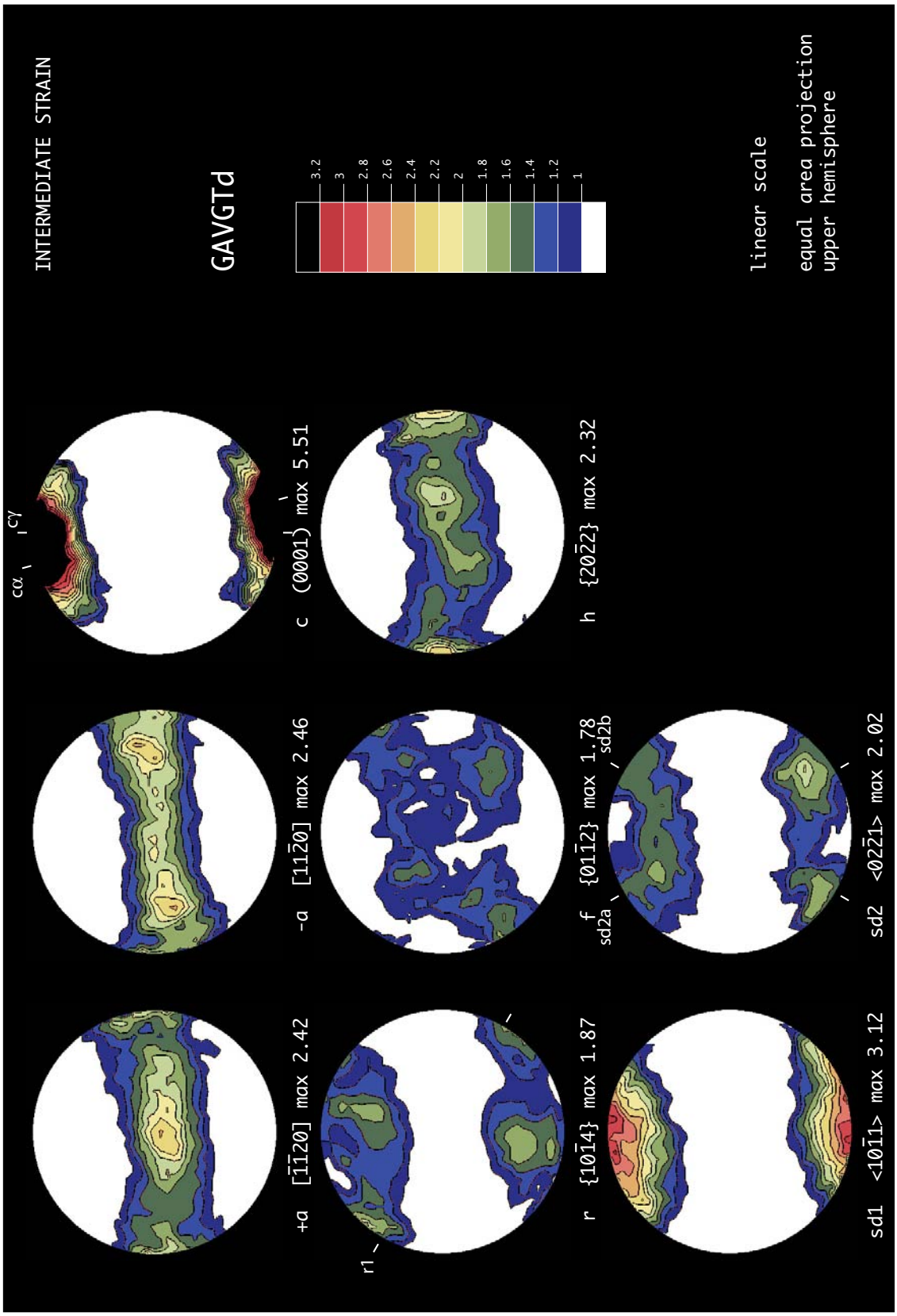


**Figure 3.39:** Complete texture analysis of sample GAVgtd. The monoclinic symmetry of the texture is mainly evidenced by the different distribution between +*a* and –*a* non reduced *a* pole figures and the r1 maximum in the *r* pole figure.

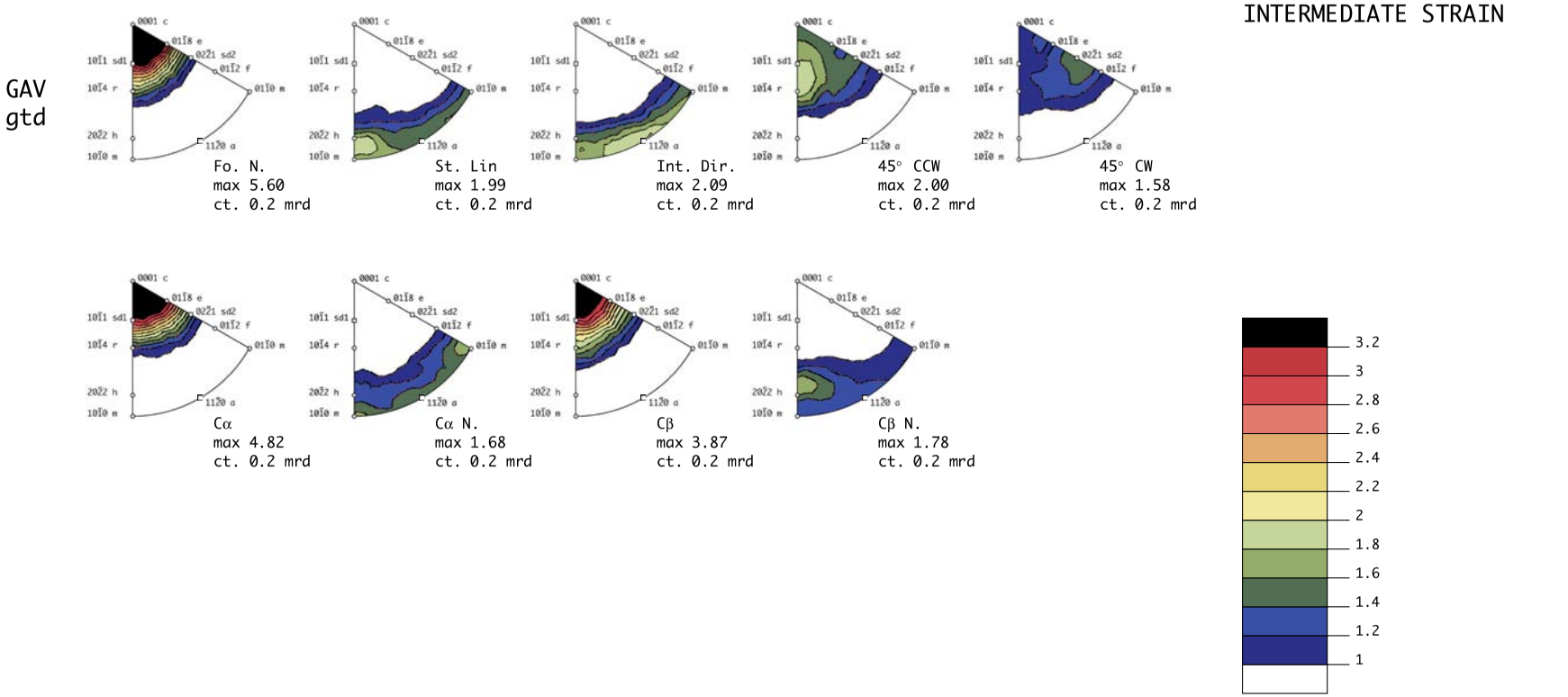


**Figure 3.40:** Inverse pole figures calculations for sample GAVgtd.
The non-orthorhombic texture symmetry is evidenced by the non-similarity between the directions at 45° from Z, cα and cβ, cαN and cβN.

## 3.6 Conclusions.

Application of the model of microfabric evolution proposed in chapter 2 for calcite ultramylonites allows the following conclusions:

1) Increasing amounts of simple shear deformation is recognized when approaching the Pelvoux crystalline massif from south to north.
2) Significant flow partitioning occurs within large-scale shear zones. It appears that ideal simple shear is rarely observed in natural shear zones.
3) The overall transport directions inferred from other methods, namely top-WNW directed shearing along the RT, top-SW directed shearing within the Eocene basal decollement and top-S directed shearing along the Gavarnie basal thrust are confirmed.

The application of calcite texture analysis for structural purposes is only possible when using microstructural investigations as well (see chapter 2). Deformation by twinning on the *e* crystallographic plane also produces tilted *c*-axis distributions. These are, however, oriented against the main shortening direction.

As depicted in the sketch presented in figure 3.41, for a given sense of shear the *c*-axis tilting documented in the case of mechanical twinning (position cT) is opposite to that observed under a regime of plastic deformation (position cα). Under conditions of coaxial kinematics, calcitic marbles plastically deformed show a broad maximum oriented normal to the macroscopic foliation. This maximum often shows a tendency to split in two position cα and cβ at 15° from Z, as described in chapter 2.

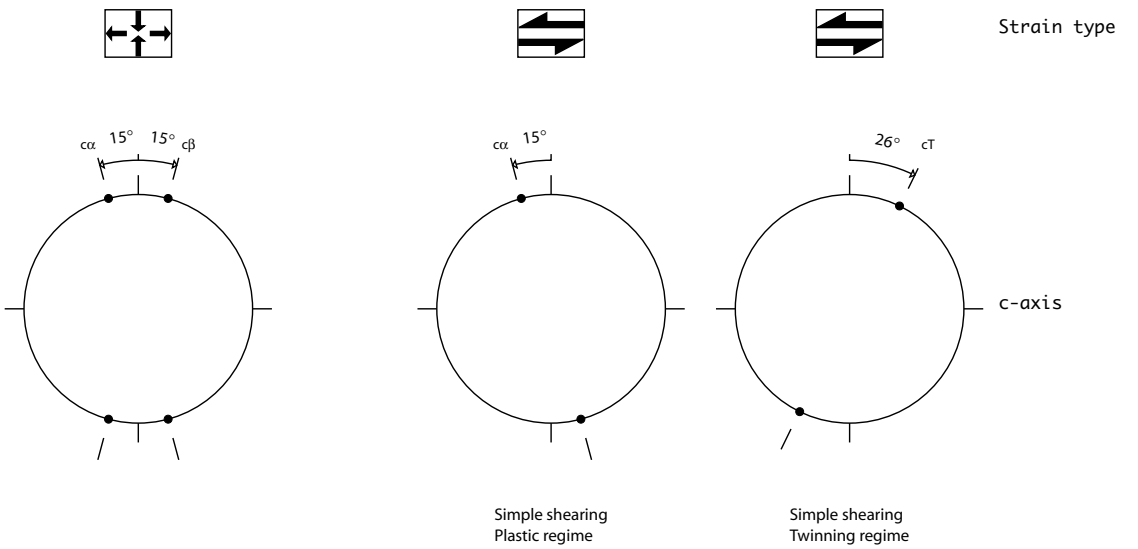


**Figure 3.41:** Sketch summarizing the main *c*-axis distributions observed in calcite mylonites deformed under conditions of coaxial and non coaxial strain. Under non-coaxial kinematics, the *c*-axis sense of tilting depends upon the active deformation mechanism.

# SYNTHESIS

This last session aims to provide a general synthesis for this work, based on the conclusions and discussions presented in the different chapters.

The main results of microfabric analysis of calcite ultramylonites are first presented. They will be incorporated in the summary of the regional structural analysis performed in the area between the Pelvoux and Argentera massifs.

## Microfabric analysis.

Exceptional outcrop exposure within a broad shear zone at the eastern rim of the Pelvoux massif allowed for a complete microfabric analysis of calcite ultramylonites recording coaxial and non-coaxial deformation.

Samples deformed under coaxial kinematics show a grain shape fabric with orthorhombic symmetry. Their textures are characterized by two *c*-axis maxima at the periphery of the pole figure, symmetrically oriented at 15° from the normal to the macroscopic foliation, as a result of activity of <10-11> and <02-21> slip along the *f* and *r* planes.

In contrast, samples having experienced simple shear deformation present a monoclinic shape fabric. Their textures are characterized by a single oblique *c*-axis maximum tilted with the sense of shear by about 15°, as resulting from duplex <*a*> slip along the basal plane.

The presence of samples showing similarities with the textures of samples coaxially deformed as well as of samples non-coaxially deformed allow to propose a model of microfabric evolution for calcitic rocks, following ideas proposed by Schmid and Casey (1986).

It is emphasized that, in the absence of twinning deformation, the new type of oblique *c*-axis maximum rotated synthetically with the sense of shear might be used as a reliable shear sense indicator.

## Field study.

Detailed investigation in the most external Subriançonnais/Briançonnais units and within the Dauphinois domain revealed the presence of several generations of structures in the area between Pelvoux and Argentera massifs.

The earliest phase of deformation is related to the Pyrenean orogeny. The corresponding deformation structures have been recognized within the Dauphinois domain either in the Mesozoic cover of the Dauphinois domain or as inverted paleograbens within the external crystalline massifs. The overall sense of transport related to this phase is top-

N directed.

The main Alpine phase affecting the external Western Alps occurs in Oligo-Miocene times during WNW-directed out of sequence thrusting along the Roselend thrust (RT), kinematically linked to dextral movements along the Rhone-Simplon line and sinistral movements at the rear of the Argentera massif. Shear senses along the RT have been deduced from meso- and microscopic shear sense criteria together with application of the model of microfabric evolution previously presented. Analysis of calcite ultramylonites deriving from limestones of different paleogeographic origin found along strike of the RT evidenced an increasing amount of simple shear deformation when approaching the Pelvoux crystalline massif.

One of the key results of the structural analysis presented in chapter 1 consists in the recognition that SW-directed movements clearly postdate earlier WNW-directed thrusting along the RT. Clear overprinting relationships have been found within the basal decollement of both Dauphinois para-autochtonous Tertiary cover and Helmenthoid Flysch of the Embrunais Ubaye nappe stack. Top-SW directed movements have again been evidenced using a combination of meso- and microscopic shear sense indicators together with the model of microfabric evolution presented in chapter 2. Important partitioning of the bulk flow into domains either dominated by coaxial or non-coaxial deformation occurs within the shear zone found at the base of the Tertiary cover.

The latest deformation features affecting the investigated area are related to normal faulting still active at present days.

## Implications for the evolution of the western Alpine arc.

This study first validates the model proposed by Ceriani et al. (2001) who proposed that during Oligo-Miocene times, the whole Adriatic indenter was thrusted onto the European plate towards the WNW along the RT.

Deformation features related to SW-directed thrusting clearly overprint earlier structures related to activity along the RT. This implies that the 90° divergence of thrusting directions from north to south of the Pelvoux massif is only apparent. Models involving a gradual change of thrusting directions are clearly not appropriate to explain the structural evolution of this part of the western Alpine arc. A possible origin for SW-directed thrusting is found in the formation of the Apennines, as a consequence of opening of the Tyrrhenian basin.

## Suggestions for further research.

The microfabric analysis of fine-grained calcite ultramylonites found in the investigated area documented that the microfabrics developed primarily by dislocation creep accompanied by dynamic recrystallisation. However, it has been noticed as well that the visible orientation distribution function maxima are built on small volume portions of the sample. This suggests that other deformation processes such as grain boundary sliding played a significant role in the overall deformation of the rock. It is therefore likely that a combined activity of both grain boundary sliding and dislocation creep occurs. Further investigations are needed to quantify the relative activity of each mechanism, notably by means of experimental deformation and electron backscattered diffraction.

Concerning the linkage between SW-directed thrusting in Dauphinois domain and formation of the Apennine chain, further work is needed to verify this hypothesis which remains speculative in the absence of deep seismic data and well-constrained phase correlation between Alpine and Apennine chains.

# APPENDICES

# APPENDIX A: Complete structural dataset and insights of the eastern rim of the Pelvoux massif.

This appendix first gives the complete dataset of structural data collected within the investigated area (appendix A.1, figures A1, A2 and A3). It then illustrates some details of the geological setting found at the eastern rim of the Pelvoux massif, i.e. between Combeynot and Rocher de l'Yret peaks (see figure A4 and figure A1 for localisation). Appendix A.2 includes a microstructural study of basement rocks showing a N-S directed strain gradient. Appendix A.3 shows some structural insights from the Rocher de l'Yret shear zone (RYSZ, see chapters 1, 2 and 3).

## Appendix A.1.

The complete set of structural data now presented is organized according to the three main deformation phases encountered, i.e. D1: WNW directed transport along the Roselend thrust, D2: SW directed movements and D3: late Neogene normal faulting. The significance of the different abbreviations is as follows: St.Lin stretching lineation, S foliation, F.axes fold axes, D3 norm.F. normal faulting related to D3 deformation phase. In order to facilitate the data presentation, the investigated area has been divided in 7 sub-areas (see figure A1): RY (Rocher de l'Yret massif), BL (La Blanche massif), Fo (Fournel valley), Do (Dormillouse valley), Vaut (Tête de Vautisse massif), Reot (Réotier locality) and Orc (Orcières locality).

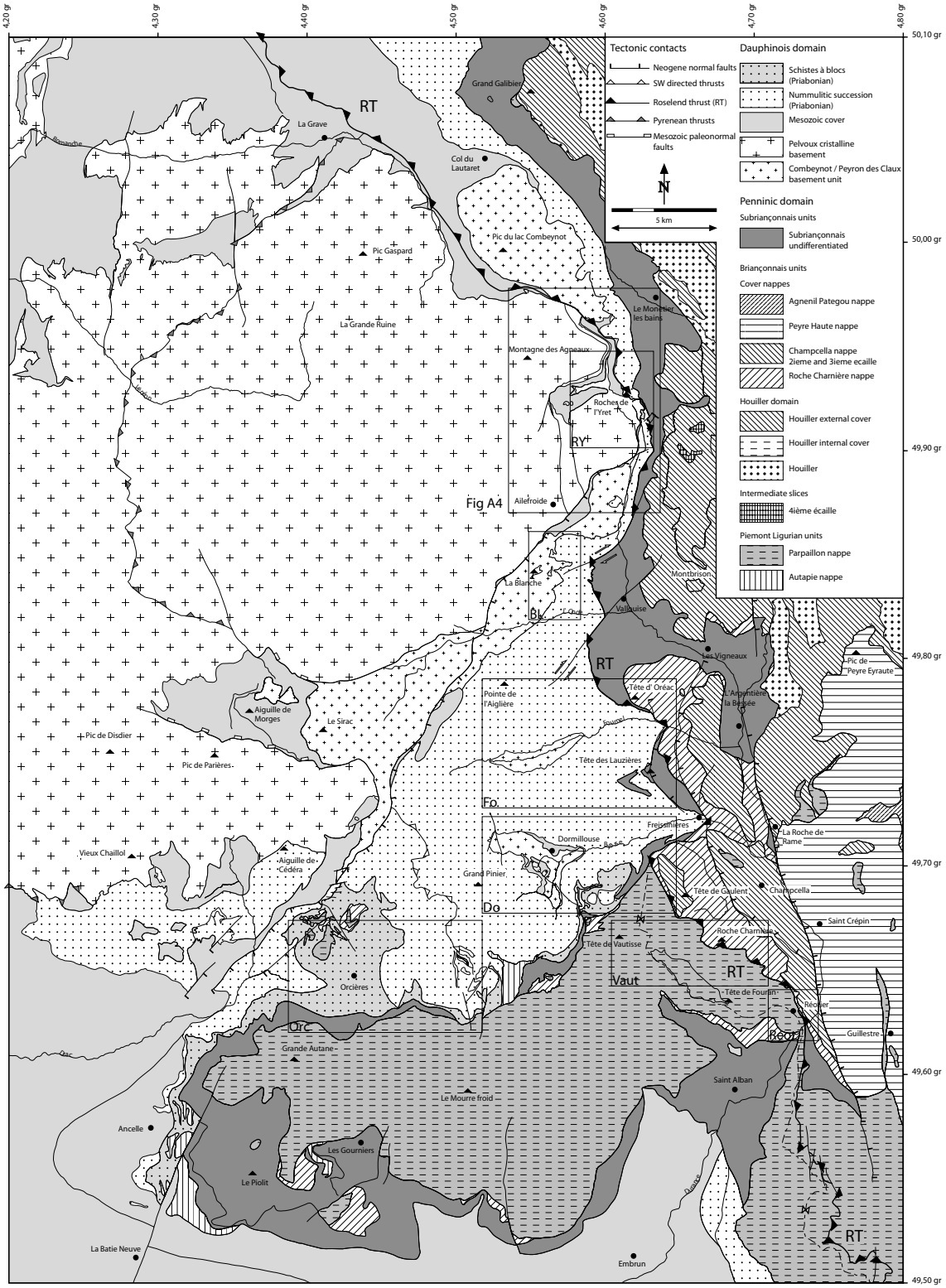


**Figure A1:** Structural map of the eastern rim of the Pelvoux massif. Sub-areas RY, BL, Fo, Do, Vaut, Reot and Orc are indicated.

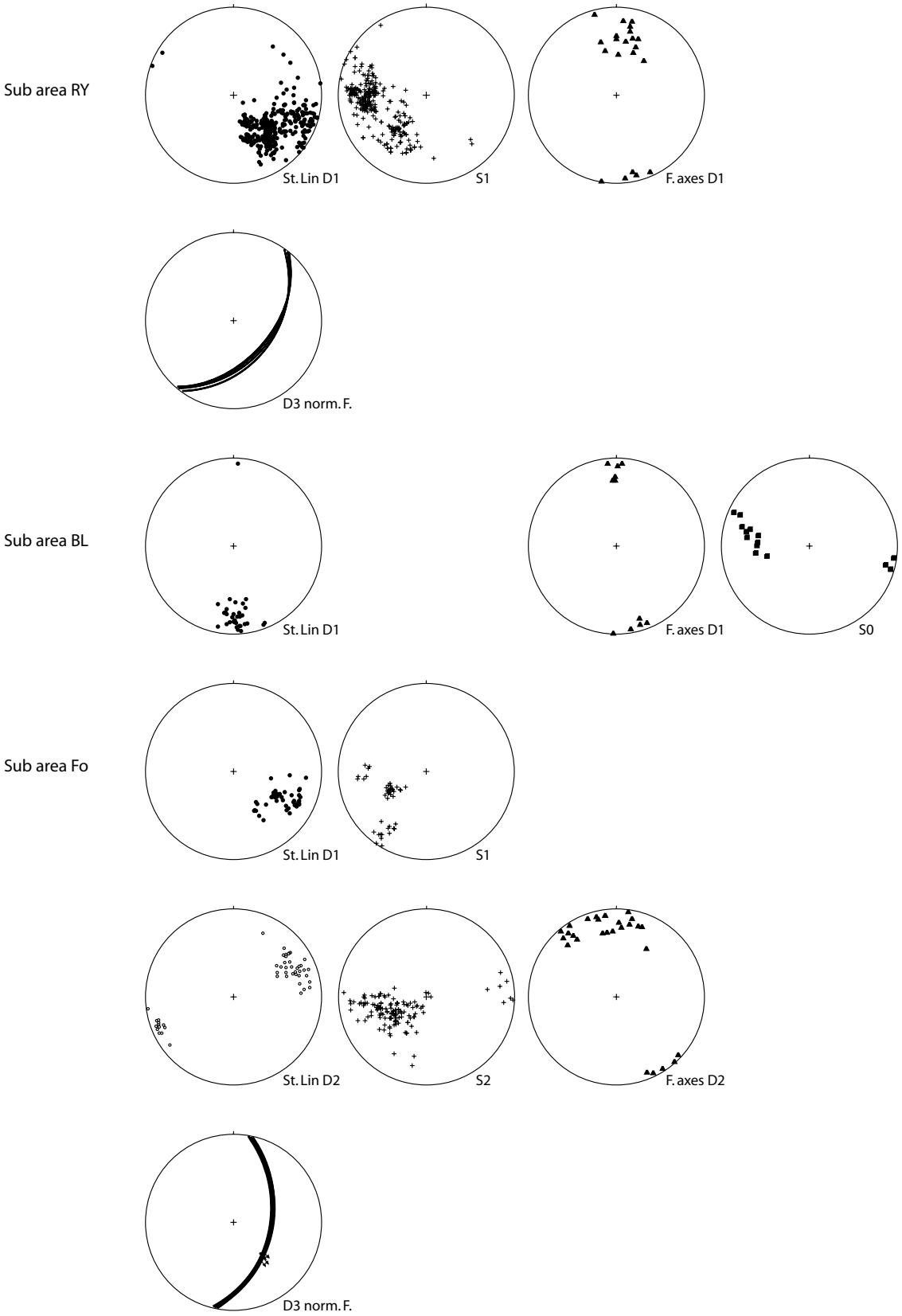


**Figure A2:** Structural data from sub-areas RY, BL and Fo.

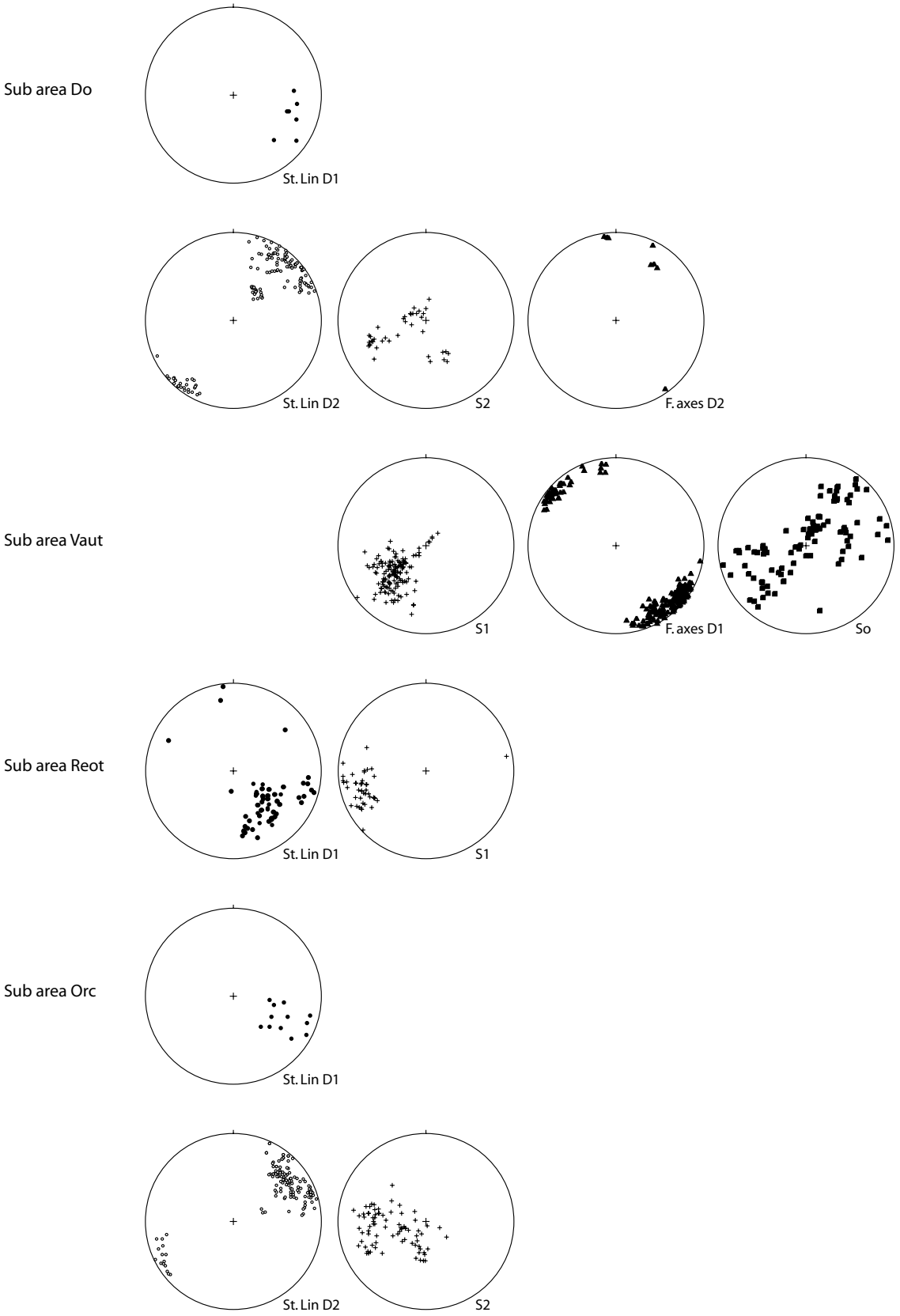


**Figure A3:** Structural data from sub-areas Do, Vaut, Reot and Orc.

## Appendix A.2.

We presented in chapter 1 the general tectonic setting of the eastern rim of the Pelvoux massif. Our data support the hypothesis of Ceriani et al. (2001) who argued that the wedging out in map view of the Combeynot massif was due to activity along the Roselend thrust (RT). We propose to illustrate this N-S deformation gradient from the microstructural point of view using three samples of basement rocks from 1) the core of the Combeynot massif in the north (point Comb 1 in figure A4), 2) the Grangettes slice above the Eychauda lake (point Grang in figure A4) and 3) the last remnants of the Combeynot massif found below the Rocher de l'Yret peak (point Yret1 in figure A4) in the south.

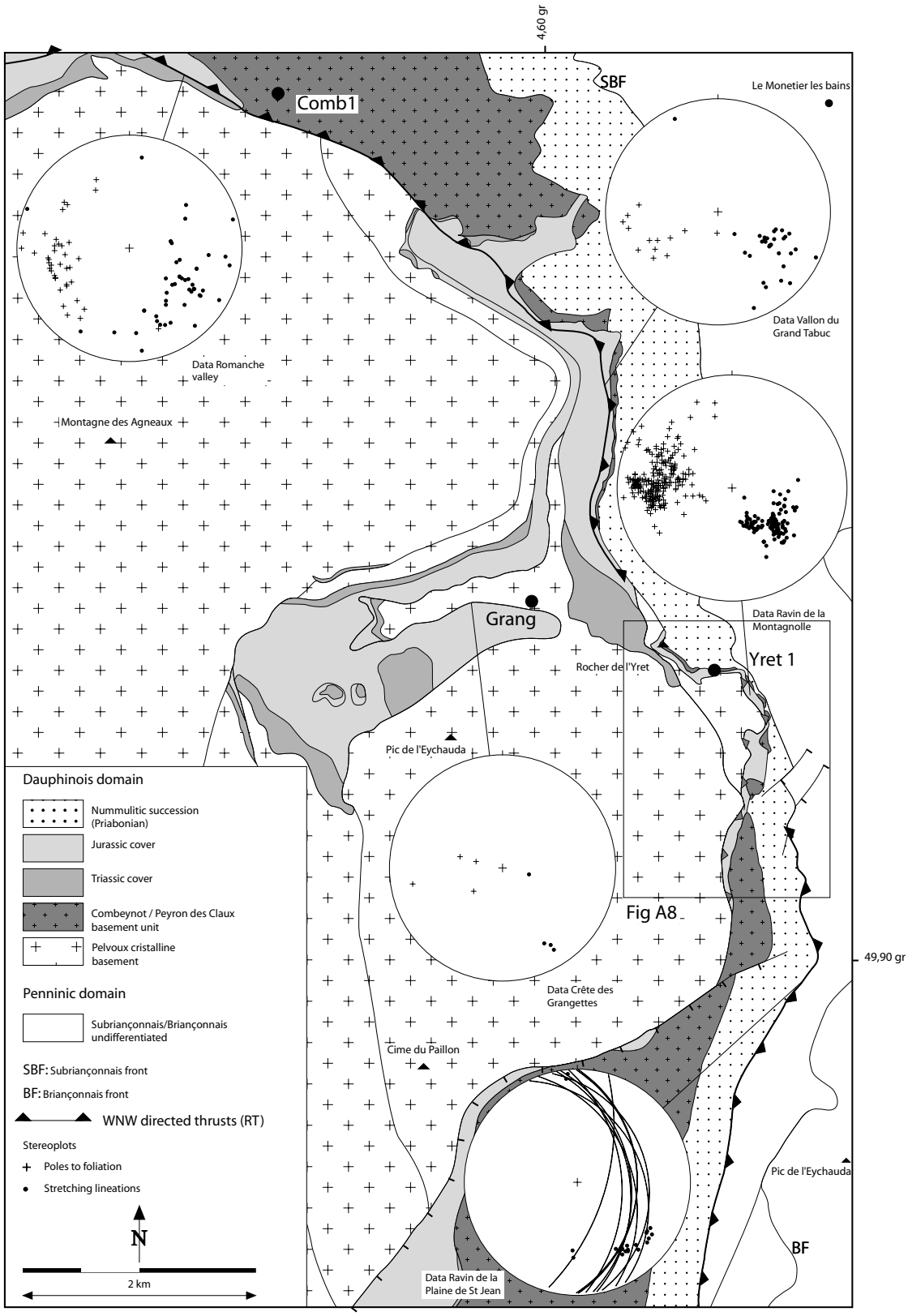


**Figure A4:** Structural map of the eastern rim of the Pelvoux massif. Sampling sites Comb 1, Grang, Yret are shown.

A sample taken from the core of the Combeynot massif is shown in figure A5. Hardly any evidence of deformation is recognizable in this thin section, as is attested by numerous triple point junctions between minerals and sharp extinction under crossed polarizers. The rock shows an association of quartz, feldspath and micas. All crystals are plurimillimetric in scale.

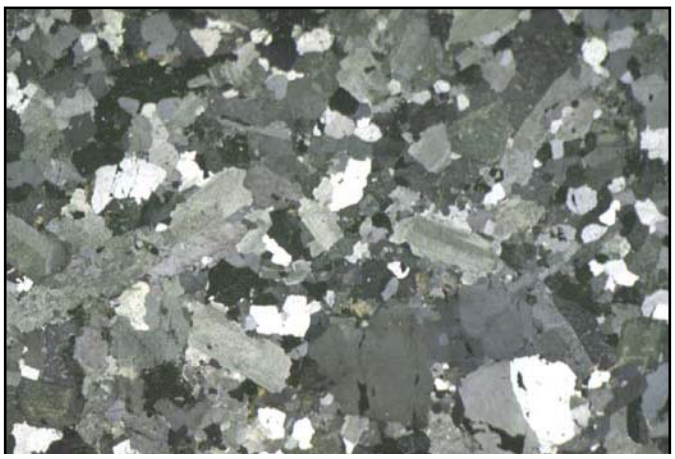

**Figure A5:** Photomicrograph from Comb 1 basement sample. Crossed polarized light.

A study of samples from the basement of the Grangettes slice revealed cataclastic deformation processes for this unit. In thin section, millimetric angular shaped fragments, composed of quartz-feldspar aggregates are recognizable (see figure A6). These fragments are cimented by a very fine-grained matrix that also includes calcitic precipitates. This matrix shows numerous traces of feldspar and mica alteration products, responsible for the overall yellowish color of the rock.

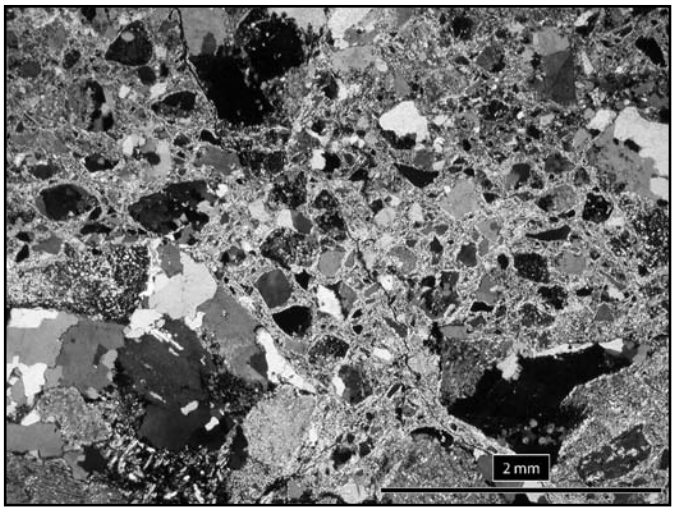


**Figure A6:** Photomicrograph from Grang basement sample. Crossed polarized light.

A microstructural investigation of samples from the lasts remnants of the Combeynot massif reveals again cataclastic deformation processes (see figure A7).

The rocks contain patches of quartz-feldspar aggregates separated by a matrix of micas and calcitic precipitates. The average grain size of the quartz-feldspath aggregates is much smaller compared to samples from the Grangettes slice. Sigma clast structures developing at the rim of quartz grains and shear bands structures are commonly observed. Exceptionally, an old foliation (probably Hercynian in age) consistent with a layering due to mineral segregations between quartz and micas has been recognized.

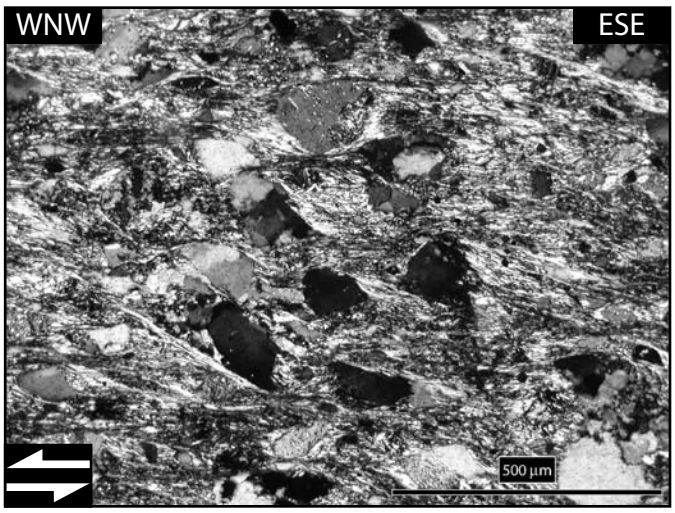


**Figure A7:** Photomicrograph from Yret 1 basement sample. Crossed polarized light.

It therefore appears that the uppermost basement units found at the RYSZ suffered much higher amounts of deformation compared to samples from the Grangettes slice.

## Appendix A.3.

The uppermost tectonic unit of the RYSZ consists of boudinaged basement units interpreted as remnants of the “Combeynot” massif tectonically reduced due to activity along the RT.

These basement boudins are affected by several complications that we analysed in details and present in the following.

A first type of local complication is found between the upper termination of the Ravin de la Montagnolle valley and the Rocher de l’Yret summit. A sinistral strike slip network affects the upper basement boudins and their Eocene cover. The related structures have been presented in chapter 2 and the reader is referred to this section for detailed description.

The second type of local complication consists in the folding of the basement boudins and their Priabonian cover. A schematic representation of these folds found along profile A (see map figure A8) is given in figures A9 and A10.

Exceptionally, interference patterns due to superposition of folding events are observable (see figure A11). This folding is associated with a crenulation cleavage, mainly observable in the underlying Mesozoic marls. This cleavage clearly overprints a first tectonic foliation consisting in a mineral segregation between calcitic and micas rich layers (see figures A12 and A13). These folds commonly evolve in fault propagation fault structures, creating imbricates between basement slices and their nummulitic cover, together with lenses of Mesozoic marls. Striations measured on the corresponding fault planes indicate a top WNW sense of movement.

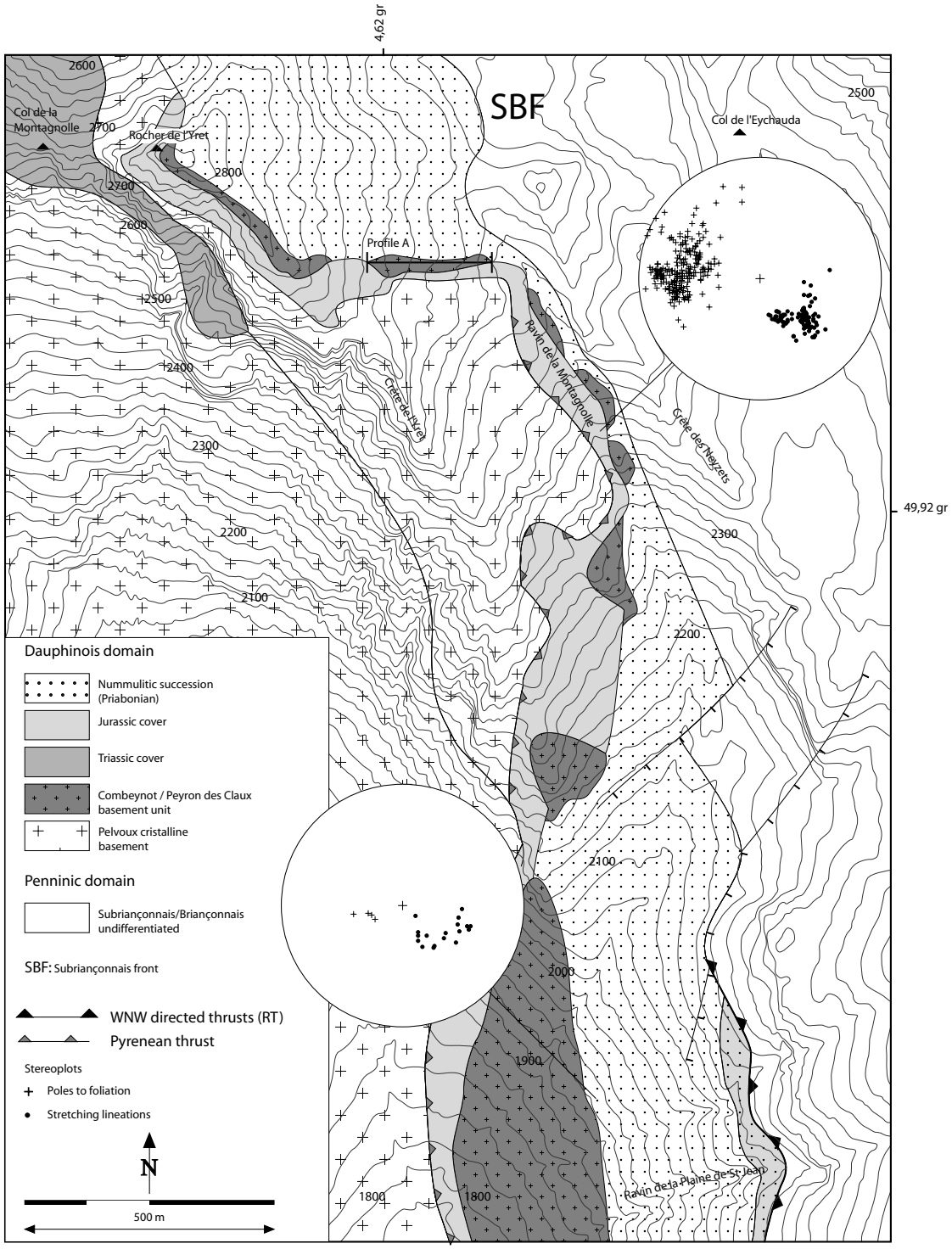


**Figure A8:** Detailed geological map of the "Rocher de l'Yret" shear zone realized after field mapping.

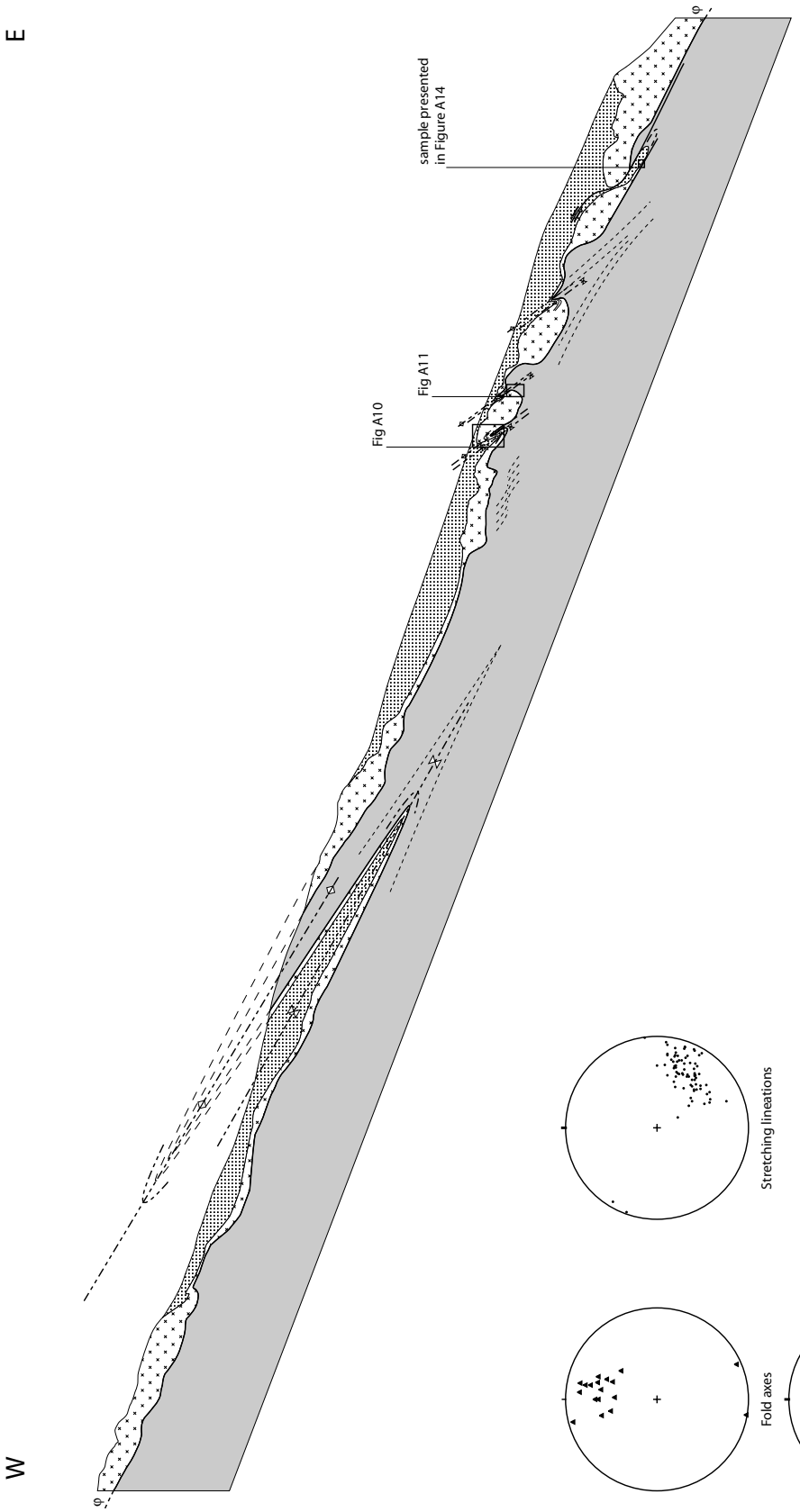


**Figure A9:** Detailed representation of the basement/cover imbricate found within the RYSZ. See figure A8 for localisation.



**Figure A10:** Insights on a small scale fold affecting the basement cover imbricate depicted in figure A9.

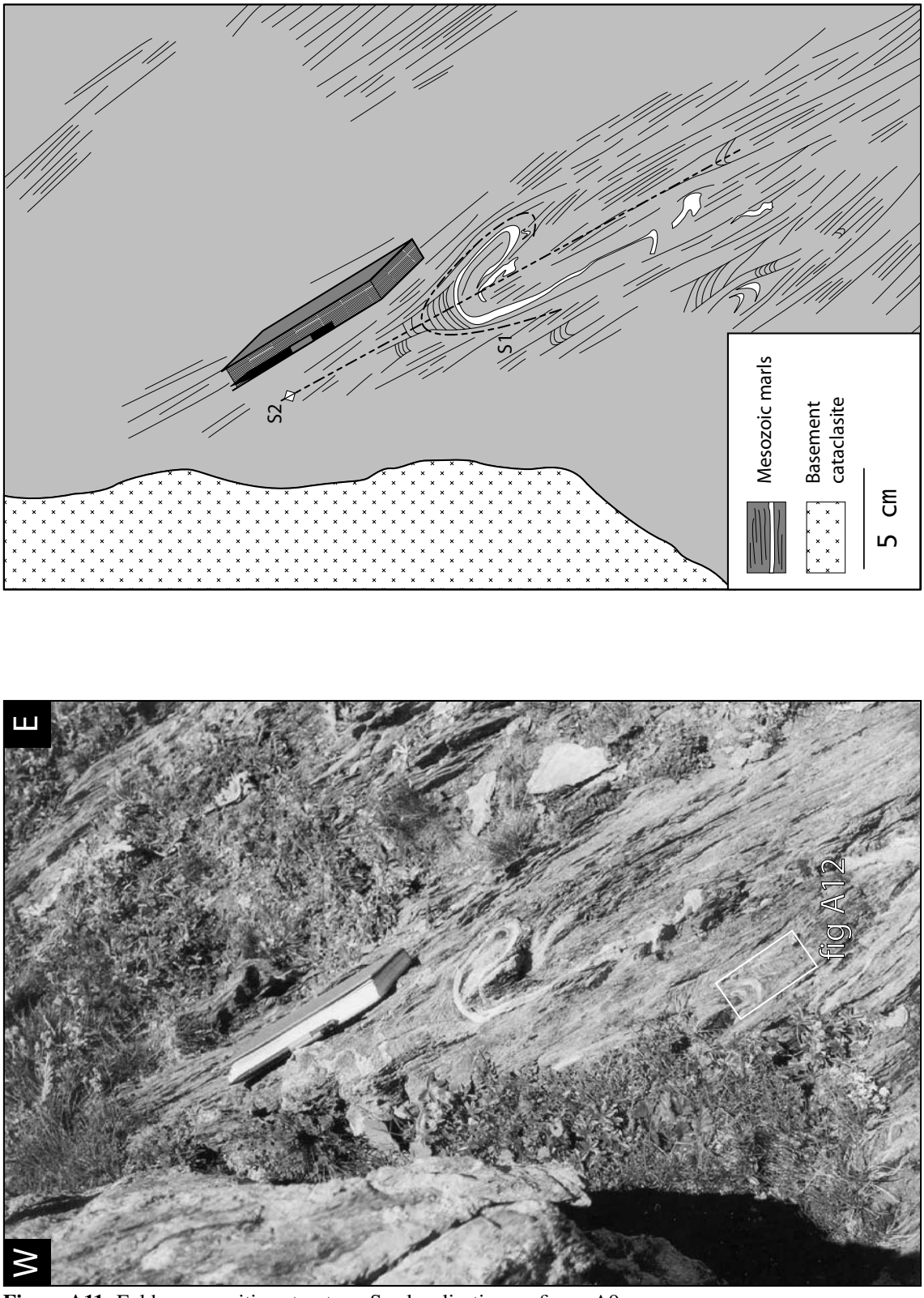


**Figure A11:** Fold superposition structure. See localisation on figure A9.

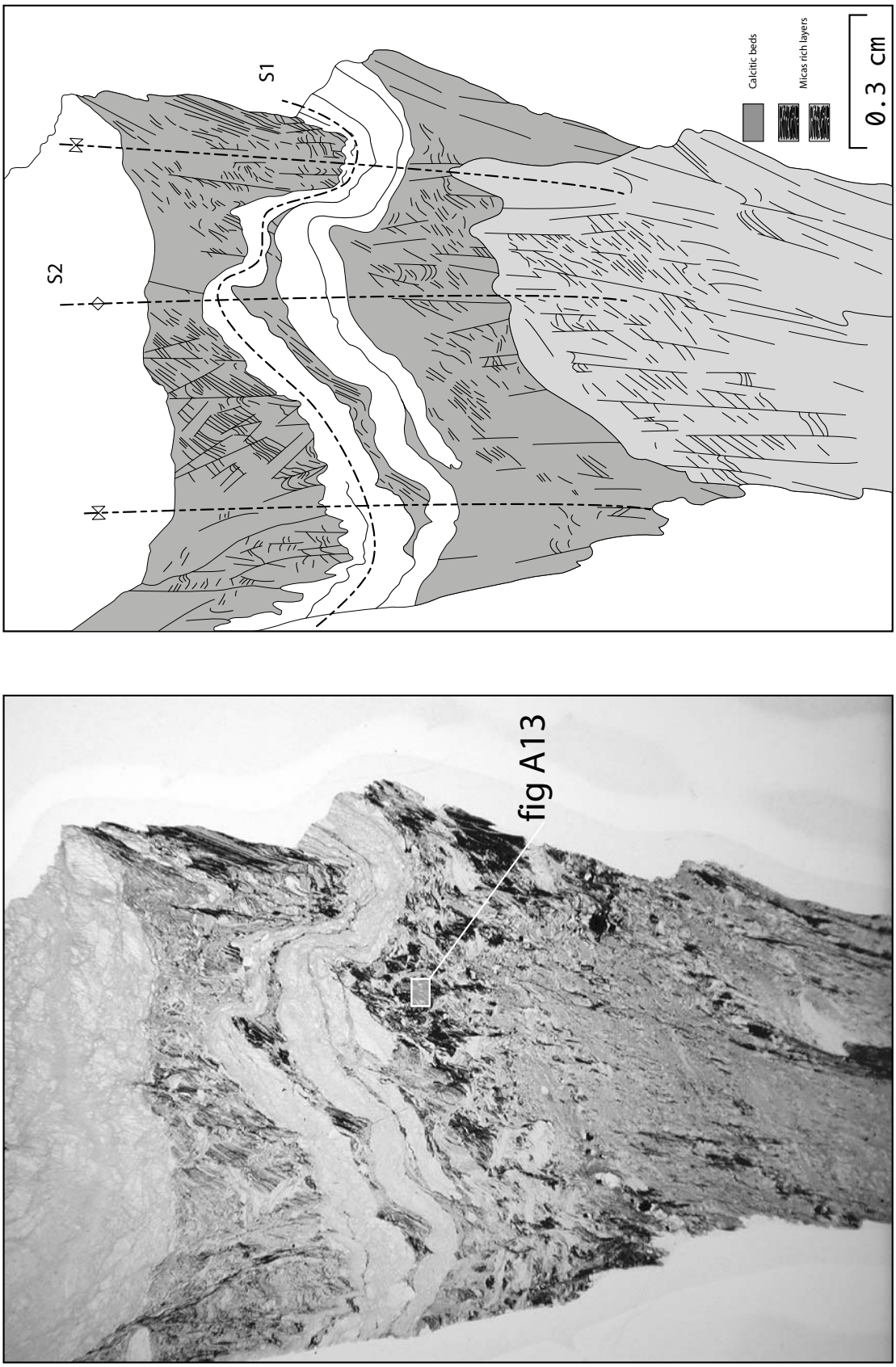


**Figure A12:** Micrograph interpretation of marl sample from outcrop depicted in figure A11. Note the superposition of two schistosities S0/1 and S2.

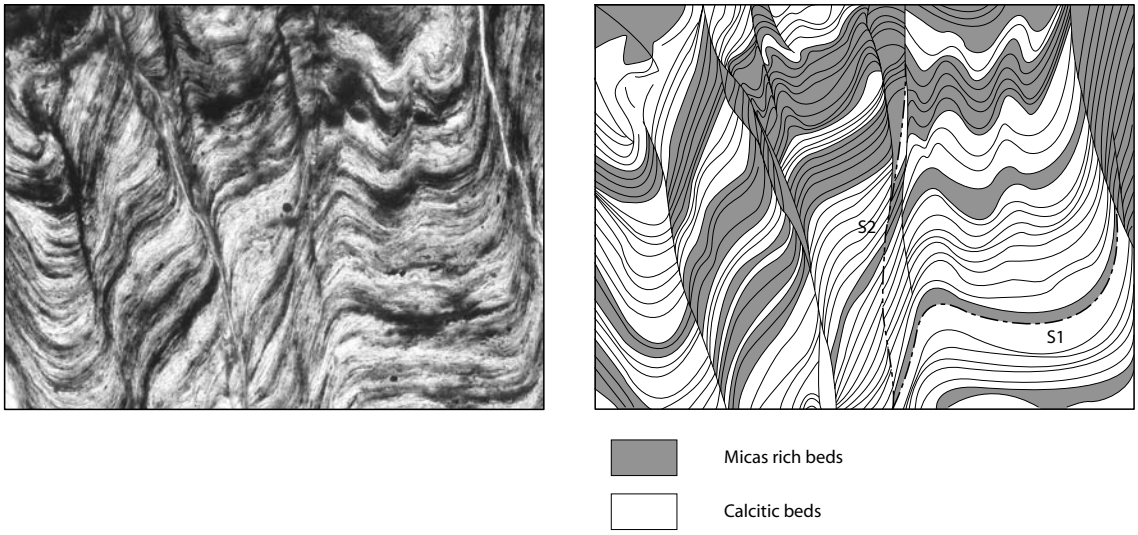


**Figure A13:** Insight of superimposition pattern between S0/1 and S2.

The nummulitic cover involved in these thrust zones suffered intense shearing, as documented by the extreme lamination of the sedimentary sequence often reduced to a few centimeters of nummulitic limestone and basal conglomerate (see figure A14a). Microstructural evidences, such as asymmetric calcite pressure fringes developed

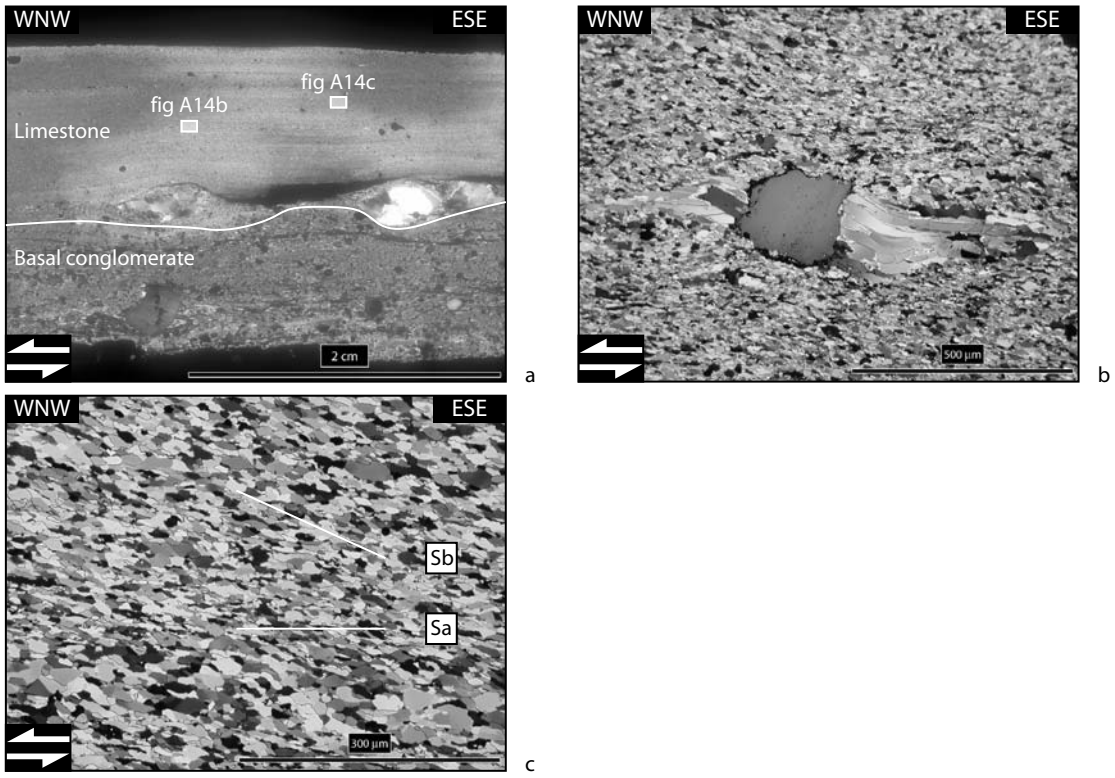


**Figure A14:** Photomicrographs of different mylonitic limestones found within profile depicted in figure A9.

at the rim of detritical quartz grains (see figure A14b) or shape preferred orientation of dynamically recrystallised crystals (see figure A14c) found in samples from these limestones also indicate WNW-directed thrusting. These calcite ultramylonites present a strong crystallographic preferred orientation, the asymmetry of which independently confirms the sinistral shearing (WNW-directed) of the rock (see chapter 2).

The third type of local complications is that also recognized by Butler (1992), who noticed in a "zone of a few hundred meters wide affecting the highest basement sheets, the presence of a series of faults cutting down through the thrust stack towards the WNW and showing net extensional offsets with respect to the tectonic pile".

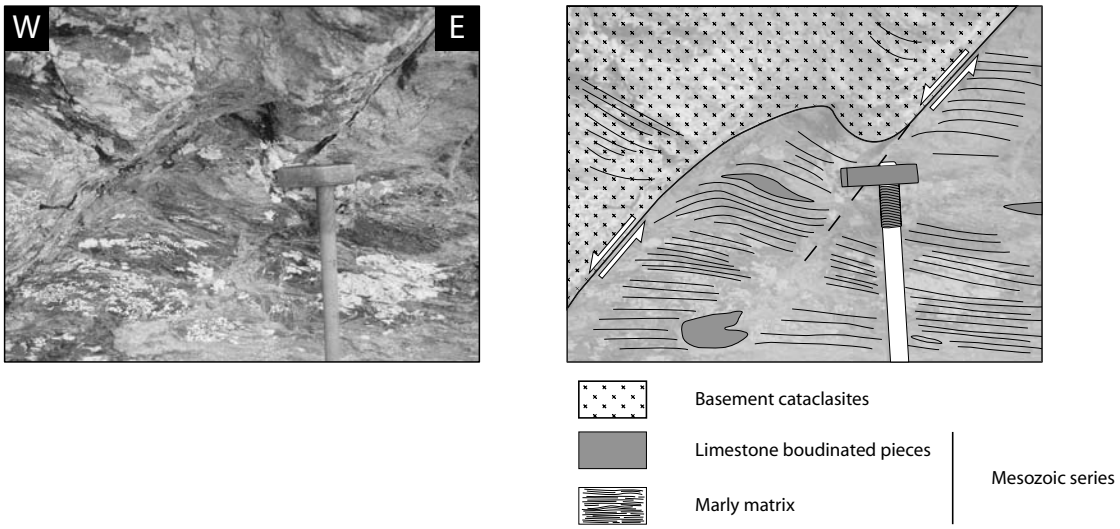


**Figure A15:** Late extentional fault found below the Rocher de l'Yret summit.

The presence of these extensional structures was confirmed (see figure A15). As argued by Butler (1992), they probably do not play a major role in the structural evolution of the RYSZ. Indeed, amounts of movement along the fault planes rarely exceed a few meters and are only noticed in the upper part of the shear zone. They may be considered as a kind of shear bands at the macroscopic scale.

Since all kinematic indicators are consistent with thrusting along the RT and because the amounts of displacement or strain accommodated by strike slip activity, folding or normal faulting show moderate values, we do not consider the above complications as being caused by a second tectonic event. Instead, we interpret these complications as being due to strain partitioning and/or progressive deformation within one and the same kinematic framework.

# APPENDIX B: Complete data set of microfabric analyses performed within the Rocher de l'Yret shear zone.

A complete microfabric analysis of calcite ultramylonites found at the eastern rim of the Pelvoux massif (Rocher de l'Yret shear zone, RYSZ see figure B1) has been presented in chapter 2. Seven samples deformed under various strain pathes have been considered as representative of the whole collection of 85 samples taken at this place.

The purpose of the present series of appendixes is to present to the reader the complete data set of:

1) Texture measurements: this includes pole figure and inverse pole figure calculations (appendixes B.1, B.2 and B.3) using input from X-ray goniometry measurements together with a picture of Computer Integrated Polarisation microscopy (Panozzo Heilbronner and Pauli 1993, 1994) (appendix B.4). Computer conversion routines used to automatically transform the different files format between MENTEX (Schaeben, 1990) and BEARTEX (Wenk et al. 1998) programs are presented as well in appendix B5.

2) Microstructural analysis: this includes grain size analysis histograms (appendix B.6) and grain shape preferred orientation diagrams (appendix B.7).

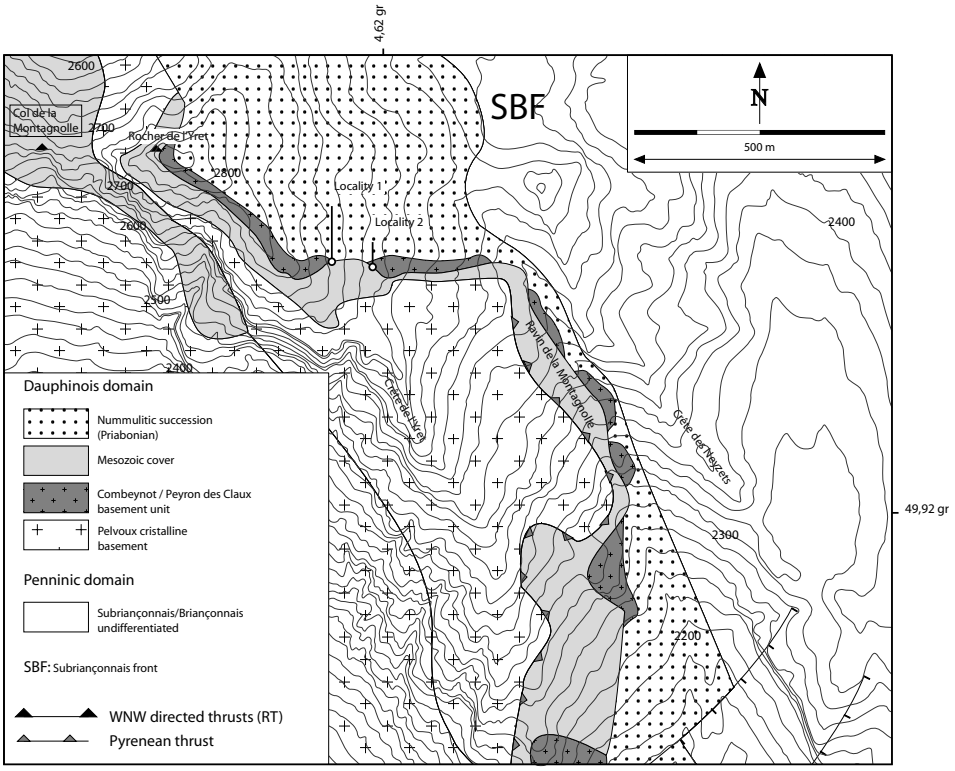


**Figure B1:** Detailed geological map of the "Rocher de l'Yret" shear zone.

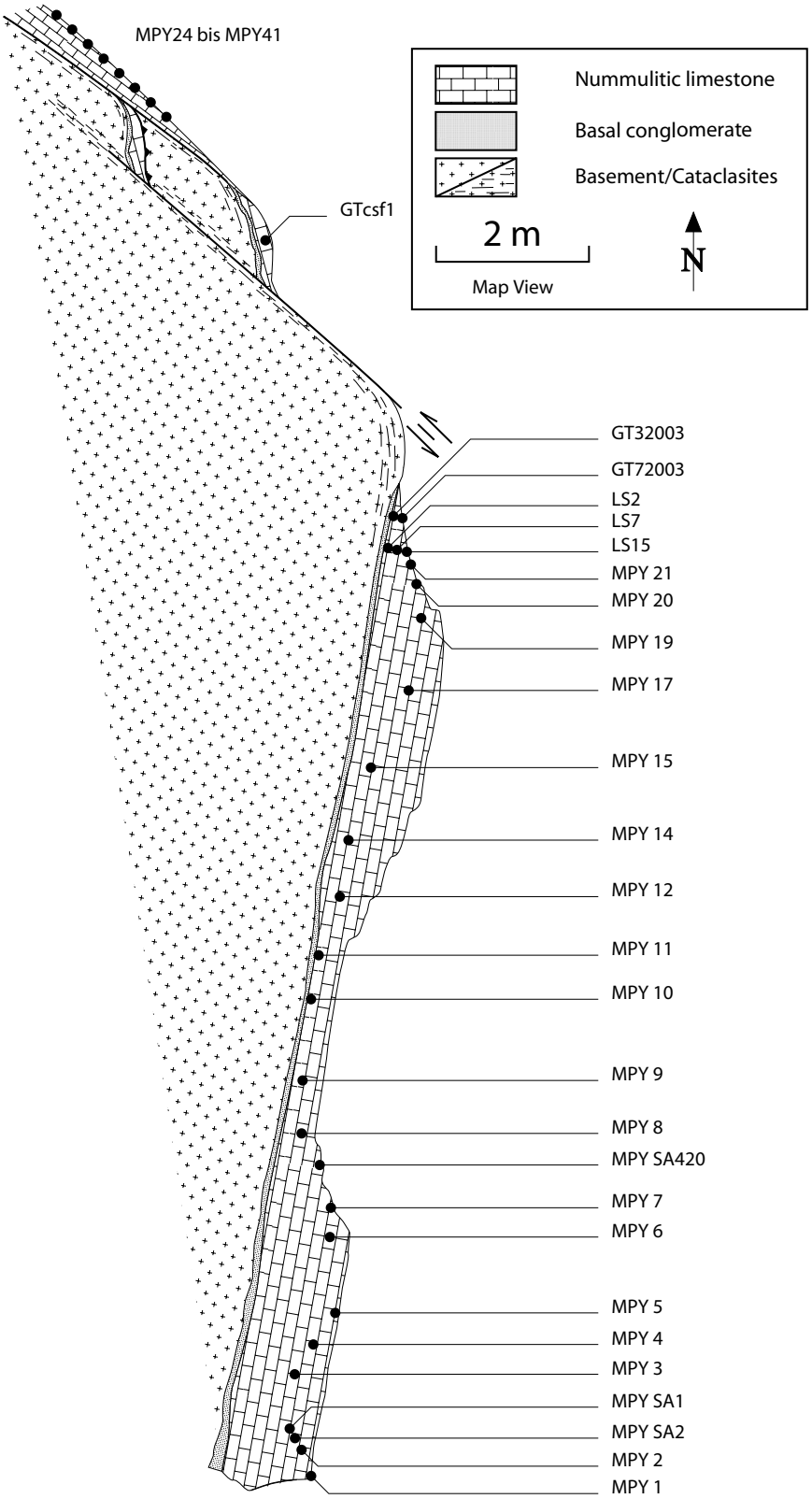


**Figure B2:** Schematic representation of the outcrop from locality 1 (see figure B1). The localisation of the different samples is reported.

The localization of the samples is given in the schematic representation found in figure B2 (outcrop from locality 1) and figure B12 (outcrop from locality 2). Each specimen, either sampled at locality 1 or 2, has been chosen large enough to extract several samples for textural goniometry. In this way, samples MPY7, MPY7b and MPY7sc, for example, refer to the same MPY7 hand specimen.

## Textures measurements.

### Appendix B.1.

This appendix presents 64 calculations of *r* and *h* crystallographic planes, reduced *a* and *sd1* slip directions and *c*-axis, determined using MENTEX (Schaeben, 1990) iteration program only.
In all cases, the orientation distribution function (ODF) was determined using an order of expansion equal to 20.

The data are presented according to their sampling origin (see figure B1), i.e. locality 1 (appendix B.1.1) or locality 2 (appendix B.1.2).

#### Appendix B.1.1.

As described in chapter 2, this outcrop consists of an isolated basement boudin and its preserved Eocene cover. This basement boudin structure is cut at its northern termination by a sinistral stike slip zone active during the last increments of deformation along the RT. Movements along this sinistral strike slip fault induces intense deformation of the nummulitic limestone layer which evolves in an ultramylonitic band parallel to the fault plane (see figure B2).

Two main samples series have been taken from this outcrop and are presented separately in the following:

1) Appendix B.1.1.1 refers to samples taken from the main mylonitic layer found at locality 1. 34 samples (MPY1bne to MPYGTLS15) are presented in figures B3 to B8.
2) Appendix B.1.1.2 refers to samples taken from the mylonitic band developped at the northern termination of the outcrop from locality 1. 13 samples (GTcsf1 to MPY41) are presented in figures B9 to B11.

Appendix B.1.1.1.

Given 1) the paleostress analysis presented in chapter 2 and 2) the very specific orientation of the nummulitic limestone found in sedimentary contact on top of the basement boudins, it has been argued in chapter 2 that all samples taken from this nummulitic limestone layer have been deformed under conditions of dominant coaxial strain (cf profile 1 in chapter 2).

All pole figures presented in this session show an orthorhombic level of symmetry. The *c*-axis distribution is consistent with a broad maximum normal to the macroscopic foliation and shows a tendency to split in two positions symmetrically disposed at 15° from Z (see notably sample MPY4b in figure B4).

The gradient of deformation found across the mylonitic layer and described in chapter 2 is clearly visible in the samples series presented here. Samples MPY8 to MPY14 (see figure B6), taken in close vicinity with the basement unit show the weakest textures while the strongest signal intensities (i.e. above 2.4 mrd) are found on the upper part of the mylonite layer (samples MPY1bne, MPY2cn and MPYSA2N see figure B3).

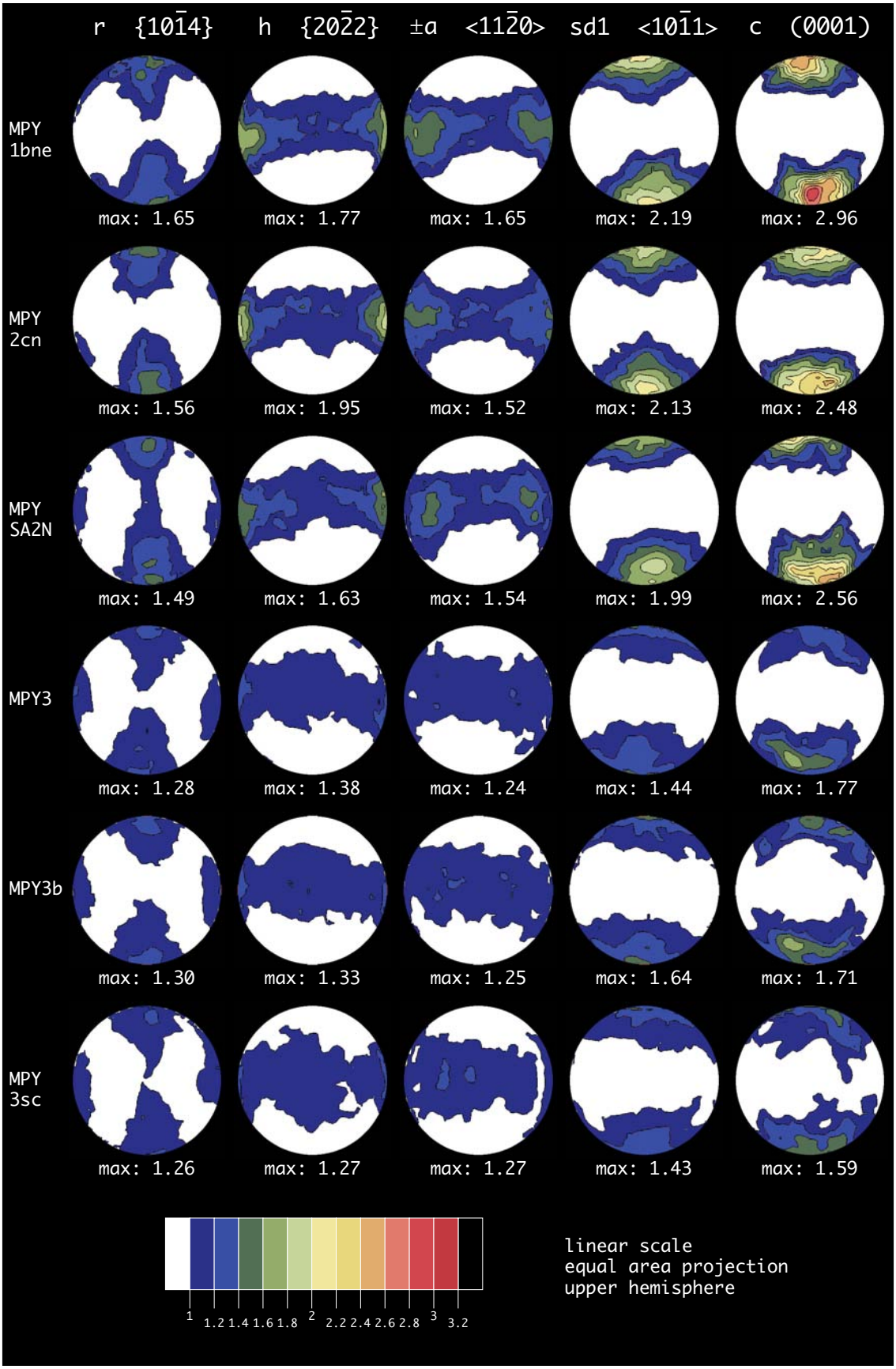


**Figure B3:** Crystallographic preferred orientation of samples MPY1bne bis MPY3sc.

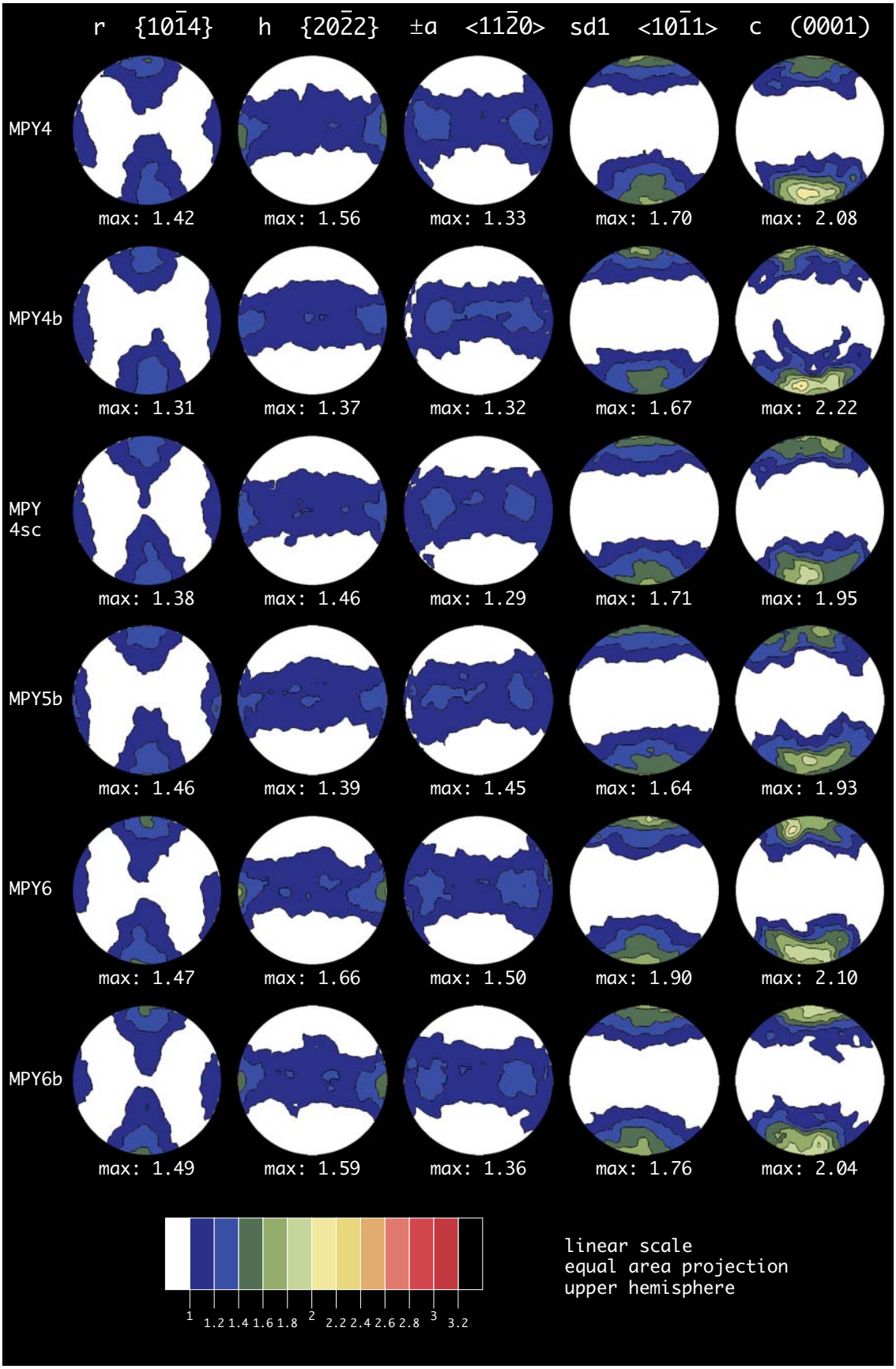


**Figure B4:** Crystallographic preferred orientation of samples MPY4 bis MPY6b.

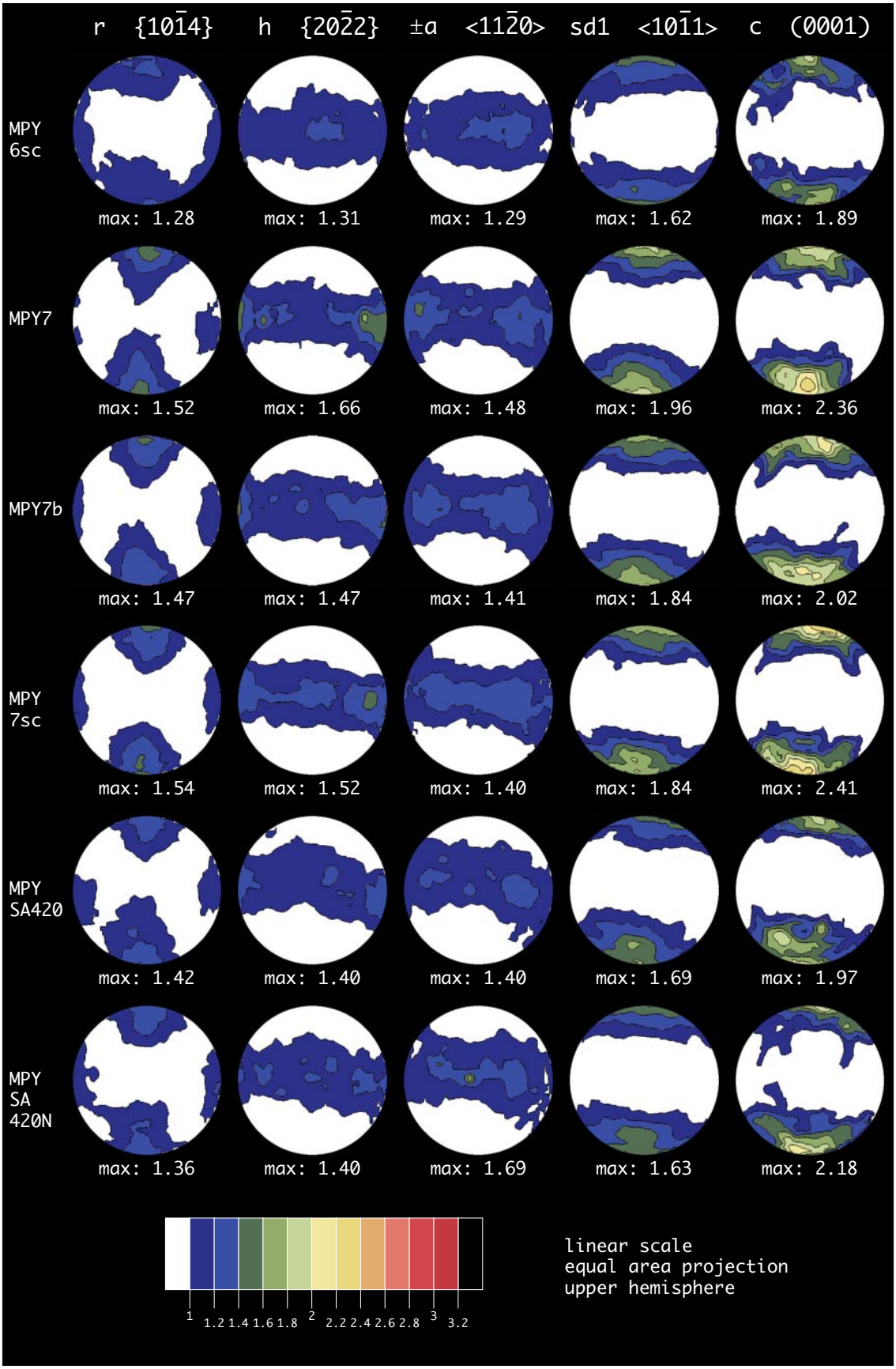


**Figure B5:** Crystallographic preferred orientation of samples MPY6sc bis MPYSA420N.

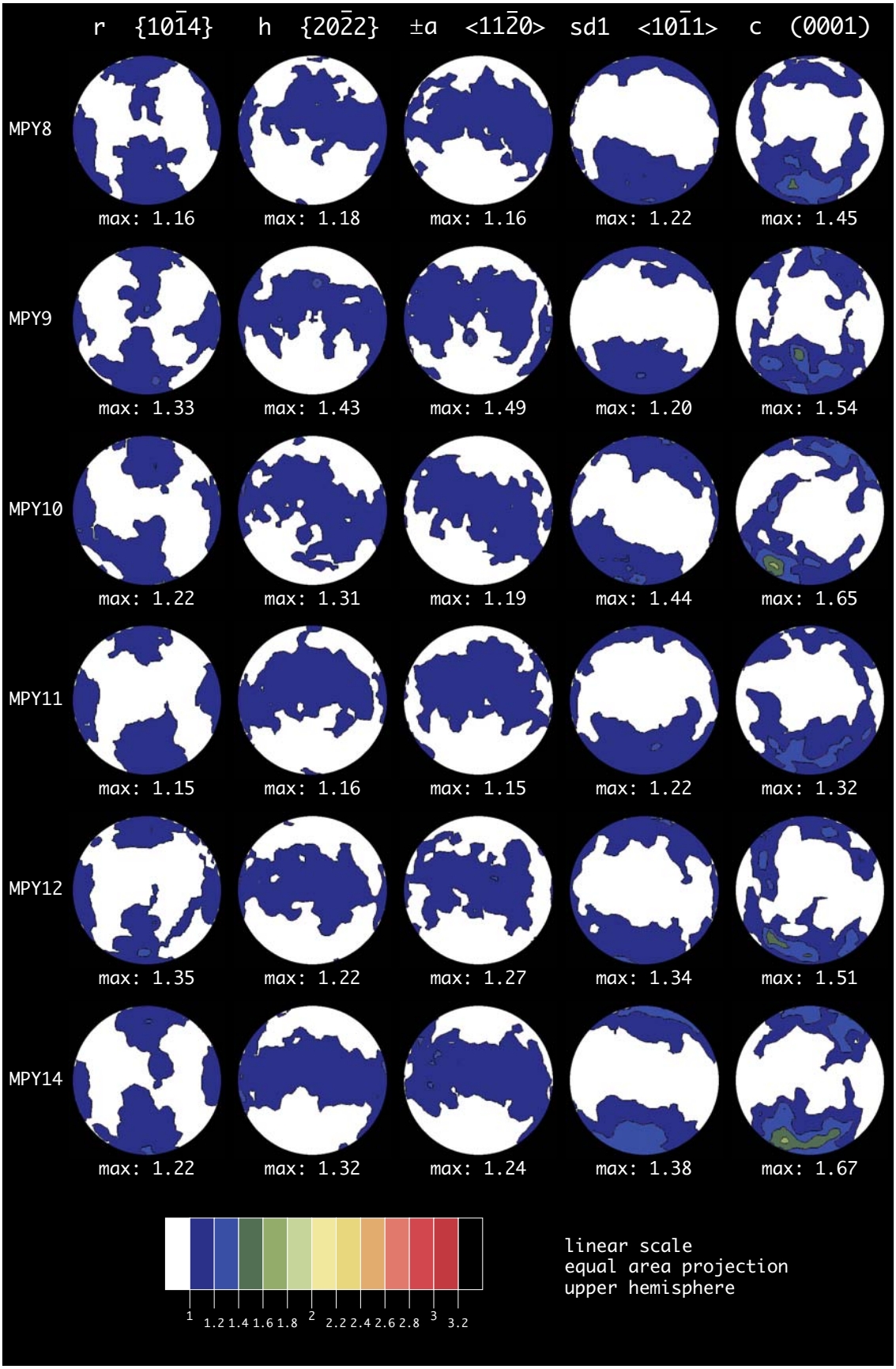


**Figure B6:** Crystallographic preferred orientation of samples MPY8 bis MPY14.

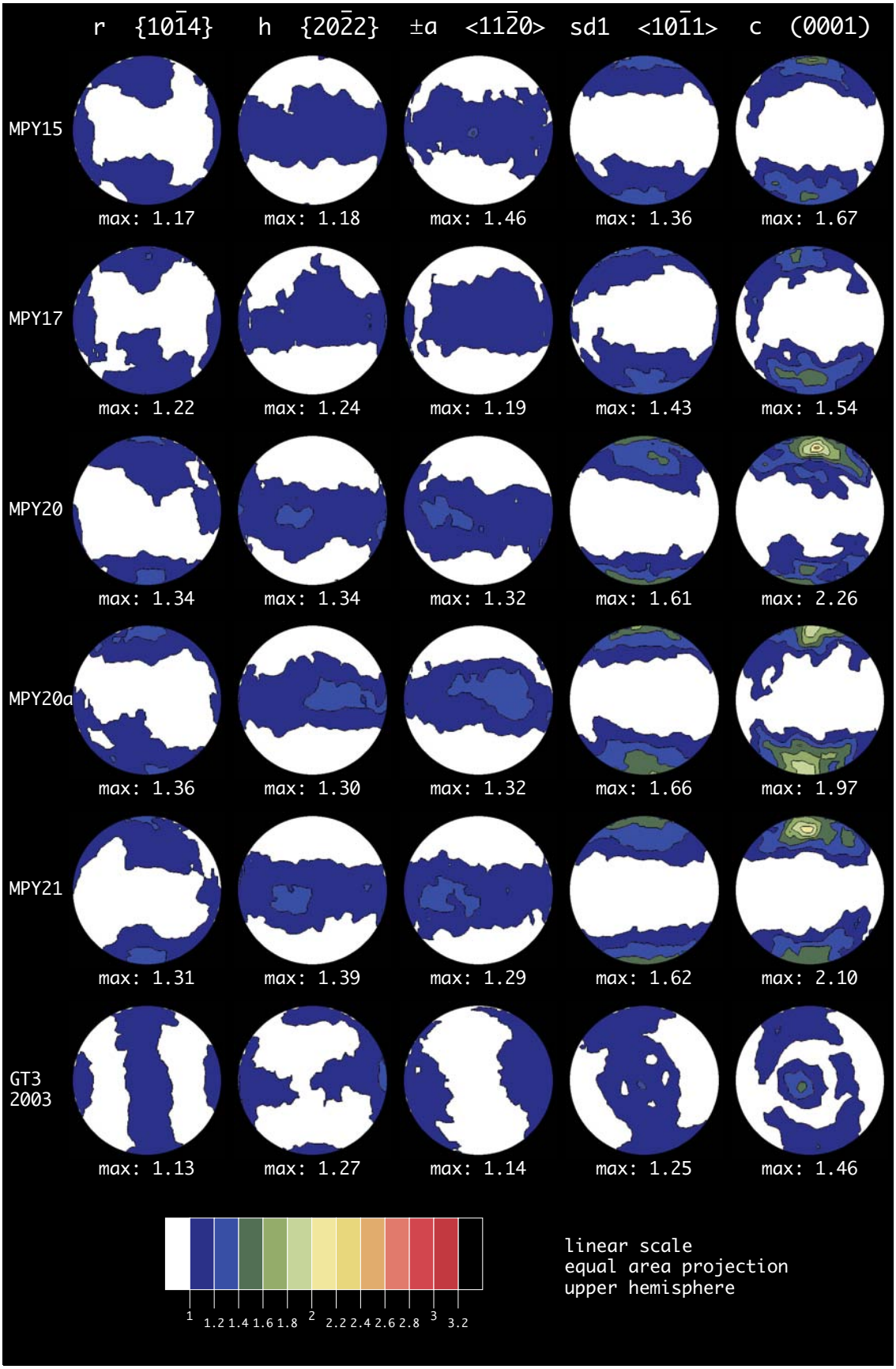


**Figure B7:** Crystallographic preferred orientation of samples MPY15 bis GT32003.

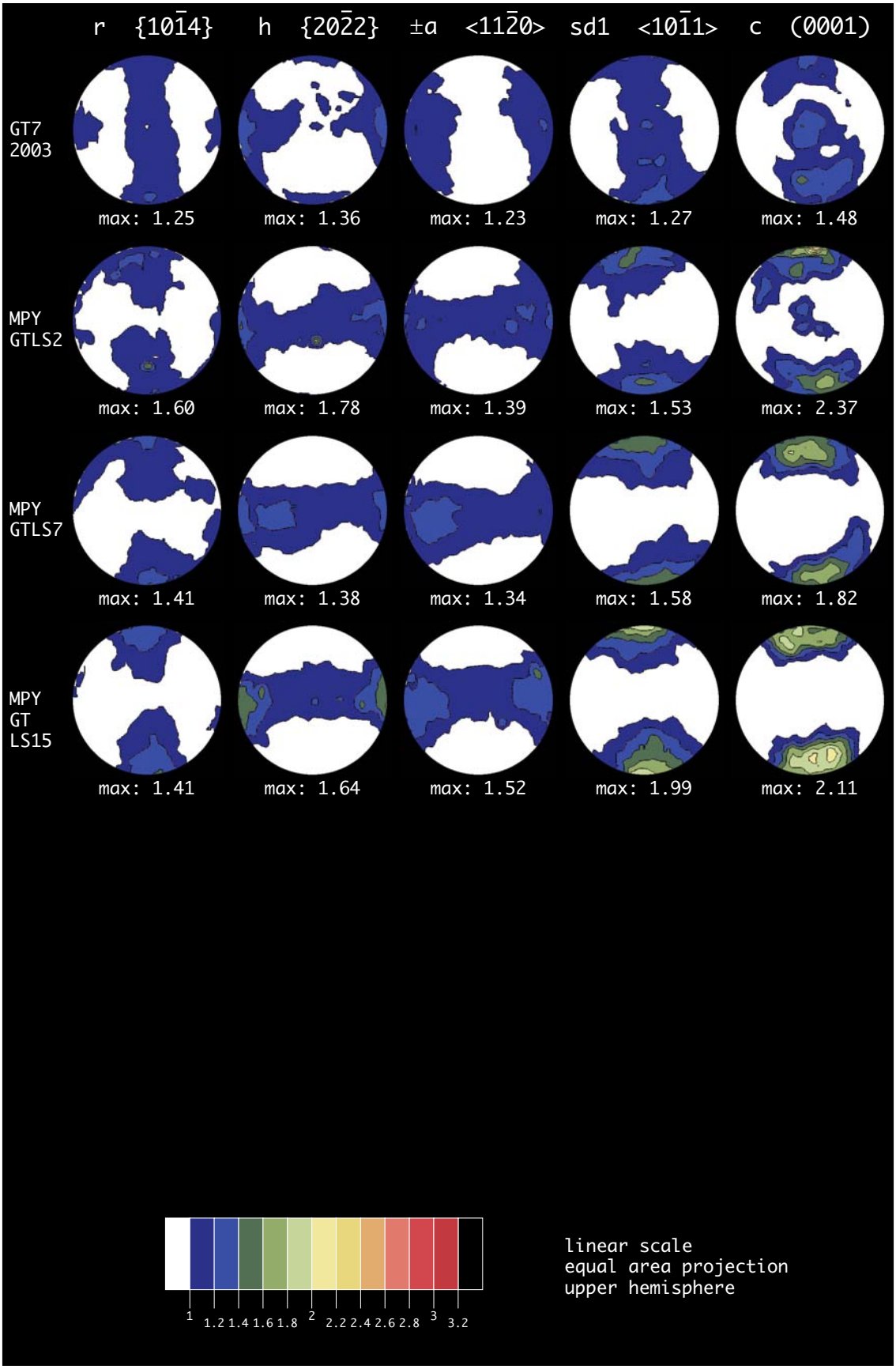


**Figure B8:** Crystallographic preferred orientation of samples GT72003 bis MPYGTLS15.

Appendix B.1.1.2.

All samples presented in this session have been taken along strike of the mylonitic band with a distance between two samples chosen approximately equal to one meter. As argued in chapter 2, these samples accomodated a dominant component of non-coaxial strain which induces the development of a monoclinic CPO well visible in all the pole figures presented. The *c*-axis distribution shows a broad maximum tilted by a constant angle of about 15° in the sense of shear (sinistral in figures B9 to B11).

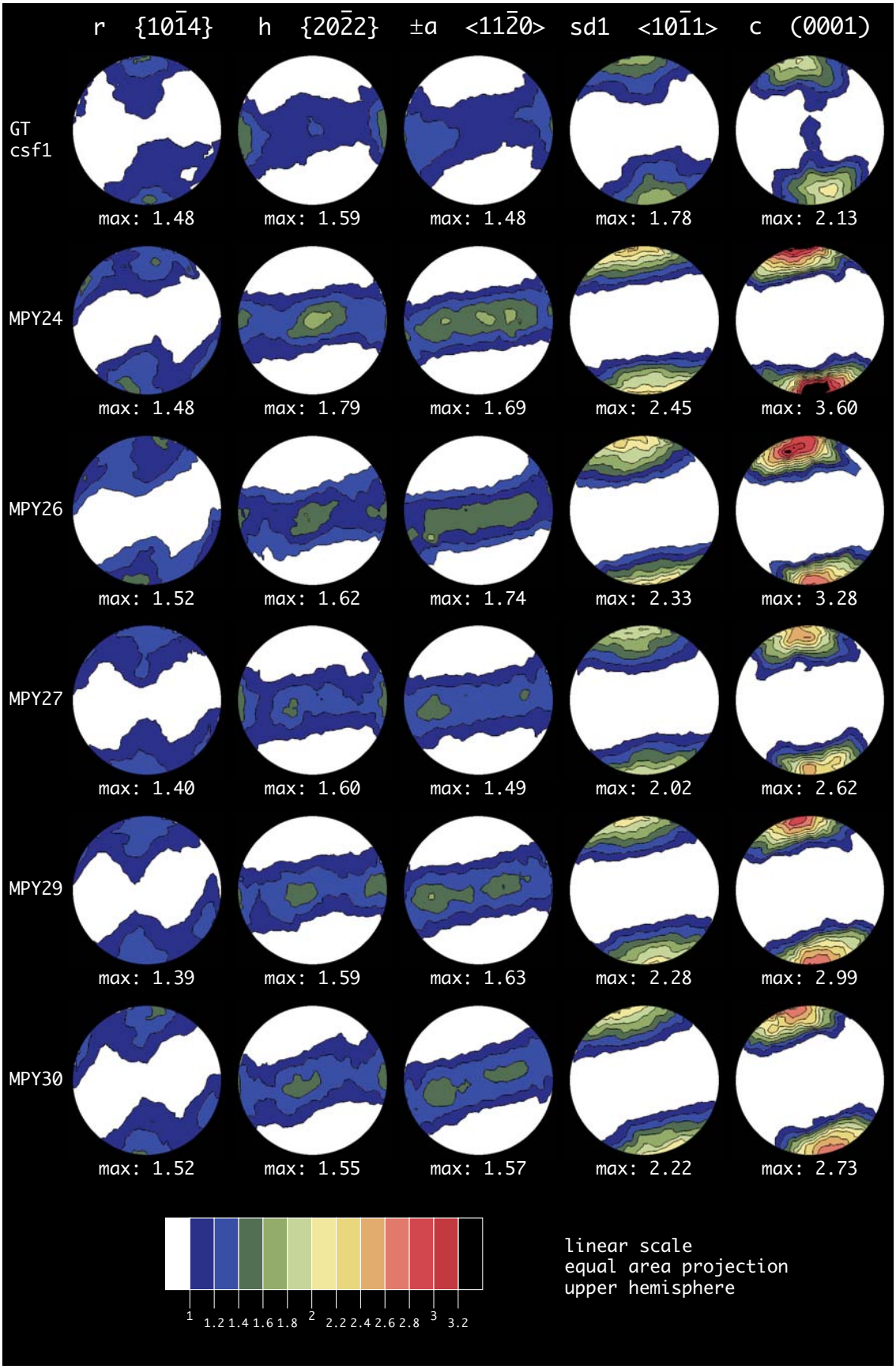


**Figure B9:** Crystallographic preferred orientation of samples GTcsf1 bis MPY30.

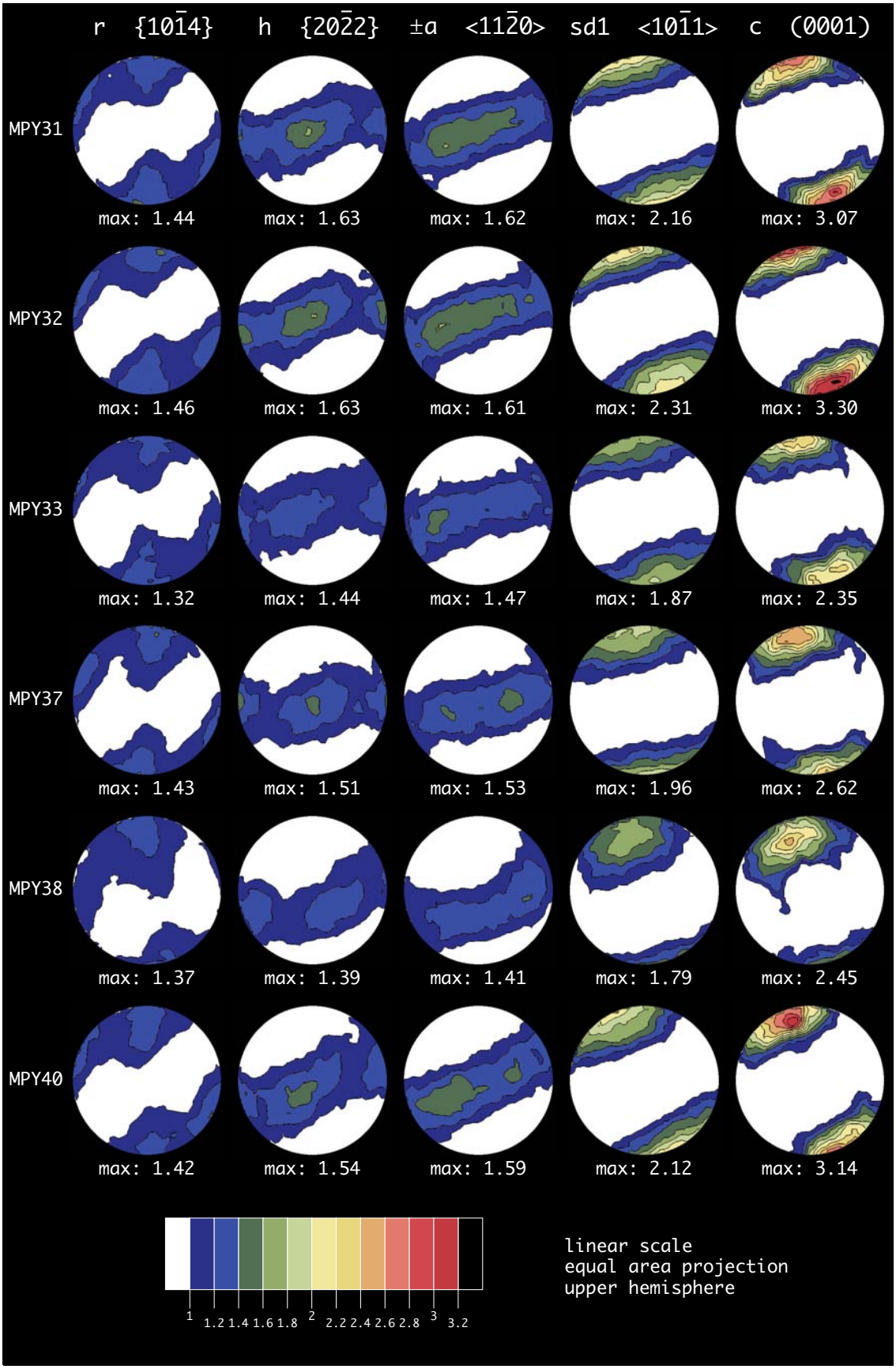


**Figure B10:** Crystallographic preferred orientation of samples MPY31 bis MPY40.

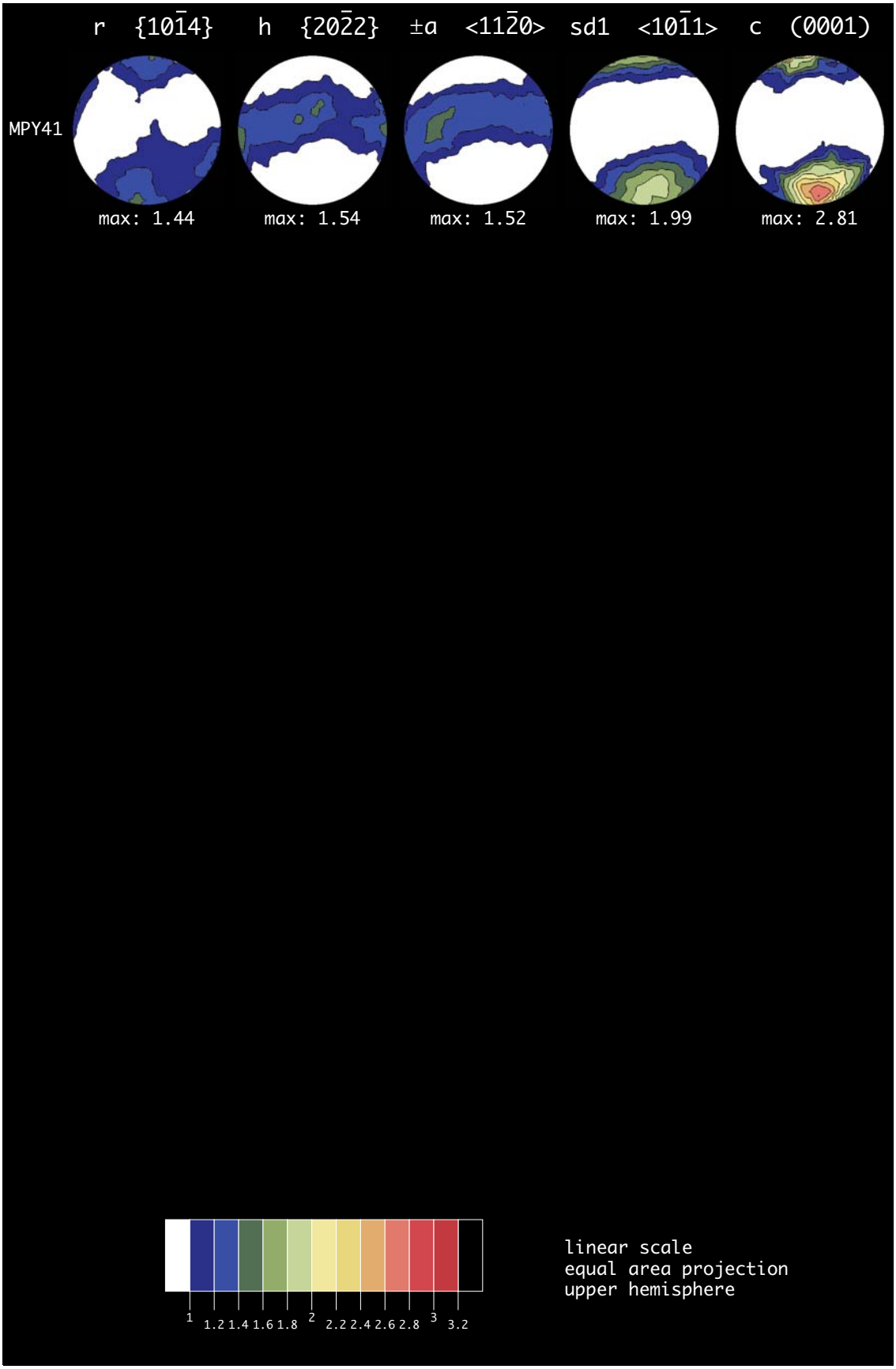


**Figure B11:** Crystallographic preferred orientation of sample MPY41.

**Appendix B.1.2.**

The 17 samples presented here have been taken from calcite ultramylonite units found within the basement cover imbricate presented in appendix A.2 (figure A9) and figure B12.

The textures are strong with *c*-axis pole figures showing intensities often above 3.5 mrd.

The level of symmetry affecting the CPO is extremely variable between the different samples. The vast majority of measurements show a clear monoclinic symmetry indicative of a dominant non-coaxial strain path. Samples 235GT, eGT235t2, eGT239t1, SA1a, SA1a1 (figure B13) and Sti2 (figure B14) however present a level of symmetry close from orthorhombic. In details, slight departures from orthorhombic symmetry are noticed notably on the *r* pole figure. Strong similarities are found between these six samples and sample Sa1a4 from the RYSZ (see chapter 2) i.e. having been deformed under conditions of "intermediate" strain regime.

It is therefore concluded that large variations in strain kinematics within locality 2 are revealed by texture analysis. These strain-partitioning processes appear related to the complicated structural setting of the outcrop studied in this session.

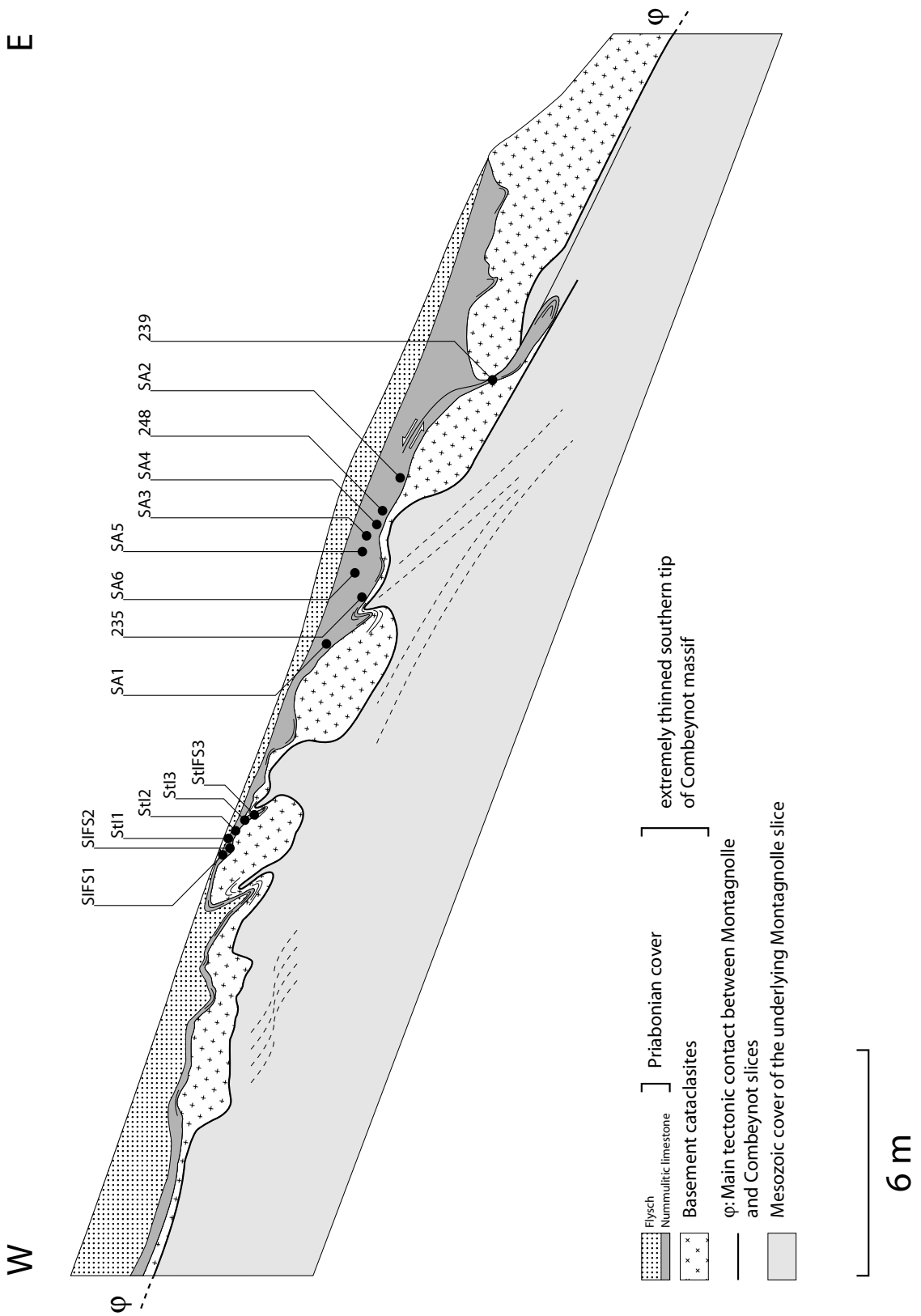


**Figure B12:** Schematic representation of the outcrop from locality 2 (see figure B1). The location of the different samples is reported.

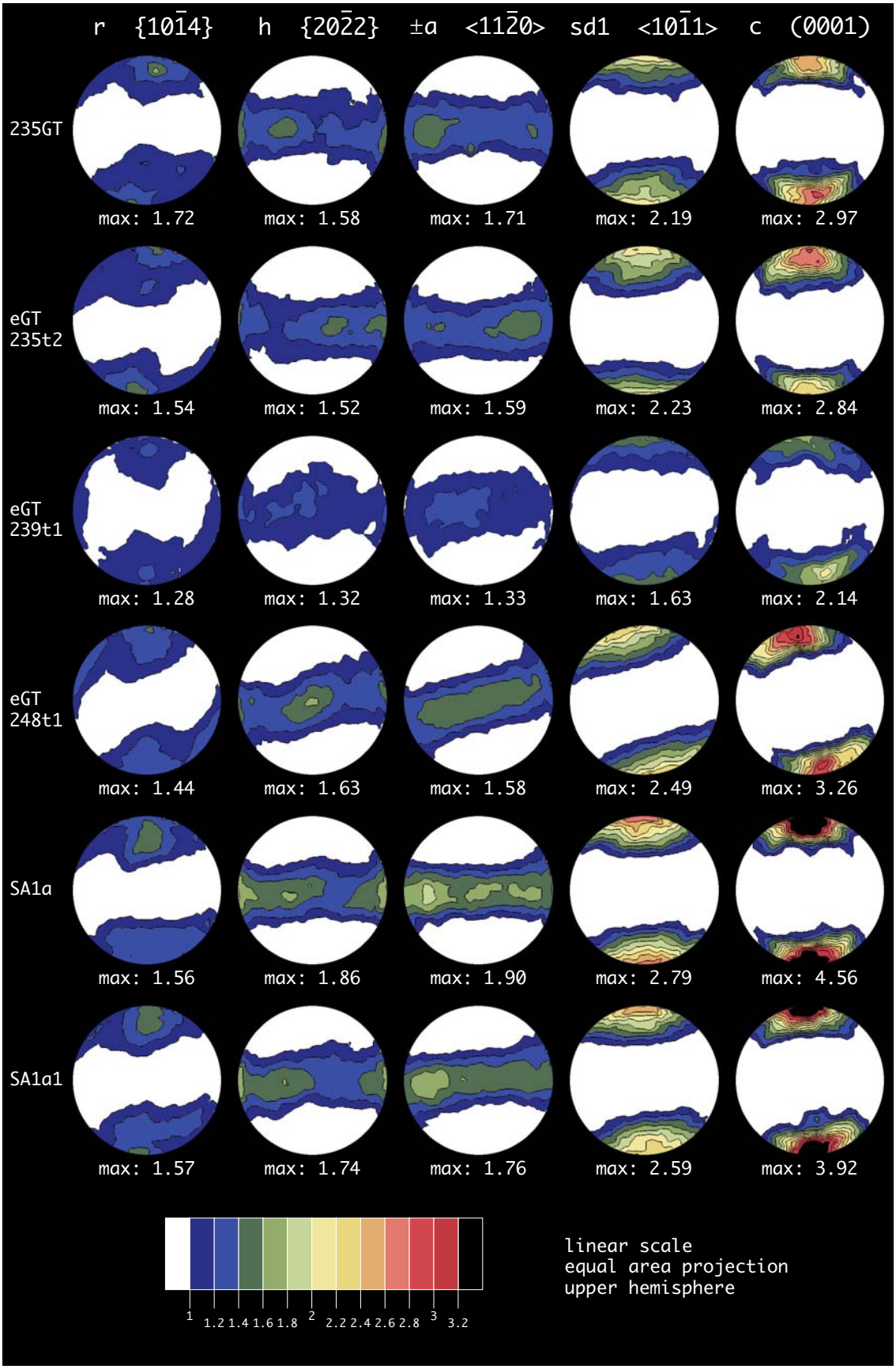


**Figure B13:** Crystallographic preferred orientation of samples 235GT bis SA1a1.

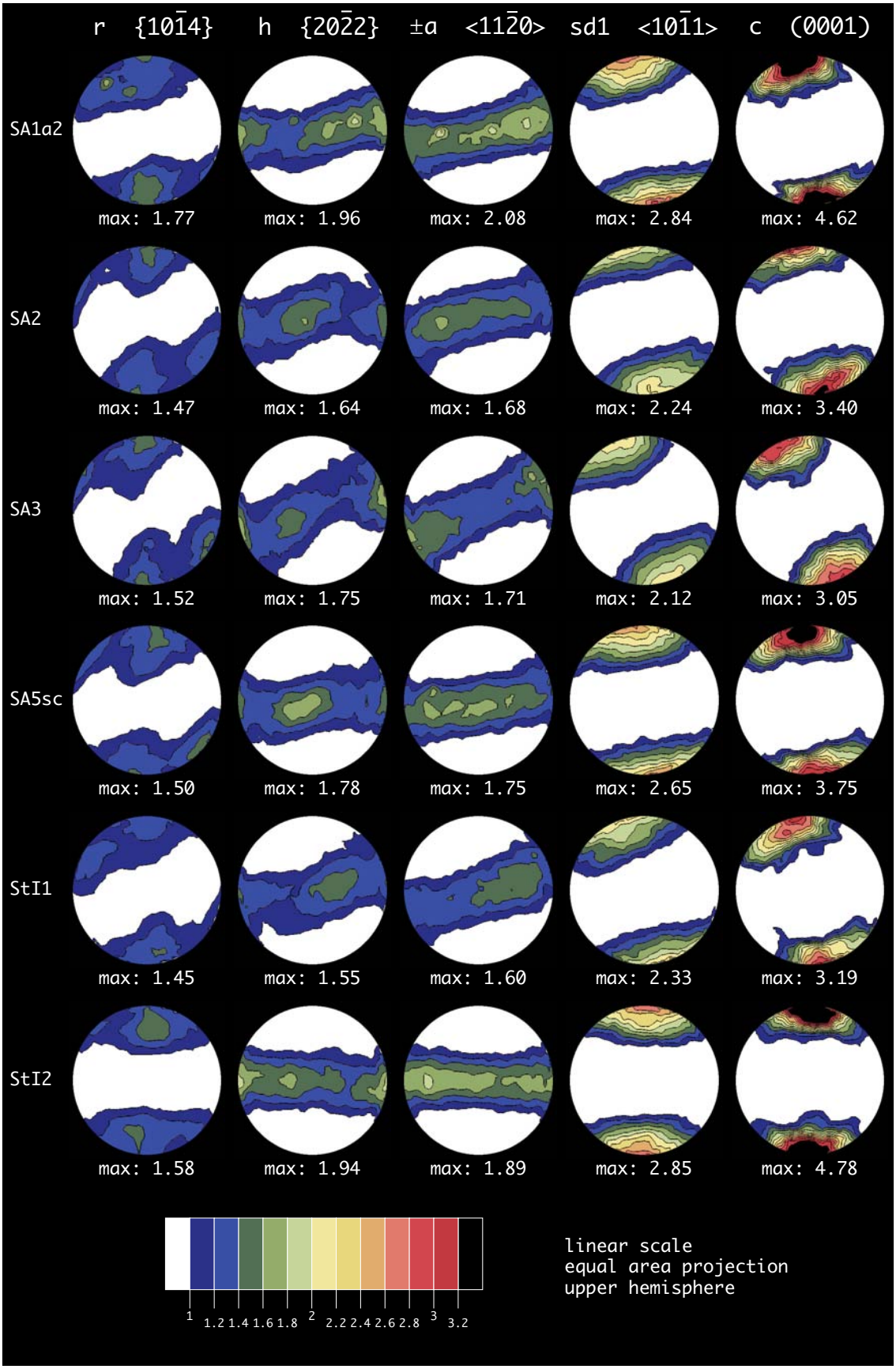


**Figure B14:** Crystallographic preferred orientation of samples SA1a2 bis StI2.

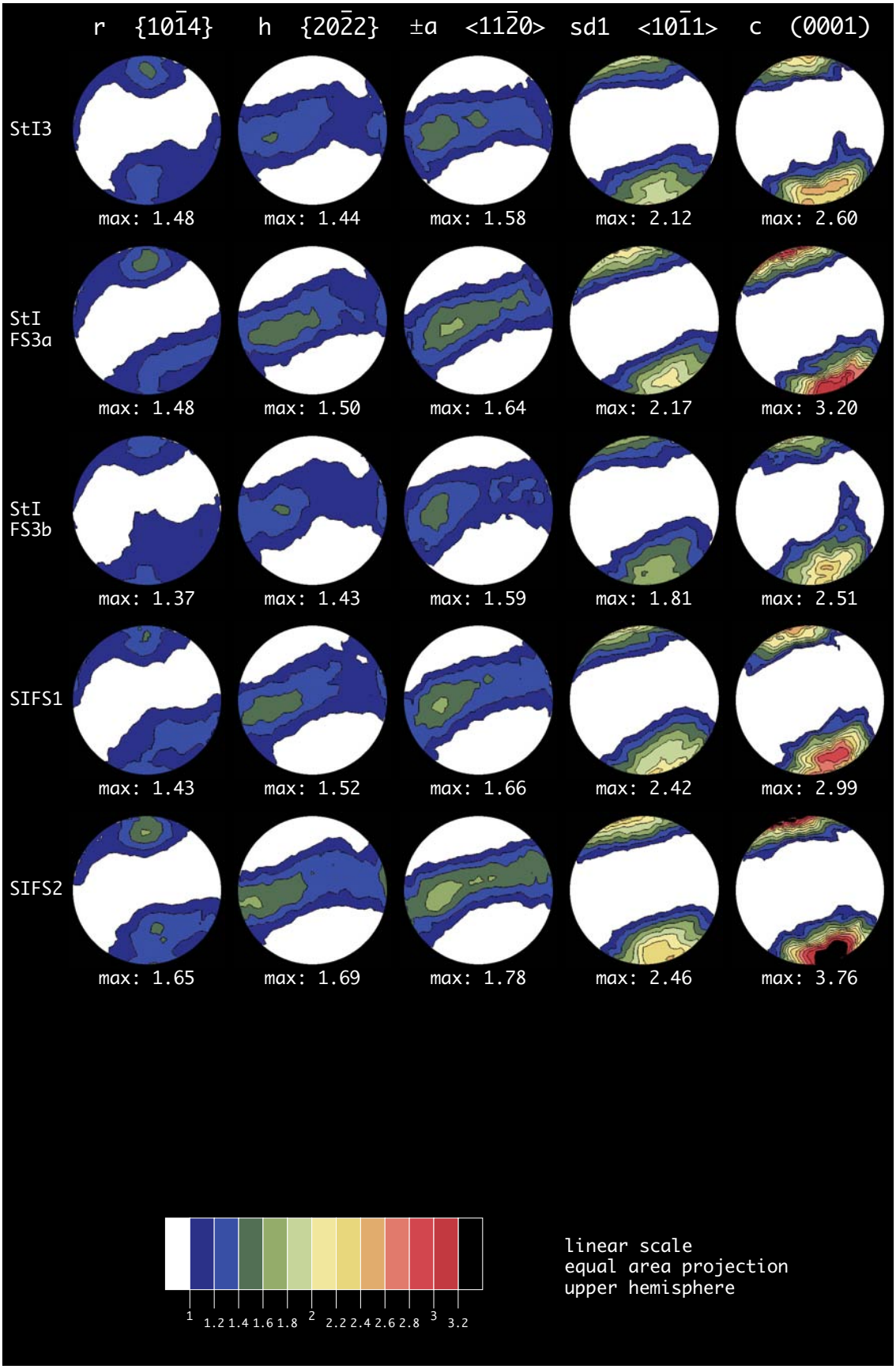


**Figure B15:** Crystallographic preferred orientation of samples StI3 bis SIFS2.

# Appendix B.2.

The purpose of this annex is to provide a set of texture analyses based on a combination of MENTEX (Schaeben, 1990) and BEARTEX (Wenk et al. 1998) softwares. A distinction is now made between the non-reduced +*a* and –*a* directions. Additionally, the *f* crystallographic plane and the *sd2* slip direction are calculated from the ODF.

The results are presented as follows:

1) Six measurements of samples showing a CPO indicative of a coaxial strain path are first given (Appendix B.2.1, see figures B16 to B18). All rocks come from the main mylonitic layer found on a preserved sedimentary contact on the basement unit at locality 1 (samples MPY19, MPYSA2n2, MPYSA12, MPY1sca2, MPY2 and MPY2b).
2) The analysis of two samples showing a CPO indicative of a so-called intermediate strain path is then presented (Appendix B.2.2, see figure B19). These two rocks come from the outcrop found at locality 2.
3) Finally, six samples having a CPO indicative of a non-coaxial strain path are shown (Appendix B.2.3, see figures B20 to B22). Four rocks come from the mylonitic layer parallel to the strike slip fault plane dissecting the northern termination of the outcrop at locality 1 (samples MPY22ne, MPY23ne, MPY25ne and MPY39ne) and two rocks come from the outcrop found at locality 2 (samples SA42 and SA6).

## Appendix B.2.1.

All pole figures show an orthorhombic level of symmetry (see figure B16 to B18). The *c*-axis show a broad distribution normal to the macroscopic foliation with a tendency to split in two positions symmetrically disposed at about 15° from Z. They correspond to positions cα and cβ defined in chapter 2.

The non-reduced +*a* and –*a* pole figures show a similar distribution with two maxima symmetrically disposed at 60° from Y.

The *sd2* pole figure shows two maxima at the periphery of the pole figure, which corresponds to positions sd2a and sd2b defined in chapter 2.

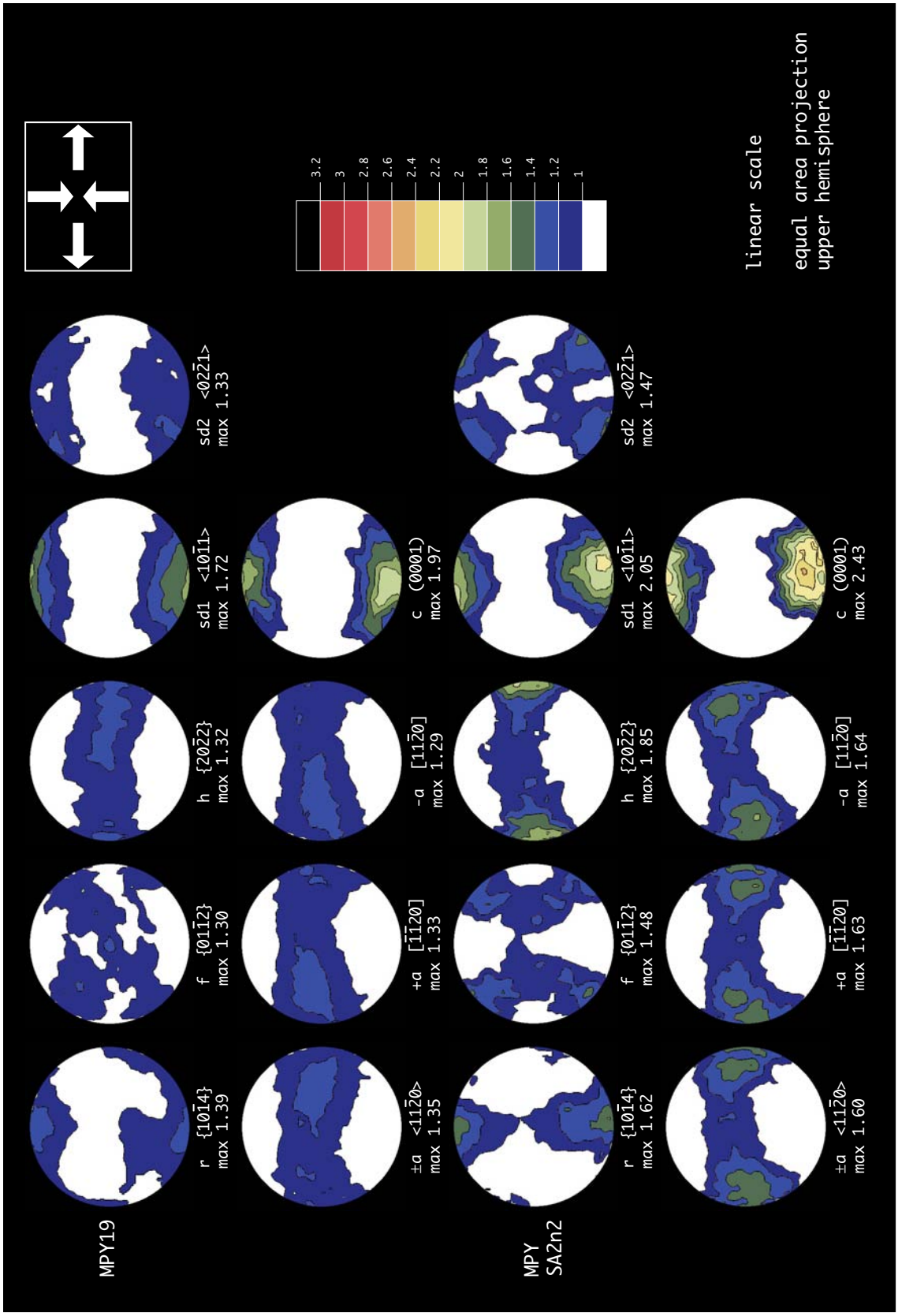


**Figure B16:** Crystallographic preferred orientation of samples MPY19 and MPYSA2n2.

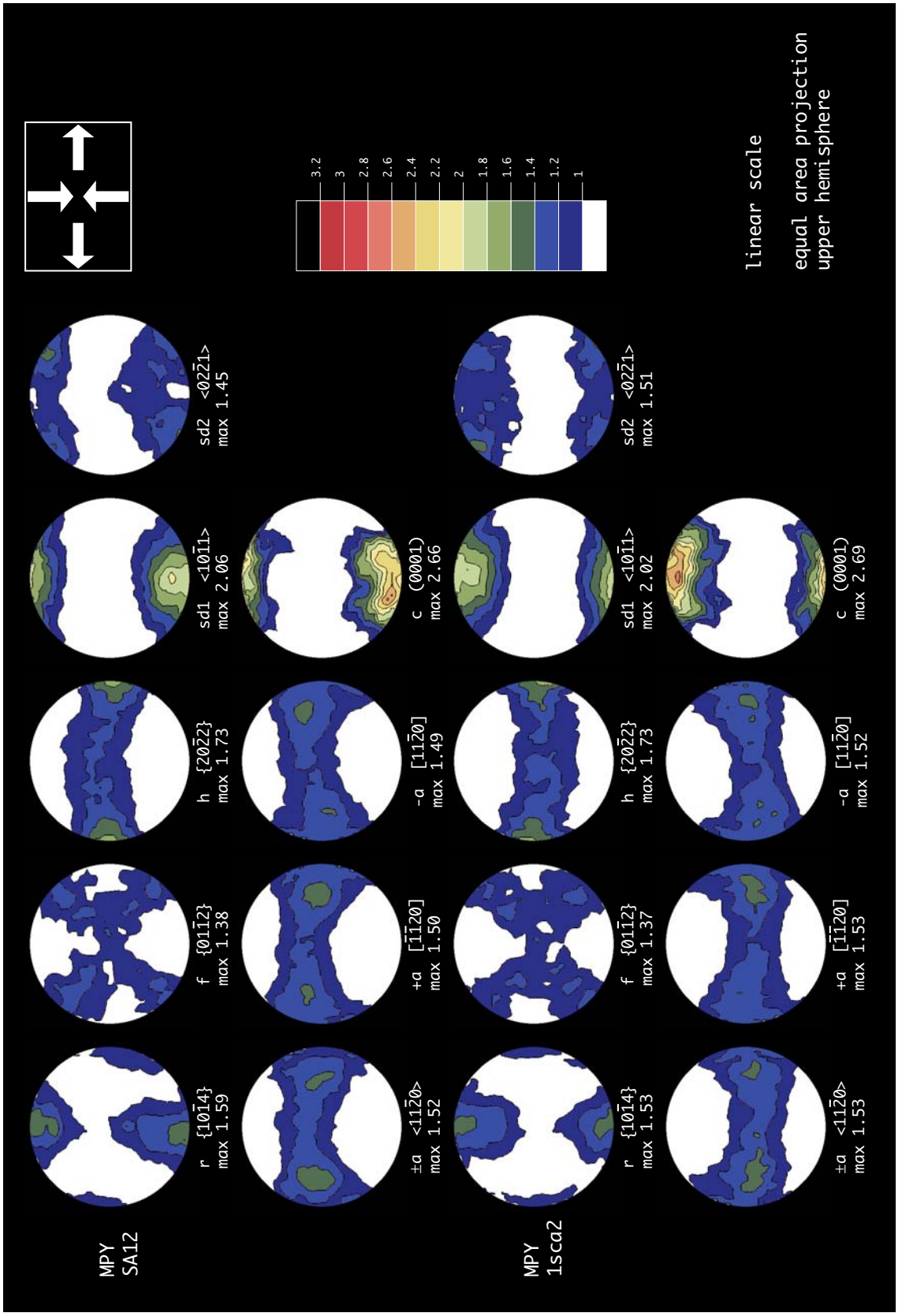


**Figure B17:** Crystallographic preferred orientation of samples MPYSA12 and MPY1sca2.

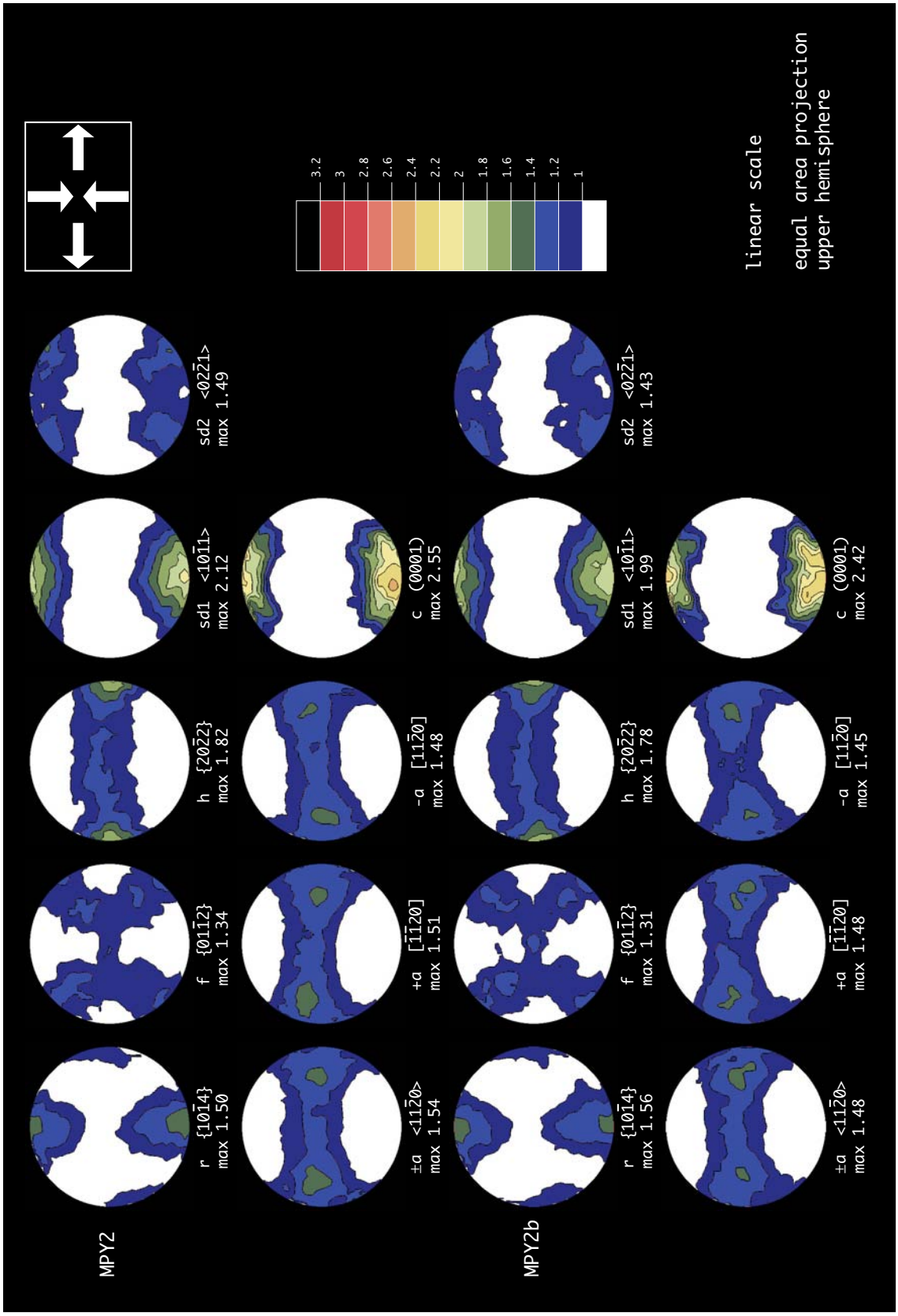


**Figure B18:** Crystallographic preferred orientation of samples MPY2 and MPY2b.

**Appendix B.2.2.**

The CPO presented here show an apparent orthorhombic symmetry with a broad *c*-axis distribution close to the normal of the macroscopic foliation (see figure B19). In details, the degree of symmetry for these two samples is lower than orthorhombic as evidenced, for example, by the non-similar distribution between the +*a* and –*a* directions.

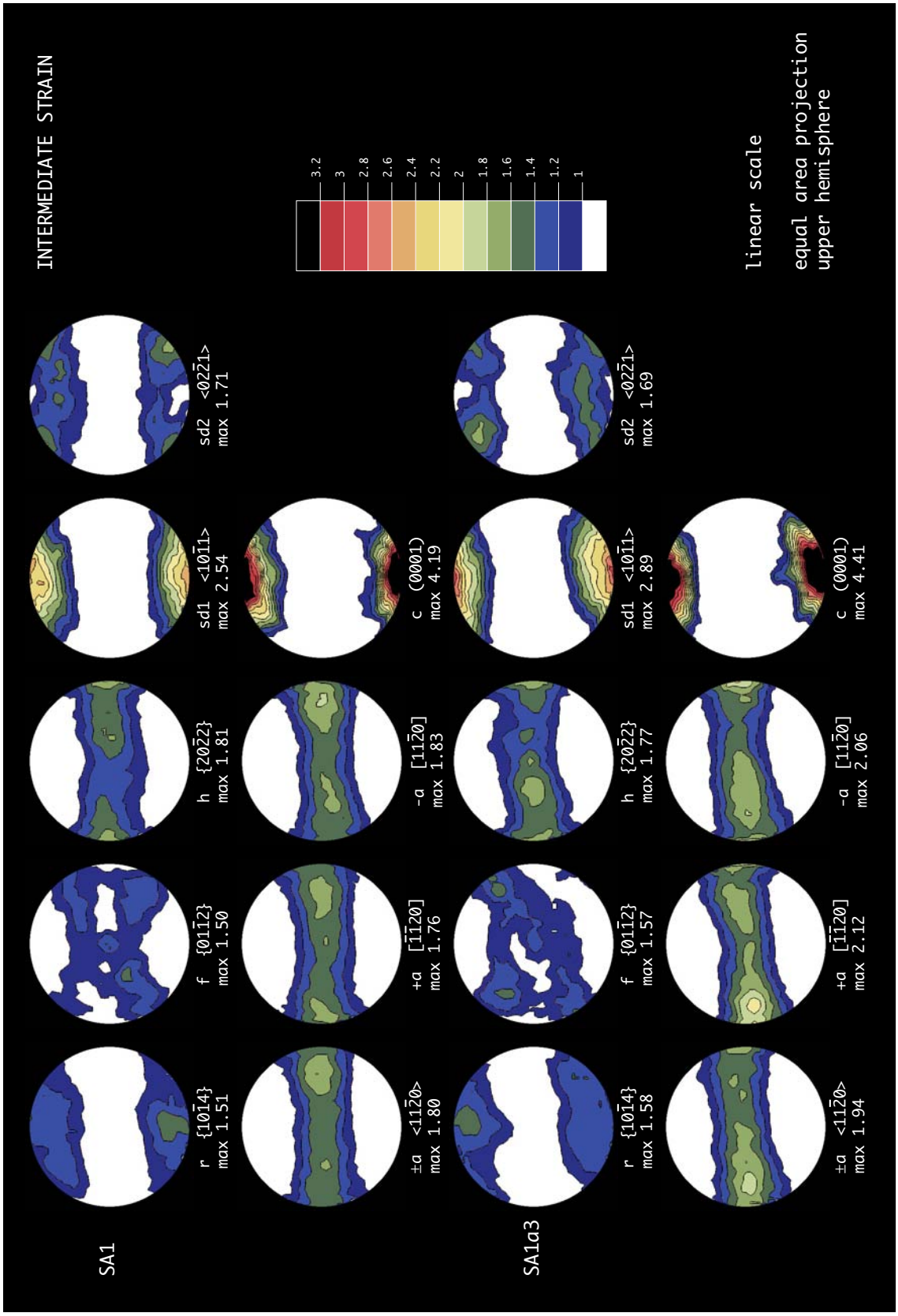


**Figure B19:** Crystallographic preferred orientation of samples SA1 and SA1a3.

**Appendix B.2.3.**

All the CPO presented in this session show a clear monoclinic symmetry (see figures B20 to B22). The *c*-axis distribution is consistent with a broad maximum rotated in the sense of shear by an angle of about 15°, which corresponds to the cα position defined in chapter 2. The monoclinic level of symmetry is also evidenced by the different distributions recorded in the +*a* and –*a* directions.

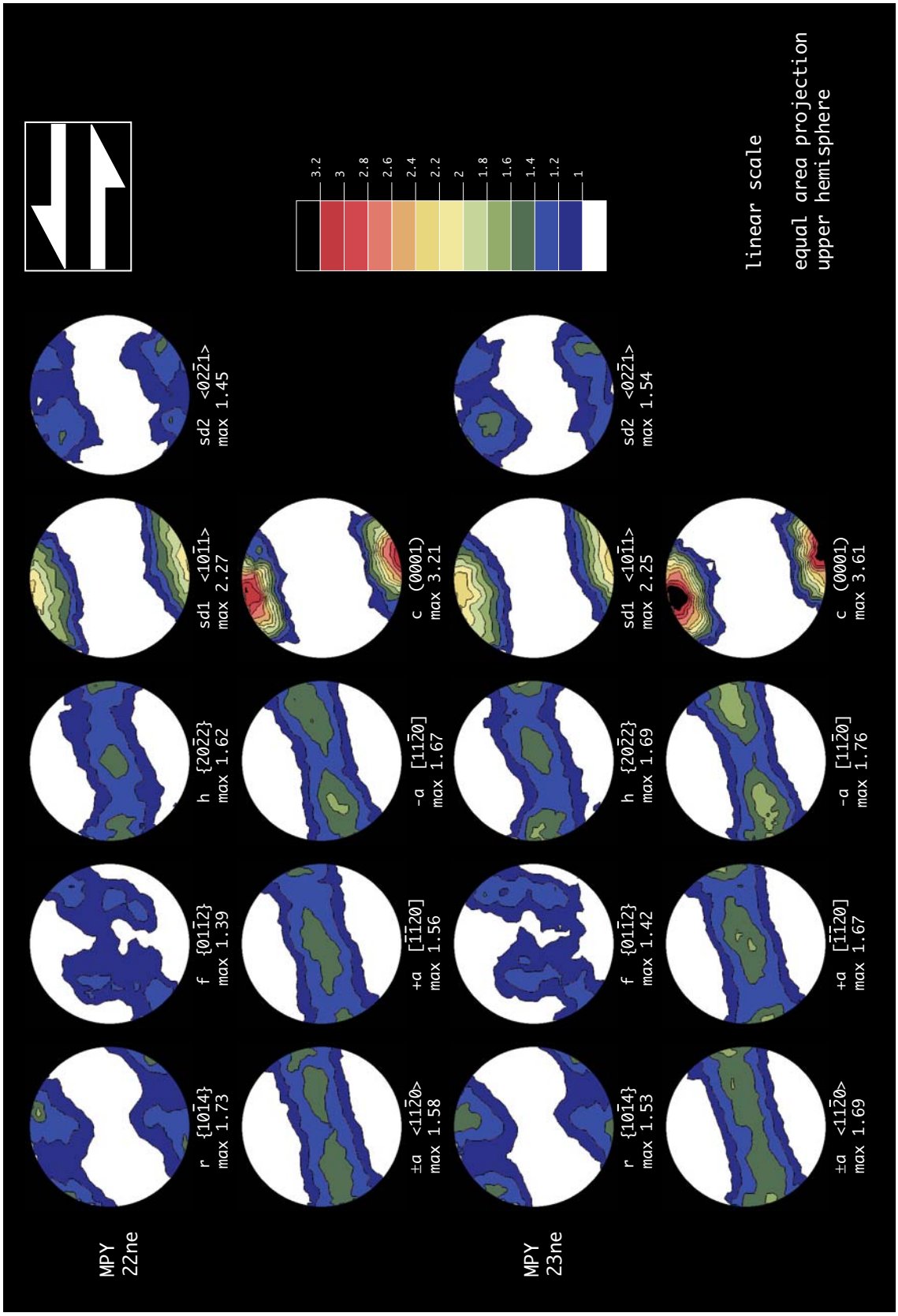


**Figure B20:** Crystallographic preferred orientation of samples MPY22ne and MPY23ne.

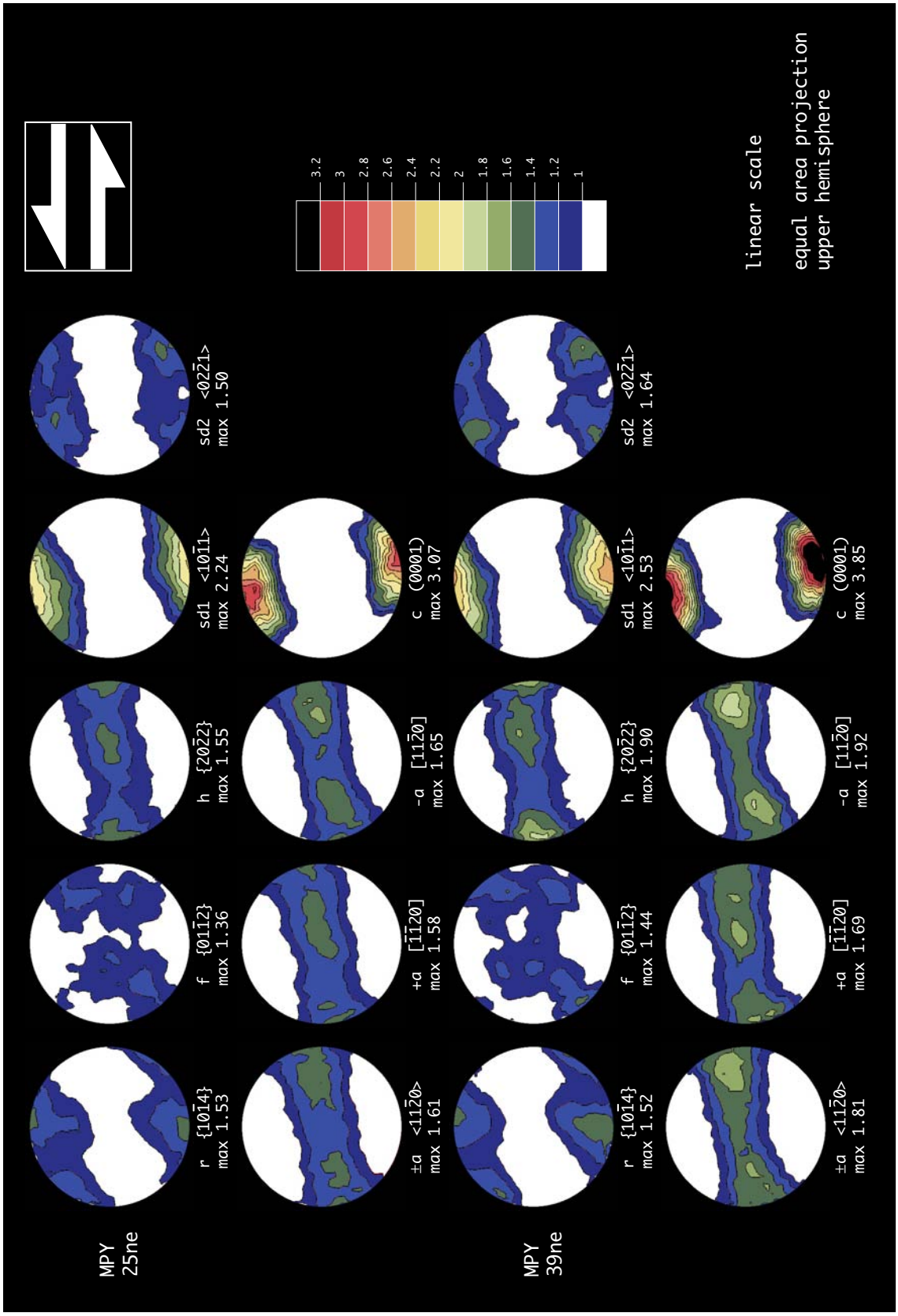


**Figure B21:** Crystallographic preferred orientation of samples MPY25ne and MPY39ne.

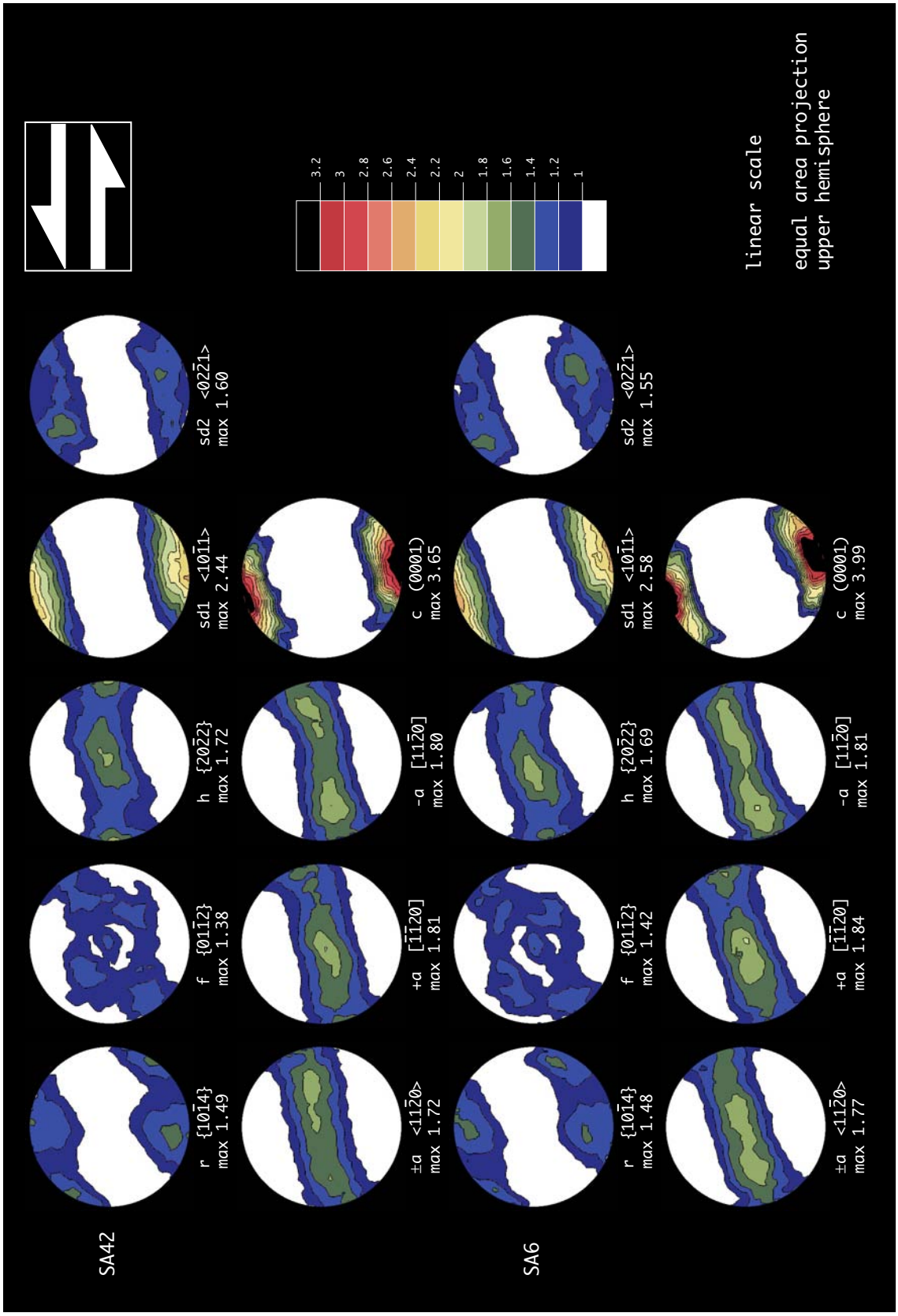


**Figure B22:** Crystallographic preferred orientation of samples SA42 and SA6.

## Appendix B.3.

In this section, the results of inverse pole figures calculations for the samples presented in appendix B.2 are given. These inverse pole figures are the ones defined in chapter 2, i.e. the foliation normal (Fo. N., i.e. Z sample direction), stretching lineation (St. Lin, i.e. X sample direction), intermediate direction (Int. Dir., i.e. Y sample direction), directions at 45° counter-clockwise (45° CCW) and 45° clockwise (45° CW) from the foliation normal, cα direction (see chapter 2) and normal to cα within the XZ plane (cα N), cβ direction (see chapter 2) and normal to cβ within the XZ plane (cβ N).

### Appendix B.3.1.

This section is dedicated to the samples series having accomodated a dominant component of coaxial strain (samples MPY19, MPYSA2n2, MPYSA12, MPY1sca2, MPY2 and MPY2b). A typical characteristic relative to the type of texture recorded in this case is the similarity between the inverse pole figures for both directions at 45° CW and CCW from Z (see figures B23 to B25). The reader is referred to chapter 2 for discussion.

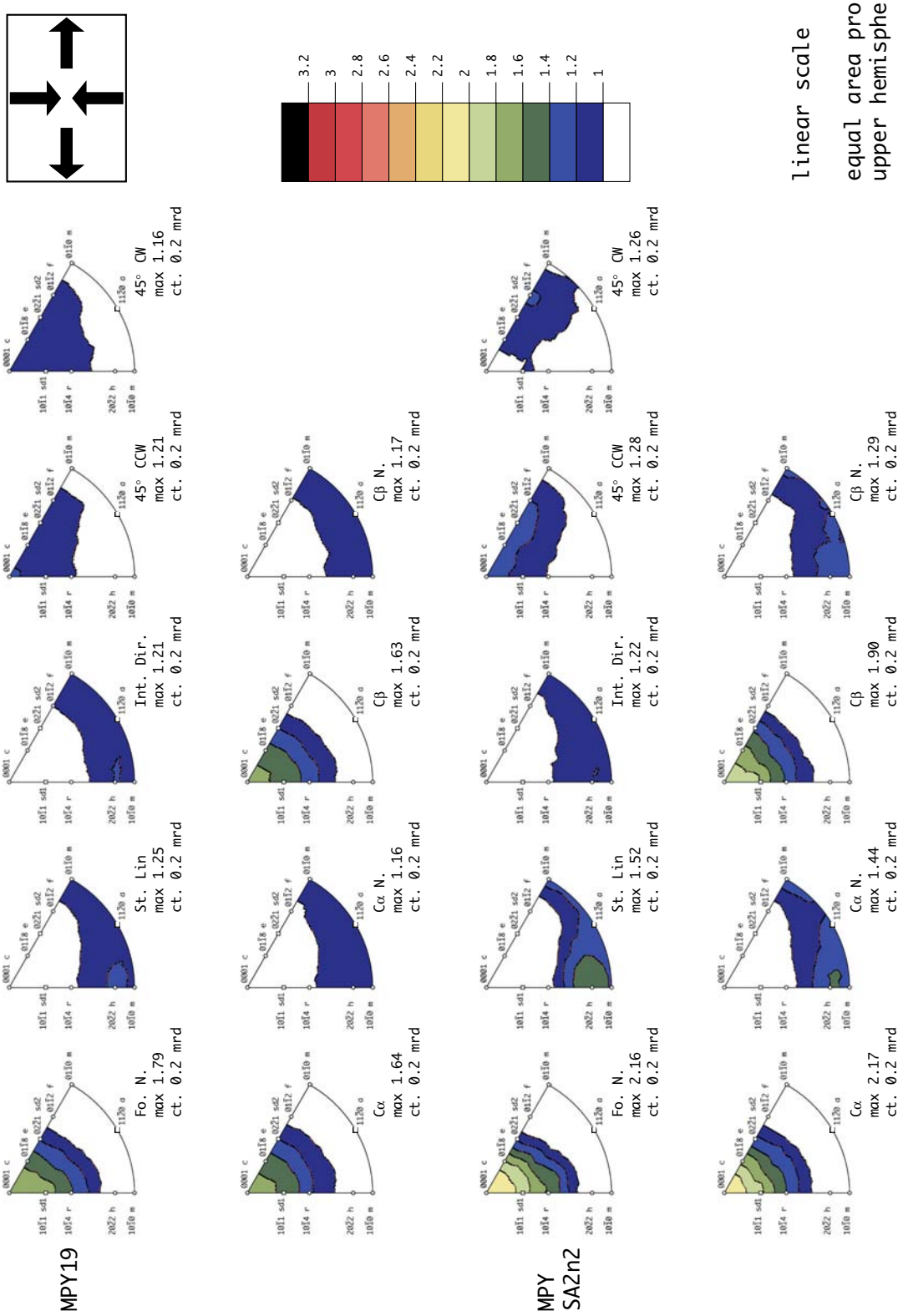


**Figure B23:** Inverse pole figures calculations for samples MPY19 and MPYSA2n2.

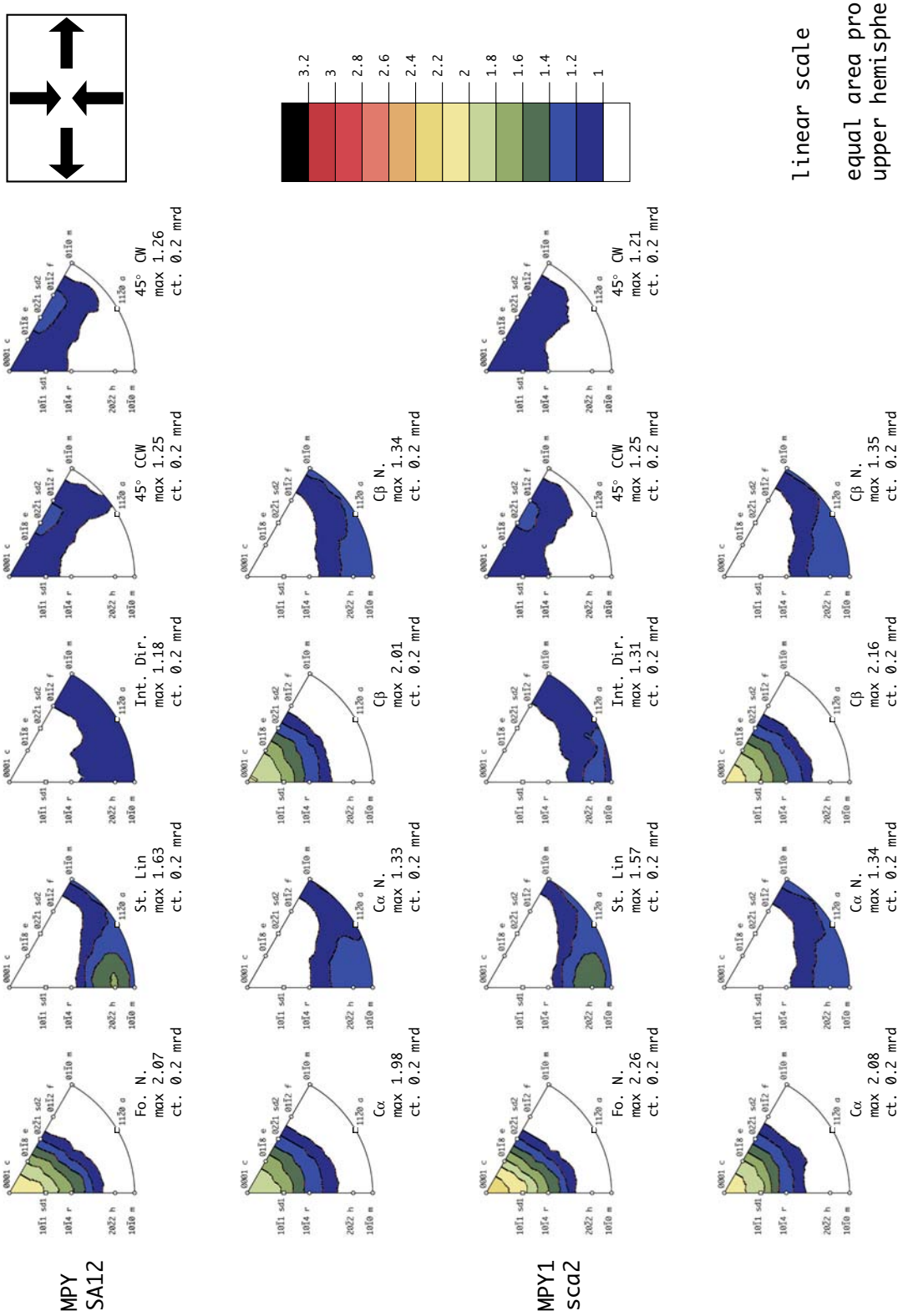


**Figure B24:** Inverse pole figures calculations for samples MPYSA12 and MPY1sca2.

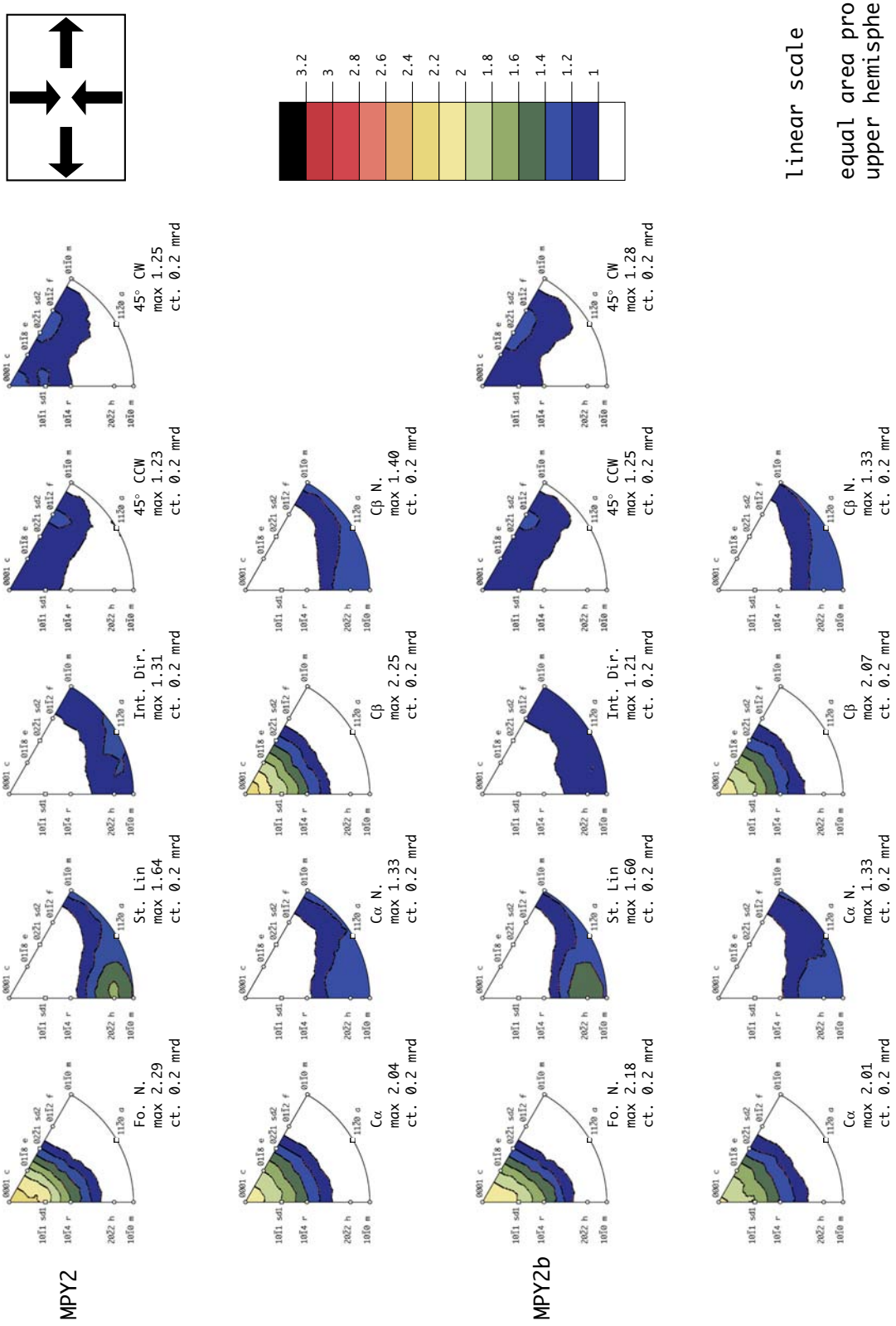


**Figure B25:** Inverse pole figures calculations for samples MPY2 and MPY2b.

**Appendix B.3.2.**

This appendix refers to samples having experienced a so-called intermediate strain regime. Note the non-similarity observed between both directions at 45° CW and CCW from Z (see figure B26). The reader is referred to chapter 2 for discussion.

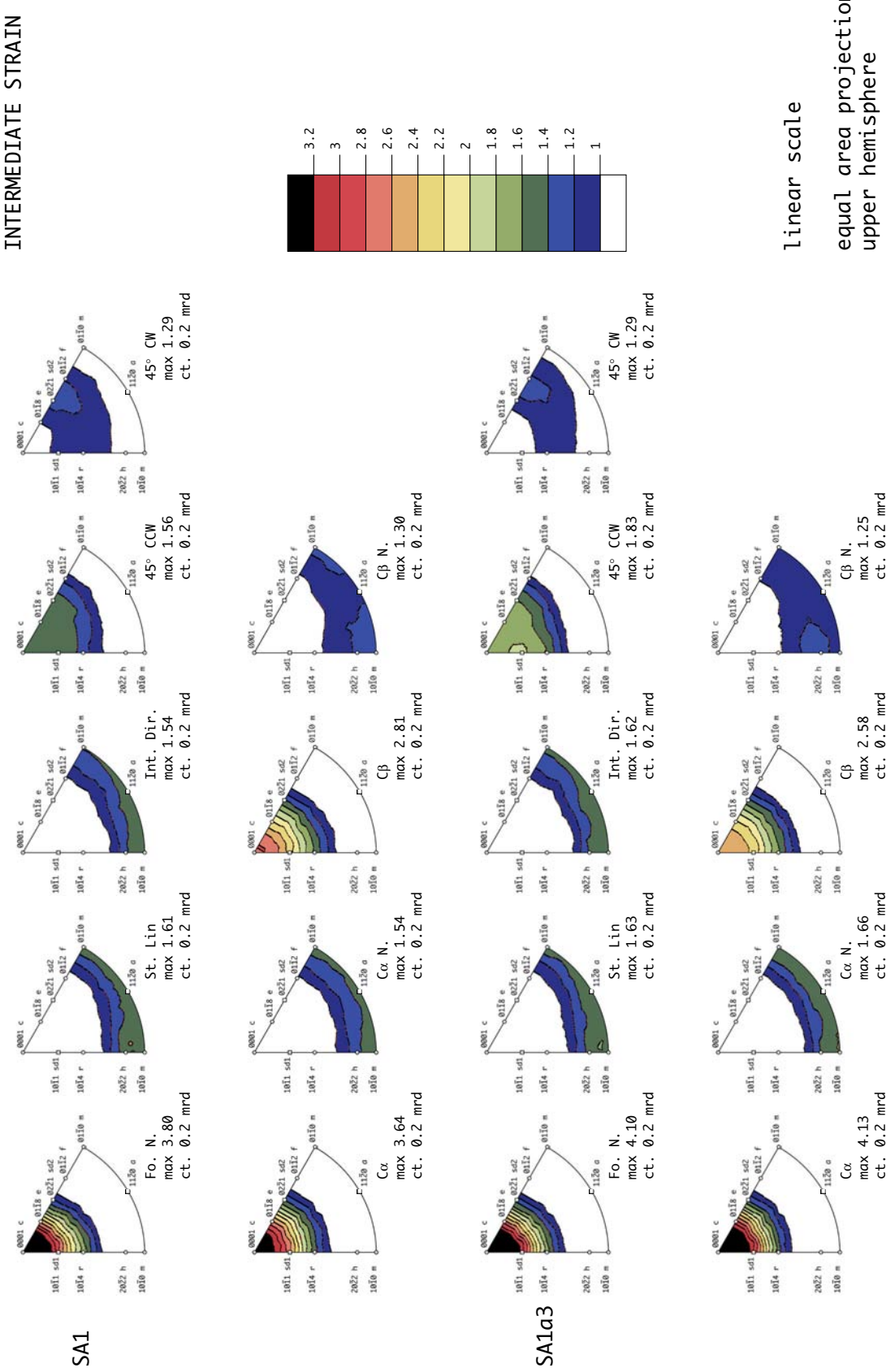


**Figure B26:** Inverse pole figures calculations for samples SA1 and SA1a3.

**Appendix B.3.3.**

Inverse pole figures calculations for samples having been deformed under conditions of non-coaxial dominated strain regime are presented. Note the strong signal concentration at *c* on the inverse pole figures for the cα direction and the girdle distribution recorded on the cαN diagrams (see figures B27 to B29). The reader is referred to chapter 2 for discussion.

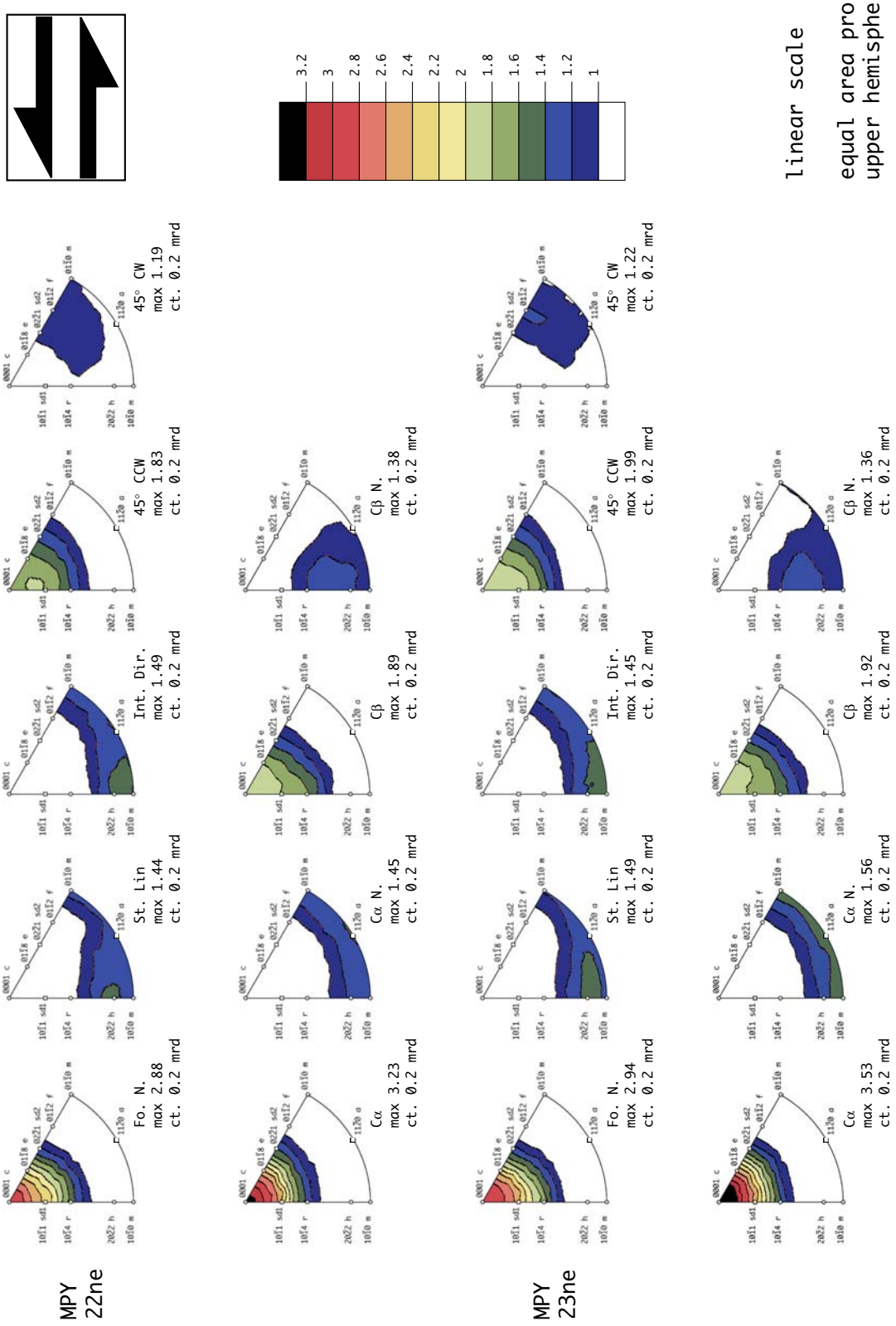


**Figure B27:** Inverse pole figures calculations for samples MPY22ne and MPY23ne.

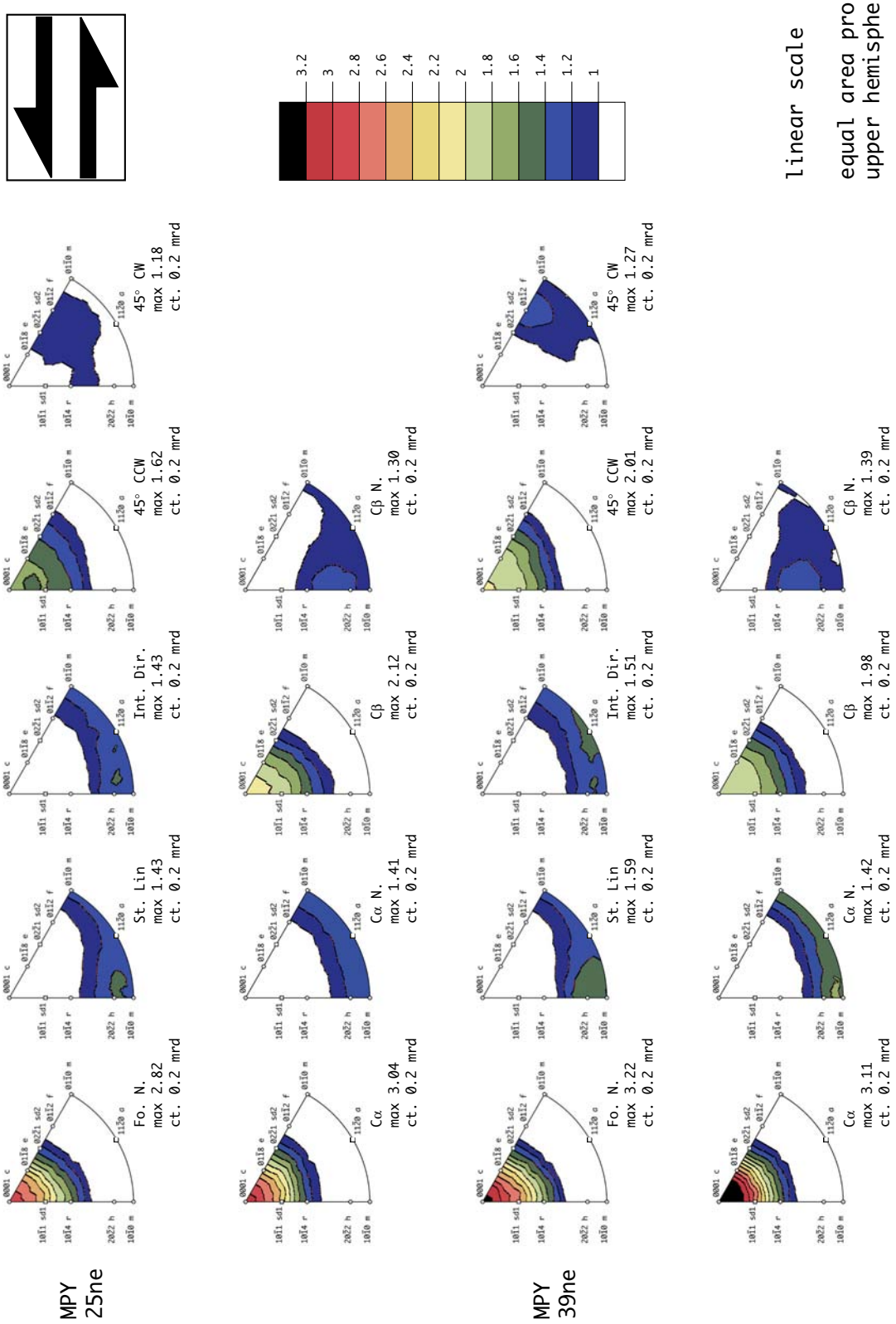


**Figure B28:** Inverse pole figures calculations for samples MPY25ne and MPY39ne.

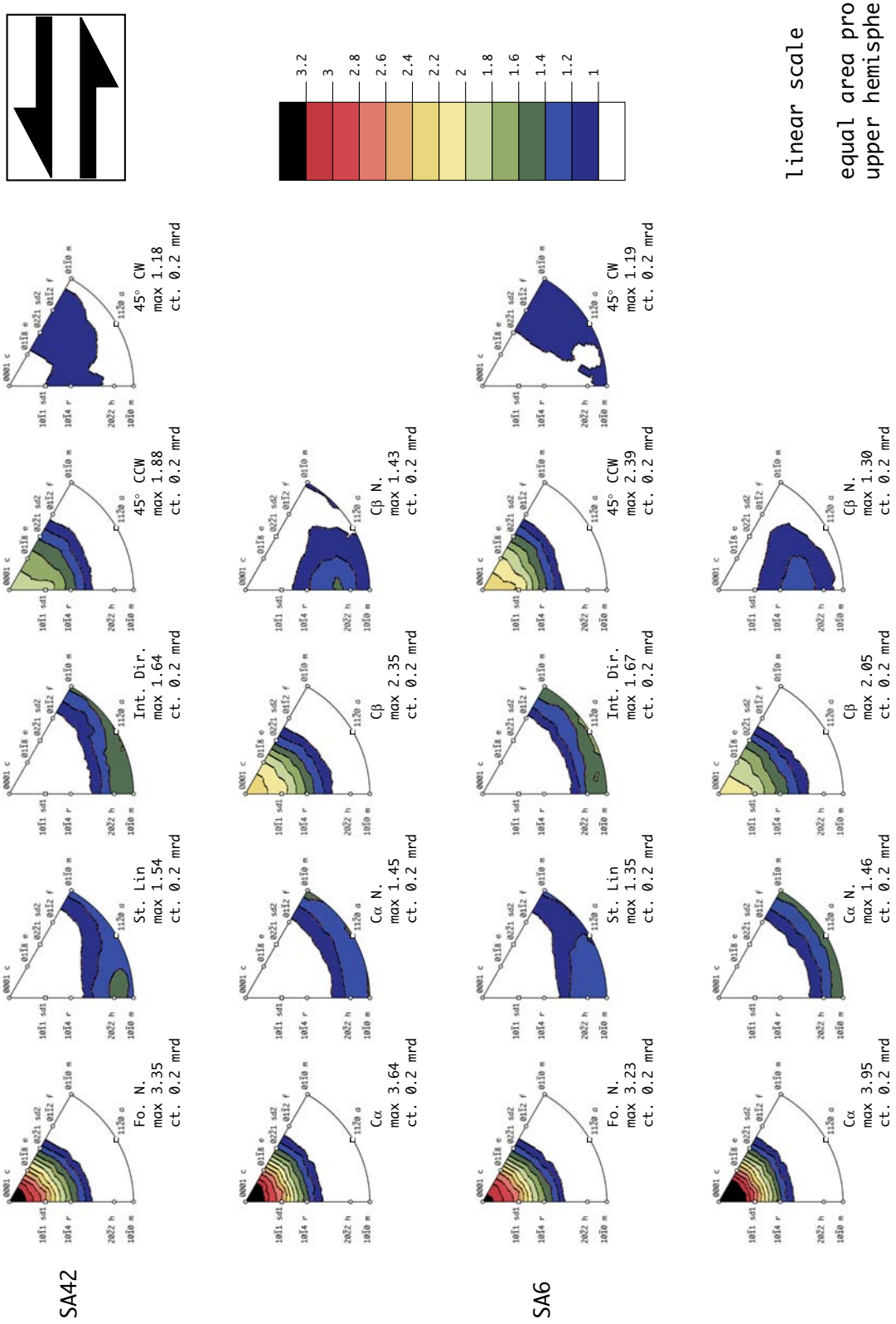


**Figure B29:** Inverse pole figures calculations for samples SA42 and SA6.

## Appendix B.4.

This appendix contains a Computer Integrated Polarization (CIP) (Panozzo Heilbronner and Pauli 1993, 1994) picture realized using an ultrathin section of about 2 micrometers thickness. The corresponding MPY2n2 sample is a calcite ultramylonite taken from the southern termination of the outcrop from locality 1. The reference frame has been chosen such that both macroscopic foliation and stretching lineation are horizontal. The pronounced horizontal SPO and the broad *c*-axis distribution around Z (see figure B30) suggest that this sample has been deformed under a coaxial dominated deformation path.

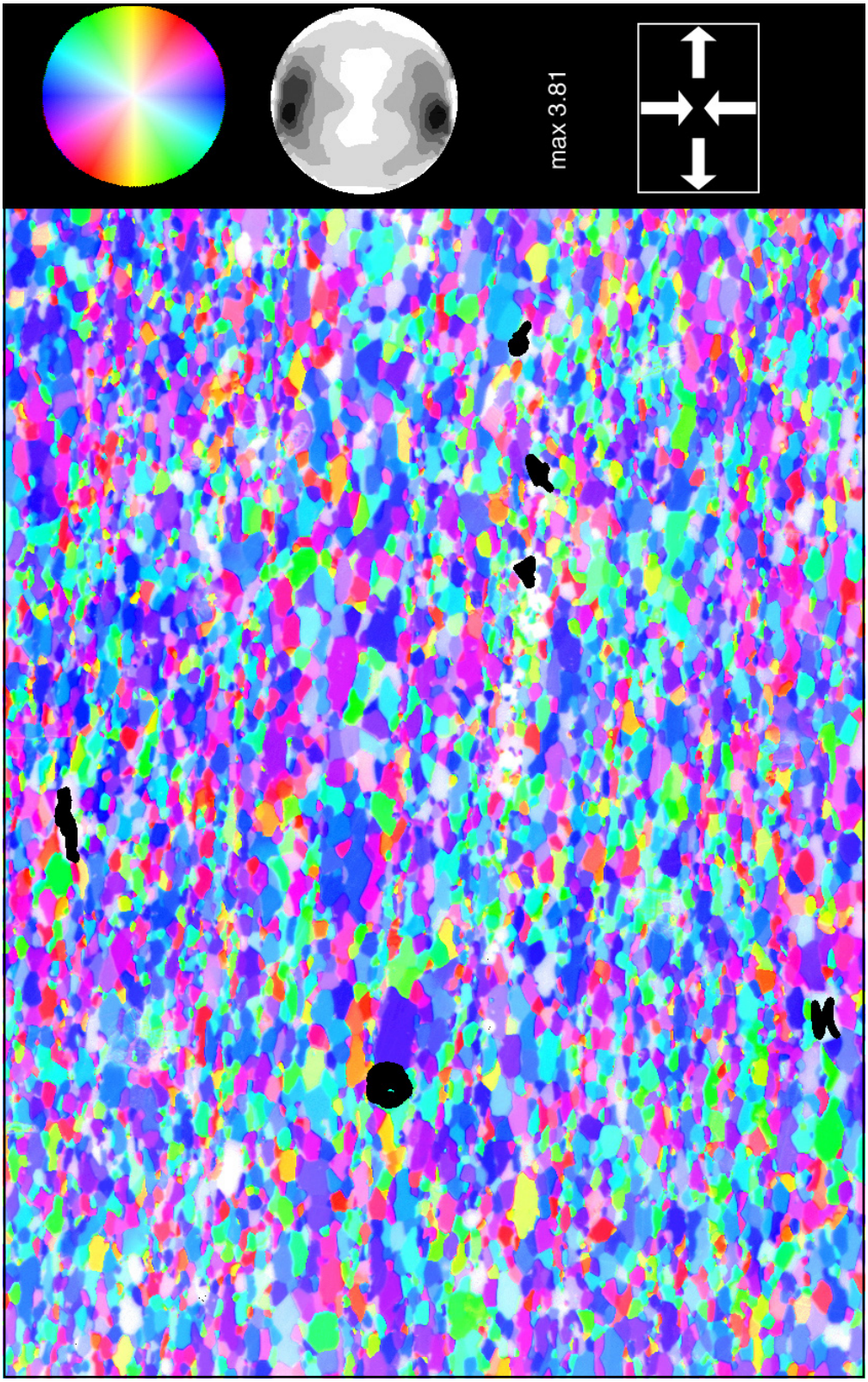


**Figure B30:** Computer Integrated Polarisation microscopy picture of sample MPY2n2

## Appendix B.5.

This appendix presents two computer programs used to convert the different files format produced by MENTEX (Schaeben, 1990) and BEARTEX (Wenk et al. 1998) iteration softwares. These two programs have been elaborated in collaboration with P. Dèzes from the Geological Institute of Basel University. They are running on any computer running a modern Unix operating system (Mac OSX, Linux...).

### Appendix B.5.1.

This first program, called “input_beartex.sh” is used to convert the measured pole figures data files calculated from MENTEX (Schaeben, 1990) software in an input file readable by the BEARTEX (Wenk et al. 1998) package.

The procedure needed to use the “input_beartex.sh” program is the following one:

- Step 1: create a folder containing both “input_beartex.sh” and the “cpf” file produced by the MENTEX software.
- Step 2: save the “cpf” file in a UNIX readable format (using BBEDIT editing software for example).
- Step 3: calculate the average values of the first four lines of raw data for each measured pole figures in the “cpf” file (values X, X2, X3 and X4, see below).
- Step 4: open the file “input_beartex.sh”. Type the name of the “cpf” and “xpa” files (lines 8 and 9 in file “input_beartex.sh”) and correct the values of X, X2, X3 and X4 (lines 12, 13, 14 and 15 in file “input_beartex.sh). Save the file.
- Step 5: open a terminal connection and type the path leading to the folder created in Step 1. Run the program using command “/input_beartex.sh”.
- Step 6: save the “xpa” output file in a DOS format. The file is now ready to be used as an input for the BEARTEX (Wenk et al. 1998) software.

```
#!/bin/bash


################################################
###    PARAMETRES A MODIFIER                 ##
###    !!!! ATTENTION AUX ESPACES !!!!!      ##
################################################
input="m13.cpf"
output="m13.xpa"
#inserer "#" entre position curseur 86 et 87 #######
titre="blably tra la la  desdfv                                        #"
x="  80"
x2=" 150"
x3=" 111"
#x4="1214"
################################################
###    PROGRAMME A PAS TOUCHER               ##
################################################
#
#premiere figure de pole
#
echo "$titre" > $output
echo "" >> $output
echo "" >> $output
echo "" >> $output
echo "" >> $output
echo "    4.990    4.990   17.064   90.000   90.000  120.000   9   1" >> $output
echo "  1  0  4  0.0 90.0  5.0  0.0360.0  5.0 1 1 1 2 3 100" >> $output
echo " $x$x$x$x$x$x$x$x$x$x$x$x$x$x$x$x$x$x$x$x" >> $output
echo " $x$x$x$x$x$x$x$x$x$x$x$x$x$x$x$x$x$x$x$x" >> $output
echo " $x$x$x$x$x$x$x$x$x$x$x$x$x$x$x$x$x$x$x$x" >> $output
echo " $x$x$x$x$x$x$x$x$x$x$x$x$x$x$x$x$x$x$x$x" >> $output
awk 'NR>=4 && NR<=75 {print "  "$0}' $input >> $output
echo "" >> $output
#
#deuxieme figure de pole
#
echo "$titre" >> $output
echo "" >> $output
echo "" >> $output
echo "" >> $output
echo "" >> $output
echo "    4.990    4.990   17.064   90.000   90.000  120.000   9   1" >> $output
echo "  1  1  0  0.0 90.0  5.0  0.0360.0  5.0 1 1 1 2 3 100" >> $output
echo " $x2$x2$x2$x2$x2$x2$x2$x2$x2$x2$x2$x2$x2$x2$x2$x2$x2$x2$x2" >> $output
echo " $x2$x2$x2$x2$x2$x2$x2$x2$x2$x2$x2$x2$x2$x2$x2$x2$x2$x2$x2" >> $output
```

```
echo " $x2$x2$x2$x2$x2$x2$x2$x2$x2$x2$x2$x2$x2$x2$x2$x2$x2"  >> $output
echo " $x2$x2$x2$x2$x2$x2$x2$x2$x2$x2$x2$x2$x2$x2$x2$x2$x2"  >> $output
awk 'NR>=229 && NR<=300 {print " "$0}' $input >> $output
echo ""  >> $output
#
#troisieme figure de pole
#
echo "$titre" >> $output
echo ""  >> $output
echo ""  >> $output
echo ""  >> $output
echo "    4.990    4.990    17.064    90.000    90.000   120.000    9    1" >> $output
echo "   2  0  2  0.0 90.0  5.0  0.0360.0  5.0 1 1 1 2 3 100"  >> $output
echo " $x3$x3$x3$x3$x3$x3$x3$x3$x3$x3$x3$x3$x3$x3$x3$x3$x3$x3"  >> $output
echo " $x3$x3$x3$x3$x3$x3$x3$x3$x3$x3$x3$x3$x3$x3$x3$x3$x3$x3"  >> $output
echo " $x3$x3$x3$x3$x3$x3$x3$x3$x3$x3$x3$x3$x3$x3$x3$x3$x3$x3"  >> $output
echo " $x3$x3$x3$x3$x3$x3$x3$x3$x3$x3$x3$x3$x3$x3$x3$x3$x3$x3"  >> $output
awk 'NR>=454 && NR<=525 {print " "$0}' $input >> $output
echo ""  >> $output
#
##quatrieme figure de pole
##
#echo "$titre" >> $output
#echo ""  >> $output
#echo ""  >> $output
#echo ""  >> $output
#echo ""  >> $output
#echo "    4.990    4.990    17.064    90.000    90.000   120.000    9    1" >> $output
#echo "   2  0  2  0.0 90.0  5.0  0.0360.0  5.0 1 1 1 2 3 100"  >> $output
#echo " $x4$x4$x4$x4$x4$x4$x4$x4$x4$x4$x4$x4$x4$x4$x4$x4$x4$x4"  >> $output
#echo " $x4$x4$x4$x4$x4$x4$x4$x4$x4$x4$x4$x4$x4$x4$x4$x4$x4$x4"  >> $output
#echo " $x4$x4$x4$x4$x4$x4$x4$x4$x4$x4$x4$x4$x4$x4$x4$x4$x4$x4"  >> $output
#echo " $x4$x4$x4$x4$x4$x4$x4$x4$x4$x4$x4$x4$x4$x4$x4$x4$x4$x4"  >> $output
#awk 'NR>=679 && NR<=750 {print " "$0}' $input >> $output
#echo ""  >> $output
```

**Appendix B.5.2.**

This second program, called “invpolfig.sh” is needed to convert the inverse pole figures files produced by the BEARTEX (Wenk et al. 1998) software (“xio” files) in order to be readable by the “INVPIMA” plotting program used by the MENTEX (Schaeben, 1990) software.

The running procedure is the following:

- Step 1: create a folder containing both “invpolfig.sh” and “xio” files produced by the BEARTEX software. The maximum number of inverse pole figures to be used is of 7.
- Step 2: save the “xio” file in a UNIX readable format.
- Step3: open a terminal connection and type the path leading to the folder created in Step 1. Run the program using command “/invpolfig.sh”.
- Step 4: save the “cpf” output file in a MAC readable format. The file is now ready to be used as an input file for the INVPIMA software.

```
#!/bin/bash

#*********************************************************************
**********************************************************************
******
#
# PLACE THIS SCRIPT IN THE SAME FOLDER AS THE FILES TO CONVERT
# WARNING!!! file names must not contain any white space (this is not good.txt but
this_is_ok.txt)
# This script has to be started by cd to the directory where the files to convert are lo-
cated ( cd /home/user/files_to_convert)
# Then just type: sh reformat.sh
#
#*********************************************************************
**********************************************************************
******

# create variable input_file by getting a list off all the names of the files to be processed
# but remove files ending with ".sh" (the script files) from the list

input_file=$(ls | sed 's/[A-Za-z0-9\._-][[A-Za-z0-9\._-]*.sh//')

# Here we make a ***set  $var; while (($# > 0)); do; shift; done*** loop to process the
name of each input_file one by one
# in order to create an output file that has ".out" appended to the name of each input_
file (called with $1.out")
# the "set" command takes the output of the input_file variable command and assigns
the output to positional parameters
# file_name1, file_name2, ....; see LINUX shells by example page 442

set $input_file
while (($# > 0)); do

        tmp="temp_file.txt"
        output_file="$1.cpf"

# START OF PIPE

# To omit the "\n" in the first {printf} function is the trick to get two successive records
into a single record
# $1 is for the name of each input file as defined from the above loop
# we select only the lines that have 18 and 7 fields "NF == 18" and "NF == 7"

        awk ' NF == 18 { printf ("%s", $0) }
                NF == 7 {printf ("%s\n", $0) }' $1 |
```

```
# remove the white space(s) at the begginning of each record
# replace the triple white space created by the above joining of 2 records into one
# delete empty lines

        sed 's/^ *//g' |
        sed 's/  / /g' |
        sed '/^$/d' > $tmp

# END OF PIPE (we now use a tmp file that will be deleted at the end of the loop)

# we want to omit the first record of data from each papragraph (original 2 first re-
cords), therefore we want records > 1, 20, 39 ... and not >=
# with BEGIN, we can recreate headers at the top of each set of records (we eliminated
headers previously by using NF == 18 && NF == 17)
# printf allows us to format the white spaces between each field (%3s means "--1" or
"-12" or "123") note the whitespace before the first %ns

        awk 'BEGIN{print ("PART1\n100  D3    5.00 5.0090.00    0    0\n 1000 0.20   10
0     EXPERIMENTAL POLE FIGURE")}
        NR > 1 && NR <= 19 {
        printf (" %3s %3s %3s %3s %3s %3s %3s %3s %3s %3s %3s %3s %3s %3s %3s
%3s %3s %3s %3s\n", $1, $2, $3, $4, $5, $6, $7, $8, $9, $10, $11, $12, $13, $14,
$15, $16, $17, $18)
        printf (" %3s %3s %3s %3s %3s %3s %3s %3s %3s %3s %3s %3s %3s %3s %3s
%3s %3s %3s %3s\n", $18, $17, $16, $15, $14, $13, $12, $11, $10, $9, $8, $7, $6,
$5, $4, $3, $2, $1)
        printf (" %3s %3s %3s %3s %3s %3s %3s %3s %3s %3s %3s %3s %3s %3s %3s
%3s %3s %3s %3s\n", $13, $14, $15, $16, $17, $18, $19, $20, $21, $22, $23, $24,
$1, $2, $3, $4, $5, $6)
        printf (" %3s %3s %3s %3s %3s %3s %3s %3s %3s %3s %3s %3s %3s %3s %3s
%3s %3s %3s %3s\n", $6, $5, $4, $3, $2, $1, $24, $23, $22, $21, $20, $19, $18,   $17,
$16, $15, $14, $13)
        }' $tmp > $output_file


        awk 'BEGIN{print ("PART2\n010  D3    5.00 5.0090.00    0    0\n 1000 0.20   10
0     EXPERIMENTAL POLE FIGURE")}
        NR > 20 && NR <= 38 {
        printf (" %3s %3s %3s %3s %3s %3s %3s %3s %3s %3s %3s %3s %3s %3s %3s
%3s %3s %3s %3s\n", $1, $2, $3, $4, $5, $6, $7, $8, $9, $10, $11, $12, $13, $14,
$15, $16, $17, $18)
        printf (" %3s %3s %3s %3s %3s %3s %3s %3s %3s %3s %3s %3s %3s %3s %3s
%3s %3s %3s %3s\n", $18, $17, $16, $15, $14, $13, $12, $11, $10, $9, $8, $7, $6,
$5, $4, $3, $2, $1)
        printf (" %3s %3s %3s %3s %3s %3s %3s %3s %3s %3s %3s %3s %3s %3s %3s
%3s %3s %3s %3s\n", $13, $14, $15, $16, $17, $18, $19, $20, $21, $22, $23, $24,
```

```
$1, $2, $3, $4, $5, $6)
        printf (" %3s %3s %3s %3s %3s %3s %3s %3s %3s %3s %3s %3s %3s %3s %3s
%3s %3s %3s %3s\n", $6, $5, $4, $3, $2, $1, $24, $23, $22, $21, $20, $19, $18,   $17,
$16, $15, $14, $13)
        }' $tmp >> $output_file


        awk 'BEGIN{print ("PART3\n001  D3    5.00 5.0090.00    0    0\n 1000 0.20   10
0     EXPERIMENTAL POLE FIGURE")}
        NR > 39 && NR <= 57 {
        printf (" %3s %3s %3s %3s %3s %3s %3s %3s %3s %3s %3s %3s %3s %3s %3s
%3s %3s %3s %3s\n", $1, $2, $3, $4, $5, $6, $7, $8, $9, $10, $11, $12, $13, $14,
$15, $16, $17, $18)
        printf (" %3s %3s %3s %3s %3s %3s %3s %3s %3s %3s %3s %3s %3s %3s %3s
%3s %3s %3s %3s\n", $18, $17, $16, $15, $14, $13, $12, $11, $10, $9, $8, $7, $6,
$5, $4, $3, $2, $1)
        printf (" %3s %3s %3s %3s %3s %3s %3s %3s %3s %3s %3s %3s %3s %3s %3s
%3s %3s %3s %3s\n", $13, $14, $15, $16, $17, $18, $19, $20, $21, $22, $23, $24,
$1, $2, $3, $4, $5, $6)
        printf (" %3s %3s %3s %3s %3s %3s %3s %3s %3s %3s %3s %3s %3s %3s %3s
%3s %3s %3s %3s\n", $6, $5, $4, $3, $2, $1, $24, $23, $22, $21, $20, $19, $18,   $17,
$16, $15, $14, $13)
        }' $tmp >> $output_file


        awk 'BEGIN{print ("PART4\n110  D3    5.00 5.0090.00    0    0\n 1000 0.20   10
0     EXPERIMENTAL POLE FIGURE")}
        NR > 58 && NR <= 76 {
        printf (" %3s %3s %3s %3s %3s %3s %3s %3s %3s %3s %3s %3s %3s %3s %3s
%3s %3s %3s %3s\n", $1, $2, $3, $4, $5, $6, $7, $8, $9, $10, $11, $12, $13, $14,
$15, $16, $17, $18)
        printf (" %3s %3s %3s %3s %3s %3s %3s %3s %3s %3s %3s %3s %3s %3s %3s
%3s %3s %3s %3s\n", $18, $17, $16, $15, $14, $13, $12, $11, $10, $9, $8, $7, $6,
$5, $4, $3, $2, $1)
        printf (" %3s %3s %3s %3s %3s %3s %3s %3s %3s %3s %3s %3s %3s %3s %3s
%3s %3s %3s %3s\n", $13, $14, $15, $16, $17, $18, $19, $20, $21, $22, $23, $24,
$1, $2, $3, $4, $5, $6)
        printf (" %3s %3s %3s %3s %3s %3s %3s %3s %3s %3s %3s %3s %3s %3s %3s
%3s %3s %3s %3s\n", $6, $5, $4, $3, $2, $1, $24, $23, $22, $21, $20, $19, $18,   $17,
$16, $15, $14, $13)
        }' $tmp >> $output_file

        awk 'BEGIN{print ("PART5\nm110  D3   5.00 5.0090.00    0    0\n 1000 0.20
10   0     EXPERIMENTAL POLE FIGURE")}
        NR > 77 && NR <= 95 {
        printf (" %3s %3s %3s %3s %3s %3s %3s %3s %3s %3s %3s %3s %3s %3s %3s
```

```
%3s %3s %3s %3s\n", $1, $2, $3, $4, $5, $6, $7, $8, $9, $10, $11, $12, $13, $14,
$15, $16, $17, $18)
        printf (" %3s %3s %3s %3s %3s %3s %3s %3s %3s %3s %3s %3s %3s %3s %3s
%3s %3s %3s %3s %3s\n", $18, $17, $16, $15, $14, $13, $12, $11, $10, $9, $8, $7, $6,
$5, $4, $3, $2, $1)
        printf (" %3s %3s %3s %3s %3s %3s %3s %3s %3s %3s %3s %3s %3s %3s %3s
%3s %3s %3s %3s %3s\n", $13, $14, $15, $16, $17, $18, $19, $20, $21, $22, $23, $24,
$1, $2, $3, $4, $5, $6)
        printf (" %3s %3s %3s %3s %3s %3s %3s %3s %3s %3s %3s %3s %3s %3s %3s
%3s %3s %3s %3s %3s\n", $6, $5, $4, $3, $2, $1, $24, $23, $22, $21, $20, $19, $18,   $17,
$16, $15, $14, $13)
        }' $tmp >> $output_file

        awk 'BEGIN{print ("PART6\nm1    D3   5.00 5.0090.00    0    0\n 1000 0.20   10
0     EXPERIMENTAL POLE FIGURE")}
        NR > 96 && NR <= 114 {
        printf (" %3s %3s %3s %3s %3s %3s %3s %3s %3s %3s %3s %3s %3s %3s %3s
%3s %3s %3s %3s %3s\n", $1, $2, $3, $4, $5, $6, $7, $8, $9, $10, $11, $12, $13, $14,
$15, $16, $17, $18)
        printf (" %3s %3s %3s %3s %3s %3s %3s %3s %3s %3s %3s %3s %3s %3s %3s
%3s %3s %3s %3s %3s\n", $18, $17, $16, $15, $14, $13, $12, $11, $10, $9, $8, $7, $6,
$5, $4, $3, $2, $1)
        printf (" %3s %3s %3s %3s %3s %3s %3s %3s %3s %3s %3s %3s %3s %3s %3s
%3s %3s %3s %3s %3s\n", $13, $14, $15, $16, $17, $18, $19, $20, $21, $22, $23, $24,
$1, $2, $3, $4, $5, $6)
        printf (" %3s %3s %3s %3s %3s %3s %3s %3s %3s %3s %3s %3s %3s %3s %3s
%3s %3s %3s %3s %3s\n", $6, $5, $4, $3, $2, $1, $24, $23, $22, $21, $20, $19, $18,   $17,
$16, $15, $14, $13)
        }' $tmp >> $output_file

        awk 'BEGIN{print ("PART7\nm2    D3   5.00 5.0090.00    0    0\n 1000 0.20   10
0     EXPERIMENTAL POLE FIGURE")}
        NR > 115 && NR <= 133 {
        printf (" %3s %3s %3s %3s %3s %3s %3s %3s %3s %3s %3s %3s %3s %3s %3s
%3s %3s %3s %3s %3s\n", $1, $2, $3, $4, $5, $6, $7, $8, $9, $10, $11, $12, $13, $14,
$15, $16, $17, $18)
        printf (" %3s %3s %3s %3s %3s %3s %3s %3s %3s %3s %3s %3s %3s %3s %3s
%3s %3s %3s %3s %3s\n", $18, $17, $16, $15, $14, $13, $12, $11, $10, $9, $8, $7, $6,
$5, $4, $3, $2, $1)
        printf (" %3s %3s %3s %3s %3s %3s %3s %3s %3s %3s %3s %3s %3s %3s %3s
%3s %3s %3s %3s %3s\n", $13, $14, $15, $16, $17, $18, $19, $20, $21, $22, $23, $24,
$1, $2, $3, $4, $5, $6)
        printf (" %3s %3s %3s %3s %3s %3s %3s %3s %3s %3s %3s %3s %3s %3s %3s
%3s %3s %3s %3s %3s\n", $6, $5, $4, $3, $2, $1, $24, $23, $22, $21, $20, $19, $18,   $17,
$16, $15, $14, $13)
        }' $tmp >> $output_file
```

```
# get rid of the tmp file

        rm $tmp

# the shift command shifts the parameter list (the filenames) once to the left until it is
empty and the loop ends

        shift

done

#awk 'sum=NR++; END {print sum}'
```

## Microstructure analysis.

### Appendix B.6.

The purpose of the present series of appendixes is to present the results of grain size analysis (GSA) of different sets of ultramylonites samples deformed under conditions of coaxial-dominated (Appendix B.6.1, 10 samples, see figures B31 and B32), intermediate (Appendix B.6.2, 7 samples, see figures B33 and B34) and non-coaxial dominated (Appendix B.6.3, 6 samples, see figures B35) strain. The average number of particles analyzed for each sample is of about 3700. The results are given using histograms of volume density (v(R), red columns) and number density (h(R), blue columns) distribution.

As announced in chapter 2, only minor variations in grain sizes are noticed between the different sets of samples. All volumetric distributions present a uni-modal distribution with a mode value ranging between 4 and 10 micrometers.

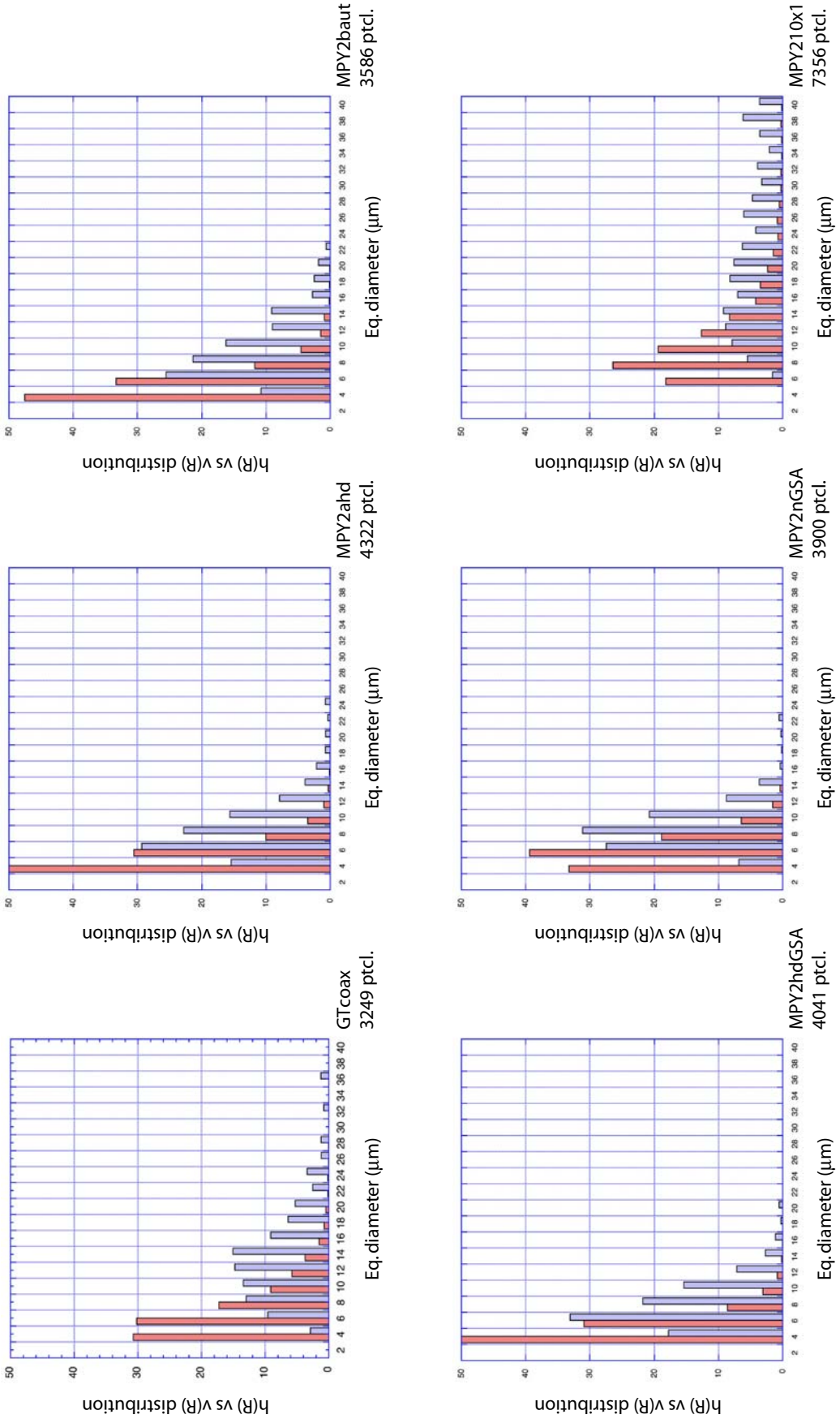


**Figure B31:** Grain size analysis of samples GTcoax bis MPY210x1.

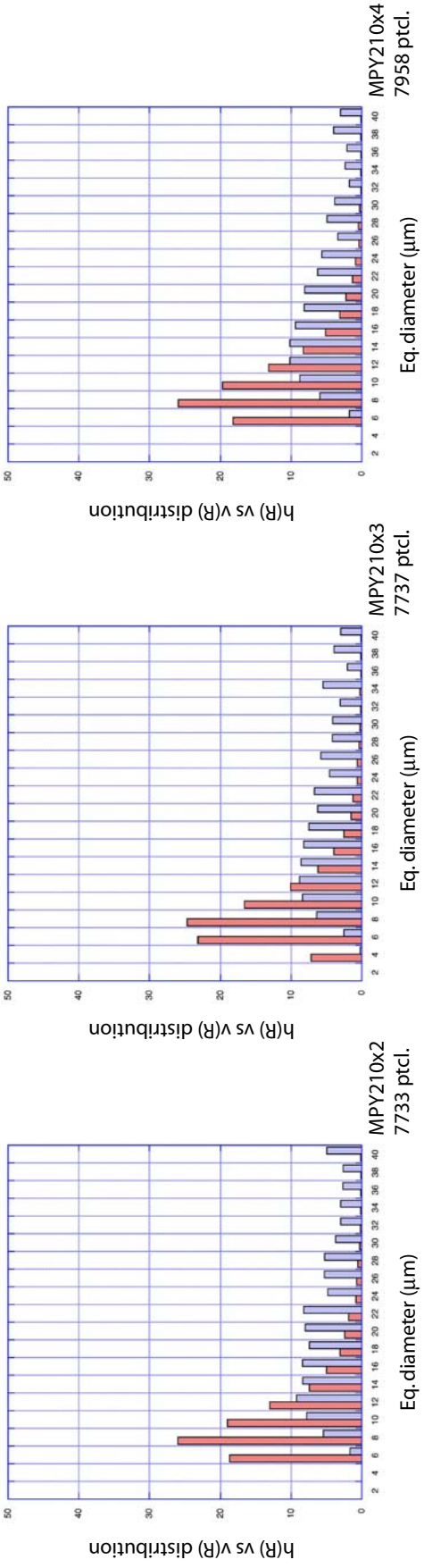


**Figure B32:** Grain size analysis of samples MPY210x2 bis MPY240x1.

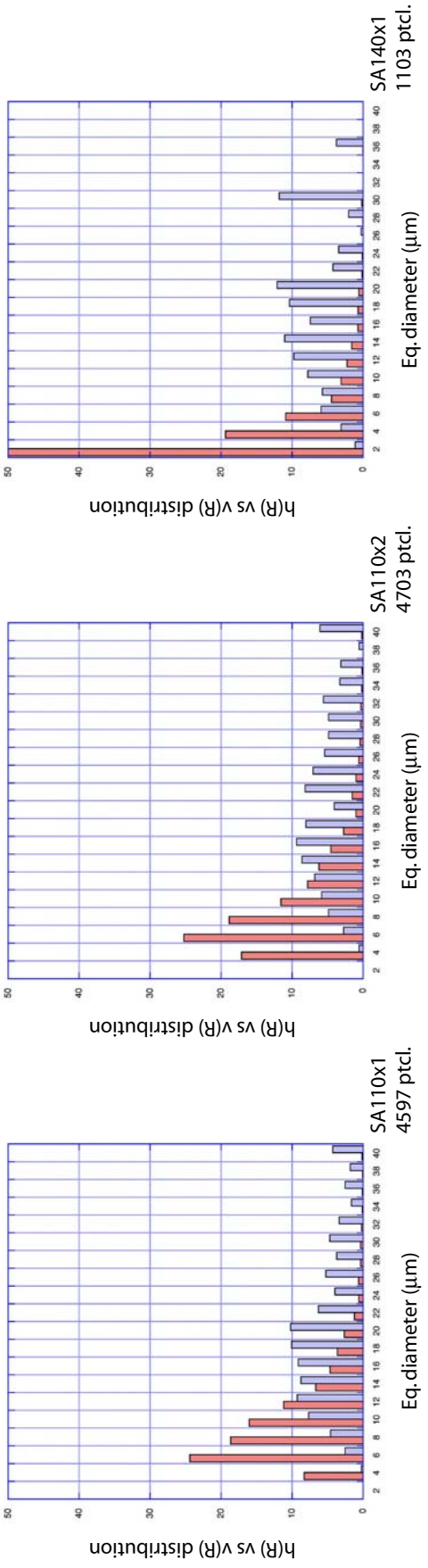


**Figure B33:** Grain size analysis of samples SA110x1 bis SA140x2.

**Figure B34:** Grain size analysis of sample SA420x2hd.

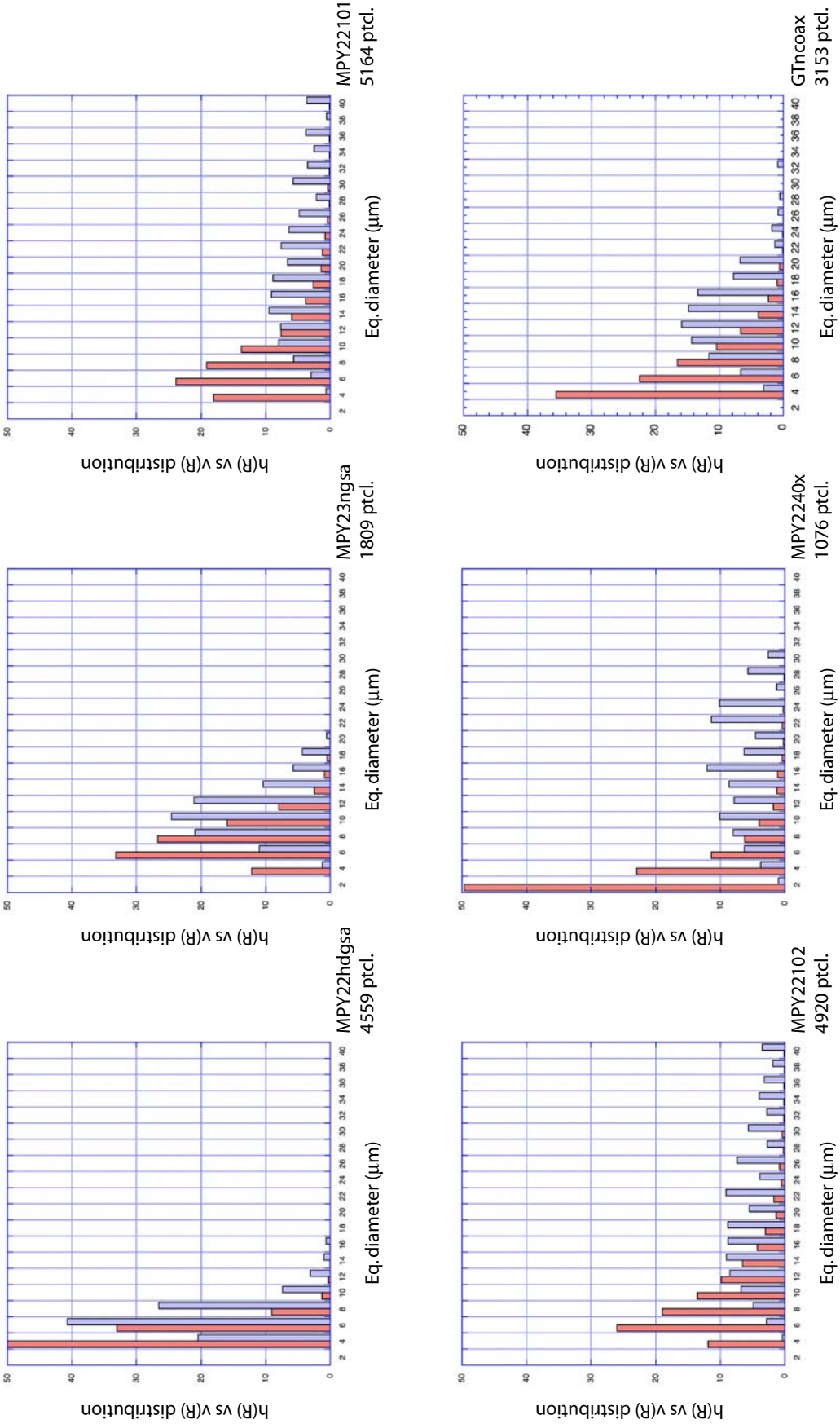


**Figure B35:** Grain size analysis of samples MPY22hdgsa bis GTncoax.

## Appendix B.7.

This appendix contains a series of GSPO analysis in XZ sections from ultramylonites samples deformed under conditions of coaxial-dominated (Appendix B.7.1, 4 samples, see figures B36 and B37), intermediate (Appendix B.7.2, 2 samples, see figure B38) and non-coaxial dominated (Appendix B.7.3, 4 samples, see figures B39 and B40) strain. For each sample, the grain boundary map is given together with PAROR and SURFOR (Panozzo, 1983, 1984) diagrams. The average number of particles analyzed is each case is of about 760.

Samples having suffered a dominant componant of coaxial strain show a strong horizontal GSPO. An average oblique GSPO at about 25° and 15° in the sense of shear is noticed for samples deformed under intermediate and non-coaxial dominated strain, respectively.

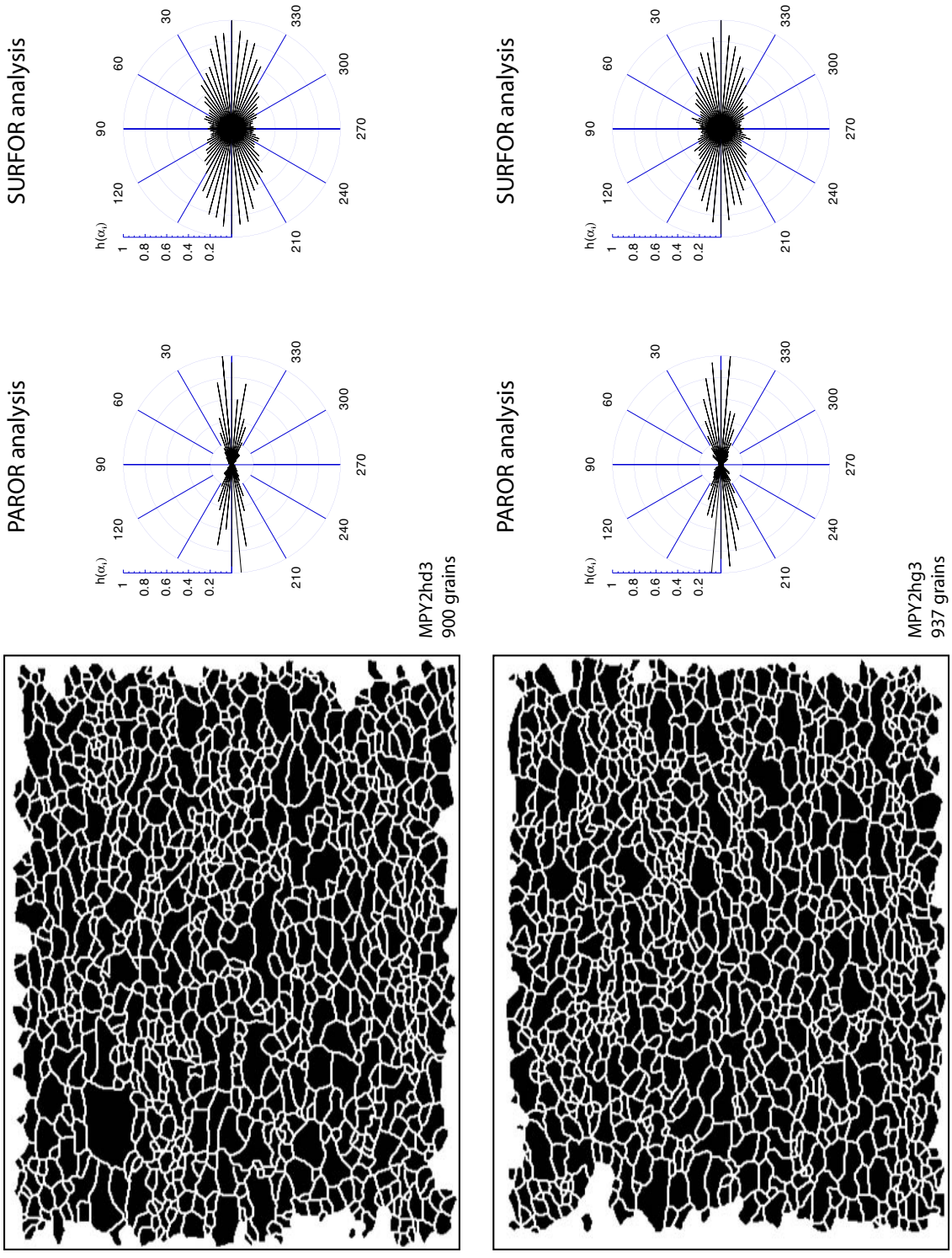


**Figure B36:** Grain shape preferred orientation analysis in XZ sections of samples MPY2bd3 and MPY2bg3.

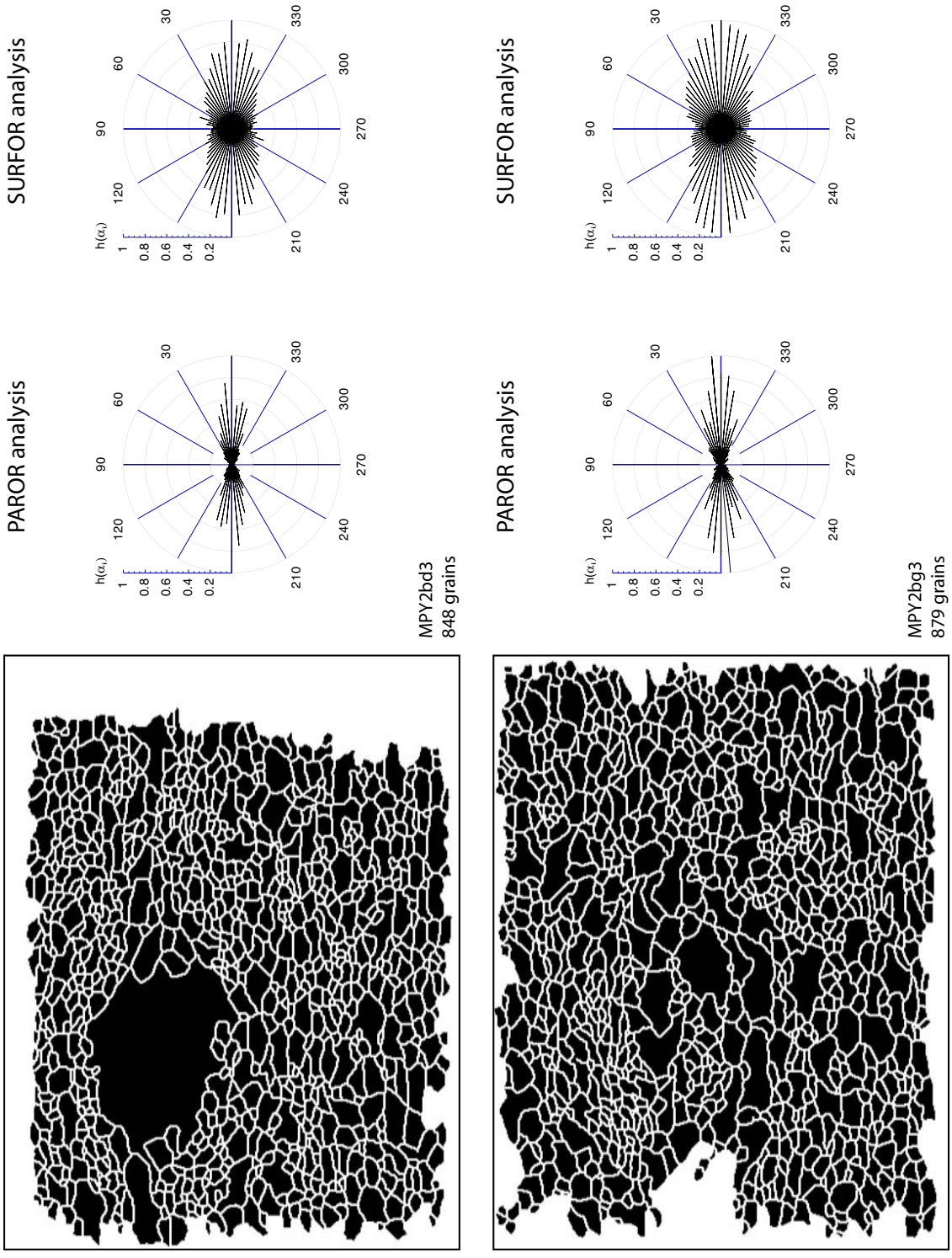


**Figure B37:** Grain shape preferred orientation analysis in XZ sections of samples MPY2hd3 and MPY2hg3.

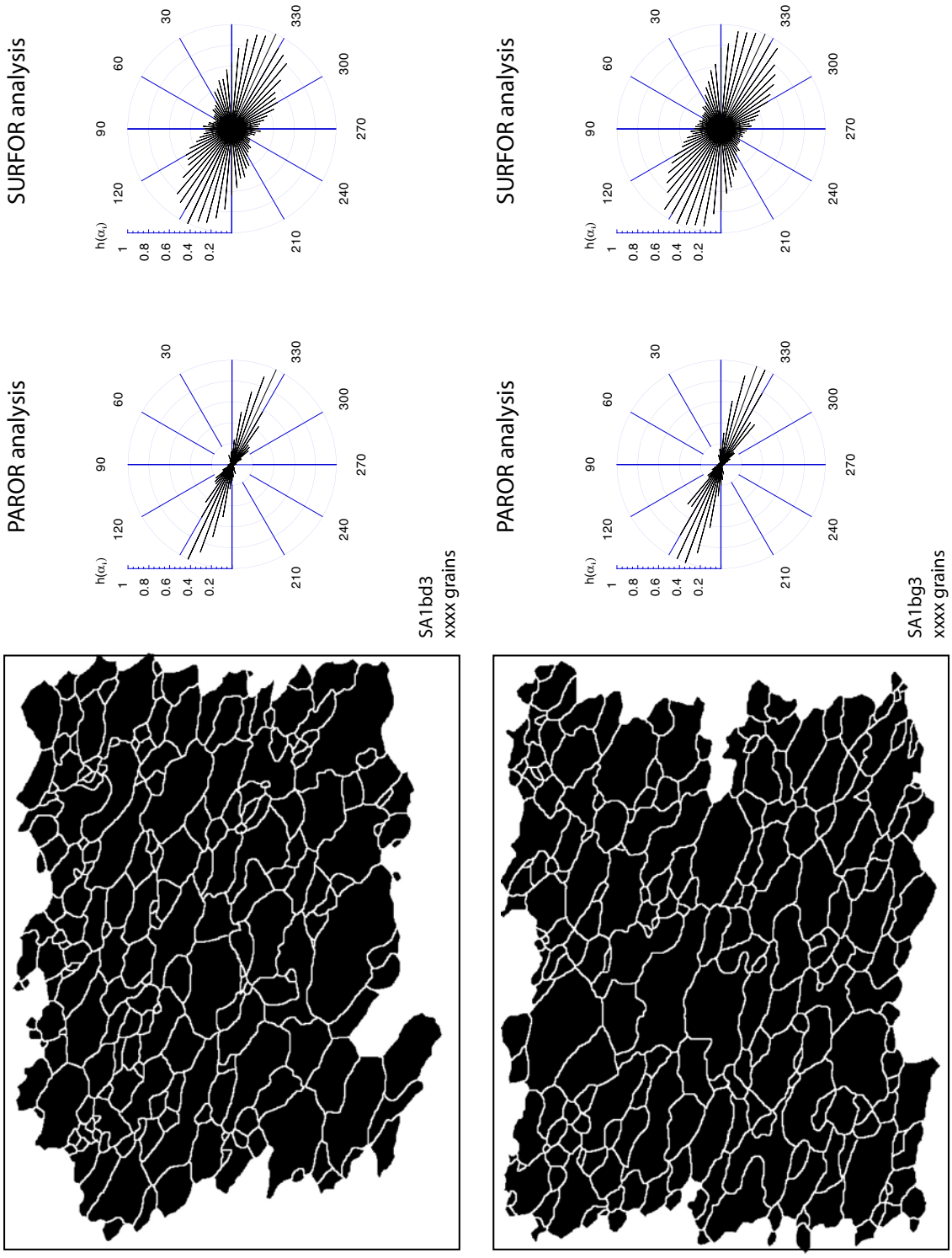


**Figure B38:** Grain shape preferred orientation analysis in XZ sections of samples SA1bd3 and SA1bg3.

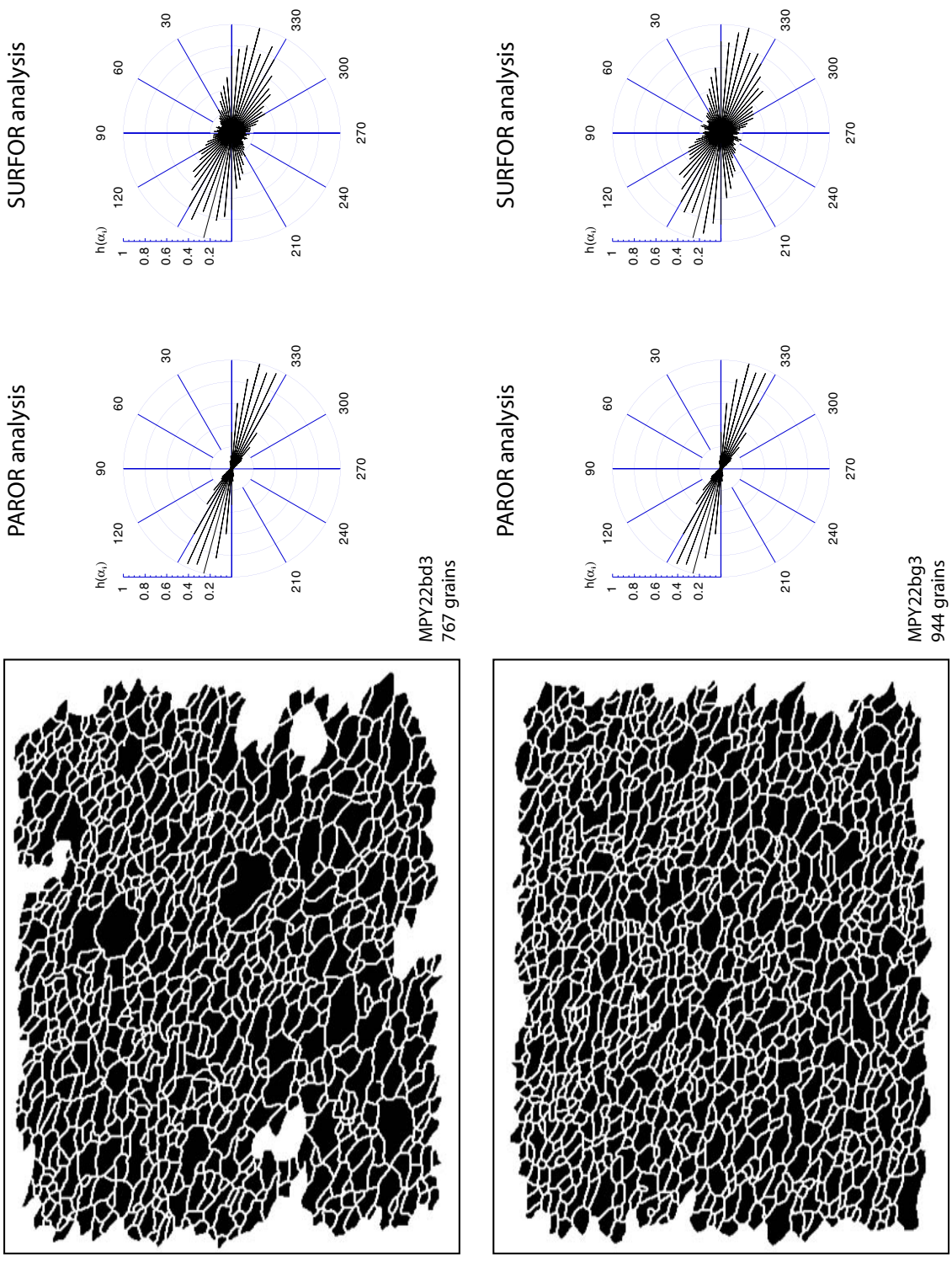


**Figure B39:** Grain shape preferred orientation analysis in XZ sections of samples MPY22bd3 and MPY22bg3.

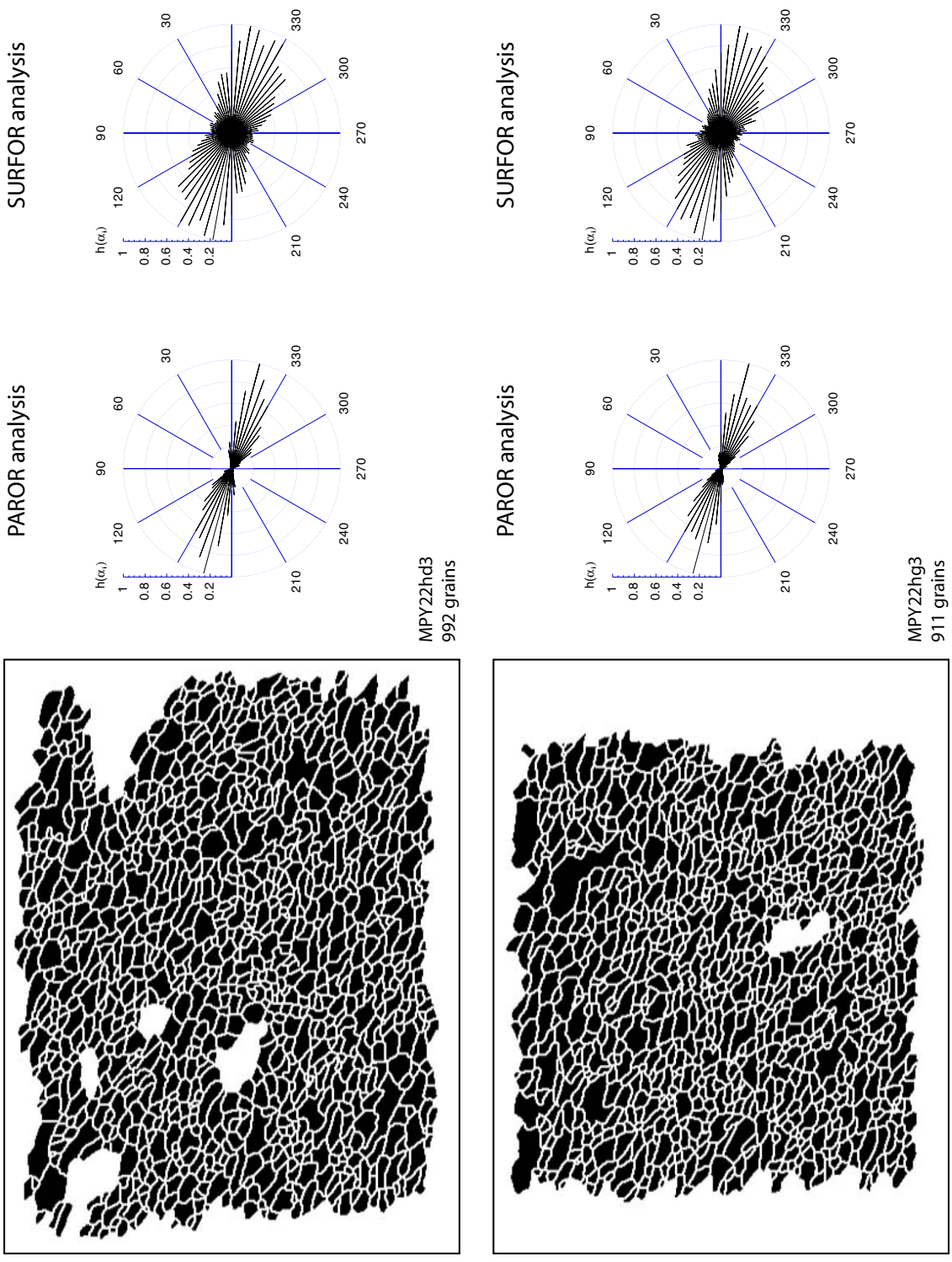


**Figure B40:** Grain shape preferred orientation analysis in XZ sections of samples MPY22hd3 and MPY22hg3.

# APPENDIX C: Metamorphic study of the Dauphinois domain at the south eastern rim of the Pelvoux massif.

This appendix presents the preliminary results of metamorphic conditions estimates within the Dauphinois cover of the southeastern rim of the Pelvoux massif. This study is the result of collaboration with Dr. S. Potel from the Institute of Geosciences of the Giessen University (Germany).

28 samples from the globigerina metamarls level of the Dauphinois cover (see figure C1) are presented. Taking samples within the same formation was chosen in order to limit the effects of the bulk rock composition on the determination of illite and chlorite "crystallinities" (Frey, 1987). Metamorphic grades have been estimated through mineral assemblages, simultaneous measurements of illite and chlorite crystallinity, K-white mica *b* cell dimension and K-white mica polytypes content.

Within the Rocher de l'Yret shear zone (RYSZ), these results are completed by a fluid inclusion study, which offers additional clues for paleogeothermal gradients estimates. Quartz-calcite precipitates found along the strike slip fault planes dissecting the uppermost basement units from the RYSZ were analysed (samples F202, F72 and FI92).

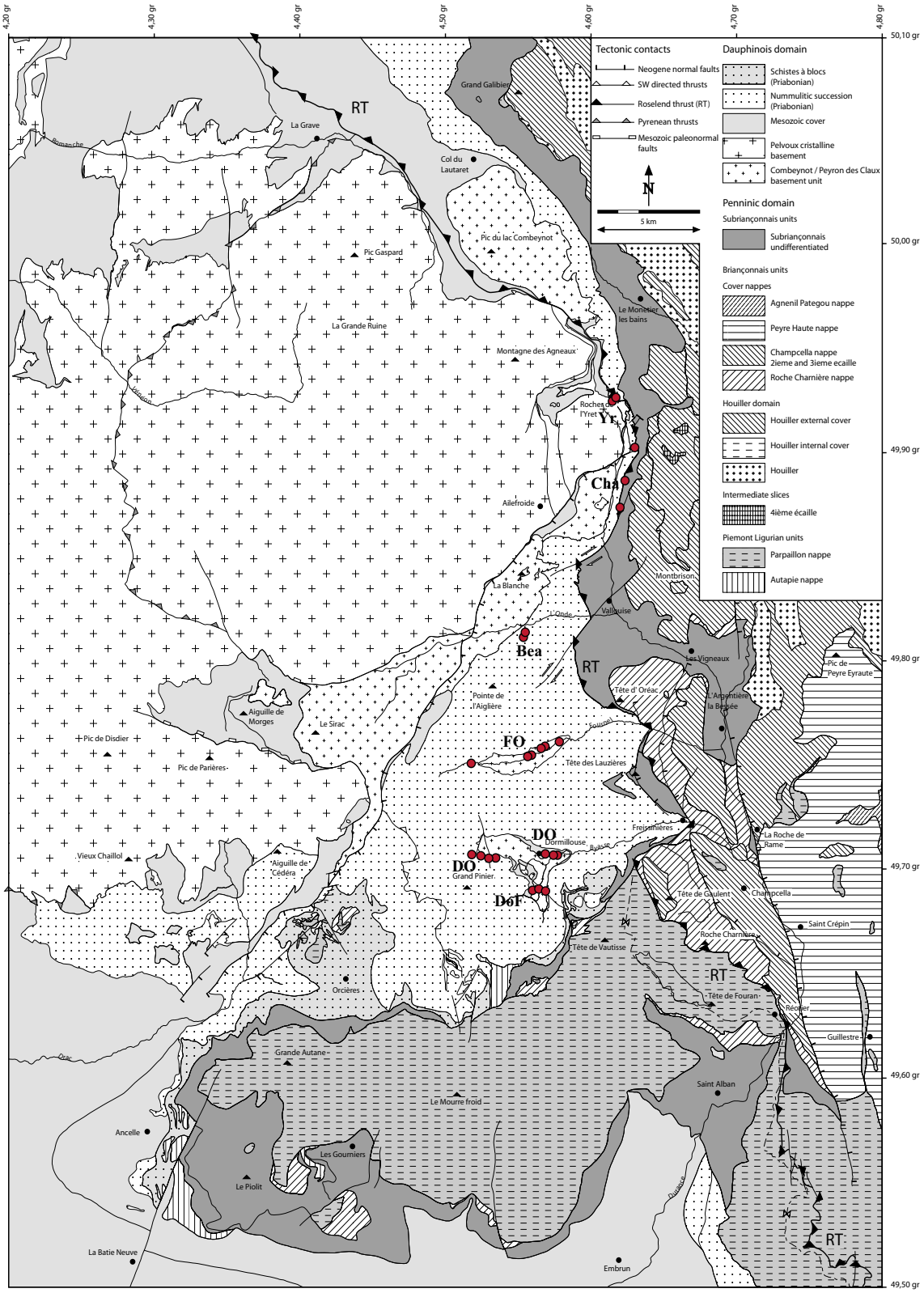


**Figure C1:** Localisation of the different sampling sites (points Yr, Cha, Bea, FO, DO and DoF).

# Methodological aspects.

## Clay minerals.

Clay mineral studies were conduced using the same preparation technique as reported by Schmidt et al. (1997). The effects of the presence of detrital material was limited using a short crushing-time and by a careful separation of the <2 μm fraction (repetition of the procedure in the Attemberg columns in order to concentrate the <2 μm fraction according to Kunert, 1999). Illite and chlorite crystallinity was measured on air-dried, glycolated preparates, on a D501 Bruker-AXS (Siemens) diffractometer, using CuKalpha radiation, 40 kV, 30 mA; divergence slits (1°) with a secondary graphite monochromator. The range of measurement, the time counting and the step size were as follow: for whole-rock paragenesis between 2 and 70 °2Θ with 1 sec and 0.02° step, for air-dried preparations between 2 and 70 °2Θ with 2 sec and 0.01° step and for glycolated preparate between 2 and 25 °2Θ with 1 sec and 0.01° step.

Illite crystallinity (IC) was calculated using the software MacDiff 4.2.5 written by R. Petschick. The IC index is defined as the full width at half maximum intensity (FWHM) of the first illite basal reflection. IC values were transformed into Kübler index (KI) values using a correlation with SW standards of Warr & Rice (1994) (KI = -0.0314 + 1.2702 * IC). KI is used to define the lower and upper limits of the anchizone. The same experimental conditions were also used to determine chlorite crystallinity on the (002) peak (ChC (002)) expressing the FHWM values of the second (7Å) basal reflection of chlorite. Furthermore, the ChC(002) measurements were calibrated with those of Warr & Rice (1994) and expressed as Árkai index (ÁI) (Guggenheim et al., 2002): ÁI = 0.0239 + 0.87755 ChC(002). The actual boundary ranges of Kübler's anchizone are KI = 0.25-0.42 Δ°2Θ, correlation with the KI gives calculated boundary values of the anchizone for ÁI = 0.24-0.30 Δ°2Θ. Mineral abbreviations used are from Kretz (1983).

K-white mica *b* cell dimensions were determined for samples free of paragonite and mixed-layered minerals. The *b* cell dimension is based on the $d_{060,331}$ spacing and on the increasing celadonite substitution that occurs with pressure increase in white mica, it is s.l. a qualitative value of the phengite content in muscovite (Ernst, 1963; Guidotti et al., 1989). Guidotti et al. (1989) presented linear regression equations that quantify the changes in the *b* cell dimensions of muscovite $2M_1$ that result from cation substitutions in the interlayer and octahedral sites. This *b*-value was determined by measurement of the (060) peak of the potassic white mica when present (Sassi & Scolari, 1974), and by using the program METRIC, which is a cell-refinement program. The measurement were done on disordered < 2$\mu$m grain-size fraction powder paste on glass using a wood glue

and sample were lightly pressed on it. The measurement was done between 2 and 70 °2Θ with 1 sec and 0.01° step.

Fluid inclusions.

Microthermal investigations on double polished thin sections were performed using the heating and cooling stage of a Linkam THM 600/S/Geo coupled to a TMS 94 temperature controller with an error of ± 1°C. The heating and cooling stage was calibrated using synthetic fluid inclusion calibration standard: $CO_2$ and $H_2O$. The measurements were achieved on double polished thin sections.

## Results.

Clay minerals.

Observed metamorphic assemblages, KI and AI values are given in Table 1. The metamarls analyzed contain Qtz + K-white mica + Chl + Fd ± Cal. In their < 2$\mu$m grain-size fraction, illite-muscovite predominates, Chl and quartz are significant.

Figure C2 shows the distribution of illite "crystallinity" (KI). The KI data correspond to high diagenetical and low-anchizonal values. The diagenetical values are observed in the south of the Dormillouse Valley and in the Yret Zone. Generally, the KI values decrease (and the metamorphic grade increases) towards the north. In the Yret zone, the values are lower probably due to the extreme deformation affecting all the Dauphinois units in this area.

Similar conclusions can be drawn from the chlorite "crystallinity" data (ÁI) (figure C3).

The correlation between KI and ÁI indexes shows a positive trend (figure C4).

The low-metamorphic grade of the samples is also confirmed by the transformation of 1Md into 2M1 illite polytypes, which is not completed (figure C5). Complete transformation is generally observed at the transition between low- and high-anchizone (Merriman & Peacor, 1999; Potel, 2001).

Pressure conditions estimates by means of K-white mica *b* dimension shows values between 9.00 and 9.03Å, which are characteristic for an intermediate pressure gradient (25-35°C/km) (figure C6).

Fluid inclusions.

The chronology of the different populations is relative and with respect to their host mineral and their overgrowth (Mullis, 1976).

Two phases fluid inclusions (i.e. vapour and liquid at room temperature) have been identified for the quartz/calcite precipitates found at the RYSZ.

In sample F202, the fluid inclusions were too small to be analysed.

In F72, all investigated fluid inclusions are of pseudo-secondary nature. Their size varies between 3 and 10 $\mu$m and their vapour/liquid ratio is estimated to 0.05. The mean $Th_I$ of these fluid inclusions is 170 °C with extreme values from 127 and 210°C.

In FI92, the fluid inclusion population observed is of pseudo-secondary nature. This population is represented by fluid inclusions of 3-7 $\mu$m size. The vapor/liquid ratio is of 0,05. The mean $Th_I$ of this sample is higher as in the F72 ($Th_I$ = 182) and the salinity is also higher with a NaCl mole% of 11.

| Name | Ms/Ill | Chl | Chl/Sm | Ill/Sm | K-Fsp | %2M1 | b-cell | KI | AI | KI Metam. Z. | AI Metam. Z. |
|---|---|---|---|---|---|---|---|---|---|---|---|
| ***Bea*** | + | + | - | - | + | 92 | 9.02 | 0,356 | 0.267 | L. Anch. | Anch. |
| ***Beb*** | + | + | - | - | + | 87 | 9.01 | 0,383 | 0.286 | L. Anch. | Anch. |
| ***CHA1*** | + | + | - | - | + | 89 | 9.01 | 0,378 | 0.283 | L. Anch. | Anch. |
| ***CHA2*** | + | + | - | - | + | 72 | 9.01 | 0,415 | 0.302 | L. Anch. | Anch. |
| ***CHA3*** | + | + | - | - | + | 84 | 9.00 | 0,364 | 0.297 | L. Anch. | Anch. |
| ***Do1*** | + | + | - | - | + | 81 | 9.00 | 0,376 | 0.296 | L. Anch. | Anch. |
| ***Do2*** | + | + | - | - | + | 57 | 9.01 | 0,405 | 0.342 | L. Anch. | Diag. |
| ***Do4a*** | + | + | - | - | + | 61 | 9.03 | 0,384 | 0.279 | L. Anch. | Anch. |
| ***Do4b*** | + | + | - | - | + | 62 | 9.02 | 0,388 | 0.290 | L. Anch. | Anch. |
| ***Do4*** | + | + | - | - | + | 96 | 9,01 | 0,342 | 0.279 | L. Anch. | Anch. |
| ***Do5a*** | + | + | - | - | + | 89 | 9.00 | 0,376 | 0.297 | L. Anch. | Anch. |
| ***Do5c*** | + | + | - | - | + | 79 | 9.01 | 0,368 | 0.285 | L. Anch. | Anch. |
| ***DoF1a*** | + | + | - | - | + |  |  | 0,410 | 0.288 | L. Anch. | Anch. |
| ***DoF1b*** | + | + | - | - | + | 73 | 9.03 | 0,446 | 0.336 | H. Diag. | Diag. |
| ***DoF2*** | + | + | - | - | + | 85 | 9.01 | 0,435 | 0.287 | H. Diag. | Anch. |
| ***DoF3*** | + | + | - | - | + | 84 | 9.02 | 0,383 | 0.282 | L. Anch. | Anch. |
| ***Fo1b*** | + | + | - | - | + | 88 | 9.02 | 0,366 | 0.284 | L. Anch. | Anch. |
| ***Fo1c*** | + | + | - | - | + | 90 | 9.01 | 0,351 | 0.265 | L. Anch. | Anch. |
| ***Fo1e*** | + | + | - | - | + |  |  | 0,376 | 0.272 | L. Anch. | Anch. |
| ***Fo2b*** | + | + | - | - | + | 95 | 9.02 | 0,371 | 0.289 | L. Anch. | Anch. |
| ***Fo2c*** | + | + | - | - | + | 90 | 9.02 | 0,358 | 0.273 | L. Anch. | Anch. |
| ***Fo3a*** | + | + | - | - | + | 82 | 9.03 | 0,350 | 0.288 | L. Anch. | Anch. |
| ***Fo3b*** | + | + | - | - | + | 81 | 9.02 | 0,420 | 0.312 | L. Anch. | Diag. |
| ***Fo3c*** | + | + | - | - | + | 70 | 9.03 | 0,461 | 0.308 | H. Diag. | Diag. |
| ***Fo4b*** | + | + | - | - | + | 90 | 9.02 | 0,406 | 0.286 | L. Anch. | Anch. |
| ***YR1*** | + | + | - | - | + | 81 | 9.02 | 0,433 | 0.322 | H. Diag. | Diag. |
| ***YR2*** | + | + | - | - | + | 65 |  | 0,395 | 0.304 | L. Anch. | Anch. |

**Table 1:** Observed metamorphic assemblages, KI and AI values.

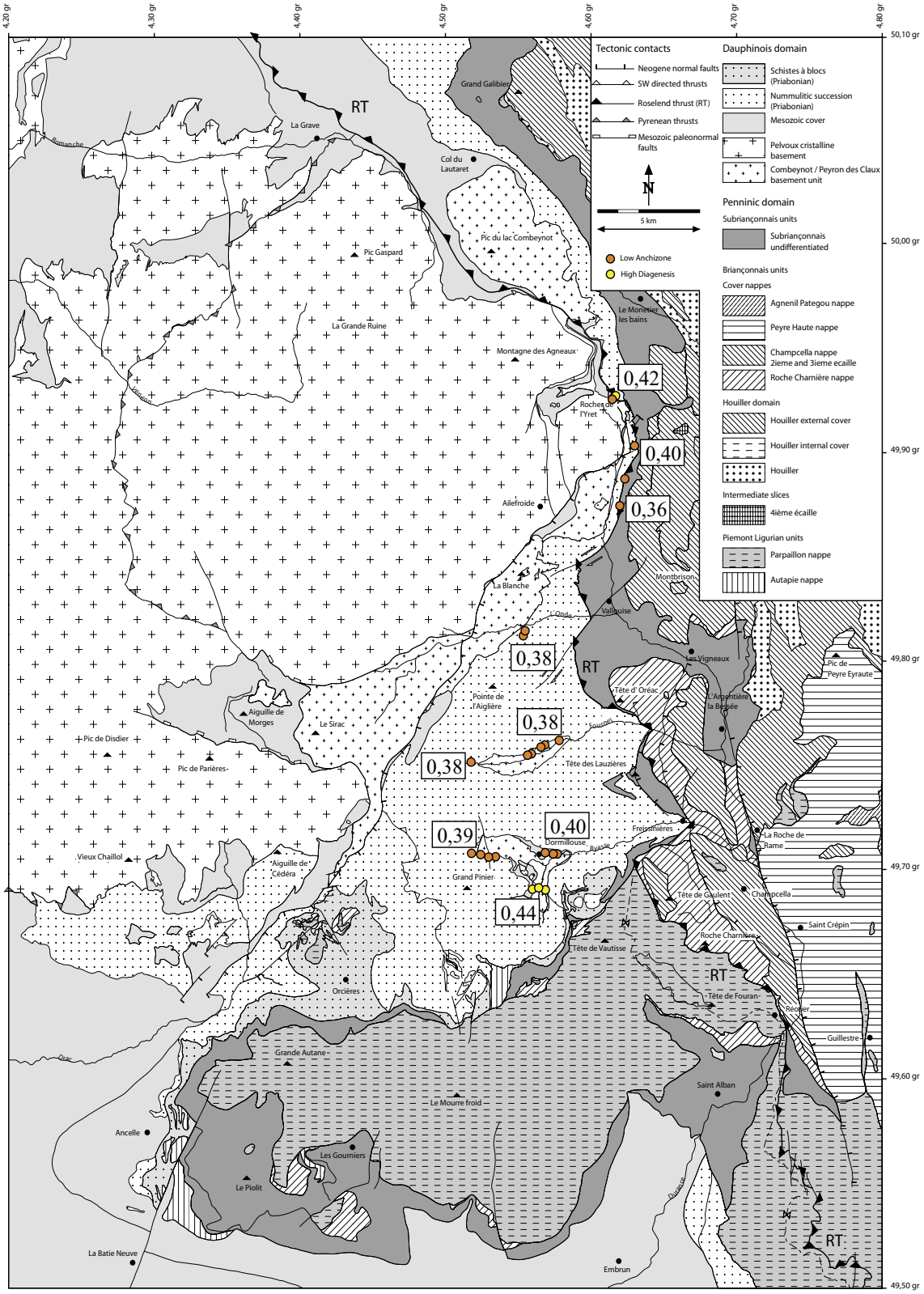


**Figure C2:** Distribution and values of Kübler index (KI) in the studied area.

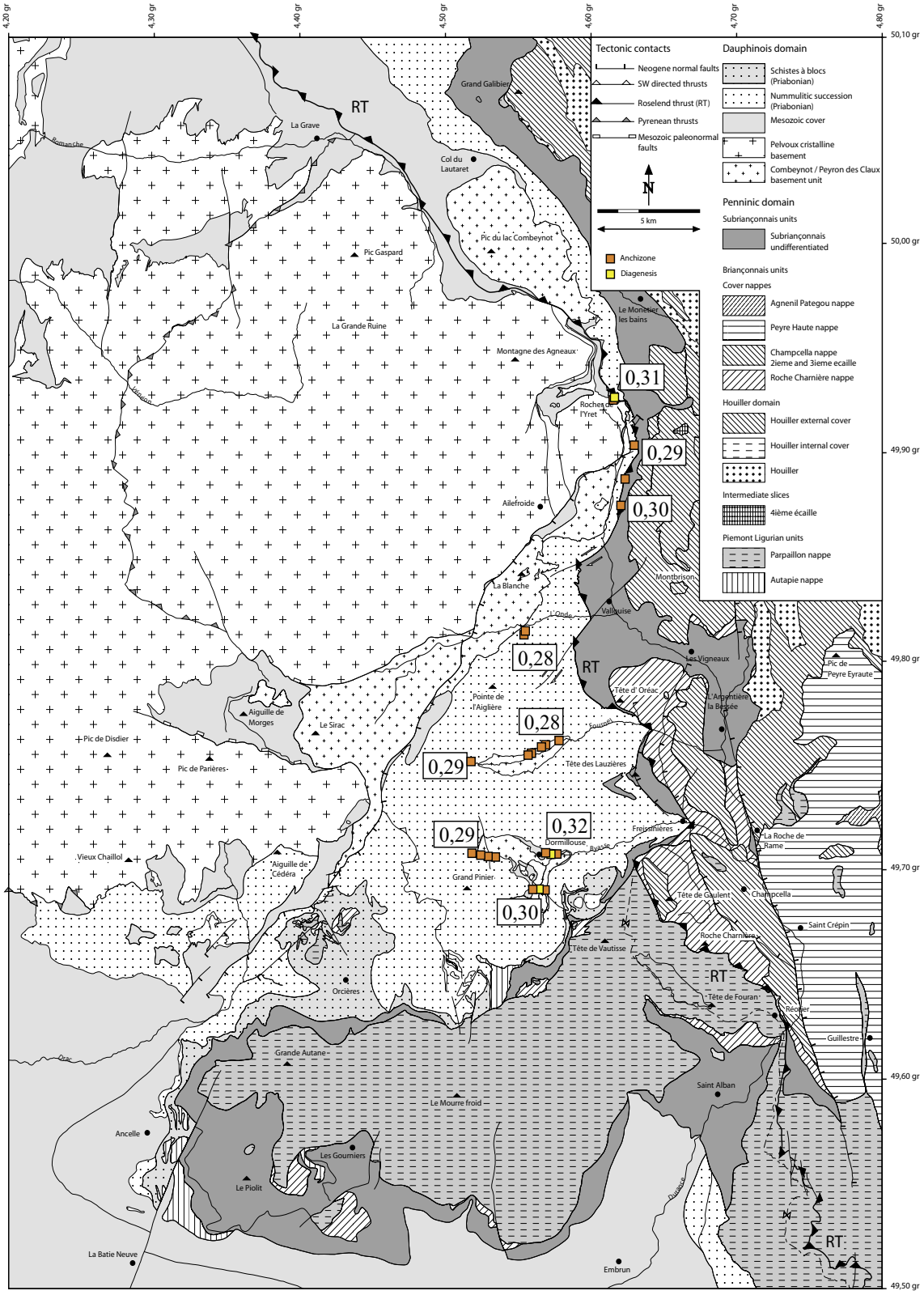


**Figure C3:** Distribution and values of Árkai index (ÁI) in the studied area.

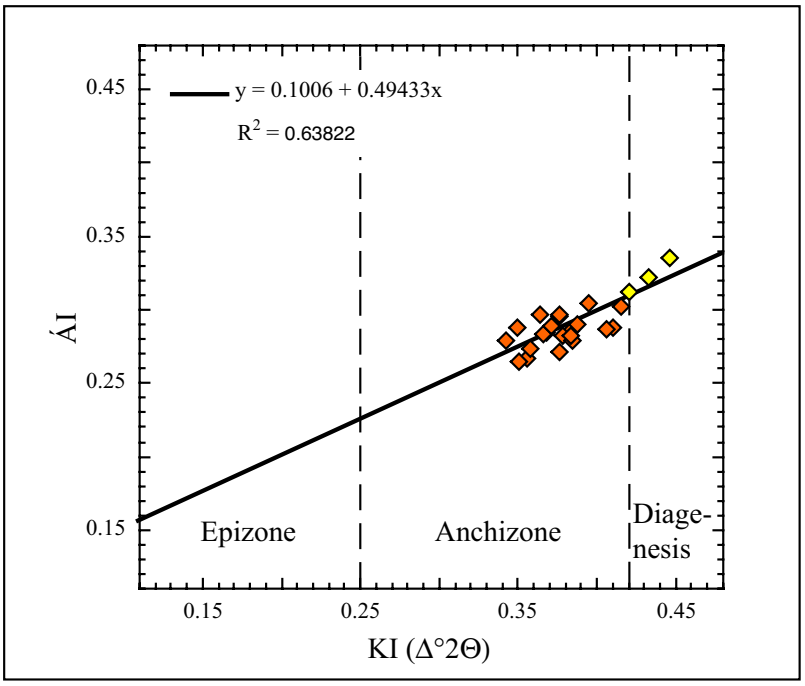


**Figure C4:** Correlation between Kübler index and Arkai index on air dried preparations.

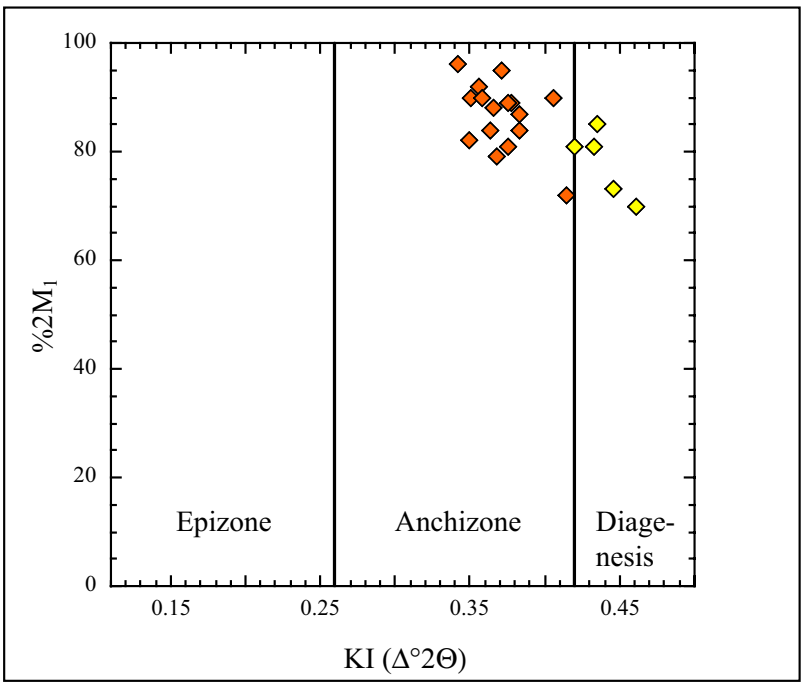


**Figure C5:** Correlation between Kübler index and 2M1 1Md illite polytypes proportion on air-dried preparations.

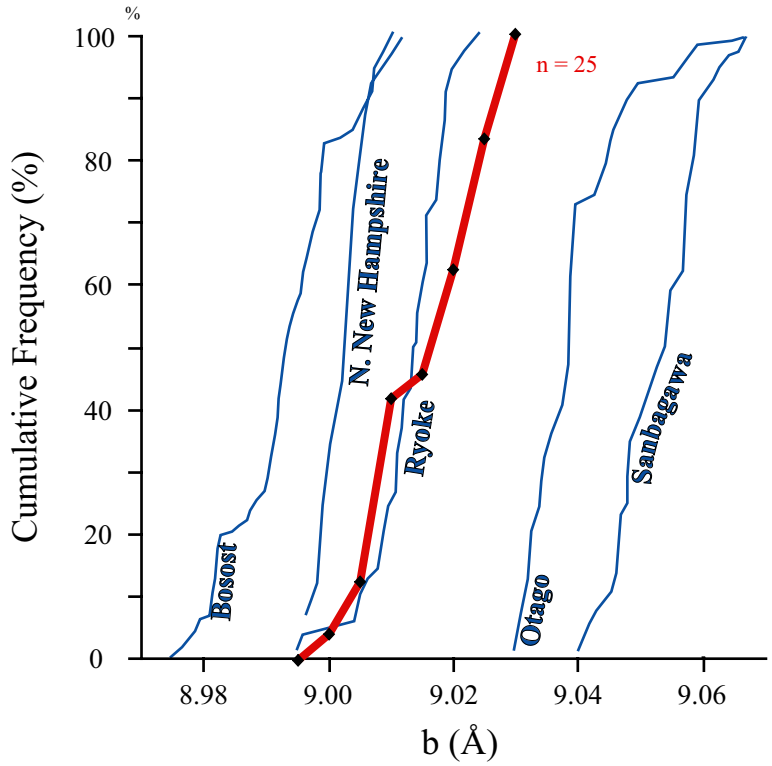


**Figure C6:** Cumulative curves of K-white mica b cell dimensions for 20 anchizonal samples from our studied area (red line).
Reference curves (blue lines) are from Sassi and Scolari (1974) and Sassi (personal communication).

## Summary.

The results reveal an increase of the metamorphic conditions from south to north (KI and ÁI values decrease) of the investigated area. The Chambran and Yret values are the only exception with values close to the diagenetic zone.

The S-N directed metamorphic gradient found at the south eastern rim of the Pelvoux massif had been already described by Aprahamian (1974, 1988). This last author, based on illite crystallinity measurements, however observed epizonal conditions within the Dormillouse and Fournel valleys. Independently to the methods used, such values were not found in the study presented here.

The findings presented in this session are instead to compare with those from Ceriani et al. (2003) in the Dauphinois and Penninic domain immediately north of the Pelvoux massif. Their results show high anchizonal metamorphic grade and medium pressure conditions deduced from illite crystallinity and K-white mica *b* cell dimension measurements.

# REFERENCES

Angelier, J. and Mechler, P., 1977. Sur une methode graphique de recherche des contraintes principales egalement utilisables en tectonique et en seismologie : la methode des diedres droits. Bulletin de la Societe Geologique de France, 19(6): 1309-1318.

Apps, G.M., Peel, F. and Elliott, T., 2004. The structural setting and palaeogeographical evolution of the Gres d'Annot Basin. Deep-water sedimentation in the Alpine Basin of SE France; new perspectives on the Gres d'Annot and related systems. Geological Society Special Publication 221: 65-96. 2004.

Aprahamian, J., 1974. La cristallinite de l'illite et les mineraux argileux en bordure des massifs cristallins externes de Belledonne et du Pelvoux (variations et relations possibles avec des evenements tectoniques et metamorphiques alpins). Geologie Alpine, 50: 5-15.

Aprahamian, J., 1988. Cartographie du metamorphisme faible a tres faible dans les Alpes francaises externes par l'utilisation de la cristallinite de l'illite. Geodinamica Acta. Volume 2(1): 25-32.

Bagnoud, A., Wernli, R. and Sartori, M., 1998. Decouverte de foraminiferes planctoniques paleogenes dans la zone de Sion-Courmayeur a Sion (Valais, Suisse). Eclogae Geologicae Helvetiae, 91(3): 421-429.

Banda, E. and Santanach, P., 1992. The Valencia Trough (western Mediterranean); an overview. Tectonophysics 208 (1-3): 183-202.

Barbier, R., Barféty, J.C., Bordet, P., Bulard, P.F., Debelmas, J., Fabre, J., Feys, R., Gréber, C., Gillot-Barbiéri, C., Lacombe, J.-C., Vialon, P., Le Fort, P., Mouterde, M., Pécher, A., Petiteville, J., Rivoirard, R., Tissot, B., Vernet, J. and Méloux, J., 1976. Carte géologique de la France (1/50000). Feuille La Grave. BRGM, Orléans.

Barféty, J.C., 1968. Importance des failles et des glissements superficiels dans le massif de Montbrison et ses environs (Briançon, Hautes-Alpes). Travaux du Laboratoire de Geologie de la Faculte des Sciences de Grenoble, 44: 49-54.

Barfety, J.-C., Lemoine, M., Mercier, D., Polino, R., Bertrand, J., Dumont, T., Aumadric du Chaffaut, S., Pêcher A., Monjuvent, G., Gidon, M., Debelmas, J., Vernet, J., Lami, A., Jaillard, E., Détraz, G., Landès, B., Jean, S. and Lavigne-Goldenberg, P., 1996. Carte géologique de la France (1/50000). Feuille Briançon. BRGM, Orléans.

Barféty, J.-C., Pécher, A., Debelmas, J., Gidon, P., Gidon, M., Mouterde, R., Vernet, J., Le Fort, P., Pécher, A., Barbieri, A., Biju-Duval, J., Gillot-Barbieri, C., Bartoli, F., Ozocak, R. and Vernet J., 1984. Carte géologique de la France (1/50000). Feuille St-Christophe-en-Oisans. BRGM, Orléans.

Barféty, J.C., Gidon, M. and Kerckhove, C., 1968. Sur l'importance des failles longitudinales dans le secteur durancien des Alpes internes francaises. Comptes Rendus Hebdomadaires des Seances de l'Academie des Sciences, Serie D: Sciences Naturelles,

267(4): 394-397.

Barféty, J.C., Gidon, M., Lemoine, M. and Mouterde, R., 1979. Tectonique synsedimentaire liasique dans les massifs cristallins de la zone externe des Alpes occidentales francaises; la faille du col d'Ornon. Comptes Rendus Hebdomadaires des Seances de l'Academie des Sciences, Serie D: Sciences Naturelles, 289(16): 1207-1210.

Barféty, J.C., Tricart, P. and Jeudy de Grissac, C., 1992. La Quatrieme ecaille près de Briancon (Alpes francaises); un olistostrome précurseur de l'orogenese pennique eocene. Comptes Rendus de l'Academie des Sciences, Serie 2, Mecanique, Physique, Chimie, Sciences de l'Univers, Sciences de la Terre, 314(1): 71-76.

Barnhoorn, A., Bystrichy, M., Burlini, L., Kunze, K., 2004. The role of recrystallisation on the deformation behaviour of calcite rocks: large strain torsion experiments on Carrara marble. Journal of Structural Geology, 26(5): 885-903.

Bartrina, M.T., Cabrera, L., Jurado, M.J., Guimera, J. and Roca, E., 1992. Evolution of the central Catalan margin of the Valencia Trough (western Mediterranean). Tectonophysics 203 (1-4): 219-247.

Beach, A., 1981. Thrust structures in the eastern Dauphinois Zone (French Alps), north of the Pelvoux Massif. Journal of Structural Geology, 3(3): 299-308.

Behrmann, J.H., 1983. Microstructure and fabric transitions in calcite tectonites from the Sierra Alhamilla (Spain). Geologische Rundschau, 72(2): 605-618.

Bergerat, F., 1987. Stress fields in the European Platform at the time of Africa-Eurasia collision. Tectonics, 6(2): 99-132.

Bestmann, M., Kunze, K. and Matthews, A., 2000. Evolution of a calcite marble shear zone complex on Thassos Island, Greece; microstructural and textural fabrics and their kinematic significance. Journal of Structural Geology, Vol. 22(11-12): 1789-1807.

Bigi, G., Cosentino, D., Parotto, M., Sartori, R. and Scandone, P., 1983. Structural model of Italy, scale 1/500000.

Blanco, M.J. and Spakman, W., 1993. The P-wave velocity structure of the mantle below the Iberian Peninsula; evidence for subducted lithosphere below southern Spain. Tectonophysics 221 (1): 13-34.

Boccaletti, M., Ciaranfi, N., Cosentino, D., Deiana, G., Gelati, R., Lentini, F., Massari, F., Moratti, G., Pescatore, T., Ricci Lucchi, F. and Tortorici, L. 1990. Palinspastic restoration and paleogeographic reconstruction of the peri-Tyrrhenian area during the Neogene. Palaeogeography, Palaeoclimatology, Palaeoecology 77 (1): 41-42.

Bonardi, G., Cavazza, W., Perrone, V., Rossi, S., 2001. Calabria-Peloritani terrane and

northern Ionian Sea. In: G.B.a.M.I.P. Vai (Editor), Anatomy of an orogen: the Apennines and adjacent Mediterranean basins. Kluwer Academic Publishers, Dordrecht, pp. 287-306.

Bouchez, J.L., 1978. Preferred orientations of quartz <a> axes in some tectonites; kinematic inferences. Tectonophysics, 49(1-2): T25-T30.

Braillon, P.a.S., J., 1976. Deformation plastique de monocristaux de calcite en compression suivant <001>. Physica Status Solidi (a), 36: 637-646.

Bravard, C. and Gidon, M., 1979. La structure du revers oriental du Massif du Pelvoux; observations et interpretations nouvelles. Geologie Alpine, 55: 23-33.

Brodie, K.H. and Rutter, E.H., 1987. The role of transiently fine-grained reaction products in syntectonic metamorphism; natural and experimental examples. Canadian Journal of Earth Sciences. 24(3): 556-564.

Bürgisser, J., 1998. Deformation in foreland basins of the Western Alps (Pelvoux massif, SE France); significance for the development of the Alpine arc., ETH, Zürich, 151 pp.

Bürgisser, J. and Ford, M., 1998. Overthrust shear deformation of a foreland basin; structural studies south-east of the Pelvoux Massif, SE France. Journal of Structural Geology, 20(11): 1455-1475.

Bunge, H.J., 1982. Texture Analysis in Material Science - Mathematical Methods. Butterworth, London.

Burrus, J., 1984. Contribution to a geodynamic synthesis of the Provencal Basin (north-western Mediterranean). Marine Geology, 55(3-4): 247-269.

Burrus, J., 1989. Review of geodynamic models for extensional basins; the paradox of stretching in the Gulf of Lions (Northwest Mediterranean). Compte rendu de la seance specialisée de la Societe geologique de France. Bulletin de la Societe Geologique de France, Huitieme Serie, pp. 377-393.

Butler, R.W.H., 1989. The influence of pre-existing basin structure on thrust system evolution in Western Alps. Geological Society Special Publications 44: 105-122.

Butler, R.W.H., 1992. Thrust zone kinematics in a basement-cover imbricate stack; eastern Pelvoux Massif, French Alps. Journal of Structural Geology, 14(1): 29-40.

Butler, R.W.H., Matthews, S.J. and Parish, M., 1986. The NW external Alpine thrust belt and its implications for the geometry of the western Alpine Orogen. Geological Society Special Publications 19: 245-260.

Carminati, E., Wortel, M.J.R., Meijer, P.T. and Sabadini, R., 1998. The two-stage

opening of the western-central Mediterranean basins; a forward modeling test to a new evolutionary model. Earth and Planetary Science Letters, 160(3-4): 667-679.

Carminati, E., Wortel, M.J.R., Spakman, W. and Sabadini, R., 1998. The role of slab detachment processes in the opening of the western-central Mediterranean basins; some geological and geophysical evidence. Earth and Planetary Science Letters, 160(3-4): 651-665.

Carminati, E., Argnani, A., Carrara, G., Dabovski, C., Dumurdzanov, N., Gaetani, M., Georgiev, G., Mauffret, A., Nazai, S., Sartori, R., Scionti, V., Scrocca, D., Séranne, M., Torelli, L. and Zagorchev, I., 2004. TRANSMED Transect III: Massif Central - Provence - Gulf of Lion - Provençal Basin - Sardinia - Tyrrhenian Basin - Southern Apennines - Apulia - Adriatic Sea - Albanian Dinarides - Balkans - Moesian Platform, The TRANSMED Atlas The Mediterranean region from crust to mantle. Springer.

Casey, M., 1981. Numerical analysis of X-ray texture data; an implementation in Fortran allowing triclinic or axial specimen symmetry and most crystal symmetries. Tectonophysics, 78(1-4): 51-64.

Casey, M., Kunze, K. and Olgaard, D.L., 1998. Texture of Solnhofen Limestone deformed to high strains in torsion. Journal of Structural Geology. 20(2-3): 255-267.

Cavazza, W., Roure, F. and Ziegler, P.A., 2004. The Mediterranean Area and the Surrounding Regions: Active Processes, Remnants of Former Tethyan Oceans and Related Thrustbelts. The TRANSMED Atlas The Mediterranean region from crust to mantle. Springer, pp. 1-29.

Cavazza, W. and Wezel, F.C., 2003. The Mediterranean region; a geological primer. International Union of Geological Sciences.

Ceriani, S., 2001. A combined study of structure and metamorphism in the frontal Penninic units between the Arc and Isère valleys (Western Alps): Implications for the geodynamic evolution of the Western Alps., University of Basel, Basel, 196 pp.

Ceriani, S., Fügenschuh, B. and Schmid, S.M., 2001. Multi-stage thrusting at the "Penninic Front" in the Western Alps between Mont Blanc and Pelvoux massifs. International journal of earth sciences 90: 685-702.

Ceriani S., Fügenschuh B., Potel S. and Schmid S.M. in press. The tectono-metamorphic evolution of the Frontal Penninic units of the Western Alps: correlation between low-grade metamorphism and tectonic phases. Schweizerische Mineralogische und Petrographische Mitteilungen, 83: 111-131.

Ceriani, S. and Schmid, S.M., 2004. From N-S collision to WNW-directed post-collisional thrusting and folding: structural study of the Frontal Penninic Units in Savoie (Western Alps, France). Eclogae Geologicae Helvetiae, 97 in press.

Claudel, M.-E., 1999. Reconstitution paléogéographique du domaine Briançonnais au Mésozoique, Université Joseph Fourier Grenoble I, Grenoble, 236 pp.

Coward, M.P., Gillcrist, R. and Trudgill, B., 1991. Extensional structures and their tectonic inversion in the Western Alps. Geological Society Special Publications 56: 93-112.

Collombet, M., 2001. Cinématique et rotations des Alpes Occidentales. Approche paléomagnétique et modélisation analogique. Université Joseph Fourier, Grenoble, 207 pp.

Collombet, M., Thomas, J.C., Chauvin, A., Tricart, P., Bouillin, J P. and Gratier, J.P. 2002. Counterclockwise rotation of the Western Alps since the Oligocene; new insights from paleomagnetic data. Tectonics. 21 (4).

Davies, V.M., 1982. Interaction of thrusts and basement faults in the French external Alps. Tectonophysics 88: 325-331.

Delacou, B., 2004. Tectonique et géodynamique actuelle de l'arc alpin -Approche sismotectonique et modélisation numérique-, 249 pp.

De Bresser, J.H.P., 1989. Calcite c-axis textures along the Gavarnie thrust zone, central Pyrenees. Geologie en Mijnbouw 68: 367-375.

De Bresser, J.H.P., Majoor, F.J.M. and Ploegsma, M., 1986. New insights in the structural and metamorphic history of the western Lys-Caillauas Massif; central Pyrenees, France. Geologie en Mijnbouw 65: 177-187.

De Bresser, J.H.P. and Spiers, C.J., 1990. High-temperature deformation of calcite single crystals by r (super +) and f (super +) slip. Geological Society Special Publications, 54: 285-298.

De Bresser, J.H.P. and Spiers, C.J., 1993. Slip systems in calcite single crystals deformed at 300-800 degrees C. Journal of Geophysical Research, 98(4): 6397-6409.

De Bresser, J.H.P. and Spiers, C.J., 1997. Strength characteristics of the r, f, and c slip systems in calcite. Tectonophysics, 272(1): 1-23.

De Ruig, M.-J., 1990. Fold trends and stress deviation in the Alicante fold belt, southeastern Spain. Tectonophysics 184 (3-4): 393-403.

Debelmas, J., 1955. Les zones Subriançonnaise et Briançonnaise occidentale entre Vallouise et Guillestre (Hautes-Alpes). Université de Grenoble, Grenoble, 169 pp.

Debelmas, J., 1983. Alpes du Dauphiné. Guides géologiques régionaux. Masson, Paris, 198 pp.

Debelmas, J. and Kerckhove, C., 1980. Les Alpes franco-italiennes. Geologie Alpine 56: 21-58.

Debelmas, J., Le Fort, P., Biju-Duval, J., Vernet, J., Monjuvent, G., Beuf, S., Debelmas, J., Kerckhove, C. and Pêcher, A., 1980. Carte géologique de la France (1/50000). Feuille Orcières. BRGM, Orléans.

Debelmas, J., Lemoine, M., Kerckhove, C., Fail, J.-P., Lavergne, M., Leduc, J., Legreneur, J., Ortollan, J., Robert, J.-P., Potié, R. and Gidon, M., 1966. Carte géologique de la France (1/50000). Feuille Guillestre. BRGM, Orléans.

Debrand-Passard, S., Courbouleix, S. and Lienhardt, M.-J., 1984. Synthèse géologique du Sud-Est de la France. Mémoire du Bureau de recherches géologiques et minières, 126.

Dewey, J.F., 1980. Episodicity, sequence, and style at convergent plate. In: The continental crust and its mineral deposits. Geological Association of Canada, pp. 553-573.

Dèzes, P., Schmid, S.M. and Ziegler, P.A., 2004. Evolution of the European Cenozoic Rift System: interaction of the Alpine and Pyrenean orogens with their foreland lithosphere. Tectonophysics, 389 (1-2): 1-33.

Dietrich, D. and Durney, D.W., 1986. Change of direction of overthrust shear in the Helvetic nappes of western Switzerland. Journal of Structural Geology 8: 389-398.

Dietrich, D. and Song, H., 1984. Calcite fabrics in a natural shear environment, the Helvetic nappes of western Switzerland. Journal of Structural Geology, 6(1-2): 19-32.

Edington, J.W., Melton, K.N., Cutler, C.P., 1976. Superplasticity. Prog. Mat. Sci., 21: 61-170.

Ernst, W. G. (1963). Significance of phengitic micas from low grade schists. American Mineralogist 48: 1357-1373.

Erskine, B.G., Heidelbach, F. and Wenk, H.R., 1993. Lattice preferred orientations and microstructures of deformed Cordilleran marbles; correlation of shear indicators and determination of strain path. Journal of Structural Geology, 15(9-10): 1189-1205.

Etchecopar, A., 1977. A plane kinematic model of progressive deformation in a polycrystalline aggregate. Tectonophysics, 39(1-3): 121-139.

Faccenna, C., Becker, T.W., Lucente, F.P., Jolivet, L. and Rossetti, F., 2001a. History of subduction and Back-arc extension in the Central Mediterranean. Geophys. J. Int., 145: 809-820.

Faccenna, C., Davy, P., Brun, J.P., Funiciello, R., Giardini, D., Mattei, M. and Nalpas, T., 1996. The dynamics of backarc basins. An experimental approach to the opening of the

Tyrrhenian Sea. Geophys. J. Int., 126: 781-795.

Faccenna, C., Funiciello, F., Giardini, D. and Lucente, P., 2001b. Episodic back-arc extension during restricted mantle convection in the central Mediterranean. Earth and Planetary Science Letters, 187(1-2): 105-116.

Faccenna, C., Mattei, M., Funiciello, R. and Jolivet, L., 1997. Styles of back-arc extension in the central Mediterranean. Terra Nova, 9(3): 126-130.

Flandrin, J., 1967. Sur l'age des principaux traits structuraux du Diois et des Baronnies. Bulletin de la Societe Geologique de France, 8(3): 376-386.

Ford, M., 1996. Kinematics and geometry of early Alpine, basement-involved folds, SW Pelvoux Massif, SE France. Eclogae Geologicae Helvetiae 89: 269-295.

Ford, M. and Lickorish, W.H., 2004. Foreland basin evolution around the western Alpine Arc. Geological Society Special Publication 221: 39-63.

Ford, M., Lickorish, H. and Kusznir, N.J., 1999. Tertiary foreland sedimentation in the Southern Subalpine Chains, SE France: a geodynamic appraisal. Basin Research, 11: 315-336.

Friedman, M. and Higgs, N.G., 1981. Calcite fabrics in experimental shear zones. Geophysical Monograph. 24: 11-27.

Frey M., 1987. Low temperature metamorphism. Chapmam and Hall, New York - USA.

Fry, N., 1989. Southwestward thrusting and tectonics of the Western Alps. Geological society special publications 45: 83-109.

Froitzheim, N., Schmid, S.M. and Frey, M., 1996. Mesozoic paleogeography and the timing of eclogite-facies metamorphism in the Alps; a working hypothesis. Eclogae Geologicae Helvetiae 89: 81-110.

Fügenschuh, B., Loprieno, A., Ceriani, S. and Schmid, S.M., 1999. Structural analysis of the Subbrianconnais and Valais units in the area of Moutiers (Savoy, Western Alps); paleogeographic and tectonic consequences. International Journal of Earth Sciences 88: 201-218.

Fügenschuh, B. and Schmid, S.M., 2003. Late stages of deformation and exhumation of an orogen constrained by fission-track data; a case study in the Western Alps. Geological Society of America Bulletin, 115(11): 1425-1440.

Galindo-Zaldivar, J., Gonzales-Lodeiro, F. and Jabaloy, A., 1993. Stress and Paleostress in the Betic-Rif cordilleras (Miocene to the present). Tectonophysics, 227: 105-126.

Gidon, M., 1965. Sur l'interpretation des accidents de la bordure meridionale du massif du Pelvoux. Travaux du Laboratoire de Geologie de la Faculte des Sciences de Grenoble, 41: 177-185.

Gidon, M., 1979. Le role des etapes successives de deformation dans la tectonique alpine du massif du Pelvoux (Alpes occidentales). Comptes Rendus Hebdomadaires des Seances de l'Academie des Sciences, Serie D: Sciences Naturelles, 288(9): 803-806.

Gidon, P., 1954. Les rapports des terrains cristallins et de leur couverture sedimentaire, dans les regions orientale et meridionale du massif du Pelvoux. Travaux du Laboratoire de Geologie de la Faculte des Sciences de Grenoble, 31: 1-199.

Gidon, P. and Vernet, J., 1952. Les accidents synclinaux de la haute vallee du Drac de Champoleon (Hautes-Alpes). Compte Rendu Sommaire des Seances de la Societe Geologique de France, 13-14: 269-270.

Giglia, G., Capponi, G., Crispini, L. and Piazza, M., 1996. Dynamics and seismotectonics of the West-Alpine arc. Tectonophysics, 267(1-4): 143-175.

Gignoux, M. and Moret, L., 1938. Description geologique du bassin superieure de la Durance. Travaux du Laboratoire de Géologie de la Faculté des Sciences de Grenoble, 21: 1-295.

Gignoux, M., Moret, L. and Schneegans D., 1933. Structure géologique de la fenêtre de L'Argentière au Sud de Briançon (Hautes-Alpes). Comptes Rendus de l'Academie des Sciences, 197(22): 1265-1267.

Gillcrist, R., Coward, M. and Mugnier, J.L., 1987. Structural inversion and its controls; examples from the Alpine Foreland and the French Alps. Geodinamica Acta, 1(1): 5-34.

Goguel, J., 1940. Tectonique de la chaine de Montbrison (feuille de Briancon au 1/ 50.000). Bulletin du Service de la Carte Geologique de la France, 203: 187-201.

Goguel, J., 1942. La chaine de Montbrison; essai de coordination tectonique (feuille de Briancon au 1/ 50.000). Bulletin du Service de la Carte Geologique de la France, 211: 109-118.

Goguel, J., 1963. Les problemes des chaines subalpines. [Fallot Memorial Vol.] (Soc. Geol. France), 2: 301-307.

Gonzalez, C.J.M. and Garcia, C.C., 1999. Calcite twins from microveins as indicators of deformation history. Journal of Structural Geology, 21(7): 875-889.

Graham, R.H., 1978. Wrench faults, arcuate fold patterns and deformation in the southern French Alps. Proceedings of the Geologists' Association, 89 Part 2: 125-142.

Gratier, J.P., Menard, G. and Arpin, R., 1989. Strain-displacement compatibility and restoration of the Chaines Subalpines of the Western Alps. Geological Society Special Publications 45: 65-81.

Griggs, D.T., Turner, F.J. and Heard, H.C., 1960. Deformation of rocks at 500 degrees to 800 degrees C. Geological Society of America. Geological Society of America, pp. 39-104.

Gueguen, E., Doglioni, C. and Fernandez, M., 1998. On the post-25 Ma geodynamic evolution of the western Mediterranean. Tectonophysics 298: 259-269.
Guggenheim S.Jr., Bain D.C., Bergaya F., Brigatti M.F., Drits V.A., Eberl D.D., Formoso M.L.L., Galan E., Merriman R.J., Peacor D.R., Stanjek H. & Watanabe T., 2002. Report of the association internationale pour l'etude des argiles (AIPEA) nomenclature committee for 2001: order, disorder and crystallinity in phyllosilicates and the use of the "crystallinity index". Clays and Clay Minerals, 50: 406-409.

Guidotti, C.V., Sassi, F.P. and Blencoe, J.G., 1989. Compositional controls on the a and b cell dimensions of 2M1 Muscovites. European Journal of Mineralogy, 1: 71-84.

Guillaume, A., 1980. Tectonophysics of the Western Alps. Eclogae Geologicae Helvetiae 73(2): 425-436.

Gupta, S., 1997. Tectonic control on paleovalley incision at the distal margin of the early Tertiary Alpine foreland basin, southeastern France. Journal of Sedimentary Research, 67(6): 1030-1043.
Haug, E., 1894. Excursion géologique dans la haute vallée du Drac. Comptes Rendus des Séances de la Société Géologique de France, 22.

Heilbronner, R.P. and Pauli, C., 1993. Integrated spatial and orientation analysis of quartz c-axes by computer-aided microscopy. Journal of Structural Geology, 15(3-5): 369-382.

Heilbronner, R.P. and Pauli, C., 1994. Orientation and misorientation imaging: integration of microstructural and textural analysis. In: H.J. Bunge, Siegesmund, S., Skrotzki, W., Weber, K. (Editor), Texture of Geological Materials. DGM Informationsgesellschaft Verlag, Oberursel, pp. 147-164.

Helming, K., Geier, St., Heinitz, J., Leiss, B., Rauschenbach, B., Schwarzer, R.A., Ullemeyer, K., Wenk, H.-R., 1994. Texture Estimates by Means of Components. Z. Metallkd., 85: 545-553.

Herwegh, M. and Kunze, K., 2002. The influence of nano-scale second-phase particles on deformation of fine grained calcite mylonites. Journal of Structural Geology, 24(9): 1463-1478.

Huyghe, P. and Mugnier, J.L., 1995. A comparison of inverted basins of the southern North Sea and inverted structures of the external Alps. Geological Society Special

Publications 88: 339-353.

Jolivet, L. and Faccenna, C., 2000. Mediterranean extension and the Africa-Eurasia collision. Tectonics, 19(6): 1095-1106.

Kerckhove, C., 1969. La 'zone du flysch' dans les nappes de l'Embrunais-Ubaye (Alpes occidentales). Geologie Alpine, 45: 5-190.

Kerckhove, C., Debelmas, J. and Cochonat, P., 1978. Tectonique du soubassement parautochtone des nappes de l'Embrunais-Ubaye sur leur bordure occidentale, du Drac au Verdon. Geologie Alpine, 54: 67-80.

Kerckhove, C., Gidon, M., Malaroda, R., Barfety, J.-C., Bogdanoff, S., Lemoine, M., Carraro, F., Jorda, M. and Monjuvent, G., 1980. Carte géologique de la France (1/250000). Feuille Gap. BRGM, Orléans.

Kerckhove, C., Gidon, M., Pairis, J.-L., Latreille, M. and Schneegans, D., 1988. Carte géologique de la France (1/50000). Feuille Chorges. BRGM, Orléans.

Kerckhove, C., Schneegans, D., Pairis, J.-L., Gidon, M. and Le Guernic, J., 1969. Carte géologique de la France (1/50000). Feuille Embrun. BRGM, Orléans.

Kern, H. and Wenk, H.R., 1983. Calcite texture development in experimentally induced ductile shear zones. Contributions to Mineralogy and Petrology, 83(3-4): 231-236.

Kretz, R., 1983. Symbols for rock-forming minerals. American Mineralogist., 68: 277-279.

Kunert V., 1999. Die Frankenwälder Querzone: Entwicklung einer thermischen Anomalie im Saxothuringikum. Unpublished PhD thesis, Univ. Gießen, 161pp.

Lafrance, B., White, J.C. and Williams, P.F., 1994. Natural calcite c-axis fabrics; an alternate interpretation. Tectonophysics, 229(1-2): 1-18.

Laubscher, H., 1991. The arc of the Western Alps today. Eclogae Geologicae Helvetiae, 84(3): 631-659.

Laubscher, H., Biella, G. C., Cassinis, R., Gelati, R., Lozej, A., Scarascia, S. and Tabacco, I., 1992. The collisional knot in Liguria. Geologische Rundschau, 81(2): 275-289.

Laubscher, H., 1971. The large-scale kinematics of the Western Alps and the northern Apennines and its palinspastic implications. American Journal of Science, 271(3): 193-226.

Law, R.D., Knipe, R.J. and Dayan, H., 1984. Strain path partitioning within thrust sheets; microstructural and petrofabric evidence from the Moine thrust zone at Loch Eriboll,

Northwest Scotland. Journal of Structural Geology, 6(5): 477-497.

Lawson, K., 1987. Thrust geometry and folding in the Alpine structural evolution of Haute Provençe., University of Wales, Swansea.

Lazarre, J., Tricart, P., Courrioux, G. and Ledru, P., 1996. Heritage tethysien et polyphasage alpin; reinterpretation tectonique du "synclinal" de l'aiguille de Morges (massif du Pelvoux, Alpes occidentales, France). Comptes Rendus de l'Academie des Sciences, Serie II. Sciences de la Terre et des Planetes, 323(12): 1051-1058.

Le Pichon, X., 1982. Land-locked oceanic basins and continental collision; the eastern Mediterranean as a case example. In: J. Hsue Kenneth (Editor), Mountain building processes. Acad. Press, London, United Kingdom, pp. 201-211.

Lefevre, R., 1983. La cicatrice de Preit; une discontinuite structurale majeure au sein de la zone brianconnaise interne entre Acceglio et l'Argentera (Alpes cottiennes meridionales). Comptes-Rendus des Seances de l'Academie des Sciences, Serie 2: Mecanique-Physique, Chimie, Sciences de l'Univers, Sciences de la Terre, 296(19): 1551-1554.

Leiss, B., Siegesmund, S., Weber, K., 1999. Texture asymmetries as shear sense indicators in naturally deformed mono- and poly-phase carbonate rocks. Textures Microstruct., 33: 61-74.

Lemoine, M., 1951. Donnees nouvelles sur la geologie du Brianconnais oriental et sur le probleme de la quatrieme ecaille. Bulletin de la Societe Geologique de France, 1: 191-204.

Lemoine, M., 1972. Rythme et Modalites des Plissements Superposes dans les Chaines Subalpines Meridionales des Alpes Occidentales Francaises. Geologische Rundschau, 61(3): 975-1010.

Lemoine, M., Bas, T., Arnaud-Vanneau, A., Arnaud, H., Dumont, T., Gidon, M., Bourbon, M., de Graciansky, P.-C., Rudkiewicz, J.-L., Megard-Galli, J. and Tricart, P., 1986. The continental margin of the Mesozoic Tethys in the Western Alps. Marine and Petroleum Geology, 3(3): 179-199.

Lemoine, M., Gidon, M. and Barféty, J.C., 1981. Les massifs cristallins externes des Alpes Occidentales; d'anciens blocs bascules nes au Lias lors du rifting tethysien. Comptes-Rendus des Seances de l'Academie des Sciences, Serie 2: Mecanique-Physique, Chimie, Sciences de l'Univers, Sciences de la Terre, 292(12): 917-920.

Lemoine, M., Graciansky, P.-C., Tricart, P., 2000. De l'océan à la chaîne de montagnes. Tectonique des plaques dans les Alpes., 205 pp.

Letouzey, J., 1986. Cenozoic paleo-stress pattern in the Alpine Foreland and structural interpretation in a platform basin. Tectonophysics 132: 215-231.

Lickorish, W.H. and Ford, M., 1998. Sequential restoration of the external Alpine Digne thrust system, SE France, constrained by kinematic data and synorogenic sediments. Geological Society Special Publications 134: 189-211.

Lickorish, W.H., Ford, M., Buergisser, J. and Cobbold, P.R., 2002. Arcuate thrust systems in sandbox experiments; a comparison to the external arcs of the Western Alps. Geological Society of America Bulletin, 114(9): 1089-1107.

Majesté-Menjoulas, C., 1979. Evolution Alpine d'un segment de la chaîne Varisque: nappe de Gavarnie, chevauchement Cinq-Monts-Gentiane, Université de Toulouse, 343 pp.

Maladora, R., Abiad, P.-L., Alesina, A., Blasi, A., Bortolami, Gc., Campanino Sturani, F., Cancelmo, C., Carraro, F., Crema, Gc., Cucchi, F., De Pol, C., Ezechieli, L., Fallot, P., Faure-Muret, A., Feltrin, F., Franceschetti, B., Francone, V., Gaiero, R., Govi, M., Grasso, F., Lorenzoni, S., Malaroda, R., Manzini Cucchi, A., Merlo, C., Perozzi, G., Ronco, P., Sacchi, R., Schiavinato, G., Sessa, N., Simonigh, A., Sodero, D., Sturani, C., Zanella, E., Zanettin Lorenzoni, E. and Zappi L., 1967. Carta Geologica del Massiccio dell' Argentera, scala 1/50000.

Malinverno, A. and Ryan, W.B.F., 1986. Extension in the Tyrrhenian Sea and shortening in the Apennines as result of arc migration driven by sinking of the lithosphere. Tectonics, 5(2): 227-245.

Mancktelow, N.S., 1987. Quartz textures from the Simplon fault zone, Southwest Switzerland and North Italy. Tectonophysics, 135(1-3): 133-153.

Merle, O. and Brun, J.P., 1984. The curved translation path of the Parpaillon Nappe (French Alps). Journal of Structural Geology, 6(6): 711-719.

Merriman R.J. & Peacor D.R., 1999. Very low-grade metapelites: mineralogy, microfabrics and measuring reaction progress. In: M.a.R. Frey, D. (Editor), Low-Grade Metamorphism. Blackwell Science, London, pp. 10-60.

Mosar, J., Stampfli, G.M. and Girod, F., 1996. western Prealpes Medianes Romandes; timing and structure; a review. Eclogae Geologicae Helvetiae 89 (1): 389-425.

Mullis, J. (1976). Das Wachstumsmilieu der Quarzkristalle im Val d´Illiez (Wallis, Schweiz). Schweizerische Mineralogische und Petrographische Mitteilungen 56: 219-268.

Nicolas, A., 1976. Flow in upper-mantle rocks; some geophysical and geodynamic consequences. Tectonophysics, 32: 93-106.

Nicolas, A., Bouchez, J.L., Blaise, J. and Poirier, J.P., 1977. Geological aspects of deformation in continental shear zones. Tectonophysics, 42(1): 55-73.

Nicolas, A., Bouchez, J.L. and Boudier, F., 1972. Interpretation cinematique des deformations plastiques dans le Massif de lherzolite de Lanzo (Alpes piemontaises); comparaison avec d'autres massifs. Tectonophysics, 14(2): 143-171.

Nicolas, A., Bouchez, J.L., Boudier, F. and Mercier, J.C., 1971. Textures, structures and fabrics due to solid state flow in some European lherzolites. Tectonophysics, 12(1): 55-86.

Nicolas, A., Boudier, F. and Boullier, A.M., 1973. Mechanisms of flow in naturally and experimentally deformed peridotites. American Journal of Science, 273(10): 853-876.

Odin, G.S. and Odin, C., 1990. Echelle numérique des temps géologiques. Géochronique, 35: 12-21.

Orszag, S.F. and Pilot, M.D., 1976. Grands traits du Neogene de Corse. Bulletin de la Societe Geologique de France, 18(5): 1183-1187.

Ortner, H., 2001. Tectonic VB 1.5a. http://geopal.uibk.ac.at/tvb/front.html.

Ott d'Estevou, P., Montenat, C., Ladure, F. and D'Autrey, L.P., 1988. Evolution tectono-sedimentaire du domaine prébétique oriental (Espagne) au Miocène. C. R. Acad. Sci. Paris Série II, 307: 789-796.

Padmanabhan, K.A., Davies, G.J., 1980. Superplasticity. Springer, 312 pp.

Panozzo, R.H., 1983. Two-dimensional analysis of shape-fabric using projections of digitized lines in a plane. Tectonophysics, 95(3-4): 279-294.

Panozzo, R.H., 1984. Two-dimensional strain from the orientation of lines in a plane. Journal of Structural Geology, 6(1-2): 215-221.
Parish, M., 1984. A structural interpretation of a section of the Gavarnie Nappe and its implications for Pyrenean geology. Journal of Structural Geology, 6(3): 247-255.

Passchier, C.W., Trouw, R.A.J., 1996. Microtectonics, 289 pp.

Perriaux, J. and Uselle, J.P., 1968. Quelques donnees sur la sedimentologie des gres du Champsaur (Hautes-Alpes). Geologie Alpine, 44: 329-332.

Pieri, M., Burlini, L., Kunze, K., Stretton, I. and Olgaard, D.L., 2001. Rheological and microstructural evolution of Carrara Marble with high shear strain; results from high temperature torsion experiments. Journal of Structural Geology, 23(9): 1393-1413.

Pieri, M., Kunze, K., Burlini, L., Stretton, I., Olgaard, D.L., Burg, J.P., Wenk, H.R., 2001. Texture development of calcite by deformation and dynamic recrystallization at 1000 K during torsion experiments of marble to large strains. Tectonophysics, 330(1-2): 119-140.

Platt, J.P. and Behrmann, J.H., 1986. Structures and fabrics in a crustal-scale shear zone, Betic Cordillera, SE Spain. Journal of Structural Geology, 8(1): 15-33.

Platt, J.P., Behrmann, J.H., Cunningham, P.C., Dewey, J.F., Helmann, M., Parish, M., Shepley, M.G., Wallis, S. and Weston, P.J. 1989. Kinematics of the Alpine arc and the motion history of Adria. Nature, 337(6203): 158-161.

Platt, J.P. and England, P.C., 1994. Convective removal of lithosphere beneath mountain belts; thermal and mechanical consequences. American Journal of Science, 294(3): 307-336.

Platt, J.P. and Vissers, R.L.M., 1989. Extensional collapse of thickened continental lithosphere; a working hypothesis for the Alboran Sea and Gibraltar Arc. Geology, 17(6): 540-543.

Potel, S., 2001. Very low-grade metamorphism of northern New Caledonia, University of Basel, Basel, 207 pp.

Principi, G. and Treves, B., 1984. Il sistema corso-appenninico come prisma di accrezione; riflessi sul problema generale del limite Alpi-Appennini. In: M. Vanossi (Editor), Atti del convegno sul tema Geologia delle Alpi Liguri. Memorie della Societa Geologica Italiana. Societa Geologica Italiana, Rome, Italy, pp. 549-576.

Ratschbacher, L., Wenk, H.R. and Sintubin, M., 1991. Calcite textures; examples from nappes with strain-path partitioning. Journal of Structural Geology, 13(4): 369-384.

Ravenne, C., Vially, R., Riche, P. and Tremolieres, P., 1987. Sedimentation et tectonique dans le bassin marin Eocene superieur-Oligocene des Alpes du Sud. Revue de l'Institut Francais du Petrole, 42(5): 529-553.
Ricou, L.E., 1981. Glissement senestre des nappes penniques le long de la bordure nord de l'Argentera; son role dans le jeu de l'arc alpin. Comptes-Rendus des Seances de l'Academie des Sciences, Serie 2: Mecanique-Physique, Chimie, Sciences de l'Univers, Sciences de la Terre, 292(18): 1305-1308.

Ricou, L.E., 1984. Les Alpes occidentales; chaine de decrochement. Bulletin de la Societe Geologique de France, 26(5): 861-874.

Ricou, L.E. and Siddans, A.W.B., 1986. Collision tectonics in the Western Alps. Geological Society Special Publications 19: 229-244.

Ritz, F., 1991. Evolution du champ de contraintes dans les Alpes du Sud depuis la fin de l'Oligocène. Implications sismotectoniques., Montpellier.

Roca, E., 2001. The Northwest Mediterranean Basin (Valencia Trough, Gulf of Lions and Liguro-Provencal basins); structure and geodynamic evolution. In: A. Ziegler Peter, W. Cavazza, H.F. Robertson Alastair and S. Crasquin Soleau (Editors), Peri-Tethys memoir

6; Peri-Tethyan rift/ wrench basins and passive margins. Ed. du Museum National d'Histoire Naturelle. Paris, France. 2001.

Roddaz, B., 1977. Le prolongement oriental de la nappe de Gavarnie et son substratum entre le Barroude et le Moudang (Pyrénées Centrales). Université de Toulouse, 131 pp.

Rollet, N., Déverchère, J., Beslier, M.-O., Guennoc, P., Réhault, J.-P., Sosson, M. and Truffet, C. 2002. Back arc extension, tectonic inheritance, and volcanism in the Ligurian Sea, western Mediterranean. Tectonics 21 (3).

Royden, L.H., 1993. Evolution of retreating subduction boundaries formed during continental collision. Tectonics, 12(3): 629-638.

Rutter, E.H. and Brodie, K.H., 1988. The role of tectonic grain size reduction in the rheological stratification of the lithosphere. Geologische Rundschau. 77(1): 295-308.

Sanderson, D.J., 1979. The transition from upright to recumbent folding in the Variscan fold belt of Southwest England; a model based on the kinematics of simple shear. Journal of Structural Geology, 1(3): 171-180.

Sassi F.P. & Scolari A., 1974. The b0 of the potassic white micas as a barometric indicator in low-grade metamorphism of pelitic schists. Contribution to Mineralogy and Petrology, 45: 143-152.

Schaeben, H., Siemes, H., Hoefler, S. and Will, G., 1990. Practical application of entropy optimization in quantitative texture analysis. Geological Society Special Publications. 54: 375-381.

Schmid, S.M., Fügenschuh, B., Kissling E. and Schuster, R., 2004. Tectonic map and overall architecture of the Alpine orogen. Eclogae Geologicae Helvetiae, 97(1): 93-117.

Schmid, S.M., 1982. Microfabric studies as indicators of deformation mechanisms and flow laws operative in mountain building. In: J. Hsue Kenneth (Editor), Mountain building processes. Acad. Press, London, pp. 95-110.

Schmid, S.M., Boland, J.N. and Paterson, M.S., 1977. Superplastic flow in finegrained limestone. Tectonophysics, 43(3-4): 257-291.

Schmid, S.M. and Casey, M., 1986. Complete fabric analysis of some commonly observed quartz c-axis patterns. Geophysical Monograph. 36: 263-286.

Schmid, S.M., Casey, M. and Starkey, J., 1981. The microfabric of calcite tectonites from the Helvetic Nappes (Swiss Alps). Geological Society of London Special Publication. 9: 151-158.

Schmid, S.M., Panozzo, R. and Bauer, S., 1987. Simple shear experiments on calcite

rocks; rheology and microfabric. Journal of Structural Geology. 9(5-6): 747-778.

Schmid S.M., 1994. Textures of geological materials: computer model predictions versus empirical interpretations based on rock deformation experiments and field studies. In: H.J. Bunge, Siegesmund, S., Skrotzki, W., Weber, K. (Editor), Texture of Geological Materials. DGM Informationsgesellschaft Verlag, Oberursel, pp. 279-301.

Schmidt, D., Schmidt, S.Th. and Mullis, J., 1997. Very low grade metamorphism of the Taveyanne formation of western Switzerland. Contributions to Mineralogy and Petrology, 129: 385-403.

Seranne, M., 1999. The Gulf of Lion continental margin (NW Mediterranean) revisited by IBS; an overview. Geological Society Special Publications 156: 15-36.

Serri, G., Innocenti, F. and Manetti, P., 1993. Geochemical and petrological evidence of the subduction of delaminated Adriatic continental lithosphere in the genesis of the Neogene-Quaternary magmatism of central Italy. Tectonophysics 223 (1-2): 117-147.

Seward, D., Ford M., Bürgisser, J., Lickorish, H., Williams, E.A., Meckel L.D., 1999. Preliminary results of fission-track analyses in the southern Pelvoux area, SE France. In: G. Gosso, F. Jadoul, M. Sella and I. Spalla Maria (Editors), 3rd workshop on Alpine geological studies. Memorie di Scienze Geologiche, 51(1): 25-31.

Seward, D. and Mancktelow, N.S., 1994. Neogene kinematics of the Central and Western Alps; evidence from fission-track dating. Geology, 22(9): 803-806.

Siddans, A.W.B., 1979. Arcuate fold and thrust patterns in the Subalpine chains of Southeast France. Journal of Structural Geology, 1(2): 117-126.

Simon Gomez, J.L., 1986. Analysis of a gradual change in stress regime (example from the eastern Iberian Chain, Spain. Tectonophysics, 124(1-2): 37-53.

Simpson, C. and Schmid, S.M., 1983. An evaluation of criteria to deduce the sense of movement in sheared rocks. Geological Society of America Bulletin, 94(11): 1281-1288.

Spakman, W.S., van der Lee and R. van der Hilst, 1993. Travel-time tomography of the European-Mediterranean mantle down to 1400 km. Physics of the Earth and Planetary Interiors 79: 3-74.

Spakman, W., and Wortel R., 2004. A Tomographic View on western Mediterranean Geodynamics., The TRANSMED Atlas The Mediterranean region from crust to mantle. Springer.

Spencer, S., 1992. A kinematic analysis incorporating incremental strain data for the frontal Pennine zones of the western French Alps. Tectonophysics, 206(3-4): 285-305.

Spiers, C.J. and Wenk, H.R., 1980. Evidence for slip on r and f in the positive sense in deformed calcite single crystals. American Geophysical Union; 1980 fall meeting. Eos, Transactions, 61(46): 1128.

Sue, C., Martinod, J., Tricart, P., Thouvenot, F., Gamont, J.-F., Fréchet, J., Marinier, D., Glot, J.-P., Grasso, J.R., 2000. Active deformation in the inner Western Alps inferred from comparison between 1972-classical and 1996-GPS geodetic surveys. Tectonophysics, 320(1): 17-29.

Sue, C., Thouvenot, F., Frechet, J. and Tricart, P., 1999. Widespread extension in the core of the Western Alps revealed by earthquake analysis. Journal of Geophysical Research, B, Solid Earth and Planets, 104(11): 25,611-25,622.

Sue, C. and Tricart, P., 1999. Late Alpine brittle extension above the frontal Pennine thrust near Briancon, Western Alps. Eclogae Geologicae Helvetiae, 92(2): 171-181.
Sue, C. and Tricart, P., 2003. Neogene to ongoing normal faulting in the inner Western Alps; a major evolution of the late alpine tectonics. Tectonics, 22 (5).

Sue, C., Tricart, P., Dumont, T. and Pecher, A., 1997. Raccourcissement polyphase dans le massif du Pelvoux (Alpes occidentales); exemple du chevauchement de socle de Villard-Notre-Dame. Comptes Rendus de l'Academie des Sciences, Serie II. Sciences de la Terre et des Planetes, 324(10): 847-854.

Tagami, T., Galbraith, R.F., Yamada, R., and Laslett, G.M., 1998. Revised annealing kinetics of fission tracks in zircon and geological implications. In: P. Van den Haute, and De Corte, F. (Editor), Advances in fission-track geochronology. Dordrecht, Kluwer Academic Publishers, pp. 99-112.

Termier, P., 1903. Les montagnes entre Briançon et Vallouise. Mém. expl. Carte géol. Fr.: 182.

Thomas, J.C., Claudel, M.E., Collombet, M., Tricart, P., Chauvin, A. and Dumont, T., 1999. First paleomagnetic data from the sedimentary cover of the French Penninic Alps: evidence for Tertiary counterclockwise rotations on the Western Alps. Earth and Planetary Science Letters, 171: 561-574.

Tricart, P., 1980. Tectoniques superposées dans les Alpes occidentales au Sud du Pelvoux; évolution structurale d'une chaîne de collision., Université de Strasbourg, France, Strasbourg, 407 pp.

Tricart, P., 1986. Le Chevauchement de la zone brianconnaise au Sud-Est du Pelvoux; cle des rapports zone externe - zones internes dans les Alpes occidentales. Bulletin de la Societe Geologique de France, Huitieme Serie, 2(2): 233-244.

Tricart, P., Bouillin, J.P., Dick, P., Moutier, L. and Xing, C., 1996. Le faisceau de failles de haute-Durance et le rejeu distensif du front brianconnais au SE du Pelvoux (Alpes

occidentales). Comptes Rendus de l'Academie des Sciences, Serie II. Sciences de la Terre et des Planetes, 323(3): 251-257.

Tricart, P., Bourbon, M., Chenet, P. Y., Cros, P., Delorme, M., Dumont, T., Graciansky, P.C., Lemoine, M., Megard, Galli J. and Richez, M., 1988. Tectonique synsedimentaire triasico-jurassique et rifting tethysien dans la nappe brianconnaise de Peyre-Haute (Alpes occidentales). Bulletin de la Societe Geologique de France, Huitieme Serie, 4(4): 669-680.

Tricart, P., Schwartz, S., Sue, C., Poupeau, G. and Lardeaux, J.M., 2001. La denudation tectonique de la zone ultradauphinoise et l'inversion du front brianconnais au sud-est du Pelvoux (Alpes occidentales); une dynamique miocene a actuelle. Bulletin de la Societe Geologique de France, 172(1): 49-58.

Tricart, P., 2004. From extension to transpression during the final exhumation of the Pelvoux and Argentera massifs, Western Alps. Eclogae Geologicae Helvetiae, in press.

Trincardi, F., Zitellini, N., 1987. The rifting in the Tyrrhenian basin. Geo-Marine Lett., 7(1-6).

Turner, F.J., Griggs, D.T. and Heard, H.C., 1954. Experimental deformation of calcite crystals. Geological Society of America Bulletin, 65(9): 883-933.

Turner, F.J.a.H., H.C., 1965. Deformation in calcite crystals at different strain rates. Univ. Calif. Publ. Geol. Sci., 46: 103-126.

Vernet, J., 1950. Les limites SE du massif du Pelvoux et de l'anticlinal amygdaloïde des Ecrins. Bulletin de la Societe Geologique de France, 5(20): 275-287.

Vernet, J., 1951. Le Synclinorium de l'Aiguille de Morges et le style des déformations alpines du Cristallin du Pelvoux. Bulletin de la Societe Geologique de France, 6(1): 169-183.

Vernet, J., 1952. Les déformations d'âge alpin du Cristallin du Pelvoux, à la lumière d'observations nouvelles. Bulletin de la Societe Geologique de France, 6(2): 175-189.

Vernet, J., 1966. Observations nouvelles sur le synclinal d'Ailefroide et les bordures du massif du Pelvoux en Vallouise. Travaux du Laboratoire de Geologie de la Faculte des Sciences de Grenoble 42: 275-280.

Vialon, P., Rochette, P. and Menard, G., 1989. Indentation and rotation in the western Alpine arc. Geological Society Special Publications 45: 329-338.

Vigliotti, L. and Langenheim, V.E., 1995. When did Sardinia stop rotating? New palaeomagnetic results. Terra Nova, 7(4): 424-435.

Wagner, F., Wenk, H.R., Kern, H., Houtte, P.V. and Esling, C., 1982. Development of preferred orientation in plane strain deformed limestone; experiment and theory. Contributions to Mineralogy and Petrology, 80(2): 132-139.

Waibel, A.F., 1990. Sedimentology, petrographic variability, and very-low-grade metamorphism of the Champsaur sandstone (Paleogene, Hautes-Alpes, France). Evolution of volcaniclastic foreland turbidites in the external Western Alps., Université de Genève, Genève.

Warr L.N. and Rice A.H., 1994. Interlaboratory standardization and calibration of clay mineral crystallinity and crystallite size data. Journal of Metamorphic Geology, 12: 141-152.

Watts, A.B. and Torne, M., 1992. Subsidence history, crustal structure, and thermal evolution of the Valencia Trough; a young extensional basin in the western Mediterranean. Journal of Geophysical Research, B, Solid Earth and Planets, 97(13): 20,021-20,041.

Weiss, L.E. and Turner, F.J., 1972. Some Observations on Translation Gliding and Kinking in Experimentally Deformed Calcite and Dolomite, Flow and Fracture of Rocks. Geophysical Monograph. 16: 95-107.

Wenk, H.R., Matthies, S., Donovan, J., Chateigner, D., 1998. BEARTEX, a Windows-based program system for quantitative texture analysis. Journal of Applied Crystallography, 31: 262-269.

Wenk, H.R., Takeshita, T., Bechler, E., Erskine, B.G. and Matthies, S., 1987. Pure shear and simple shear calcite textures; comparison of experimental, theoretical and natural data. Journal of Structural Geology. 9(5-6): 731-745.

Wenk, H.R., Venkitasubramanyan, C.S., Baker, D.W. and Turner, F.J., 1973. Preferred Orientation in Experimentally Deformed Limestone. Contributions to Mineralogy and Petrology, 38(2): 81-114.

Wortel, M.J.R. and Spakman, W., 1992. Structure and dynamics of subducted lithosphere in the Mediterranean region. Proceedings of the Koninklijke Nederlandse Akademie van Wetenschappen (1990), 95(3): 325-347.

Wyckoff, R.W.G., 1920. The crystal structures of some carbonates of the calcite group. American Journal of Science, 50: 317-360.